"The Wavelength Dependence of the Photoplethysmogram and its Implication to Pulse Oximetry"

by Damianos Damianou, MSc

Thesis submitted to the University of Nottingham

for the degree of Doctor of Philosophy, October, 1995

ABSTRACT

Since the early 1980s the increase in use of pulse oximeters in many clinical situations has been quite remarkable, turning it into one of the most important methods of monitoring in use today. Pulse oximetry essentially uses photoplethysmography to calculate oxygen saturation. Consequently the wavelength dependence of the photoplethysmogram (PPG) is of direct relevance in the performance of pulse oximeters.

The experimental results obtained on the wavelength dependence of the AC, DC and AC/DC PPG components for the 450 - 1000nm range are undoubtedly different to the ones predicted by the current simple pulse oximeter model based on the Lambert-Beer law. Moreover, they show unexpected phenomena regarding the magnitude of the above components over the whole range, with distinct differences between the reflection and transmission modes. This is of significance to the technique of pulse oximetry suggesting that perhaps other wavelengths should be considered for use, and that use of both "reflection" and "transmission" probes on the same oximeter may lead to inaccurate readings in one of the modes.

A finger model was developed and results from Monte Carlo simulations of photon propagation obtained. The results did not correspond to the experimental results, this is most probably due to either wrong parameters or model.

Recent advances in the use of reflection pulse oximeters on fetal monitoring during labour, have raised the question of possible artifacts which may arise due to inadequate probe application in the birth canal. The importance of complete opposition of the reflectance probe was examined on an adult finger. False low oxygen saturation readings were recorded with malpositioned probes. A new probe with modified geometry was designed which offered an improved performance in reducing this artifact and further suggestions were given for its possible elimination.

Finally, a proposal for a novel, visible multi-wavelength reflection pulse oximeter is presented with the aim of replacing current pulse oximeters in certain situations where their use is questionable.

CONTENTS

ACKNOWLEDGEMENTS

I would like to thank my supervisor Dr John Crowe for all his time, help and encouragement. Without his continuous backing this thesis would just not have been possible.

I am also grateful to the staff and students of the Department of Electrical and Electronic Engineering for providing such excellent facilities and support.

Finally I must thank my family and friends who throughout encouraged me to persevere with this sometimes frustrating but ultimately interesting and valuable study.

CHAPTER 1

INTRODUCTION

The most common cause of preventable disaster in the operating theatre and critical care environments, is patient hypoxia. An instrument that would continually and accurately monitor the oxygen saturation of a patient's blood, preferably non invasively, would facilitate detection of hypoxia before clinical signs are apparent, and enable the physician to initiate corrective actions before it is too late. Until the early 1980s, oxygen saturation was mainly calculated by obtaining arterial blood and examining the profile of the blood gases. However, the disadvantages of this method are that it is *in vitro*, with the risk of sample contamination, and more importantly is invasive and also not continuous. Although, several other ways of monitoring oxygen saturation optically have been proposed, like the Wood oximeter (Wood, 1948) and the Hewlett-Packard ear oximeter (Saunders, 1976), their success was limited.

Since the early 1980s a new technique, namely pulse oximetry,

has become widely used. Pulse oximeters (Yoshiya, 1980; Taylor, 1986; Griffiths, 1988; Blackwell, 1989) are used in many clinical settings, such as intensive care, surgery and emergency medicine to name just a few, for the continuous, *in vivo*, non invasive monitoring of "arterial" oxygen saturation. The current situation regarding pulse oximetry is that of an extremely commercially successful instrument, mainly because of the ease of operation. Although several problems have been reported relating to the use of pulse oximeters, it has to be emphasized that pulse oximeters are very reliable clinical instruments in most cases, and this has been clearly proved over the last few years. Nevertheless it is widely acknowledged that the precise mechanism of their operation is not totally understood.

In the following sections of the introduction the clinical background of oxygen transport is reviewed along with oxygen saturation monitoring techniques. Also the theory and uses of photoplethysmography, the technique utilised by Pulse Oximetry for monitoring oxygen saturation, are presented. In Chapter 2 the present theory, uses and limitations of pulse oximetry are examined. Finally an outline of the objectives of this thesis is given. Chapter 3 describes the instrumentation (both hardware and software), the system set up and experimental procedure for the capture and analysis of the photoplethysmogram within the 450 to 1000nm wavelength range. In Chapter 4 the consequences of the wavelength dependence of the photoplethysmogram to pulse oximetry are considered and discussed.

Chapter 5 gives an introduction to the structure and optics of the skin, a description of the Monte Carlo technique used for simulating light transport in tissue and results relating to the wavelength dependence of the photoplethysmogram, obtained from a series of Monte Carlo simulations on a model finger. In Chapter 6 results are presented from studies relating to the effect of pulse oximeter probe malposition, principally in reflection mode but also in transmission. In Chapter 7 a suggestion for a novel reflection pulse oximeter based upon the observations in Chapter 4 is given. Final conclusions are given in chapter 8.

1.1 CLINICAL BACKGROUND

In this section the cardiovascular system and the respiratory functions of blood are explained. It is not intended to be a very detailed description, but sufficient to enable the principles of pulse oximetry to be explained and discussed.

1.1.1 Circulation of the blood

The blood circulates through the arterial system present in the tissues of the body. The blood volume is about 8% of the total body volume and it consists of cells suspended in a fluid called plasma. Each of the blood constituents is adapted for a special purpose and the main function of blood is that of transport. Blood carries all the materials that

cells need to function correctly, that is fats, amino acids, sugar, vitamins, salts, water, hormones and most importantly oxygen. Moreover, blood carries all the waste products of metabolism of cells, such as carbon dioxide and urea away from the tissues to the organs of excretion.

Blood is continually pumped by the heart through a closed system of blood vessels. The energy required to drive the blood through the series of blood vessels is provided by the rhythmic contractions of the heart, the heart being nothing more than a muscular pump. In reality, the heart can be thought off as two pumps in series with each other. From the left ventricle blood is driven to the tissues through thick walled vessels, the arteries. In the tissues blood is driven through a meshwork of fine vessels, the capillaries, where an exchange of materials between the blood and the tissues occurs. The capillaries drain through venules into veins and eventually back to the right atrium. This is the systemic circulation. From the right atrium blood flows to the right ventricle and then it is pumped through the pulmonary arteries to the lungs. In the thin walled capillaries of the lungs the blood equilibrates with the O_2 and CO_2 in the alveolar air. It then is carried by the pulmonary veins to the left atrium. This represents the pulmonary circulation. The pulmonary and systemic circulation of blood are shown in Fig. 1.1.

The exchange of gases between blood and tissues, and blood and alveolar air is treated with some detail in section 1.1.3.

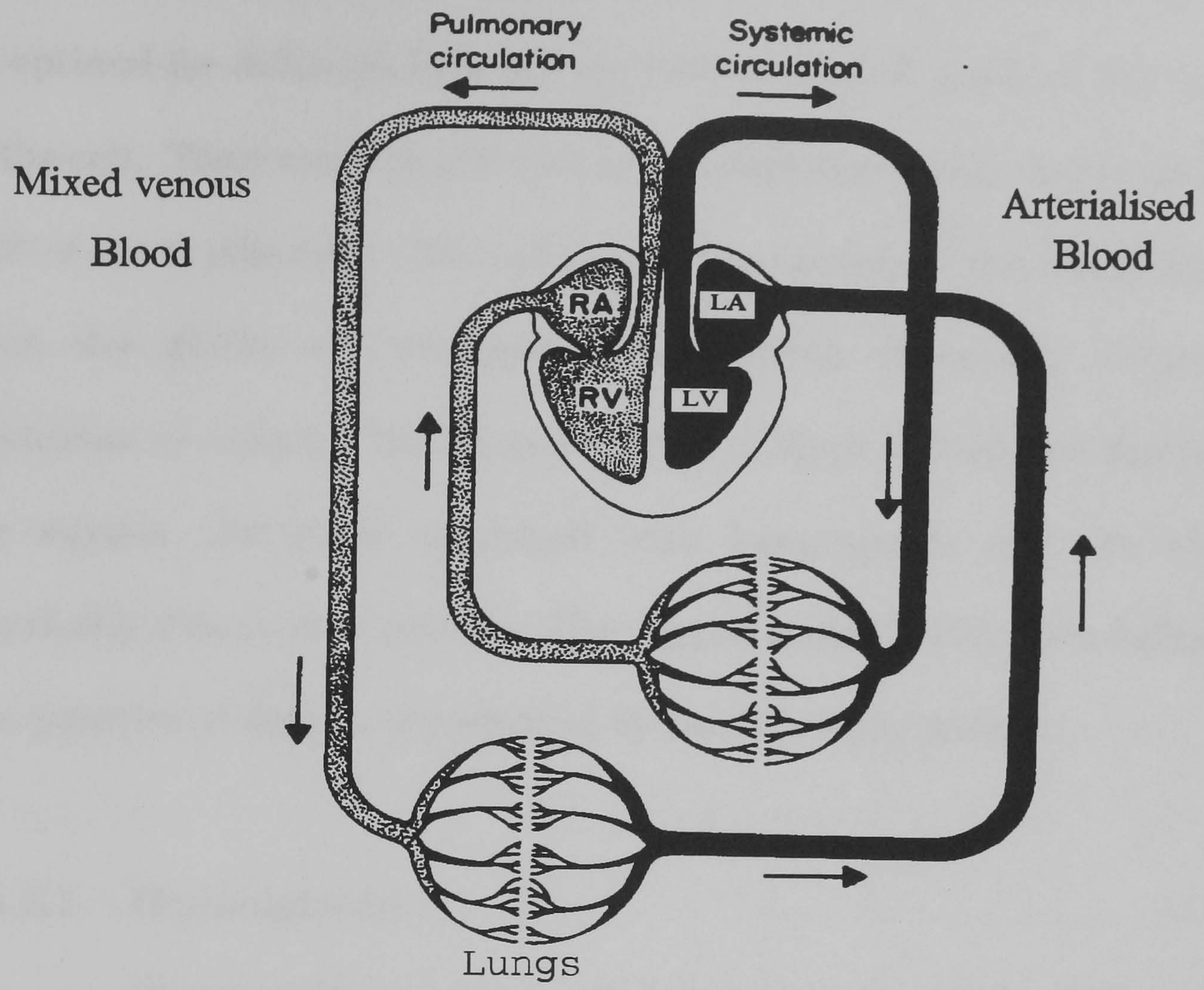

Figure 1.1: The pulmonary and systemic circulation.

1.1.2 Oxygen Transport - Blood Constituents

Oxygen is necessary for life because it is fundamental to cellular respiration. As mentioned above oxygen is transported from the lungs to the tissues and organs of the body by the blood. Although oxygen does dissolve in plasma its solubility is such that the amount of dissolved oxygen alone carried in the plasma, is not sufficient for man's oxygen requirements. Sufficient oxygen quantities are carried by one of the blood constituents, the erythrocytes. The function of erythrocytes (or red blood cells) is central to the respiratory functions of blood, which is to transport oxygen from the lungs to the tissues and organs. Erythrocytes are non-nucleated cells, their shape being a biconcave disc with mean diameter of

7.2μm and mean thickness of 2μm. This configuration has been found to be optimal for diffusion between the surface and all parts of the interior of the cell. Their main constituent is haemoglobin, which makes up about 94% of the erythrocyte. Most of the oxygen carried by the blood depends upon the ability of haemoglobin to combine chemically with large quantities of oxygen. The oxygen content of blood is therefore the sum of the oxygen chemically combined with haemoglobin and the oxygen physically dissolved in plasma. The oxygen content of blood is defined as the quantity of oxygen transported by the blood per minute.

1.1.2.1 Haemoglobin

Haemoglobin is a conjugated protein and consists of the protein globin united to the iron containing substance haem. The haemoglobin molecule is composed of four haem groups and four protein chains. Each of the four iron atoms can combine one O_2 molecule.

$$Hb + O_2 \rightleftharpoons HbO_2 \tag{1.1}$$

This combination is not an oxidation but an oxygenation. This gives haemoglobin its most important property, to combine rapidly and reversibly with oxygen. The oxygenated form of haemoglobin is known as oxyhaemoglobin (HbO_2) and the deoxygenated is known as reduced haemoglobin or deoxyhaemoglobin (Hb).

The percentage saturation of haemoglobin (ie the ratio of oxygenated haemoglobin over total haemoglobin) is a function of the

oxygen's partial pressure (pO_2), which is described by the oxygen dissociation curve. The characteristic sigmoid shape of the oxygen dissociation curve (Fig. 1.2) is due to the shifting affinity of Hb for O_2. That is combination of the first haem in the Hb molecule with O_2 increases the affinity of the second haem for O_2 which in turn increases the affinity of the third haem which in turn increases the affinity of the fourth. The sigmoid shape of the dissociation curve is highly relevant to the function of haemoglobin. The flat section which is principally concerned with oxygen uptake, ensures that arterial blood leaves the lungs well saturated even when partial pressure is reduced to about 67 mm Hg (by living at altitude or by modest lung disease). The steep lower portion ensures an adequate oxygen supply to tissues by releasing large amounts of oxygen for relatively small decreases in partial pressure.

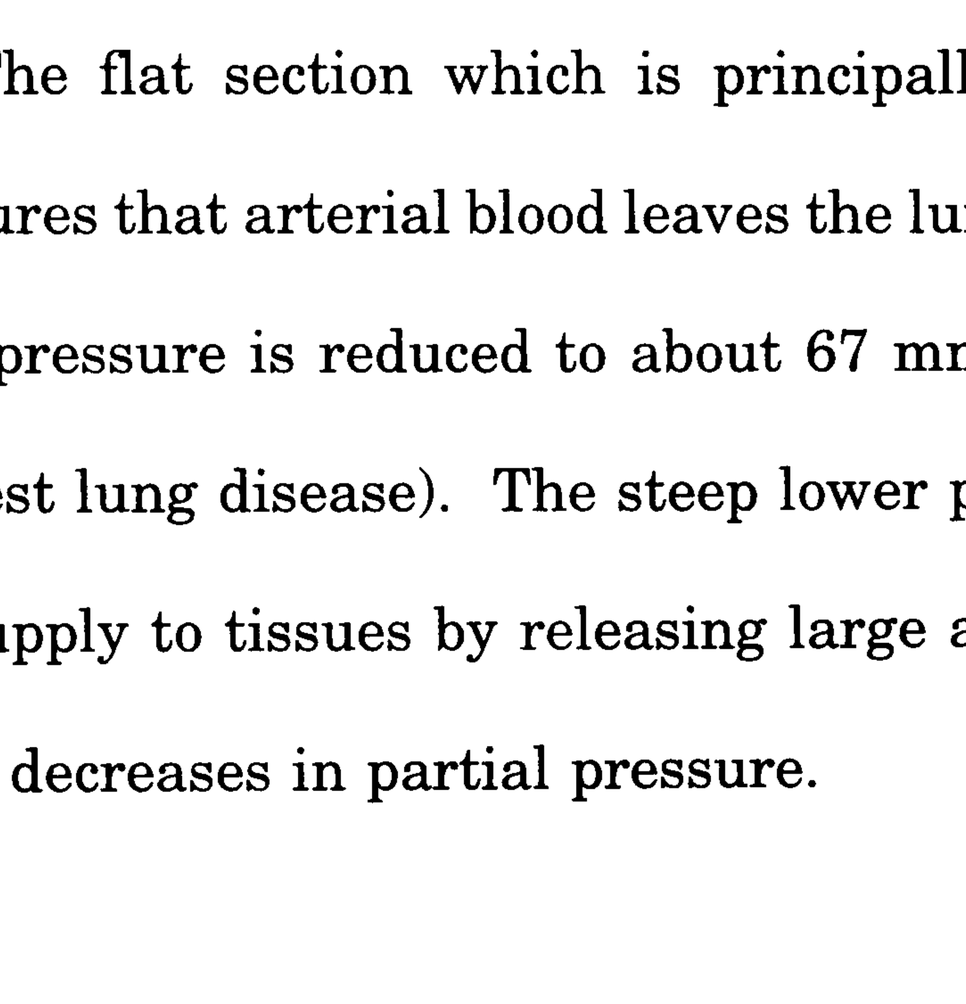

Figure 1.2: Oxygen haemoglobin dissociation curve.

Different factors shift and may alter the shape of the oxygen

dissociation curve. These include temperature, partial pressure of CO_2 (pCO_2) and concentration of 2,3-diphosphoglycerate. A fall in blood pH, which is due to its CO_2 content rising, or an increase in temperature shifts the curve to the right. The right shifting due to the increase in pCO_2 is known as the Bohr effect. In the tissues the pO_2 is between 10 and 40mm Hg. Therefore, a shift of the curve to the right means that at a given tissue pO_2, oxyhaemoglobin unloads more of its oxygen. This is of clear physiological value, as an active tissue has a relatively high pCO_2, low pH and higher temperature and all these changes result in more oxygen being unloaded.

1.1.2.2 Other forms of haemoglobin

Other forms of haemoglobin are also present in blood. These can sometimes be so significant that they demand specific consideration. When blood is exposed to various drugs the ferrous iron in the Hb molecule is converted to its ferric form, forming methaemoglobin (MetHb). Methaemoglobin is incapable of combining reversibly with oxygen and thus cannot act as an oxygen carrier. Some oxidation of haemoglobin to methaemoglobin occurs normally, but an enzyme system in the red cells, the NADH-methaemoglobin reductase system, converts methaemoglobin back to haemoglobin.

Carbon monoxide also reacts with Hb to form carboxyhaemoglobin (COHb). As the affinity of Hb for O_2 is much less

than that of Hb for CO, high levels of carboxyhaemoglobin result in a reduction of the oxygen carrying capacity of blood, because CO binds irreversibly to Hb.

1.1.3 Transfer of Gases

In alveolar air at normal atmospheric pressure and at a body temperature of 37^0 C the partial pressure of oxygen is 100mm Hg and of carbon dioxide is 40mm Hg. In the tissues at rest the partial pressure of oxygen is 35mm Hg and of carbon dioxide 46mm Hg. The net transfer of gas between alveolar air and blood as well as between blood and tissue continues as long as there is a pressure gradient. Oxygen passes from the alveolar air to blood because the partial pressure of oxygen in the air is higher than in the blood. Carbon dioxide passes in the opposite direction because its partial pressure is higher in blood than in the air. In the case of tissues the above situation is reversed, with oxygen passing from blood to the tissues and carbon dioxide passing from the tissues to blood (Ganong, 1973). This is indicated in Fig. 1.3.

1.2 MONITORING OXYGEN SATURATION

Oxygen saturation is defined as the oxygen content expressed as a percentage of the total oxygen capacity and the degree of blood oxygenation can be described by either the functional oxygen saturation or the fractional oxygen saturation, given in equations 1.2 and 1.3

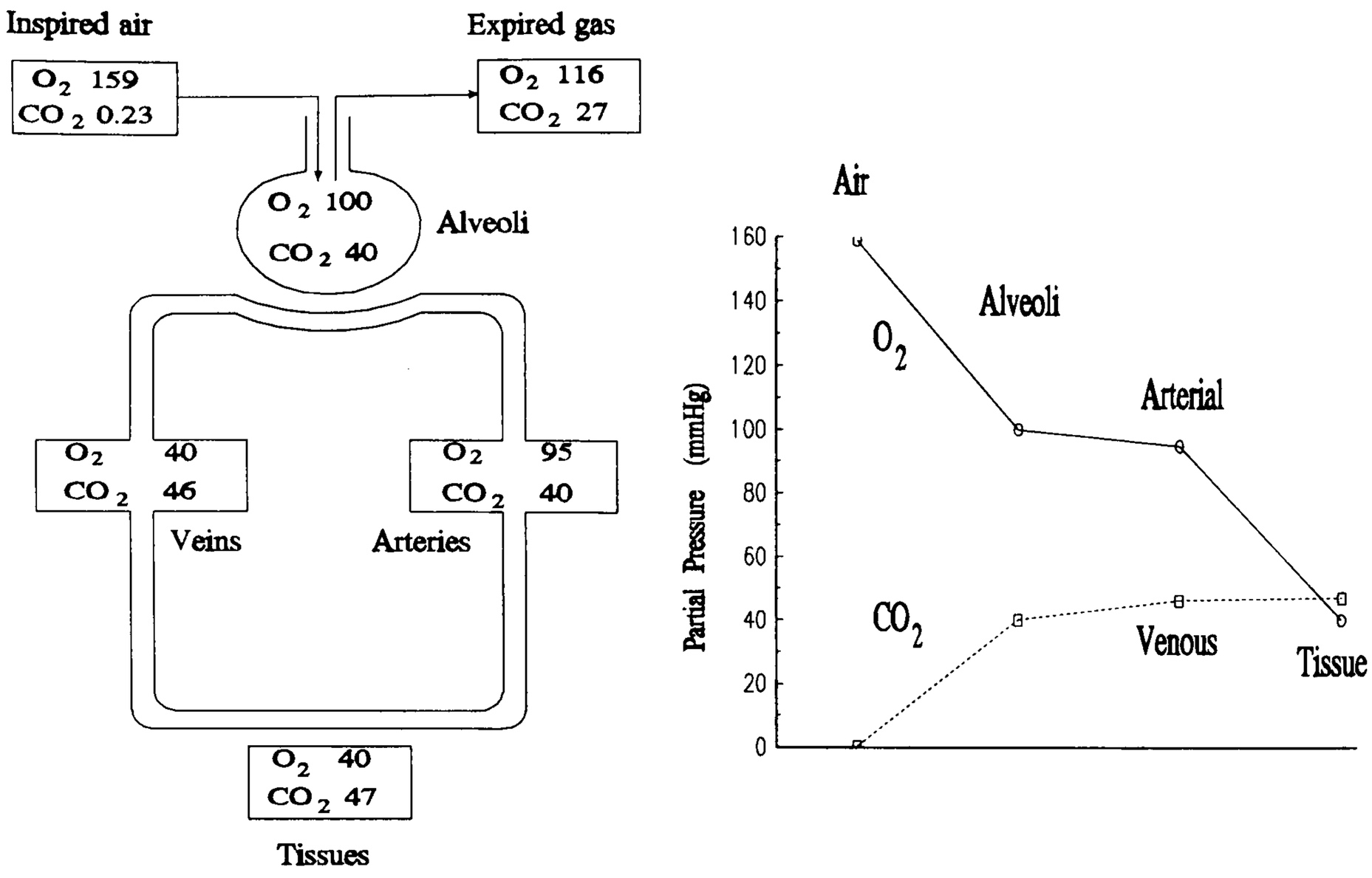

Figure 1.3: The partial pressures of oxygen and carbon dioxide in the gas transport system and the pressure gradients for oxygen (solid line) and carbon dioxide (dotted line).

respectively.

$$Functional\ SaO_2 = \frac{C[HbO_2]}{C[HbO_2]+C[Hb]} * 100\% \qquad (1.2)$$

$$Fractional\ SaO_2 = \frac{C[HbO_2]}{C[HbO_2]+C[Hb]+C[MetHb]+C[COHb]} * 100\% \qquad (1.3)$$

where: C[Hb] concentration of haemoglobin

C[HbO_2] concentration of oxyhaemoglobin

C[MetHb] concentration of methaemoglobin

C[COHb] concentration of carboxyhaemoglobin

The fractional oxygen saturation takes into account the fact that

other forms of haemoglobin are present in the blood (section 1.1.2.2) which affect the degree of blood oxygenation, thus the ratio of oxyhaemoglobin to total haemoglobin is also used. In normal healthy people the arterial blood saturation is usually between 96 - 100%.

Utilisation of the physician's senses (sight, hearing, touch, smell) has from the beginning of medicine been the mainstay in diagnosis and tracking the course of disease. The first ever method used for assessing blood oxygenation levels was that of skin colour or cyanosis. The word cyanosis is derived from the Greek word κυανο, meaning dark blue. Unfortunately, cyanosis is only a late sign of significant desaturation. Moreover, detection of cyanosis depends on skin pigmentation and perfusion and on the haemoglobin concentration in blood. Thus, with an anaemic patient the oxygen saturation would have to be much lower to detect cyanosis whereas a polycythaemic patient would show signs of cyanosis much earlier. In a study by Comroe (Comroe, 1947) it was found that cyanosis is not a reliable clinical sign of hypoxemia, clearly indicating that other means to complement the physician's senses are required, in order to assess blood oxygenation levels accurately.

Several electrochemical methods for blood gas analysis have been developed over the years, with a complete historical review on the subject given by Astrup and Severinghaus (Astrup, 1986) and Ziljstra (Ziljstra, 1953). A different way of determining oxygen saturation is using optical measurements of haemoglobin and these techniques come under the name of oximetry.

1.2.1 Oximetry

As mentioned in section 1.1, virtually all oxygen transported around the body is carried in the red cells as oxyhaemoglobin, which is the oxygenated form of haemoglobin. Oximetry, which is defined as the determination of the oxygen saturation of blood, is based upon the existence of differences in the absorption spectra (Alexander, 1989; Wukitsch, 1988) of oxyhaemoglobin and deoxyhaemoglobin as shown in Fig. 1.4 (Data from Zijlstra, 1991).

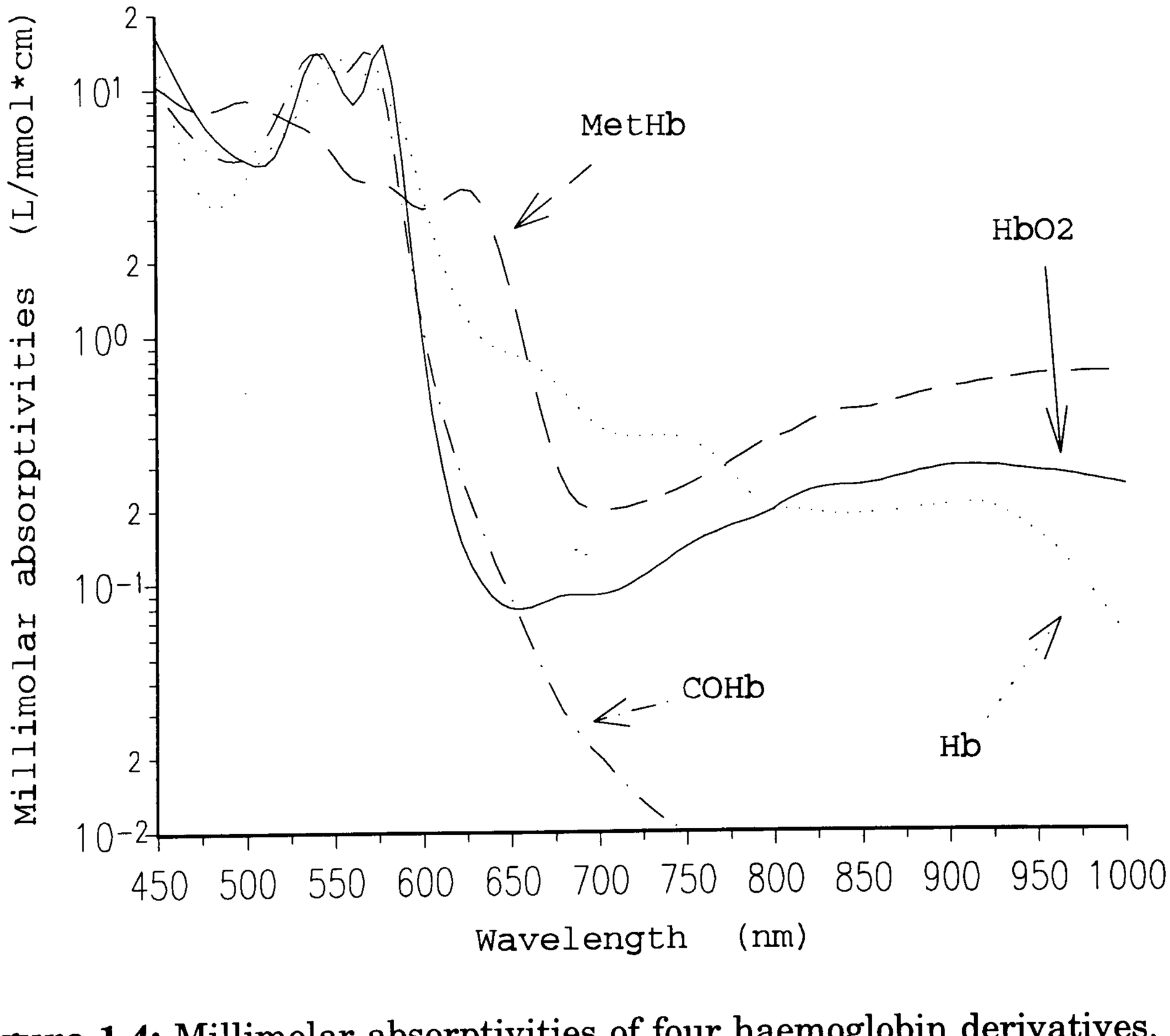

Figure 1.4: Millimolar absorptivities of four haemoglobin derivatives.

An oximeter is an optical-electronic device in which the difference in light absorption between haemoglobin species can be measured, and thus oxygen saturation, by using standard spectrophotometric techniques.

The field of oximetry started developing rapidly in the early 1930s where much of this research was associated with anaesthesia. Later oximetry was associated with aviation medicine, encouraged by experiments using unpressurized aeroplanes flying at high altitudes during World War 2.

There are several methods of assessing blood oxygenation levels depending on the means of processing. These can be divided into two groups; *in vitro* methods and *in vivo* methods.

Most of these techniques are based, or were originally based, on the Lambert-Beer law. This law states that the transmission of light through a solution is a logarithmic function of the concentration of the absorbent.

$$I_t = I_o \, 10^{-A} , \qquad A = \epsilon \, C \, L \tag{1.4}$$

where: I_t : the transmitted light intensity

I_o : the incident light intensity

A : the absorption

ε : the extinction coefficient of the absorbent in L mmol^{-1} cm^{-1}.

C : the concentration of the absorbent in mmol L^{-1}

L : the path length in cm

Where several absorbents are present in a solution, then the absorption A is given by :

$$A = \epsilon_1 C_1 L_1 + \epsilon_2 C_2 L_2 + ... + \epsilon_n C_n L_n \qquad (1.5)$$

Some of the technological breakthroughs in oximetry along the years and present techniques are presented here.

1.2.1.1 In vitro methods

The *in vitro* methods are of course invasive since they require an arterial blood sample. Haemolysed or non-haemolysed (whole) blood can be used according to the particular method used. The theory of oximetry on haemolysed blood is given in Appendix A.

The CO-Oximeter is an automated spectrophotometer that uses four specific wavelengths to measure the relative concentration of oxyhaemoglobin, deoxyhaemoglobin, carboxyhaemoglobin and methaemoglobin (Shapiro, 1982). The four wavelengths were chosen based on the absorption characteristics of the above haemoglobins. In the case of adult haemoglobin no corrections are needed when using the CO-Oximeter. However, in the case of fetal haemoglobin there are dissimilarities in spectral properties at the wavelengths used by the CO-Oximeter and the readings must be corrected (Cornelissen, 1983; Zijlstra, 1983). Although this technique is invasive, *in vitro* and non continuous it is today considered as the "gold standard" in oximetry due to the accurate

results it produces.

1.2.1.2 In vivo methods

Reports of using ear oximeters for determining oxygen saturation go back to the 1940s. In the Millikan oximeter (Millikan, 1942) the instrument was preset to indicate an oxygen saturation value of 100% when the subject was breathing 100% oxygen. Therefore any consequent readings of oxygen saturation were only relative.

The Wood oximeter (Wood, 1948) used a rather different approach to the problem. It used Lambert-Beer law analysis on the ear, with the ear acting as a cuvette. The absorption in the ear tissues was distinguished from the absorption due to arterial blood. This was achieved by squeezing out the blood by simply compressing the ear. Measurements of light intensity were taken at two wavelengths for the same reasons described in Appendix A. These served as the baseline. The compression was then released and two new measurements of light intensity were taken after the arterial blood was re-admitted. The procedure of this technique is shown in Fig. 1.5. The difference between the new measurements and baseline is due to arterial blood absorption and this was used to calculate oxygen saturation.

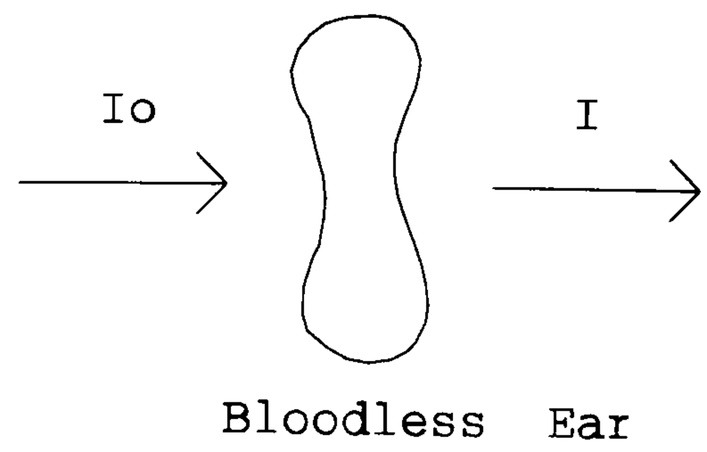

Figure 1.5: Wood's ear oximeter.

Referring to Fig. 1.5 from the Lambert-Beer law the absorbance $A_{b.e.}$ of the bloodless ear is given by:

$$A_{b.e.} = \log \frac{I_o}{I} \tag{1.6}$$

Again from Fig. 1.5 the absorbance $A_{e.}$ due to ear tissues and arterial blood is:

$$A_{e.} = \log \frac{I_o}{I'} \tag{1.7}$$

The difference of the two gives the absorption $A_{a.b.}$ due to arterial blood only.

$$A_{a.b.} = A_{e.} - A_{b.e.} = \log \frac{I}{I'} \tag{1.8}$$

For the two wavelengths employed the absorptions due to the arterial blood, ignoring scattering effects, are:

$$A_{a.b.\lambda 1} = L\ (\epsilon_{\lambda 1}[HbO_2]C[HbO_2] + \epsilon_{\lambda 1}[Hb]C[Hb]) \qquad (1.9)$$

$$A_{a.b.\lambda 2} = L\ (\epsilon_{\lambda 2}[HbO_2]C[HbO_2] + \epsilon_{\lambda 2}[Hb]C[Hb]) \qquad (1.10)$$

From now on the analysis and calculation of SaO_2 is exactly the same as for haemolysed samples as given in Appendix A. In practice the Wood oximeter used a red and an isobestic wavelength in the near infrared, thus the equation for SaO_2 is in the form of equation A.5.

The advantage of the Wood oximeter was that it provided absolute rather than relative values of oxygen saturation, and the influence of earlobe thickness, or skin pigmentation was eliminated. However, in practice it suffered from the long time needed to operate the oximeter, the need to compress the ear and the associated difficulty in excluding all arterial blood for the baseline measurements.

Although the above methods were available for many years they failed to gain any major clinical use. The reluctance to use ear oximetry can partly be explained by reservations concerning its accuracy and partly due to the practical difficulties in operating these early instruments.

The Hewlett Packard ear oximeter (Saunders, 1976) overcame the calibration problems of the above oximeters. It used eight narrow wavelengths (obtained from a rotating filter wheel) and the light was

piped to the ear by using fibre bundles. A large number of wavelengths were used because the ear was again considered as a cuvette but with several absorbing components; with oxyhaemoglobin and deoxyhaemoglobin being two of them. The Hewlett Packard oximeter was relatively insensitive to changes in earpiece position.

The use of fiberoptics for oximetry began in the early 1960s (Polyani, 1960, 1962; Enson, 1962; Kapany, 1967). Oxygen saturation measurements were made from blood in major vessels or the heart using catheterisation. A fibre bundle was incorporated at the tip of the catheter, with half of the bundles acting as the transmitter and the other half acting as the receiver. When the light enters the blood it is scattered by the red blood cells illuminating an area around the catheter tip. A portion of the light after it is scattered and absorbed by the red cells returns to the tip of the catheter and via the receiving bundle to the detection device. As with other spectroscopic methods of oxygen saturation two wavelengths are used (red and infrared). The ratio of the backscattered light at the two wavelengths is used to compute oxygen saturation. A variation of this oximeter was used by Johnson (Johnson, 1971) where solid state devices were mounted on the tip of the catheter.

Despite all previous work, oxygen saturation monitoring was revolutionised in the late 1970s by Pulse Oximetry. Pulse oximetry gives continuous *in vivo* non invasive functional oxygen saturation readings. The reasons that this new technique succeeded and gained wide acceptance are several and these are explained and analysed in detail in

chapter 2. It is the simplest method yet to be used, since it does not require any on-site calibration and is easy to apply. This method essentially uses the photoplethysmography technique and therefore, before explaining pulse oximetry the photoplethysmography technique is reviewed.

1.3 PHOTOPLETHYSMOGRAPHY

Photoplethysmography refers to the monitoring of time varying changes in the intensity of light scattered from tissue *in vivo*. Although the human body is normally assumed to be opaque to light transmission, most soft tissues will transmit both visible and near-infrared radiation. Light is therefore shone onto an area of the skin and a photodetector is used to detect the emergent light arriving after its interaction with the skin, blood and other tissue. The amount of light measured by the photodetector depends upon a number of factors:-

a) the optical properties of the tissues at the measurement site.

b) the wavelength, direction of emission and output power of the light source.

c) the sensitivity of the detector.

d) the interface between emitter and detector and the skin.

e) the geometry of the emitter and detector.

Conventionally two components are considered to be observed

during photoplethysmography, the "AC" component and the "DC" component as shown in Fig. 1.6.

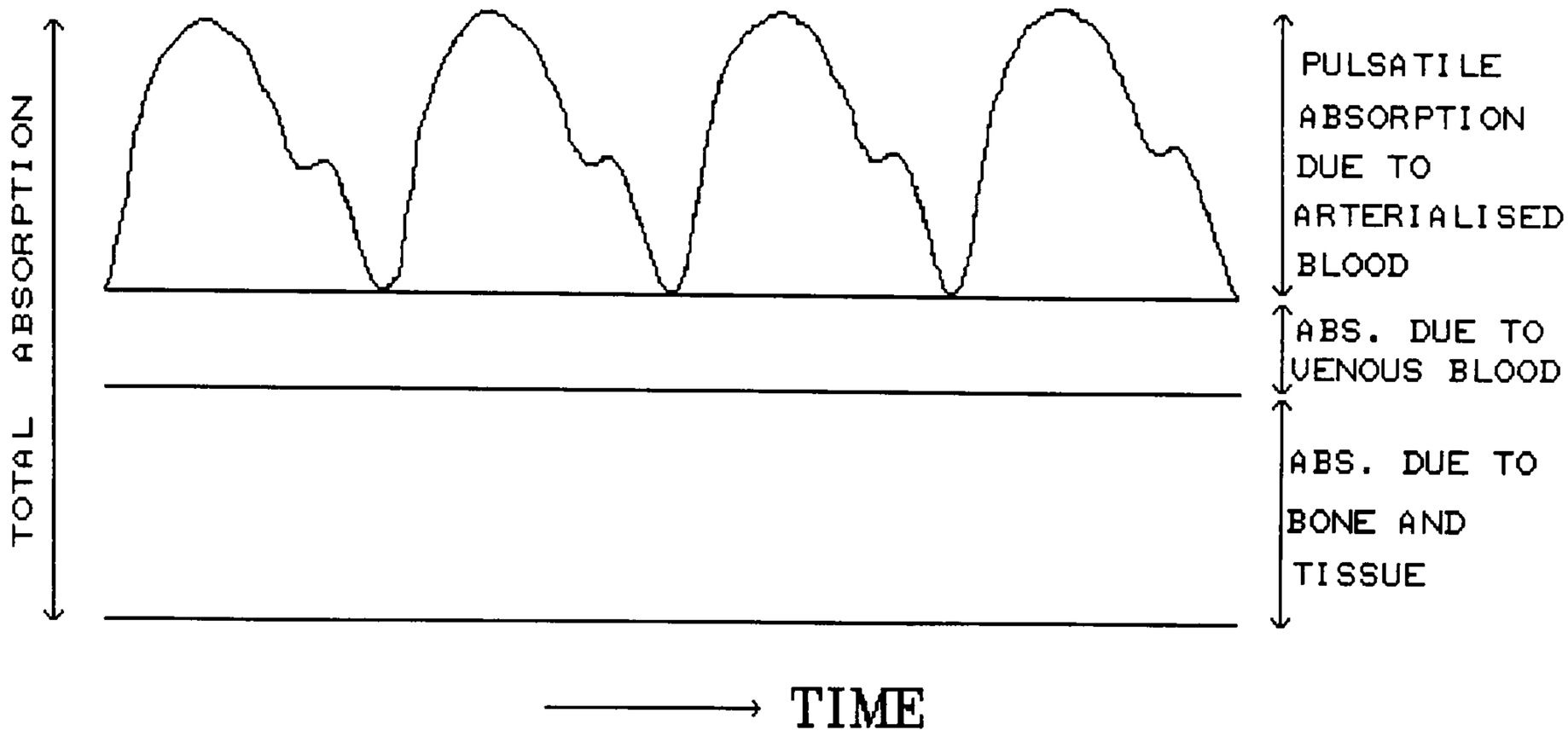

Figure 1.6: Light absorption through living tissue as a function of time.

The AC component is a cardiac synchronous signal caused by the arterial pulse. The DC component is a very slowly varying signal which is thought to be largely due to the total blood volume in the skin.

With the PPG method there are also two modes of measurement, the Transmission mode and the Reflection mode as illustrated in Fig. 1.7.

In the Transmission mode the light source is at one side of the skin under investigation and the photodetector is placed at the opposite side of the skin. This mode is obviously limited to only a few areas of the body, such as fingers, toes, ear lobes, where the distance between the source and the detector is not too great.

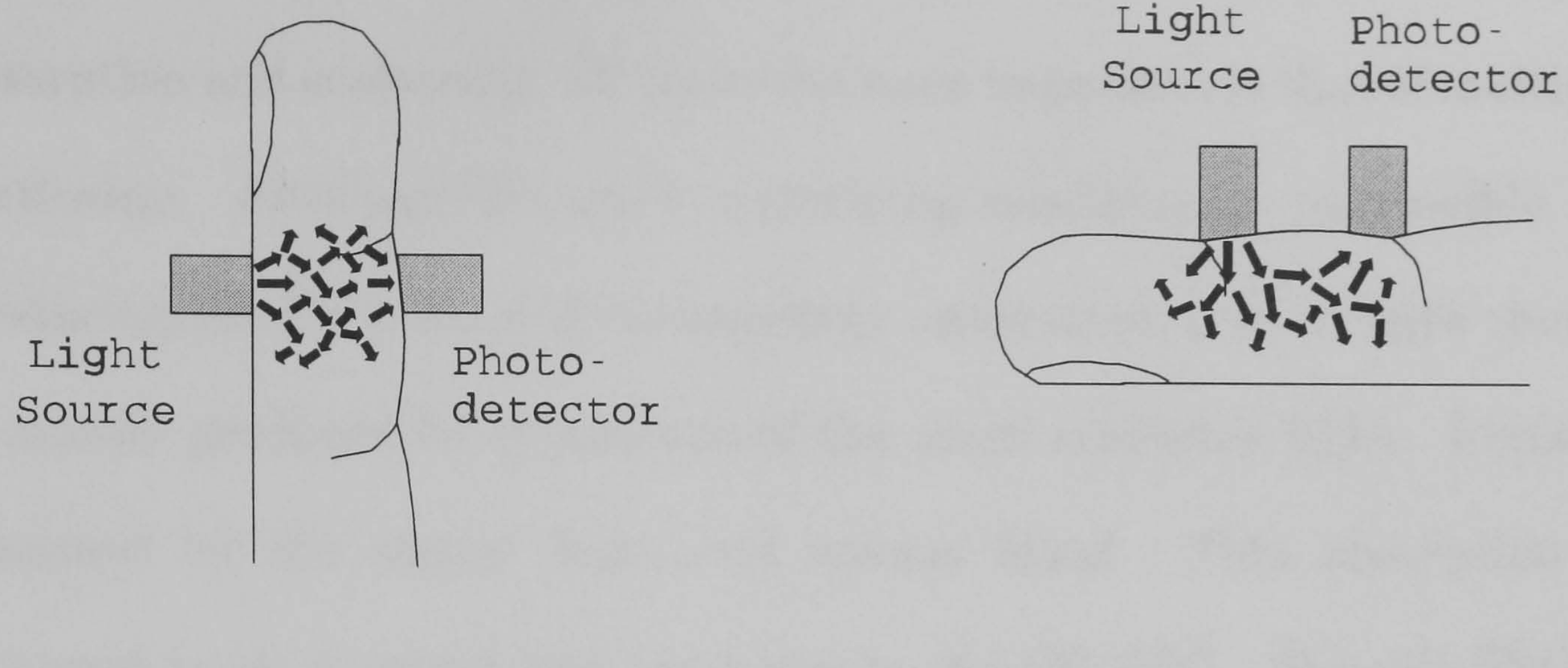

Transmission Mode Reflection Mode

Figure 1.7: Transmission and Reflection modes as used in Photoplethysmography.

In the Reflection mode the light source and the photodetector are positioned side by side. A proportion of the light entering the skin is back scattered and emerges from the skin adjacent to the light source. Therefore, the photodetector placed next to the light source will detect this light. The further apart the photodetector is from the light source, the more difficult it is to detect the light. This source - detector configuration is much more versatile, thus allowing measurements to be performed on virtually any skin area.

It has to be remembered that although the terms "transmission" and "reflection" are used here, the process is that of overall forward scattering and back scattering respectively.

Looking at the interaction of light with the skin in more detail, light leaving the source undergoes many optical processes as it passes

through the skin. These optical processes are reflection, refraction, absorption and scattering. Of these the most important is that of multiple scattering. Although the exact underlying mechanisms responsible for producing the PPG are still incompletely understood, it is thought that it is mainly produced by absorption of the multi scattered light. Light is absorbed by the tissue, bone and venous blood. This absorption is assumed to be constant and gives rise to the DC PPG. The AC PPG is again believed to be produced by an absorption process, with the incoming arterial pulse causing an increase in the blood volume and consequently a decrease in the received light intensity. An added complication with the AC component is that the creation of this alternating signal may be due to a change in the optical transmittance of blood. This was demonstrated by Challoner (Challoner, 1979) in an experiment using a rigid tube. Since a rigid tube excludes any volume changes, the change in the optical transmittance of blood was attributed to changes in the orientation of erythrocytes. In the case of the DC signal the orientation of erythrocytes does not apply, and the measurement of the total blood volume is due predominantly to the absorption of the multi-scattered light.

In both transmission and reflection photoplethysmography the PPG signal is produced by an absorption process, thus the blood volume and light intensity pulses are in antiphase. However, in the reflection mode under certain physiological conditions PPG signals have been observed that are in phase with the blood volume pulse (Nijboer, 1982). This signal is generally referred to as the "inverted" PPG, Fig. 1.8.

Nijboer found that the "inverted" PPG is a local phenomenon restricted to the reflection mode. It is thought to be caused by a relative increase in the optical density of the surrounding tissue in relation to the arterial vessels.

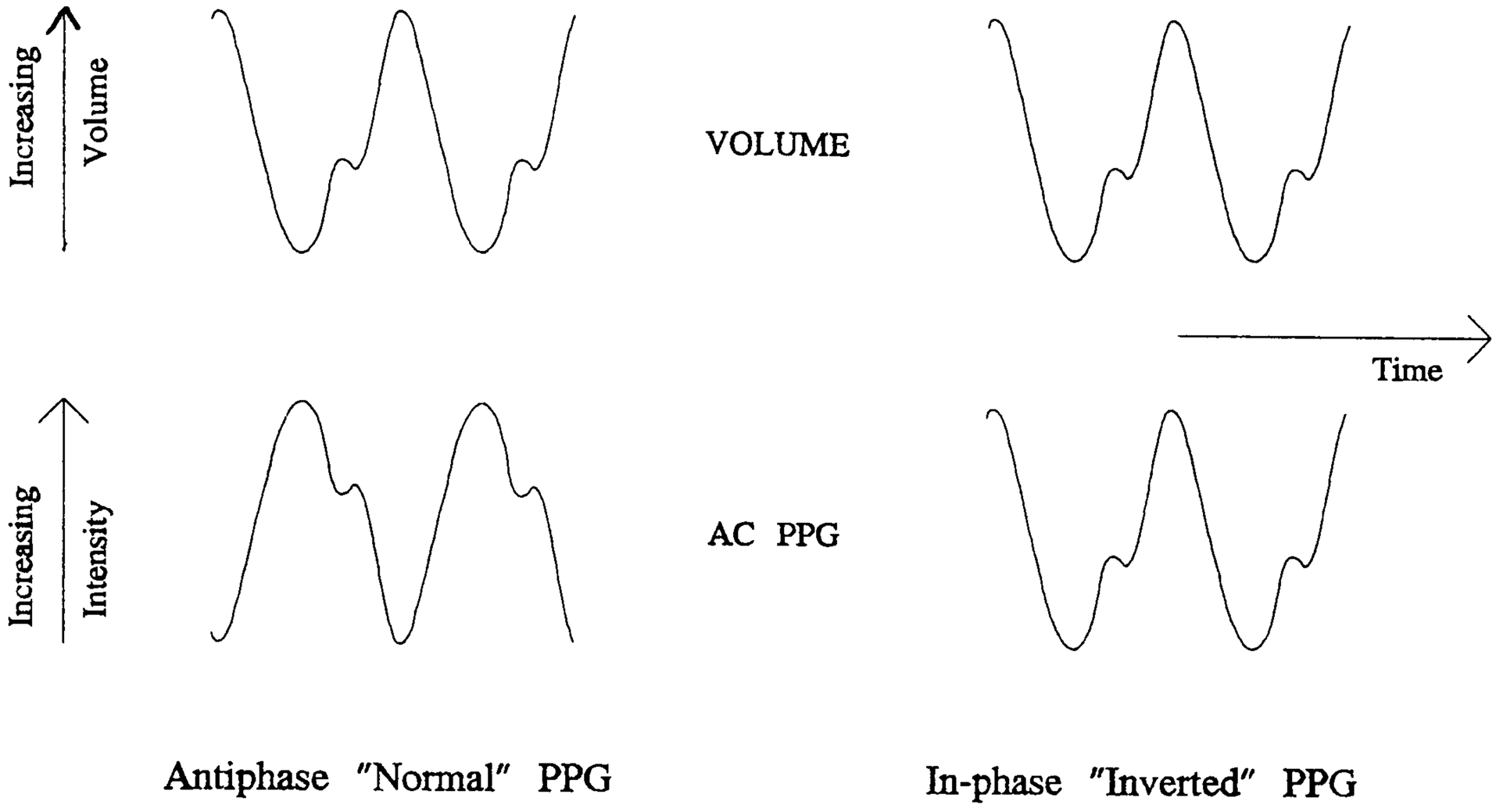

Figure 1.8: "Normal" and "inverted" AC PPG signals.

1.3.1 Uses of Photoplethysmography

Although Photoplethysmography has found its major use in pulse oximetry (as explained in the following section), it has been used in many other applications. Some of them are presented here:-

The photoplethysmogram was first introduced by Hertzman in the late 1930s (Hertzman, 1937) for the measurement of blood volume in skin. Photoplethysmography does not yield a quantifiable measurement of blood volume in absolute units. This is because the amount of light arriving at the photodetector depends on the vascular bed which varies from individual to individual. Assuming that during the measurement

parameters like temperature, humidity and ambient lighting which alter the optical properties of the skin remain constant, then the method measures variation in blood volume relative to an arbitrary reference level, thus it provides information on skin blood volume changes. Most of the pioneering work and use of the photoplethysmogram to investigate cutaneous blood flow was done by Hertzman in the 1930s and 40s (Hertzman, 1938; 1946). However, technical limitations with the detectors and light sources at that time, prevented this technique becoming popular until recently. Challoner and Ramsay used photoplethysmography for assessing blood flow (Challoner, 1974), especially after some external action, such as after injection of drugs or irradiation. Two probes were used, one at the test site the other at the control site. The results obtained are qualitative as the changes at the test site are always compared with the adjacent control site.

Kamal, Harness and Mearns (Kamal, 1989) used the frequency analysis of the photoplethysmogram to extract information about the autonomic nervous system control of the cardiovascular system. This information is similar to that which can be obtained from heart rate variability studies.

The frequencies of thermoregulation, baroreception (blood pressure control) and breathing represent the main activities of the autonomic nervous system. All these appear in the frequency spectrum of the photoplethysmogram as frequency components below 0.5 Hz. These natural frequencies may be moved by using an external stimulus and this

has given rise to the concept of forcing frequency testing (Mearns, 1985) as a technique to test the autonomic and cardiovascular system. In the frequency range 0.5 - 2 Hz the major peak is due to the mean heart rate and also as explained by Kamal et al (Kamal, 1989) frequency components which are due to the modulation of the heart rate by the frequencies below 0.5 Hz. The information above 2 Hz is due to the harmonics and has minimal clinical value. In Figures 1.9 and 1.10 the frequency spectrum of the photoplethysmogram is shown in the range 0.0097 - 4.9902 Hz (DC component removed). These results (Damianou, 1989) are from studies on the same subject breathing at 0.31 Hz and 1.2 Hz in Fig. 1.9 and Fig. 1.10 respectively.

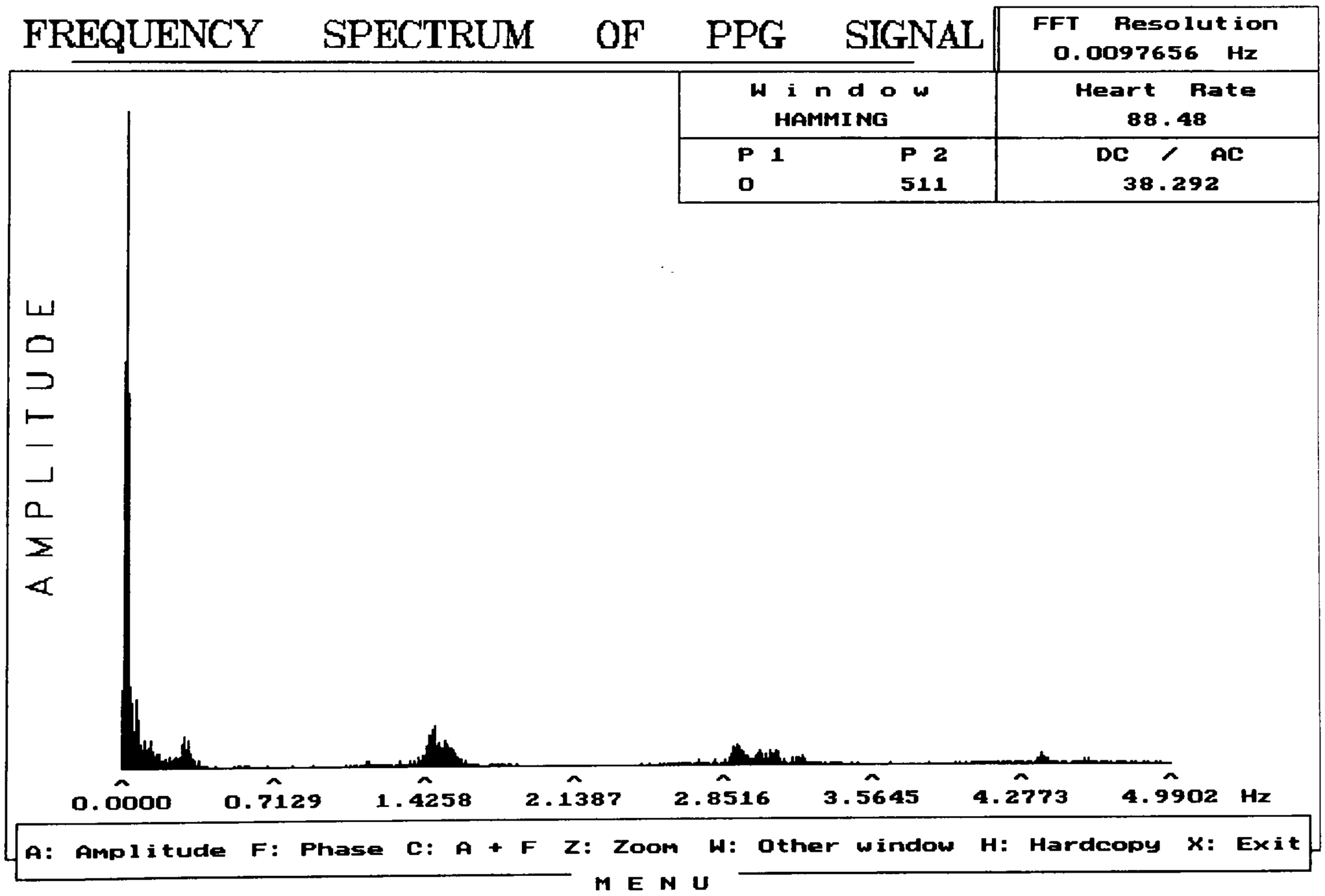

Figure 1.9: Frequency spectrum of the photoplethysmogram with the subject breathing at 0.31 Hz.

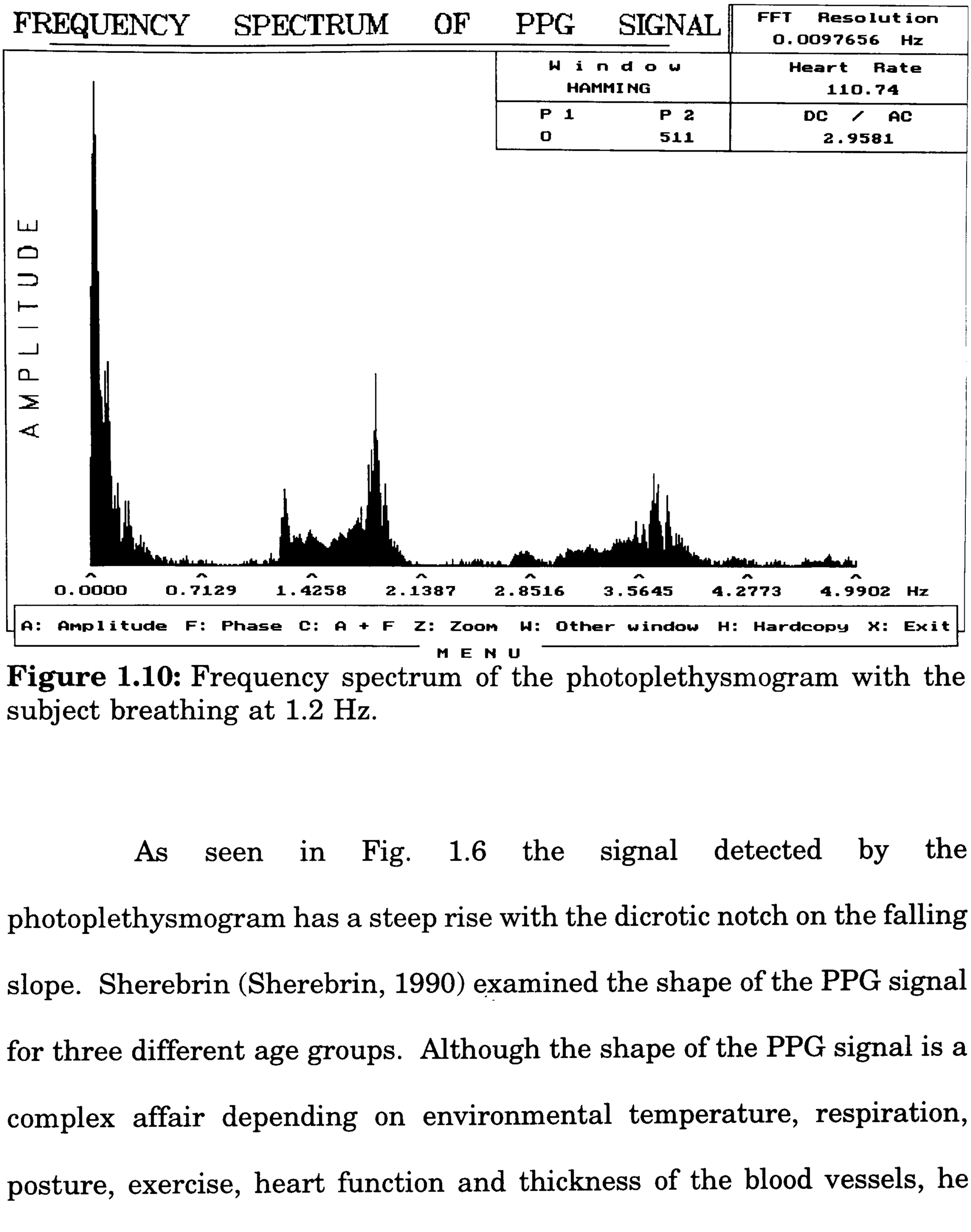

Figure 1.10: Frequency spectrum of the photoplethysmogram with the subject breathing at 1.2 Hz.

As seen in Fig. 1.6 the signal detected by the photoplethysmogram has a steep rise with the dicrotic notch on the falling slope. Sherebrin (Sherebrin, 1990) examined the shape of the PPG signal for three different age groups. Although the shape of the PPG signal is a complex affair depending on environmental temperature, respiration, posture, exercise, heart function and thickness of the blood vessels, he found that in most older groups the rise and fall of the signal was more gradual and the dicrotic notch less pronounced. He also examined the power spectrum of the PPG signal with respect to the fundamental for each of the three age groups. A decrease in harmonic content of the signal was observed with age. The object is to use this information from the shape of the AC PPG signal in order to measure non invasively the elastic

properties of the vascular tree as a function of disease and aging.

Diverse applications include investigating sexual fantasies in women (Meuwissen, 1991). The extent to which a number of themes in a female sexual fantasy questionnaire were rated as sexually arousing, correlated with the levels of physiological response recorded by vaginal photoplethysmography while women engaged in fantasy employing these themes.

Simpler applications of the photoplethysmogram can be found in heart rate monitors used in sports equipment, either incorporated in exercise machines or watches for "serious joggers".

CHAPTER 2

PULSE OXIMETRY

2.1 PULSE OXIMETRY THEORY

Although the principles of oximetry (described in the previous chapter) have been known since the turn of the century it was not until the early 1980s that the technique found widespread clinical use in the form of pulse oximetry. Since then the increase in use of pulse oximeters in all critical care situations has been quite remarkable, turning it into one of the most important methods of monitoring in use today.

All forms of oximetry rely upon the differences in the absorption spectra of haemoglobin (Hb) and oxyhemoglobin ($Hb0_2$). What has made pulse oximetry a success where other earlier oximeters failed is its processing of the cardiac synchronous component of light scattered from tissue, related to the arrival of the "pulse".

The theory of pulse oximetry has been developed by adapting the theory of *in vitro* oximetry. Consequently, the Lambert-Beer law has been

used as the basic theory for the operation of pulse oximetry. This theory as is often presented and explained in the literature is discussed here in detail. The assumptions of this theory and therefore the limitations of pulse oximetry are highlighted.

Since, pulse oximetry uses the pulsatile component of the PPG signal (see Fig. 1.6) and **assumes** that this component is solely due to the arterial oxygenated blood, the DC and the AC components of the photoplethysmogram can be thought of to be analogous to measurements on the compressed and blood-filled ear respectively in the Wood's oximeter. Application of the same theory as for the Wood's oximeter provides a basic description of the operation of pulse oximeters.

Assuming pulse oximetry monitoring on the finger, the finger can be modelled as a cuvette of length L, consisting of blood, skin and bone. This cuvette expands by a further length ΔL with the influx of arterial blood, as shown in Fig. 2.1. In this figure A and I are the absorption and transmitted light intensity respectively due to the 'nonblood' compartment and the blood present at the end of the outflow phase. A' and I' are the absorption and transmitted light intensity respectively due to the 'nonblood' compartment, the blood present at the end of the outflow phase **and** the arterial blood that flows into the finger.

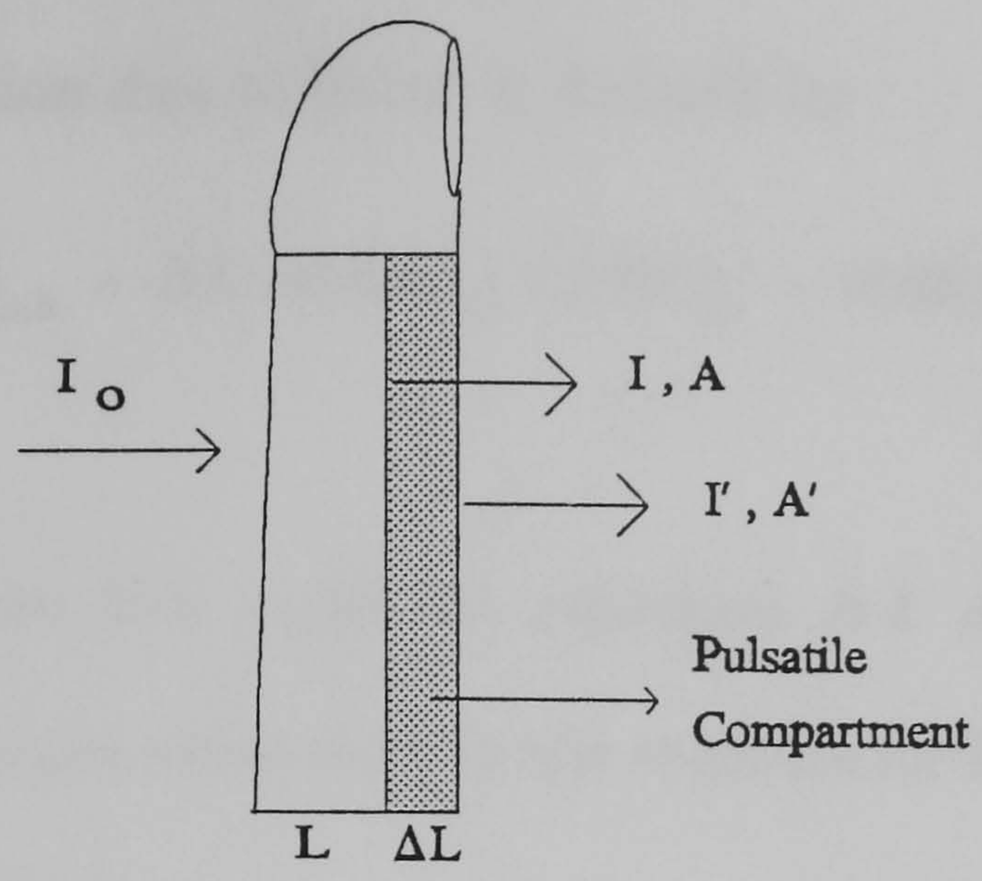

Figure 2.1: Simple model used to explain pulse oximetry, assuming the finger to be a cuvette of length L which expands by a further length ΔL with the influx of arterial blood.

Therefore, according to the Lambert-Beer law:

$$A = \log(\frac{I_o}{I}) \tag{2.1}$$

and

$$A' = \log(\frac{I_o}{I'}) \tag{2.2}$$

As for the Wood oximeter theory, the absorption $A_{a.b.}$ due to the arterial blood is:

$$A_{a.b.} = A' - A = \log(\frac{I}{I'}) \tag{2.3}$$

Also the absorption due to blood is defined by:

$$A_{a.b.} = \Delta L \left(\epsilon[HbO_2]\ C[HbO_2] + \epsilon[Hb]\ C[Hb]\right) \qquad (2.4)$$

This is of course the same as equation A.1 and the analysis and calculation of oxygen saturation is the same as for haemolysed samples as given in Appendix A.

The resulting oxygen saturation expression is therefore:

$$SaO_2 = \frac{\epsilon_{\lambda 1}[Hb] - \frac{A_{\lambda 1}}{A_{\lambda 2}}\epsilon_{\lambda 2}[Hb]}{(\epsilon_{\lambda 2}[HbO_2] - \epsilon_{\lambda 2}[Hb])\frac{A_{\lambda 1}}{A_{\lambda 2}} - (\epsilon_{\lambda 1}[HbO_2] - \epsilon_{\lambda 1}[Hb])} \qquad (2.5)$$

Note that from now on oxygen saturation references due to pulse oximetry will be denoted by SpO_2. This is to differentiate them from *in vitro* oxygen saturation readings on arterial blood denoted by SaO_2. This is the currently accepted notation.

In Fig. 2.1 intensities I and I' give rise to the DC and DC+AC PPG signals respectively, as explained in section 1.3.

Thus the ratio $A_{a.b.\lambda 1} / A_{a.b.\lambda 2}$ in equation 2.5, in terms of the AC and DC PPG signals is:

$$\frac{A_{a.b.\lambda 1}}{A_{a.b.\lambda 2}} = \frac{\ln(\frac{DC+AC}{DC})_{\lambda 1}}{\ln(\frac{DC+AC}{DC})_{\lambda 2}} \qquad (2.6)$$

In deriving the above expression for the oxygen saturation several assumptions have been made. The first assumption was that the

blood consists of haemoglobin and oxyhaemoglobin only and thus the Lambert-Beer law is valid. However, whole blood is a turbid medium which means that light is not only transmitted but is also scattered. It has been shown (Kramer, 1951; Loweinger, 1964; Anderson, 1967) that the Lambert-Beer law is not valid for whole blood, since for this law to be valid the incident light should be equal to the transmitted plus the absorbed light. Moreover, it is assumed that the increase in light attenuation during the contraction of the heart is solely due to arterial blood and that the path length for the two different wavelengths is the same. The effect of these assumptions in the performance and accuracy of pulse oximeters is examined in the following sections.

2.1.1 Commercial Pulse Oximeters

The first pulse oximeters were developed in Japan by Yoshiya and Shimada (Yoshiya, 1980) and by Konishi (Konishi, 1976) for determining oxygen saturation in the fingertip and by Nakajima (Nakajima, 1975) for determining oxygen saturation in the ear. In the Yoshiya pulse oximeter, light is produced by a halogen lamp and delivered to the fingertip via an optical fibre. The transmitted light passes through another fibre to the optical detection system where two narrow band filters, one at 650nm the other at 805nm, selectively transmit light at these wavelengths. A pair of photocells perform the photoelectric conversion for each wavelength and the computing section calculates the arterial oxygen saturation using equation 2.5 derived by the method

described above. The pulse oximeter calibration graph as derived by equation 2.5 is shown in Fig. 2.2.

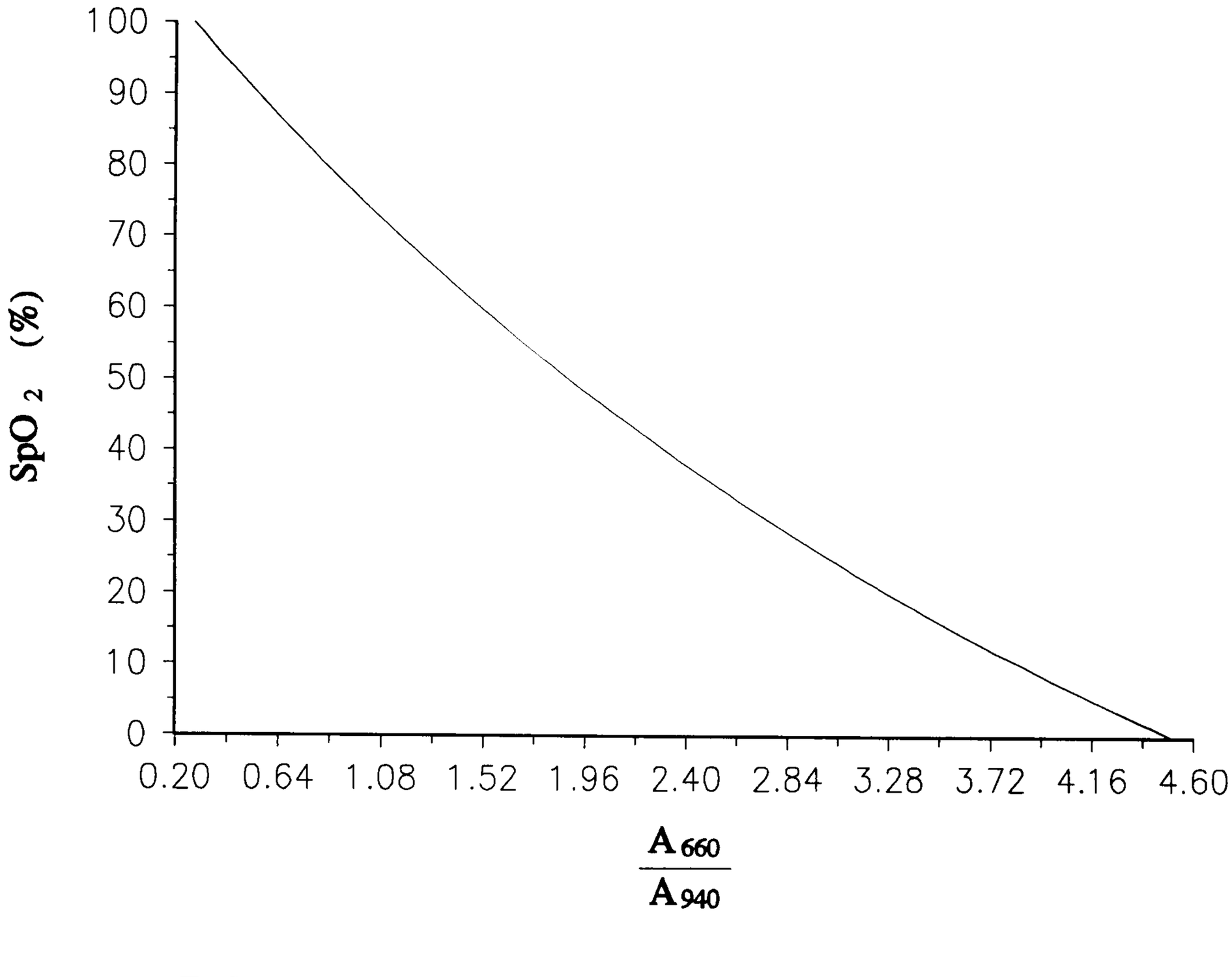

Figure 2.2: Pulse oximeter calibration curve according to the Lambert-Beer model.

Although in his first model Shimada mentioned the effects of multiple scattering he stated that these effects would be negligible because they could be minimised by the mathematical subtraction of the DC component from the total attenuation and the analysis at the two different wavelengths. However, the results obtained from these first pulse oximeters which were calibrated using equation 2.5 were of poor correlation with *in vitro* readings and a tendency to overestimate oxygen saturation readings below 90% was reported (Sarnquist, 1980). This forced Shimada and others to re-examine the effects of multiple scattering

on the accuracy of pulse oximeters and reported at a later stage (Shimada, 1984) a new device which took into account these effects in its calculation of oxygen saturation. It soon became evident to those in this field that due to the reasons mentioned above using equation 2.5 or even the modified version of it, alone to calibrate pulse oximeters was unacceptable.

Because of this, nowadays all pulse oximeters are calibrated using empirically derived data obtained from human subjects. Moreover, modern pulse oximeters use the ratio AC/DC , instead of the ratio ln(DC+AC / DC), which is in fact the first order approximation of the last term. This is to reduce processing time, since calculating the ratio $A_{a.b.\lambda1}$ / $A_{a.b.\lambda2}$ involves logarithmic calculations. Therefore, the output of pulse oximeters giving the ratio of recorded intensities at the two wavelengths becomes:

$$\frac{A_{a.b.\lambda1}}{A_{a.b.\lambda2}} = \frac{\ln(\frac{AC+DC}{DC})_{\lambda1}}{\ln(\frac{AC+DC}{DC})_{\lambda2}} = \frac{(\frac{AC}{DC})_{\lambda1}}{(\frac{AC}{DC})_{\lambda2}} \qquad (2.7)$$

This ratio is in fact the ratio of the **normalised** AC components at the two wavelengths λ1 and λ2. In the literature it is known as the ratio **R** and from equation 2.7 for the two wavelengths red (660nm) and infrared (940nm), is defined as:

$$R = \frac{(\frac{AC}{DC})_{660}}{(\frac{AC}{DC})_{940}} \qquad (2.8)$$

In practice this normalisation process can be achieved in two ways, either by dividing AC/DC mathematically, or by equalising the DC components at both wavelengths. This is made possible by adjusting the intensities of both light sources. The effect of the normalisation process is shown graphically in Fig. 2.3.

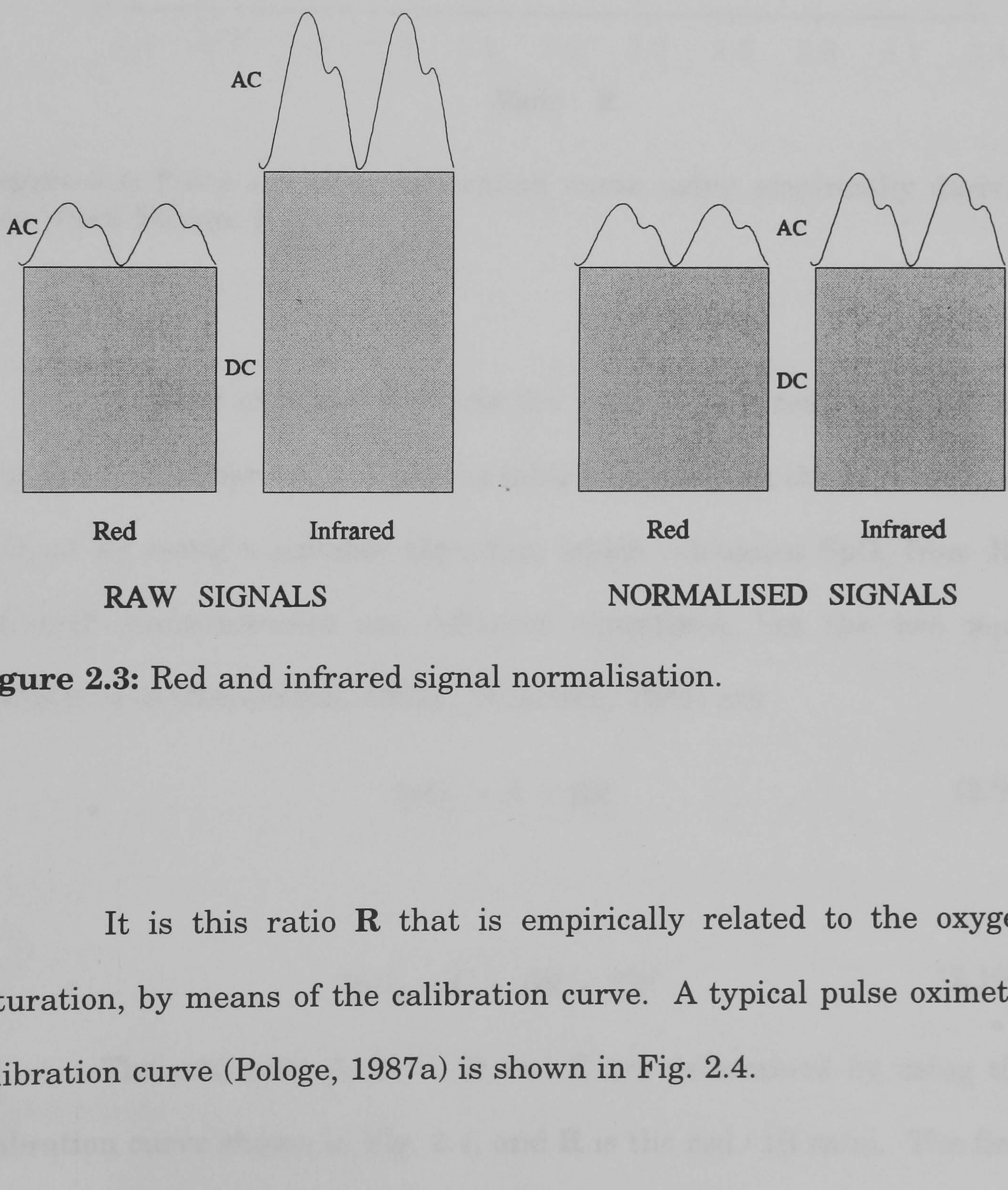

Figure 2.3: Red and infrared signal normalisation.

It is this ratio **R** that is empirically related to the oxygen saturation, by means of the calibration curve. A typical pulse oximeter calibration curve (Pologe, 1987a) is shown in Fig. 2.4.

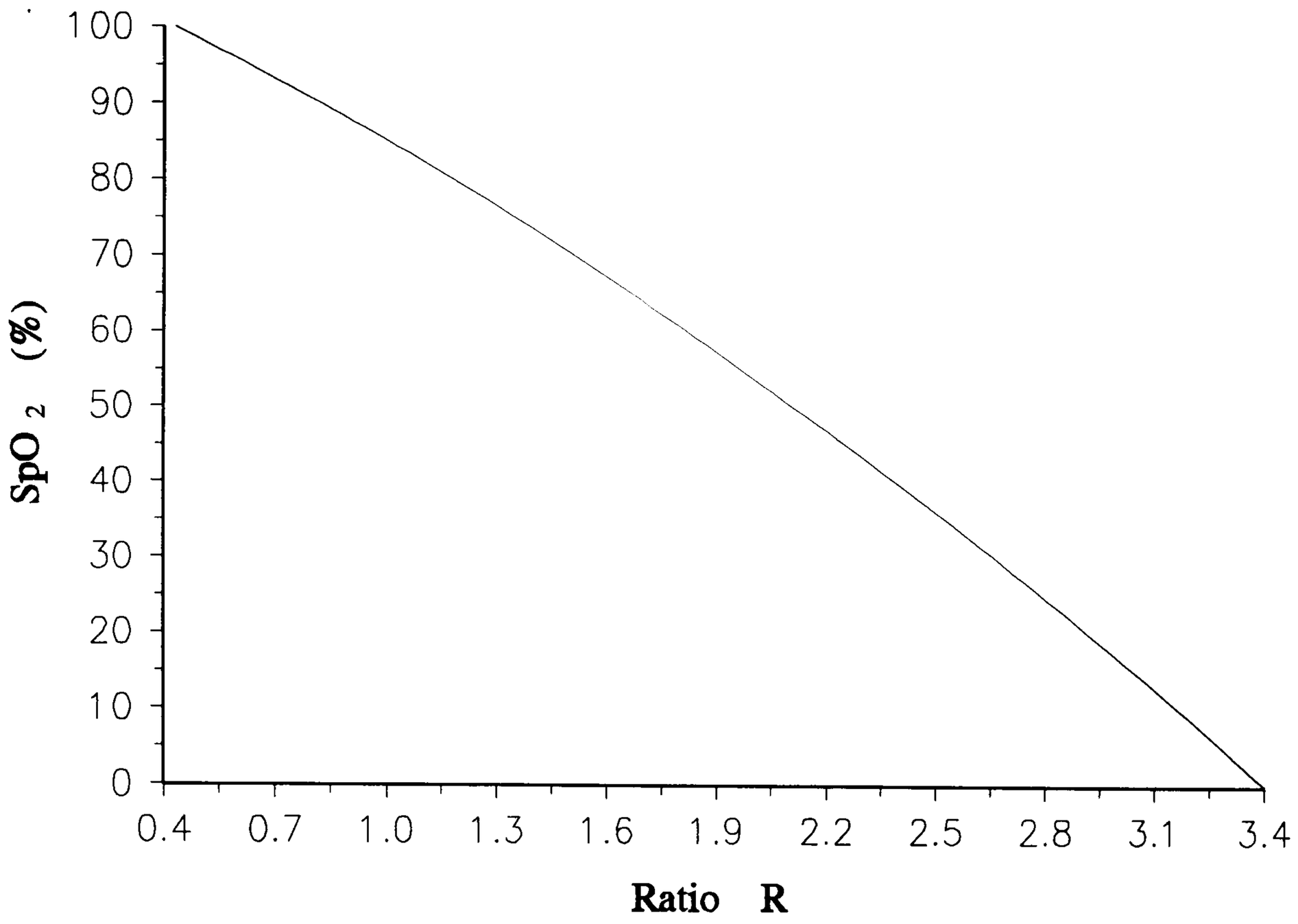

Figure 2.4: Pulse oximeter calibration curve using empirically derived data (from Pologe, 1987a).

A pulse oximeter converts the ratio **R** to a reading of oxygen saturation by either using a look-up table which relates the **R** value to an SpO_2 or by using a suitable algorithm which calculates SpO_2 from **R**. Different manufacturers use different algorithms, but the two most common ones (Mendelson, 1988a; Wukitsch, 1987) are :

$$SpO_2 = A + BR \tag{2.9}$$

$$SpO_2 = C + DR + ER^2 \tag{2.10}$$

The constants A, B, C, D and E are determined by using the calibration curve shown in Fig. 2.4, and **R** is the red / IR ratio. The first

and more simple algorithm approximates the calibration curve to a straight line, whereas the second algorithm employs a quadratic term and is a better approximation of the calibration curve. It has to be emphasised that the SpO_2 reading is only as accurate as the empirical calibration curve used. This is in turn only as accurate as the *in vitro* laboratory oximeter and the experimental procedure used to determine the calibration curve.

The calibration curve is derived by inducing a progressive steady-state hypoxemia to healthy volunteers. This is achieved by adjusting and controlling the fractional inspired oxygen concentration (FiO_2) to produce step decrements in SaO_2. Light absorption data is then associated with the *in vitro* measurements of SaO_2. Because of the dangers involved in desaturating healthy subjects to less than 65%, the calibration curve is usually extrapolated below 70% and verified on patients with chronically low saturation.

2.1.1.1 Choice of Wavelengths

The choice of the wavelengths $\lambda 1$ and $\lambda 2$ is critical for the operation and accuracy of the pulse oximeter. As shown in Fig. 1.4 oxyhaemoglobin absorbs less red light than deoxyhaemoglobin, whereas in the near infrared region the opposite is true. In a commercial system the light source consists of two light emitting diodes (LEDs) one emitting at 660nm and the other at 940nm. Originally the 805nm wavelength was used which is an isobestic point. This simplified equation 2.5 above to the

form shown in A.5, and therefore simplified the design of the analogue electronic circuitry for the calculation of SpO_2. Nowadays, since microprocessors are used for the signal processing, using the isobestic point does not offer any advantages. Moreover, it might actually reduce the accuracy of the pulse oximeter since the denominator of the expression for **R** (equation 2.8) remains constant with any change in saturation. As only one photodetector is used, each LED is switched on and off at a frequency of several hundred Hertz (depending on the manufacturer), so that the photodetector can differentiate between the two wavelengths. Some manufacturers include a third state in their timing diagram where both LEDs are off, Fig. 2.5. The third state where both LEDs are off is used so that the oximeter can measure any ambient light. This reading is then subtracted from the red and infrared readings in order to exclude ambient light effects.

2.1.1.2 Signal Processing

Most, if not all, of the recent commercial pulse oximeters employ a microprocessor with associated support circuitry for controlling all aspects of the signal processing operation including the signal input and output and intermediate processing. The intermediate processing is that of converting the photoplethysmographic signals to an oxygen saturation reading. Several different ways of data processing can be applied to the digitized DC and AC PPG signals in order to calculate a value for the ratio

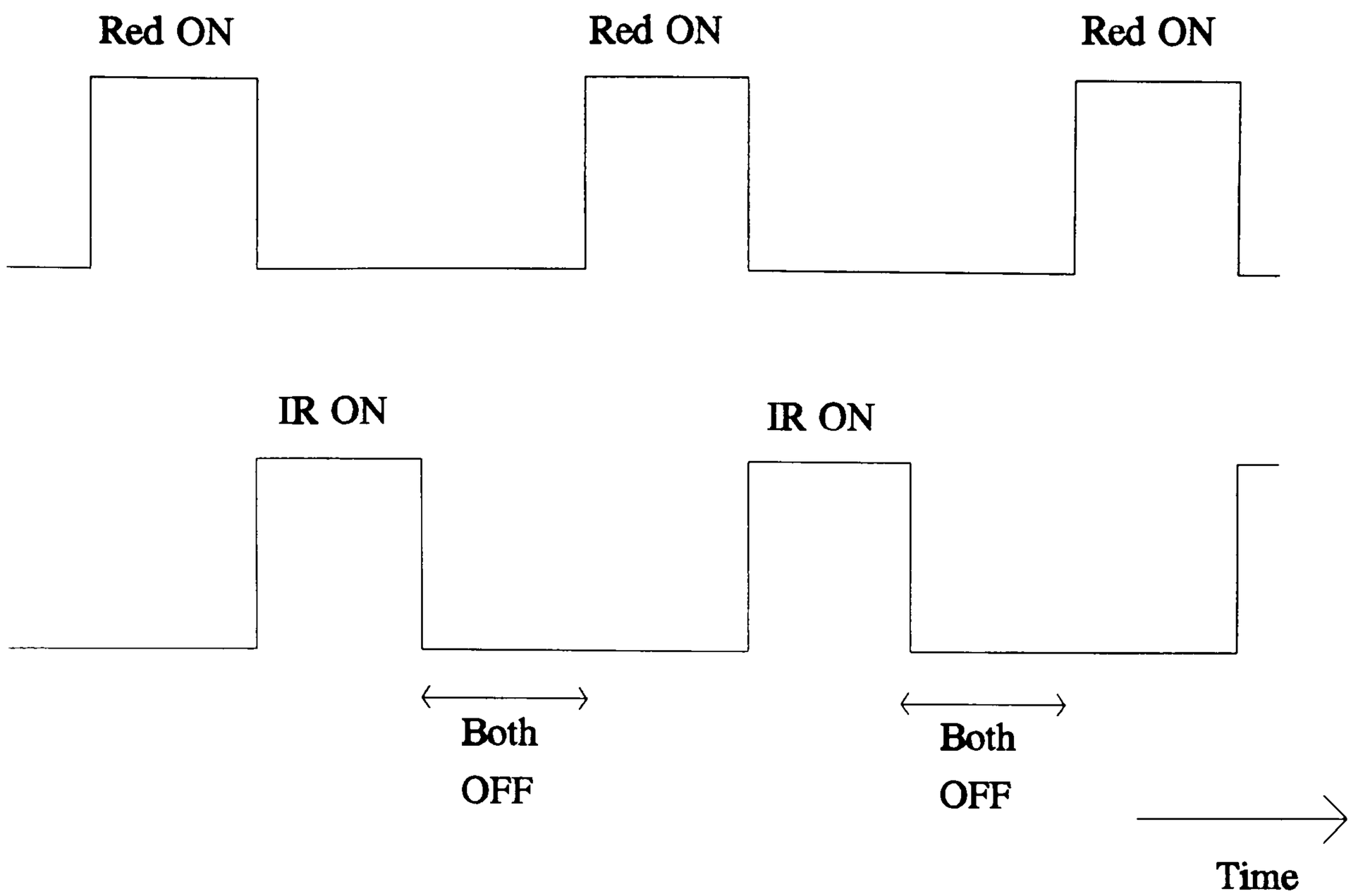

Figure 2.5: LEDs drive timing signals.

R and thus obtain an SpO_2 reading, ranging from the very simplistic ones to quite complicated ones. Indeed, signal processing methodologies can distinguish a good pulse oximeter from a basic one, and usually become the hard selling point for pulse oximeter manufacturers. A wide selection of intermediate signal processing methodologies are considered and discussed here.

The first method is using the minimum and maximum values of the red and infrared AC waveforms (see Fig. 2.6), their difference Δ giving the corresponding AC amplitude used in the calculation of the ratio R. The disadvantages of this method is that calculation of SpO_2 values is possible only once per heart beat. This in conjunction with some form of averaging in order to minimize artifacts, results in a pulse oximeter with a slow response time.

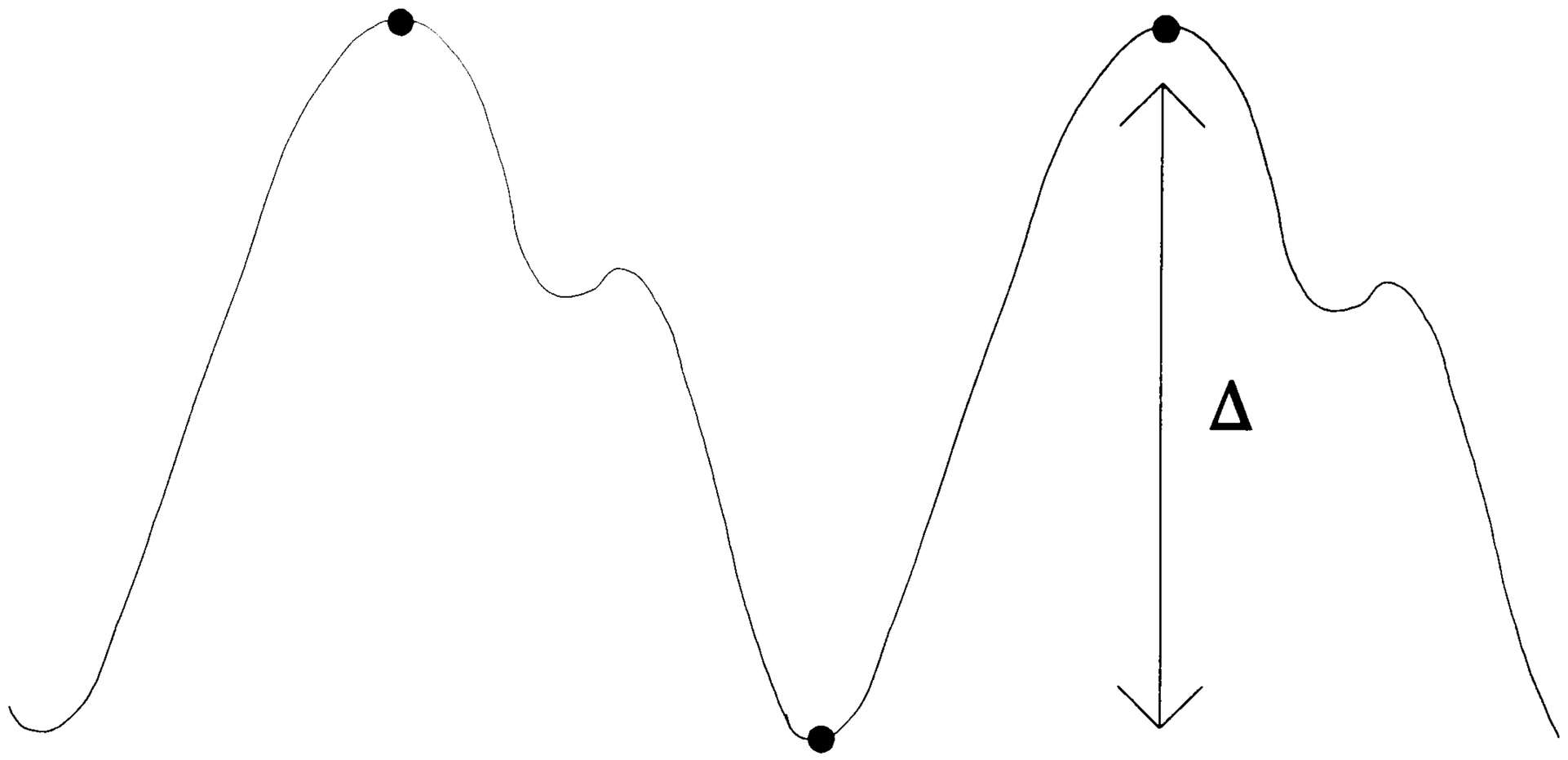

Figure 2.6: Determination of the AC amplitude Δ using the minimum and maximum values of the AC PPG signal.

The second method of data processing uses the principle that the sum of parts equals the whole. Thus the pulse oximeter samples the red and infrared PPG signals at a rate much faster than the heart rate. In this type of processing the red and infrared AC signals are normalised first by making their respective DC signals equal, as shown previously in Fig. 2.3. The instantaneous difference δ_i between successive samples (see Fig. 2.7) of the red and infrared signals is then used to calculate the oxygen saturation. The advantage of this method is that a large number of instantaneous oxygen saturation readings are obtained in a short time interval, regardless of the heart rate. Further signal processing weights each saturation reading depending on a number of predefined criteria, such as the instantaneous pulse height δ, the part of the cardiac cycle where the reading was taken and how well the new value correlates with previous values. This weighted average method of processing offers very good immunity to motion artefacts in conjunction with rapid response.

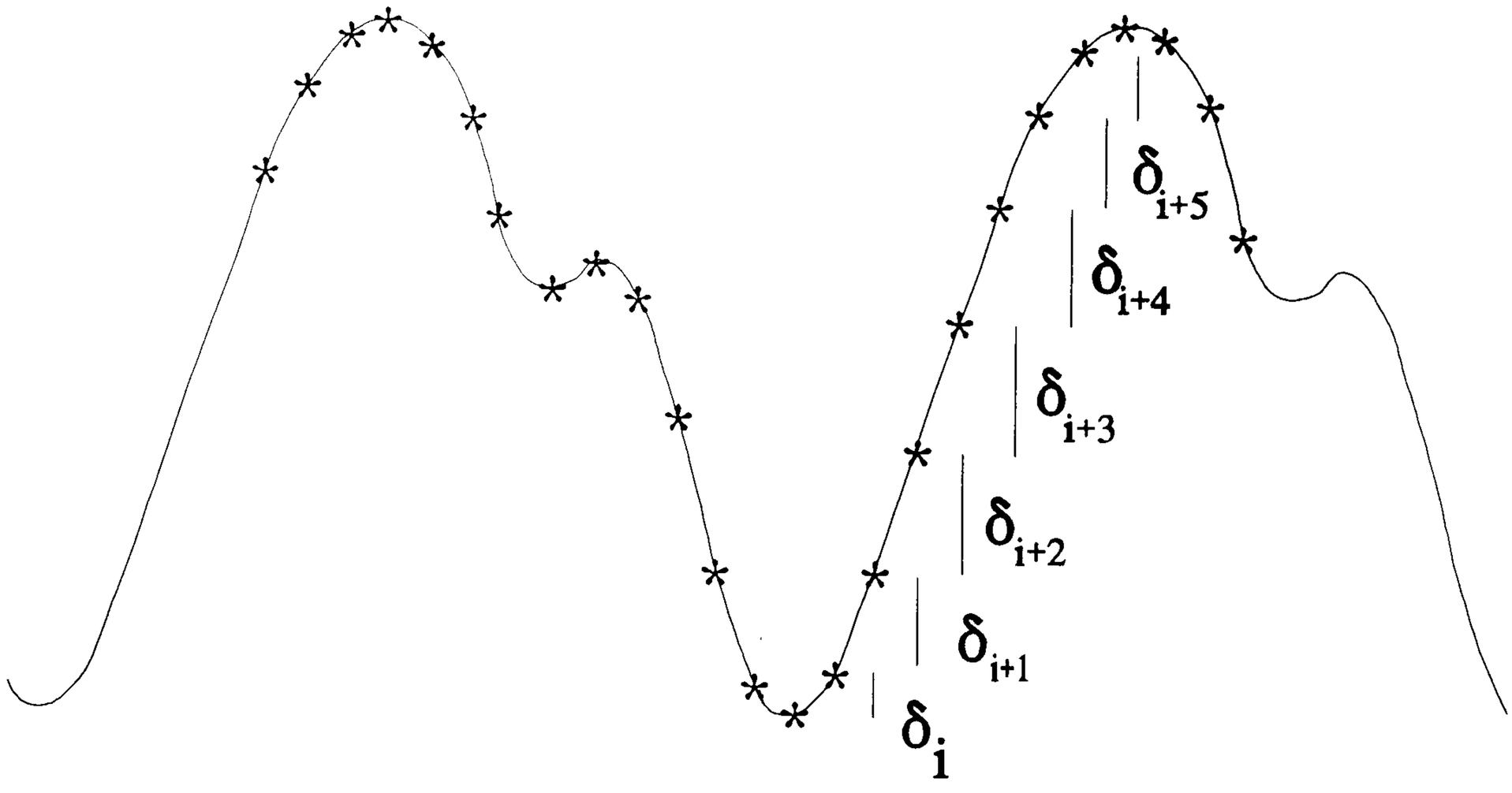

Figure 2.7: Calculation of the ratio **R** by using the instantaneous differences δ_i from normalised red and infrared AC PPG signals.

A totally different way of signal processing was adopted by Nellcor Inc. (Nellcor Inc., 1989). In the Nellcor setup the detected optical signals are transformed from the time domain to the frequency domain. By analysing the spectral components of the frequency spectrum information is extracted to calculate the ratio **R**. More specifically, the frequency spectrum of the photoplethysmographic signal (see also section 1.3.1 and Figures 1.9 and 1.10) consists of a zero frequency at the constant background intensity level, a fundamental frequency corresponding to the heart rate, additional harmonic frequencies at multiples of the fundamental frequency and finally frequencies that spread across the spectrum and are due to noise, spurious signals and motion artifacts.

The ratio **R** (red/infrared) is calculated by dividing the energy at the fundamental frequency by the zero frequency background intensity for each wavelength (red and infrared), then dividing the red modulation by

the infrared modulation. In practice the relative amplitudes of the red and infrared fundamentals at the heart rate were found by searching the frequency spectrum in the region of expected heart rates for a relative maximum and ensuring that this was the fundamental by determining the existence of another relative maximum at twice this rate. In some models determining the fundamentals was assisted by the use of an ECG input. The advantage of this processing in the frequency domain is that it offers an improvement in the SpO_2 accuracy and reliability by using only the periodic information derived from the heart rate and rejecting all aperiodic information corresponding to noise, spurious signals and motion artifacts.

2.2 PROBLEMS, LIMITATIONS AND ACCURACY OF PULSE OXIMETRY

In this section the problems, technical and clinical limitations and the accuracy of pulse oximeters are discussed.

2.2.1 Problems and Limitations

2.2.1.1 Dyshaemoglobins and dyes

This method described above assumes that the only forms of haemoglobin present in the blood are oxyhaemoglobin and deoxyhaemoglobin. In real life other species of haemoglobin are present in the blood, that is carboxyhaemoglobin (COHb) and methaemoglobin (MetHb) (see Fig. 1.4). It is for this reason that some manufacturers take

into account the concentrations of carboxyhaemoglobin and methaemoglobin when deriving their empirical data. For example, the Ohmeda Biox 3700 was calibrated (Pologe, 1987b) on healthy non smoking adults with an average COHb level of 1.6 % and a MetHb level of 0.4 %. As long as the concentration of carboxyhaemoglobin and methaemoglobin are within the normal range this does not present a source of error, but in higher concentrations oximeters might display erroneous and potentially dangerous results (Tremper, 1989; Barker, 1987; Eisenkraft, 1988). To be more specific, as carboxyhaemoglobin absorbs almost identically to oxyhaemoglobin at 660nm, the pulse oximeter, being a two wavelength device, cannot discriminate between oxyhaemoglobin and carboxyhaemoglobin, thus the reading of the oximeter will be overestimated, reflecting the sum of the above two haemoglobins.

In the case of increased methaemoglobin concentrations in studies performed on dogs (Barker, 1989b), the output of the pulse oximeter decreased and then stabilised to 85%. This is explained by looking at the absorption spectrum of methaemoglobin, where the absorption values for 660nm and 940nm are similar. Therefore for increased concentrations of methaemoglobin, absorption at these wavelengths increases, thus driving the ratio **R** towards unity and saturation reading to 85% (see Fig. 1.4 and Fig. 2.4).

Another problem associated with pulse oximeters is erroneous readings due to different dyes used for diagnostic purposes (Bowes, 1989; Sidi, 1987; Kessler, 1986). For example methylene blue which is used for

the treatment of methaemoglobinaemia, has a similar absorption at 660nm as deoxyhaemoglobin, resulting in artificially low oxygen saturation readings from the pulse oximeter, with reported readings as low as 1% (Scheller, 1986). This again is connected with the inability of the oximeter to monitor only oxy- and deoxy- haemoglobin.

2.2.1.2 Motion artifacts

Most pulse oximeters, with the use of weighted and averaging processing (see section 2.1.1), allow for artifacts produced by patient movement. However, it is still possible that signals caused by motion artifacts can be mistaken for true signals, or patient movement can result in extra or missed beats leading to erroneous calculation and display of heart rate and consequently oxygen saturation. To try and overcome this problem some pulse oximeters use the R wave of the electrocardiographic (ECG) signal, obtained from conventional electronic heart rate monitoring, together with the pulsatile PPG signal (Blitt, 1990). If the two signals are not synchronous then the oxygen saturation value is rejected and not used in the averaging.

2.2.1.3 Probe malposition

Another artifact is that of poorly applied probes resulting in total loss of signal and consequently inability to obtain oxygen saturation readings. A more worrying aspect of poorly applied probes is that sometimes false oxygen saturation readings are obtained even though

what appears to be a good photoplethysmographic signal is displayed by the pulse oximeter.

This type of artifact has been reported in the late 1980s for transmission pulse oximetry with probes used on digits (Kelleher, 1989b) and is known as the Penumbra effect. This effect was also reported in monitoring newborn babies when a pulse oximeter probe was used on the baby's big toe (Southall, 1992).

In his experiment, shown in Fig. 2.8, Kelleher varied the position of the probe on the finger. Initially the probe was placed at 11mm from the fingertip (standard position) and then moved along the y-axis towards the fingertip in steps of 1mm.

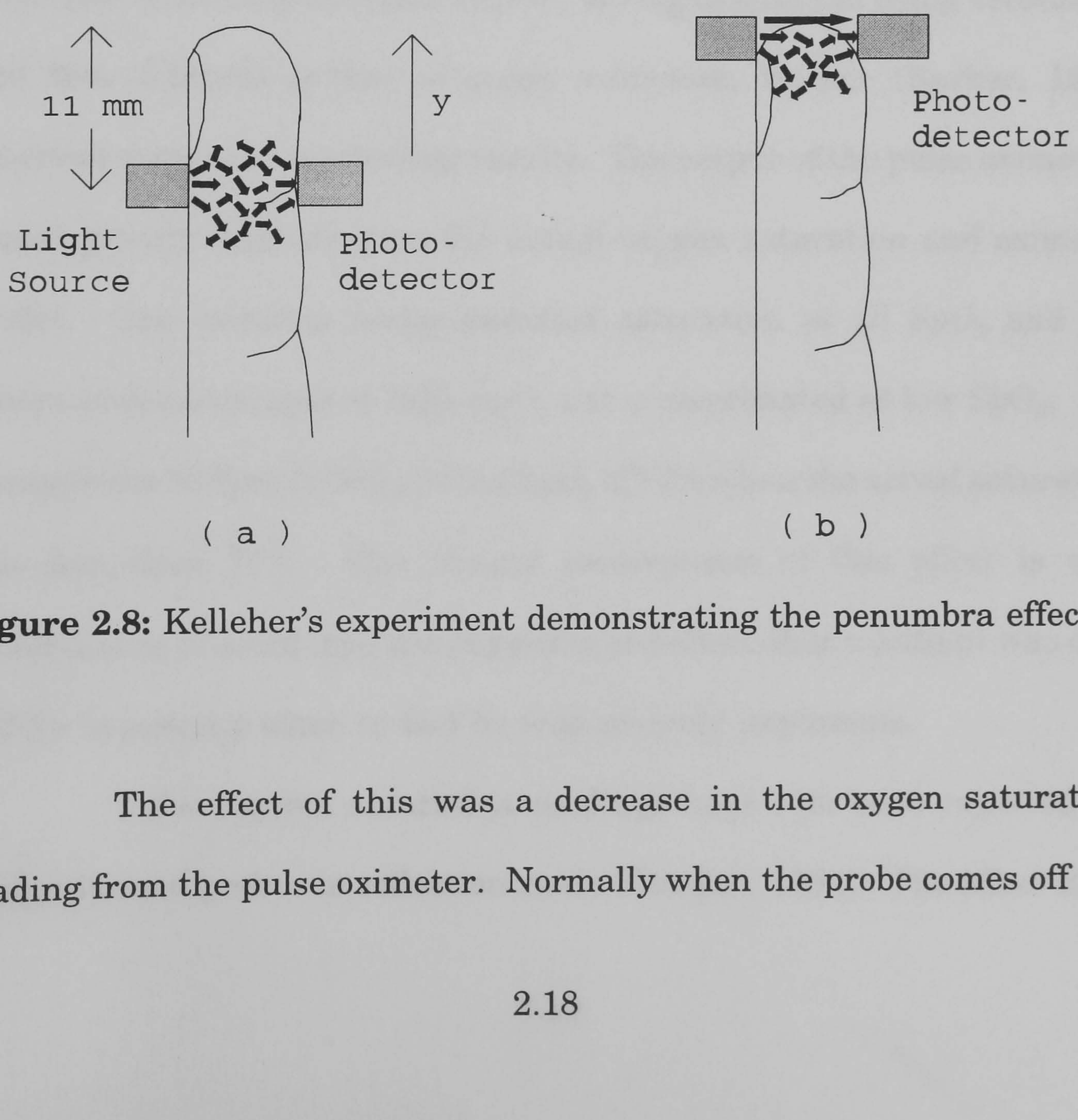

Figure 2.8: Kelleher's experiment demonstrating the penumbra effect.

The effect of this was a decrease in the oxygen saturation reading from the pulse oximeter. Normally when the probe comes off the

finger, most pulse oximeters offer an ambient light warning. If, however, the probe does not come completely off (Fig. 2.8b), the direct illumination of the sensor by the LEDs may not be significant enough for the ambient light warning to function. The poorly interposed tissue between the sensor and the LEDs may block the optical path enough to allow illuminat0ion of the vascular bed and production of a pulsatile signal. The result of the direct illumination (optical shunt) of the sensor by the LEDs can be thought of as a noise source, with pulsatile signal and noise added at each wavelength. As the contribution of noise for both wavelengths is increased the ratio of the two wavelengths tends toward unity, corresponding to an oxygen saturation reading of 85%.

In a clinical study of the behaviour of transmission pulse oximeters with malpositioned sensors during hypoxemia using volunteers and five different makes of pulse oximeters, Barker (Barker, 1993) observed some very interesting results. The output of the pulse oximeters varied greatly depending on the actual oxygen saturation and oximeter model. One oximeter underestimated saturation at all SpO_2 and the others underestimated at high SpO_2 but overestimated at low SpO_2. For example the Nellcor N-100 yielded SpO_2 of 92% when the actual saturation was less than 70%. The clinical consequence of this effect is very important as it could lead the physician to believe that a patient was only mildly hypoxemic when in fact he was severely hypoxemic.

False oxygen saturation readings have also been reported for malpositioned probes in reflection mode (Gardosi, 1991). The effect of an

increasing gap between reflection probe and skin on oxygen saturation readings is investigated in detail in chapter 6.

2.2.1.4 Spectral characteristics of light sources

Pulse oximeters use two LEDs in their probe design. Although LEDs emit power in a very narrow spectral range they are not ideal monochromatic light sources. Moreover, the centre wavelength of the emission spectrum varies even among LEDs of the same type from the same manufacturer. For any given type of LED the centre wavelength variability can be as great as ±15nm. The effect of this is an error in the oxygen saturation calculation because of a change in the measured extinction coefficients of oxy- and deoxyhaemoglobin. This problem is corrected in one of two ways. Firstly, probes can be manufactured from carefully selected LEDs that have a very narrow range of centre wavelengths. This method is time consuming and expensive due to the number of LEDs that are rejected. The second method allows for centre wavelength variability by using a set of calibration curves instead of only one. The pulse oximeter is programmed to accept several LED centre wavelengths and selects the appropriate calibration curve depending on the set of LEDs connected on it. This of course requires a mechanism for relating the LED wavelength to the pulse oximeter. One common technique for achieving this is to code each probe with a fixed resistor that the oximeter checks when the probe is connected on it (Physio-Control,1993).

Another problem reported with LED spectral range, was that some red LEDs emit infrared light as well. This creates a big problem and makes the pulse oximeter to malfunction completely (Personal communication).

2.2.1.5 Ambient light

In the clinical literature (Costarino, 1987) it has been reported that ambient light occasionally causes pulse oximeters to display false readings, even though pulse oximeters are designed to exclude ambient light (see Fig. 2.5 and section 2.1.1). Also modulated light sources present in the operating theatre interacted with pulse oximeter readings (Brooks, 1984; Amar, 1989). Shielding of the probe generally alleviates the problem.

2.2.1.6 Low Perfusion

Only if an adequate AC PPG signal is detected the pulse oximeter can calculate oxygen saturation. In cases where the amplitude of the pulsatile signal is very low or undetectable, pulse oximeter readings can be intermittent or unavailable. Low signal levels due to poor perfusion can be due to a number of different reasons such as hypothermia, hypotension, hypovolemia, vasoconstrictor infusions or cardiac bypass.

2.2.2 Accuracy

As described in section 2.1.1 all pulse oximeters are calibrated empirically using data derived from measurements on healthy volunteers. The calibration curve is extrapolated below 70% saturation. Therefore, accuracy above 70% is generally better than for values below that. Moreover, the accuracy of instruments from different manufacturers varies, this usually being a direct result of calibration procedures. Between 80% and 100% SpO_2 manufacturers quote accuracies of ±4% with a 95% confidence limit (Gravenstein, 1990). Several evaluations of pulse oximeters for studies above and below 70% saturations have been reported (Yelderman, 1983; Kagle, 1987; Severinghaus, 1987).

However, extensive use of pulse oximeters over a wide range of situations and conditions (other than tests on healthy volunteers) has shown that readings can vary over a relatively wide band. Moreover, pulse oximeters are often used without being subjected to routine performance assessment to verify their accuracy. Simulators have recently become available (O'Reilly, 1994; Amoore, 1994) that can be used to test pulse oximeters. An *in vitro* test system using a flexible blood filled cuvette as a model finger, capable of producing signals similar to those obtained from pulsatile arterial blood in the finger, has been proposed (Reynolds, 1992a; de Kock, 1991). The response of ten commercially available pulse oximeters has been compared using the above proposed test system (Reynolds, 1992b). The performance of test systems like the

above solely depends on the performance of the model finger. Once a model finger is devised that will function optically as close as a real finger, then a system like the above can be used for pulse oximeter calibration for any value of oxygen saturation. Clearly a standard procedure of testing the accuracy of pulse oximeters, over a wide range of saturations, from different manufacturers is needed.

While low accuracy below 70% diminishes the value of pulse oximeters as a scientific instrument, from the clinical point of view, accuracy at these low saturation levels is not that important, as the physician is more concerned with raising the patient's oxygen saturation.

Also different makes of pulse oximeters give systematically different results when compared under the same conditions. In a study by Thilo (Thilo, 1993) it was found that for example the Nellcor N-100 consistently gave saturation results 1.5 to 2% higher than those of the Ohmeda Biox 3700. The difference in these results can be explained by the different empirical calibration curves used by each manufacturer and also on the way pulse oximeters display oxygen saturation. Specifically, the Biox instrument takes into account normal levels of MetHb and COHb in its calculations (see section 2.2.1.1) and therefore displays fractional oxygen saturation whereas the Nellcor displays functional oxygen saturation.

2.3 USES OF PULSE OXIMETRY

Although several problems and limitations have been reported (see section 2.2), pulse oximetry offers simplicity in its use, continuous, *in vivo* and non invasive monitoring of blood oxygenation. Moreover, pulse oximeters are excellent trend recorders, and can alert the physician to falling SpO_2 before cyanosis appears. For all the above reasons pulse oximetry has gained widespread acceptance throughout the medical community.

Pulse oximetry can be used in a number of different ways. Some of them have proved to be of some importance, others still need more investigation. Basically, any clinical situation associated with respiratory or circulatory compromise may benefit from oxygen monitoring. However, PaO_2 measurements need to be taken when it is desired to calculate shunts, or when there is suspicion about patients being poisoned with carbon monoxide or affected by dyes.

The major use of pulse oximetry is in early detection (with some exceptions, see Desiderio, 1988 and Barker, 1989a) and treatment of hypoxaemia. In a carefully designed study of 152 paediatric patients undergoing surgery, Cote (Cote, 1988) tried to determine whether pulse oximetry helps to diagnose hypoxaemic episodes that can be missed by an anaesthetist relying only on clinical signs, such as cyanosis, change in heart rate or respiratory pattern. A pulse oximeter was made available to the anaesthetists for half of the patients. The pulse oximeter probe was placed on the patient's finger or toe and the SpO_2 minimum limit alarm

was set for 85%. For the other half of the patients the pulse oximeter data was not made available to the anaesthetists, so they had to rely on clinical data only. The pulse oximeter diagnosed hypoxaemia before the clinical signs of hypoxaemia became apparent. The anaesthesia team without the oximetry data managed to detect only 10 of 24 episodes of major hypoxaemia even though all 24 episodes were associated with SpO_2 readings below 73%.

In a further study of 2000 incidents reported to the Australian incident monitoring study (Runciman, 1993; Webb, 1993), in order to study the role of several monitors used in patients undergoing general anaesthesia, the pulse oximeter scored highest in detecting common incidents. This does not mean that other monitors should not be used, but that pulse oximetry plays an important role and should be used in conjunction with other front-line monitors.

Monitoring is important intraoperatively and during critical care, as well as during transport to the recovery room and in the recovery room itself. A special case can be argued for the use of pulse oximeters in cardiac surgery preparations where hypoxaemia is possible during preoperative placement of invasive monitors in combination with the pre anaesthetic medication (Kelleher, 1989).

Another use is during oxygen therapy and respiratory care, where it was found that the use of the pulse oximeter can assist in finely adjusting inspired oxygen levels and ventilatory assistance. In patients with acute respiratory failure a combination of a pulse oximeter with a

pulmonary artery oximeter can enable accurate titration of continuous positive airway pressure (Rasanen, 1988).

A relatively new area for use of pulse oximeters is paediatrics. In neonatal asphyxia the pulse oximeter can help in assessing and determining normality or not of the commonly encountered changes in SpO_2 immediately after delivery (Bowes, 1989). A number of intraoperative procedures in neonates can give rise to desaturation, hence continuous monitoring of SpO_2 in paediatric anaesthesia, during for example the repair of congenital heart defects, is of vital importance (Kelleher, 1989). Remote monitoring (ie from outside the treatment room) may be significant to avoid unnecessary exposure to ionizing radiation. Hence this is a special role of pulse oximetry for monitoring SpO_2 levels in children undergoing radiotherapy under general anaesthetic given to ensure immobility of the patient (Kelleher, 1989).

It is interesting to note how widespread the use of pulse oximetry is, by looking at the number of papers published (BIDS, 1995) in the last few years as shown in Fig. 2.9.

2.4 REFLECTION PULSE OXIMETRY

In the preceding sections when pulse oximeters were referred to it is assumed that they operate in the transmission mode, that is the light emitter is at one side of the skin under investigation and the photodetector

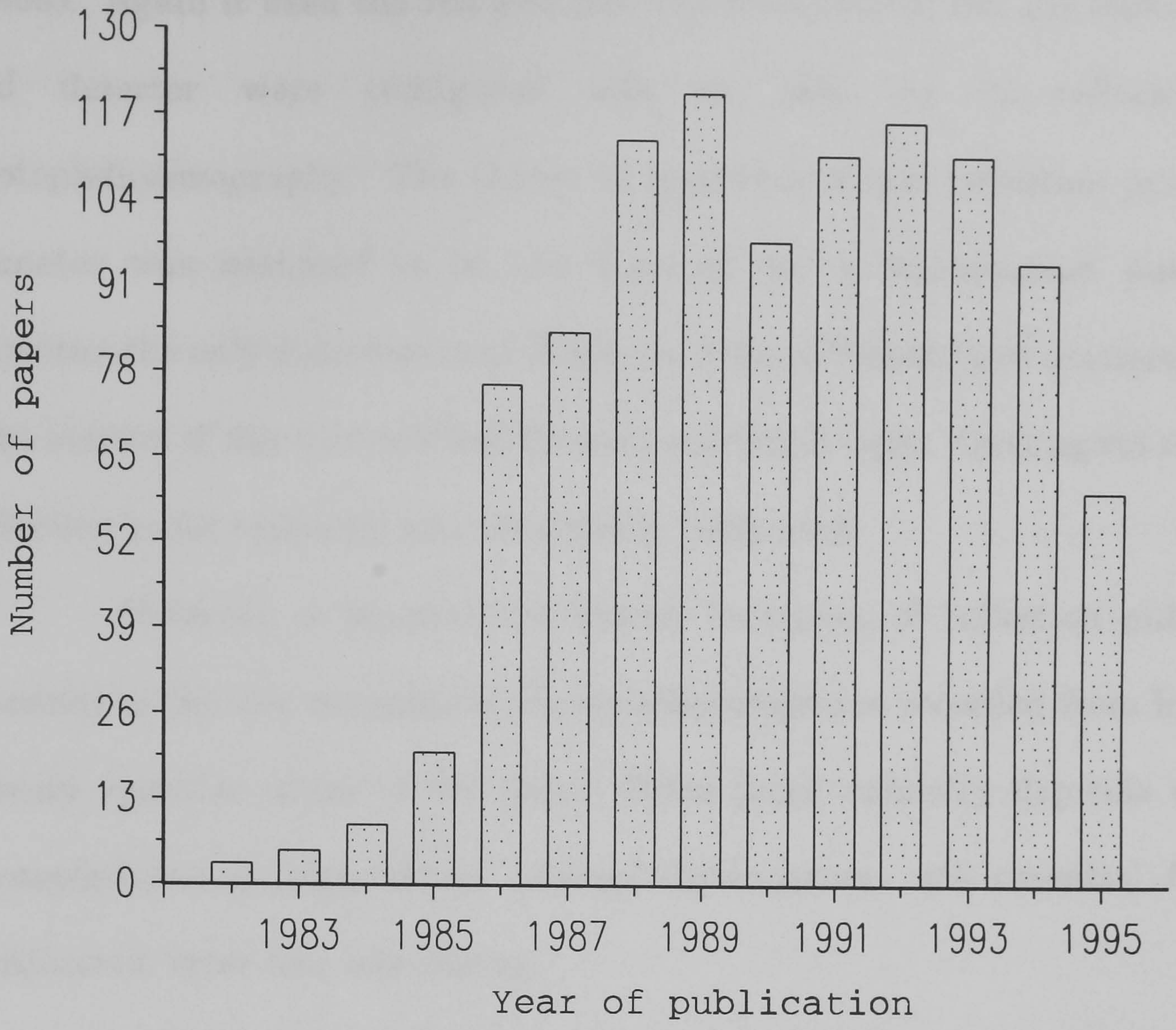

Figure 2.9: Pulse oximetry papers from 1982 to date.

at the opposite side. Practically transmission pulse oximetry is limited to a few specific locations on the body. In adults these are the fingertip, ear lobe and toes. In infants additional sites such as the wrist, palm and feet can be used. To overcome this limitation and enable one to monitor oxygen saturation at any site, reflection pulse oximetry has been developed. A further advantage of reflection pulse oximetry might be in the assessment of localized tissue oxygenation after skin transplantation and regeneration after microvascular surgery.

A prototype non invasive pulse oximeter utilising skin reflectance photoplethysmography was first described by Mendelson (Mendelson,

1988a). Again it used the red and infrared wavelengths but the emitter and detector were configured side by side, as in reflection photoplethysmography. The theory of operation of this reflection pulse oximeter was assumed to be the same as for a transmission pulse oximeter; the only difference was that it used the reflected (back scattered) light instead of the transmitted (forward scattered) light. Once again the reflection pulse oximeter was empirically calibrated.

However, a practical (technical) limitation of reflection pulse oximetry is the low magnitude photoplethysmograms recorded from low density vascular areas of the skin. Since pulse oximetry depends on photoplethysmography, strong photoplethysmograms are essential for continuous, error free monitoring.

Recent research has been concentrated in designing an optical sensor for reflectance pulse oximetry that can reliably detect sufficiently strong photoplethysmograms. Two different paths have been followed in order to enhance signal levels; either increase the emitted light or increase the amount of detected light. Mendelson (Mendelson, 1988b) proposed a sensor with two red (660nm) and two infrared (930nm) LEDs in the middle and six silicon photodiodes arranged symmetrically in a hexagonal configuration round the LEDs in order to increase the amount of detected light. He also introduced a heated sensor (Mendelson, 1991) since local heating helps vasodilate the microvascular bed and thus increases the signal to noise ratio. In a previous study Mendelson (Mendelson, 1988a) showed that a four to fivefold increase in the AC PPG magnitude is

possible with local heating to a temperature above 40^0 C. However, care should be taken with localised heating, especially in long monitoring times, to avoid skin burn injuries.

Takatani (Takatani, 1992) used a sensor with four red (665nm) and four infrared (820nm) LEDs all arranged round a central photodiode. Since the physical area of LEDs is smaller than photodiodes the overall size of this sensor was smaller than Mendelson's. Local heating was used only if inadequate signal levels were detected. In a study with critically ill patients the errors in reflection oxygen saturation were similar, and even slightly less, to those of a standard transmission pulse oximeter.

In terms of signal processing for calculating oxygen saturation both Mendelson and Takatani used the relationship between SpO_2 and **R** as described by equation 2.9. Mendelson used a commercially available transmission pulse oximeter to interface his reflectance probe and thus the conversion of the **R** ratio to reflection SpO_2 values was achieved by using the transmission calibration data. Later he used the same transmission pulse oximeter for instrumentation purposes but derived his own constants A and B for equation 2.9, following a calibration and performance study for the reflectance probe.

In his design, Takatani from the beginning derived calibration data specifically for the reflection pulse oximeter, since he used a different infrared wavelength than transmission pulse oximeters.

2.5 THESIS OBJECTIVES

Pulse oximeters operate by assuming that absorbance measurements are performed on arterial blood that flows in the finger. As presented in the theory, pulse oximeters use the AC/DC ratio of the photoplethysmographic signal at 660 and 940nm to calculate the oxygen saturation. These instruments are still empirically calibrated and therefore the study of the wavelength dependence of the magnitude of the pulsatile and non-pulsatile components of light scattered from tissue, is of extreme importance in trying to assess and understand the way that pulse oximeters really operate, whether in reflection or transmission mode.

This ties up with a new trend of using transmission pulse oximeters with multi-site sensors which can be used in either transmission or reflection mode. Consequently any observed deviations either from the wavelength dependence predicted by existing pulse oximetry theory or between reflection and transmission mode would suggest that the output from pulse oximeters should perhaps be viewed with caution. The wavelength dependence of the photoplethysmographic signal in both refection and transmission modes from 450nm to 1000nm in studies on the fingertip is therefore investigated. Moreover, the possibilities of using other wavelengths, instead of 660 and 940nm, especially in the visible region is examined with the aim of improving the accuracy and overcoming certain limitations of existing instruments.

In addition the possibility of defining a model finger for Monte Carlo simulations of light transport in tissue is investigated. The aim is

that simulation results on the wavelength dependence of the photoplethysmograph are compared with the experimental ones. A successful definition of such a model will allow future simulation prediction of the behaviour of pulse oximeters due to the variation of relevant parameters.

Finally, a new area in which the use of reflection pulse oximetry is currently under investigation is that of fetal monitoring during labour. Preliminary observations reported false low SpO_2 readings associated with malpositioned reflectance probes and this new artifact is examined here in detail; the objectives being to both quantify and suggest ways of eliminating it.

CHAPTER 3

INSTRUMENTATION

3.1 INTRODUCTION

In order to study the wavelength dependence of the photoplethysmogram, a system capable of obtaining the "AC" and "DC" components of the photoplethysmogram over the wavelength range 450 - 1000nm in "transmission" and "reflection" modes was constructed. This chapter describes this system which is shown schematically for transmission mode in Fig. 3.1. The system configuration for the reflection studies is essentially the same, apart from a change in the fibre bundles arrangement. The optical and electronic components and the software developed to control the system and analyse the captured data are explained in detail in the following sections.

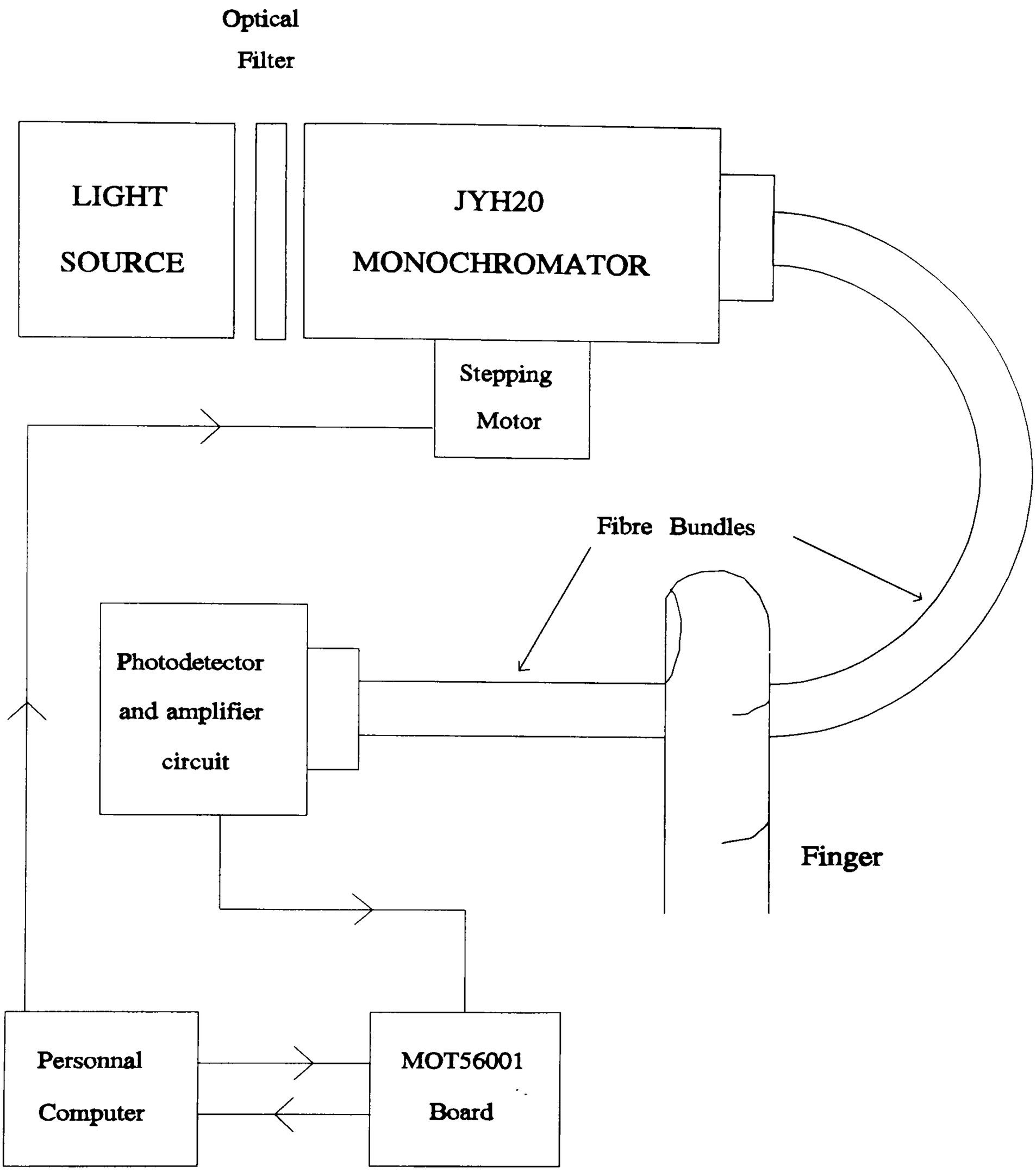

Figure 3.1: System configuration for the wavelength dependence studies of the photoplethysmogram. The fibre bundle arrangement as used in the transmission mode is shown.

3.2 LIGHT SOURCE

The light source used was a 70W quartz covered iodine vapour lamp, with a spectral range of 220nm - 2μm. The relative spectral distribution of this light source is shown in Appendix B. A spherical mirror focused the lamp filament on the entrance slit and a lens placed on

the entrance slit of the monochromator coupled the spherical mirror and the grating.

The lamp was originally powered by a 24V AC supply. However, the power supply was later modified to a stabilised 24V DC one in order to provide a more stable light intensity. This was after previous experiences with AC powered light sources, where as expected a slight fluctuation of intensity at twice the supply frequency was observed.

3.3 MONOCHROMATOR

A commercially available monochromator, the JYH20 (I.S.A. Jobin Yvon, France), was used for these studies. It was fitted with a concave holographic (600 grooves/nm) grating, covering the 400 - 1600nm wavelength range. The entrance and exit slits were aligned, and were straight and interchangeable. Dispersion in the plane of the slits was 4nm/mm. The instrument was supplied with slits of 0.5, 1 and 2mm width, thus corresponding to bandwidths of 4, 8 and 16nm respectively. Wavelength scanning was linear with direct reading on a mechanical counter. The grating was driven by a stepper motor which was controlled by the PC. Scanning along the wavelength range was performed in steps, whilst the step value, the number of steps, the number of samples taken at each step and also the sampling frequency were controlled by the PC.

In order to eliminate light output due to second order diffractions from the monochromator's grating, optical filters at the input of the

monochromator were used. The filter's specifications were matched to the wavelength range. For wavelengths up to 700nm no optical filters were used. For the wavelength range between 600nm to 1000nm a long pass filter with a cut off wavelength of 520nm was used.

3.4 PIPING OF LIGHT

To guide the light from the monochromator to the finger and from the finger to the detection circuit, fibre bundles were used. All were obtained from Eurotec Optical Fibres Ltd. For the transmission studies two 3mm optical diameter bundles were used. For the reflection studies a 5mm common end optical diameter bifurcated bundle was used and also two 1.5mm optical diameter ones placed side by side. All were of 50cm length. The fibres were protected by a PVC covered steel sheathing which offered substantial mechanical protection. The end terminations were turned brass ferrules with the fibres optically ground and polished.

3.5 PHOTODETECTORS

Different photodetectors were necessary to cover the entire 450 - 1000nm range. The choice of which photodetector to use at a specific wavelength range was dictated by the principles of operation of each photodetector.

3.5.1 Photodiodes

The photovoltaic effect states that a voltage is generated across a p-n junction when the junction is exposed to light. Photodiodes make use of this effect. The photovoltaic effect occurs only when the energy of absorbed photons is higher than the band gap energy, E_g. Therefore, the spectral responsivity at long wavelengths depends on the band gap with the maximum wavelength, λ_{max}, determined by the condition $\lambda_{max} = h\,c\,/\,E_g$ (where h is the Planck constant and c the speed of light in vacuum). The minimum wavelength is determined by the surface absorption, as the charge is lost before reaching the junction.

The Centronics OSD60-5T silicon photodiode was used, with a $62mm^2$ active area (7.9mm x 7.9mm). A typical spectral response curve for this photodiode is shown in Appendix B.

3.5.2 Photomultiplier tube

The photomultiplier tube is an optical detector which offers high current amplification and low noise, thus making it ideal for detecting very low optical signals. It consists of a photoemissive cathode, focusing electrodes, the dynodes and an anode. As photons strike the photocathode, the photocathode emits photoelectrons into the vacuum. The photoelectrons are then directed by the focusing electrodes to the dynodes, the dynodes being an electron multiplier system. The dynode system consists of electrodes covered with special materials exhibiting secondary emissions. The photoelectrons hit the first dynode where a secondary

emission occurs. The electrons emitted from the first dynode, are directed towards the second dynode, where more secondary emissions occur and so on. The number of dynodes in a photomultiplier tube ranges from 5 to 16. Electrons emitted from the last dynode are collected by the anode, this being the output current.

The spectral response of the photomultiplier tube is determined by the photocathode and window materials. The Hamamatsu 1P28 photomultiplier was used and operated at 1 kV. A typical spectral response curve for this photomultiplier tube is shown in Appendix B.

3.6 DETECTION CIRCUITS

All photodetectors used the same circuit design with slight modifications to the amplification stages. The zero bias (or unbiased) configuration was used. The photodiode was connected to an operational amplifier, which was used as a current-to-voltage converter, as shown in Fig. 3.2. Since the point E is a virtual earth, then the photodiode load resistor is nearly zero, and therefore all of the generated photocurrent (I_{ph}) flows through the feedback resistor R_f.

This circuit has a linear response and is low noise. The main disadvantage of this circuit is its slow speed of response. Speed of response can be improved by biasing the photodiode. However, for the studies undertaken here this did not present a problem since we were dealing with low frequency biological signals.

In Fig. 3.3 the complete circuit and block diagrams are shown.

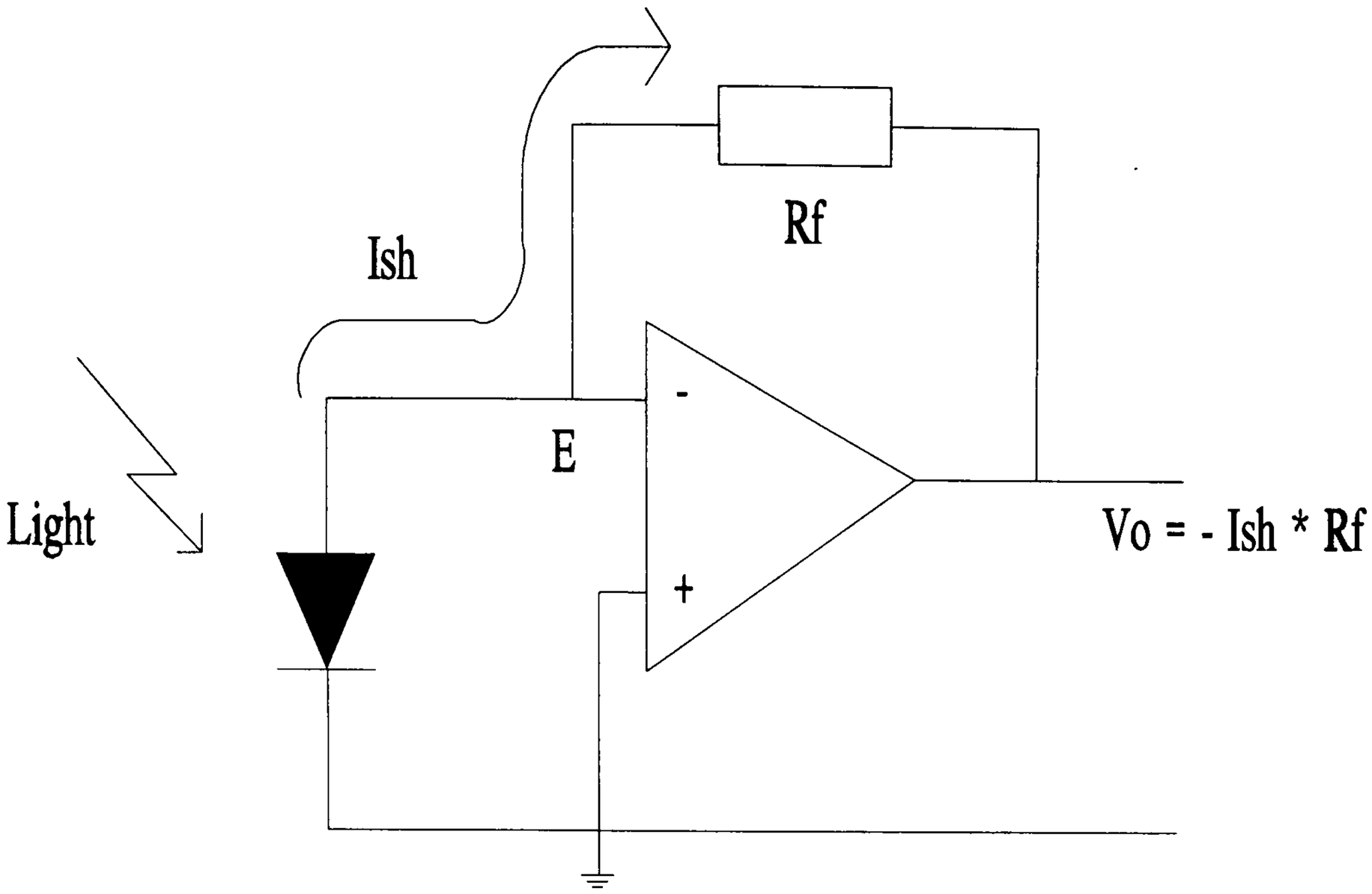

Figure 3.2: : Photodiode operational circuit with zero bias.

The function of this circuit was firstly to perform the light intensity measurements on the light scattered from the finger, and secondly to process this signal in order to obtain the AC and DC photoplethysmograms. The first function was performed by the photodetector preamplifier described in Fig. 3.2 above and a low-pass filter to remove any high frequency noise.

The output from this stage was a composite signal, consisting of a large DC signal and a small AC signal. The DC PPG was obtained from this composite signal. Although this is not the true DC PPG, as it is discussed in section 3.7.1 the effect of not rejecting the AC signal at this stage is not important. Moreover, it is in agreement with the method used by pulse oximeters. The following stages of the circuit were used to extract the AC PPG from this composite signal. It was high-pass filtered at 0.27Hz (-3dB point) to discard the high DC component, amplified (the

amplification value was variable depending on signal strength) and then low-pass filtered at 15.9Hz. The theoretical frequency response (using the Microcap 383 simulation package) of the circuit is given at Fig. 3.4. The limits of this band-pass filtering were chosen so that a flat response was obtained for the expected frequency range of the AC PPG. All circuitry was enclosed in a metal box to reduce electromagnetic interference.

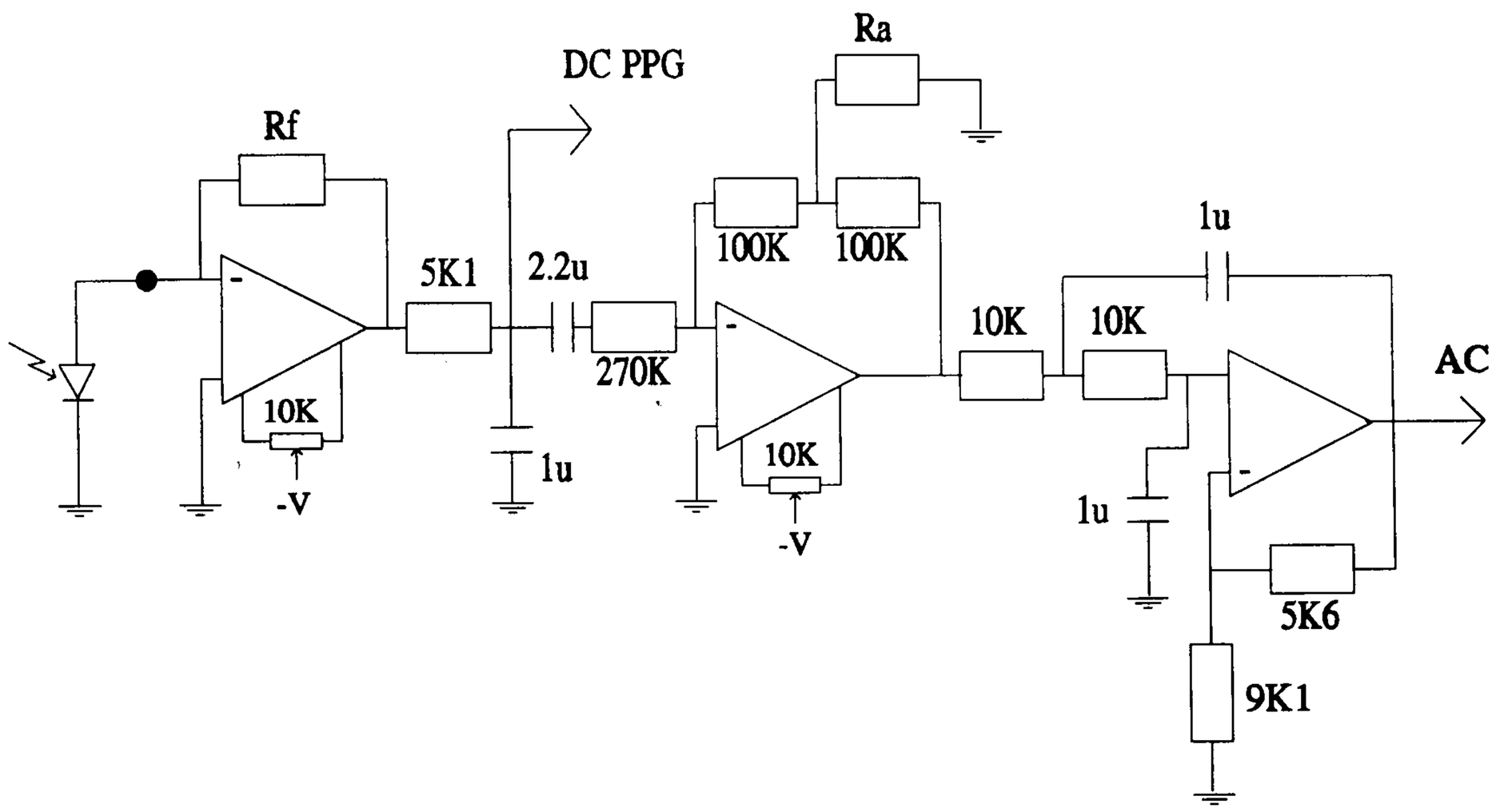

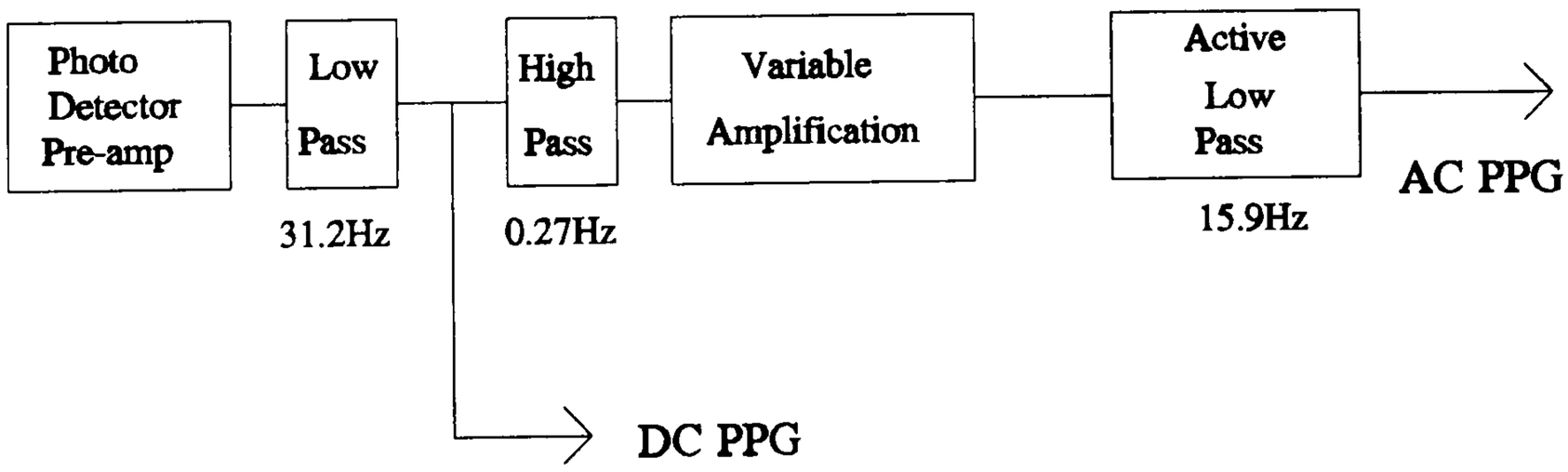

Figure 3.3: Circuit and block diagram showing the photodetector, filtering and amplification stages.

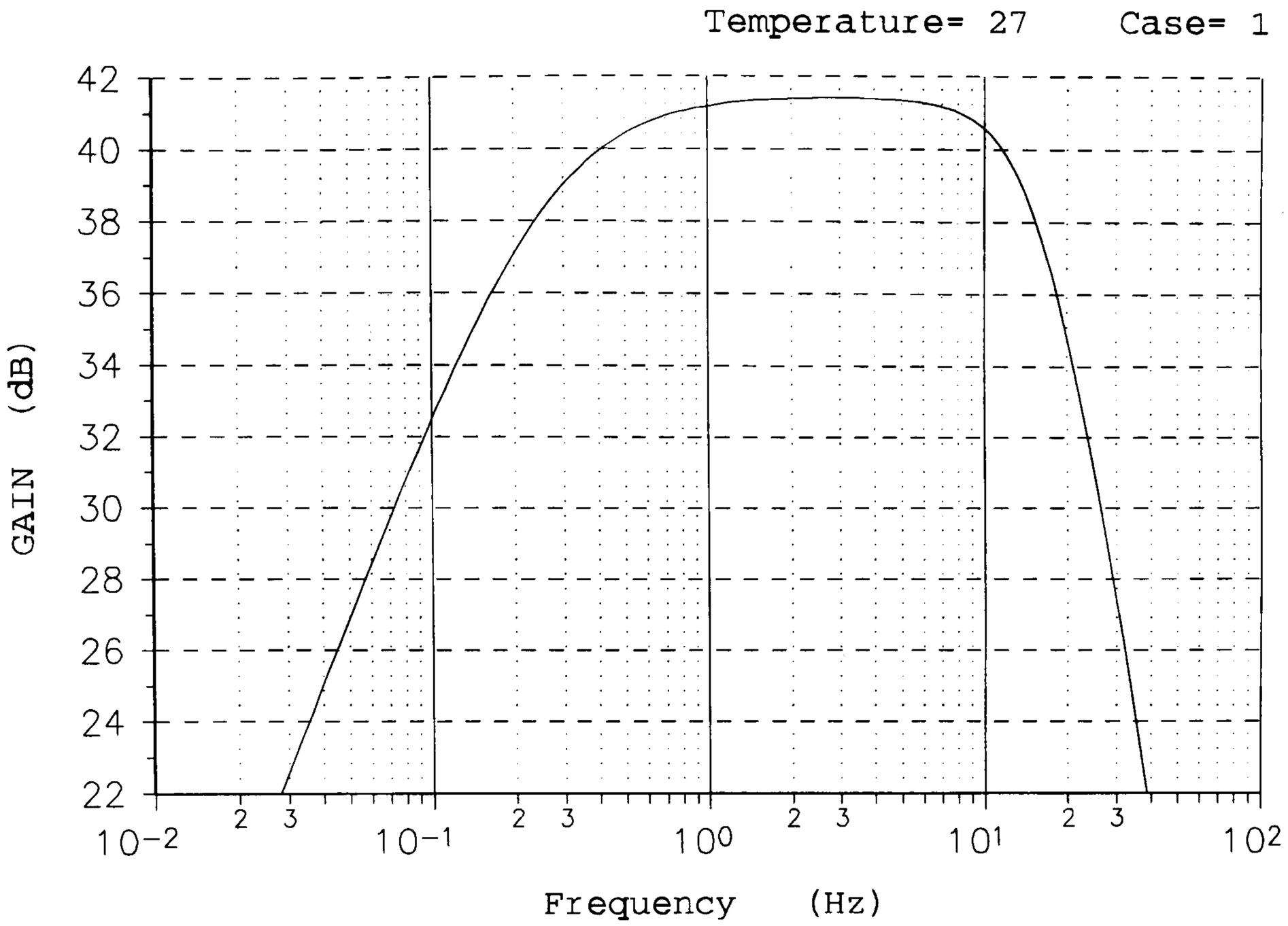

Figure 3.4: Circuit's frequency response for the AC PPG signal, as predicted by the Microcap 383 simulation package.

3.7 EXPERIMENTAL PROCEDURE

As described in previous sections due to the physical limitations of optoelectronic devices a number of photodetectors were used in order to exploit their maximum performance for a given situation. To summarize, the choice of photodetector, filter, detection circuit and fibre arrangement to cover a specific wavelength range for each mode of operation is shown in table 3.1.

Transmission 3mm bundles	Reflection 1 3mm Bifurcated bundle	Reflection 2 1.5mm bundles side by side
490 - 590 nm 1mm slit Photomultiplier No filter step 10nm	450 - 590 nm 0.5mm slit Silicon No filter step 10nm	
600 - 1000 nm 1mm slit Silicon Long pass (500nm) step 20nm	600 - 1000 nm 0.5mm slit Silicon Long pass (500nm) step 20nm	600 - 1000 nm 1mm slit Silicon Long pass (500nm) step 20nm

Table 3.1 : Range to detector - filter combination.

3.7.1 Data Acquisition and Display

In order to capture, analyze and display the data from these experiments, an IBM compatible personal computer (PC) and a Motorola DSP56001 digital signal processor (DSP) board were used. The DSP board contained two analog input channels and two analog output channels. The Analogue to Digital and Digital to Analogue devices were 16 bits, and they operated at ±3V for full scale conversions. The software requirements and the interface of the DSP board with the PC are dealt with in section 3.8.

At the beginning of each experiment the monochromator was initialised by the PC. This involved selecting a wavelength range and a step value. As the monochromator was scanned in steps, the AC and DC PPG signals were digitised (16 bit precision) at each wavelength, with a sampling frequency of 53 Hz, for a period of 19.3 seconds (taking 1024

samples). For example, for a heart rate of 80 bpm (beats per minute) this corresponds to 25.7 AC PPG cycles with about 40 samples describing each cycle.

In the case of the AC signal the amplitude of each PPG cycle was first calculated. This was achieved by searching for the minimum and maximum values of each PPG cycle, and subtracting the former from the latter. The detection routine searched for global minima and maxima only, avoiding any localised changes. Ignoring any local maxima and minima detection, avoided possible errors in calculating the AC amplitude due to the shape of the PPG cycle (dicrotic notch), movement artifacts or noise (see figures 3.7 and 3.8). The overall AC amplitude was the average of amplitudes of all captured cycles.

As shown in Fig. 3.3 the DC PPG used for these experiments is actually a signal that includes the AC PPG. The amplitude of the DC PPG was obtained by taking the average of the 1024 samples at each wavelength. Consequently, the contribution of the AC PPG, which in any way is of the order of a 1-5 %, was even less.

At each wavelength the raw signals and their respective calculated amplitudes were displayed on a colour monitor. In the case of the AC PPG signal pointers were displayed at the detected minima and maxima for visual checking. The raw signals were also displayed on a storage oscilloscope which served solely the purpose of double checking. At the end of each run both AC and DC signal amplitudes were corrected by using the pre-calculated calibration factors (see section 3.7.2) and the

AC/DC ratio at each wavelength was calculated and expressed as a percentage. The calibrated AC and DC PPG signal amplitudes, the AC/DC ratio and the calibration factors used were then displayed on a colour monitor for the specific wavelength range in graphical and tabular form.

3.7.2 Calibration

Before attempting to analyse the results and draw any conclusions from them, it is necessary to ensure that the above mentioned signals are independent of the system's performance. However, one of the problems of spectral analysis is that the efficiency of the monochromator, the output of the light source and the sensitivity of the photodetector are all wavelength dependent. This means that each wavelength has its own calibration factor which must be applied to the captured data in order to obtain corrected spectral distributions, that is distributions which will be independent of the system's specifications.

There are two methods from which corrected spectral distributions can be obtained. The first one is to actually calculate them theoretically using the available spectral performance graphs of the individual parts of the whole system. However, this is not really practical as the graphs supplied by manufacturers are typical ones and not specific ones for each part.

The second method is more sophisticated and ideal for these experiments as a computer was used to control the equipment. The first step was to select the working wavelength range. Then the

monochromator was scanned in steps with nothing placed between the light source and the monochromator. In order to avoid saturating the detector the two fibre bundles were placed opposite each other, slightly misaligned, as shown in Fig. 3.5. This assumes no wavelength dependence on angle of emerging light.

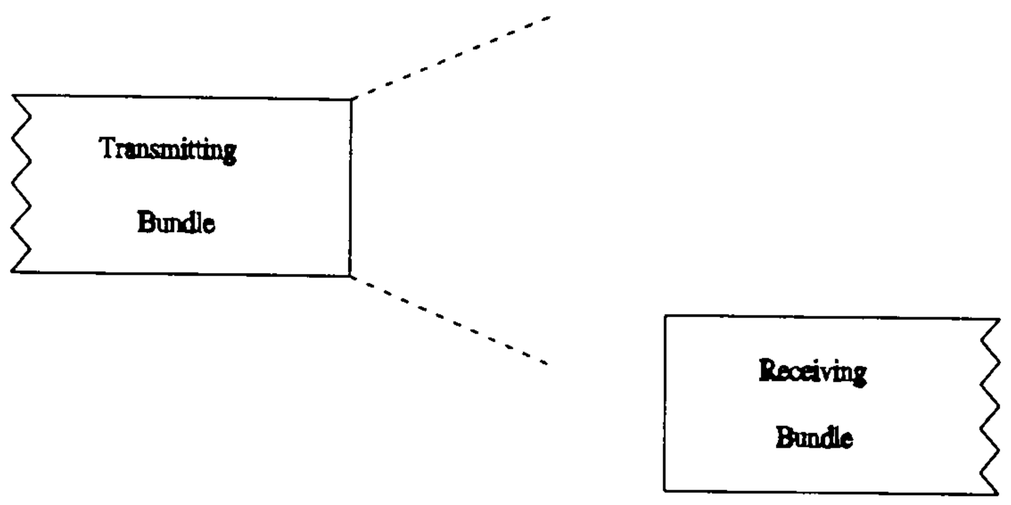

Figure 3.5: Fibre misalignment procedure for obtaining calibration factors.

The output from the photodetector was captured by the PC, this output being the overall spectra of the whole system. From this the calibration factors were then calculated and stored in a file. Calibration files for all wavelength ranges under examination have been obtained. When the sample (here the subject's finger) was then placed in position the calibration factors were automatically retrieved from the appropriate file and applied to the detector signal as the wavelength range was scanned, thus getting the true spectral response of the sample. Therefore, the results are presented in terms of the calibrated AC and DC PPG signals.

3.8 SOFTWARE REQUIREMENTS

Two programs were required to run at the same time; the first running on the DSP56001 board and the other running on the PC. All software was developed by the author.

3.8.1 DSP Programs

Two DSP programs were written in Motorola DSP56000 assembly language. They were tested and debugged using a monitor program supplied by Loughborough Sound Images Ltd.

The first program was called PPGACDC.ASM and was used to capture the AC and DC PPG signals. It effectively set up the two A/D channels and took 1024 samples for each channel. Once sampling was finished the DSP signalled to the PC that it was ready for the captured data to be transferred.

The second program was called CALIB.ASM and was used to capture the spectral response of the overall system in order to calculate the calibration factors as described above. It was essentially the same as PPGACDC.ASM but only used the DC input channel.

The method used to clock the A/D converters was by using the on board interval timer, which is clocked at 10 MHz. This timer is a 16 bit counter, which is loaded by a value and the starts counting down to zero. At zero an interrupt is created and the counter is reloaded and the process repeated. The lowest limit to the sampling frequency this timer can generate is approximately 153 Hz. However, for these experiments a

sampling frequency lower than 153 Hz was required. To achieve this the timer was set for a sampling frequency of 159 Hz but a sample was taken in every three interrupts, thus producing an effective sampling frequency of 53 Hz.

A description of the PPGACDC.ASM DSP program is given in Appendix C.

3.8.2 PC Program

The program running on the PC was originally written in Turbo Pascal, but later changed to Borland Turbo C, to take advantage of several routines supplied with the DSP board which interfaced with the PC. It provided the PC with overall control of the monochromator driver, by selecting the wavelength range, step value and position; and of the DSP board, by initialising data capture and data exchange. Moreover, it performed all the analysis and display functions as described in section 3.7.1.

The whole process was fully automatic with minimum input from the operator. Functions for saving new data in specified directories, reloading previously recorded data and dumping the displayed results to a printer were also incorporated.

During system testing it was observed that the output of the DSP board channel 1 A/D converter (used for capturing the DC PPG) introduced a DC offset error to the input waveform. Although the DSP56001 board provided an offset adjustment, this proved to be inaccurate and

inadequate. Therefore, an automatic DC offset adjustment function was incorporated in the software, which took the reading of channel 1 at the beginning of each experiment, when that was held at ground potential and then subtracted this offset value from all subsequent DC measurements.

A functional description of the PPGACDC.C program and hardcopies of the screen menus and of typical results are given in Appendix C.

3.8.3 PC - DSP Interface

As mentioned above it was necessary to interface the DSP56001 board with the PC as data had to be transferred from one processor to the other. This was achieved by using the **dsp56** interface library (Loughborough Sound Images Ltd) which provided several functions for transferring single words or blocks of data.

3.9 SYSTEM EVALUATION

Once the full system was constructed its performance was evaluated by comparing the spectra of known samples with the ones obtained using this system. The transmission spectrum of a long pass optical filter, with a cut-off wavelength of 520nm, was captured. This is shown in Fig. 3.6 and compared with the spectrum provided by the manufacturer for this specific filter. The left y-axis shows the captured response and the right y-axis the data provided by the manufacturer. The

responses were normalised and the left y-axis was deliberately offset slightly to provide clearer comparison. From this figure it can be seen that the captured response compares extremely well with the data provided by the manufacturer. The correlation factor was 0.999576 confirming that this system was capable of fulfilling its design criteria.

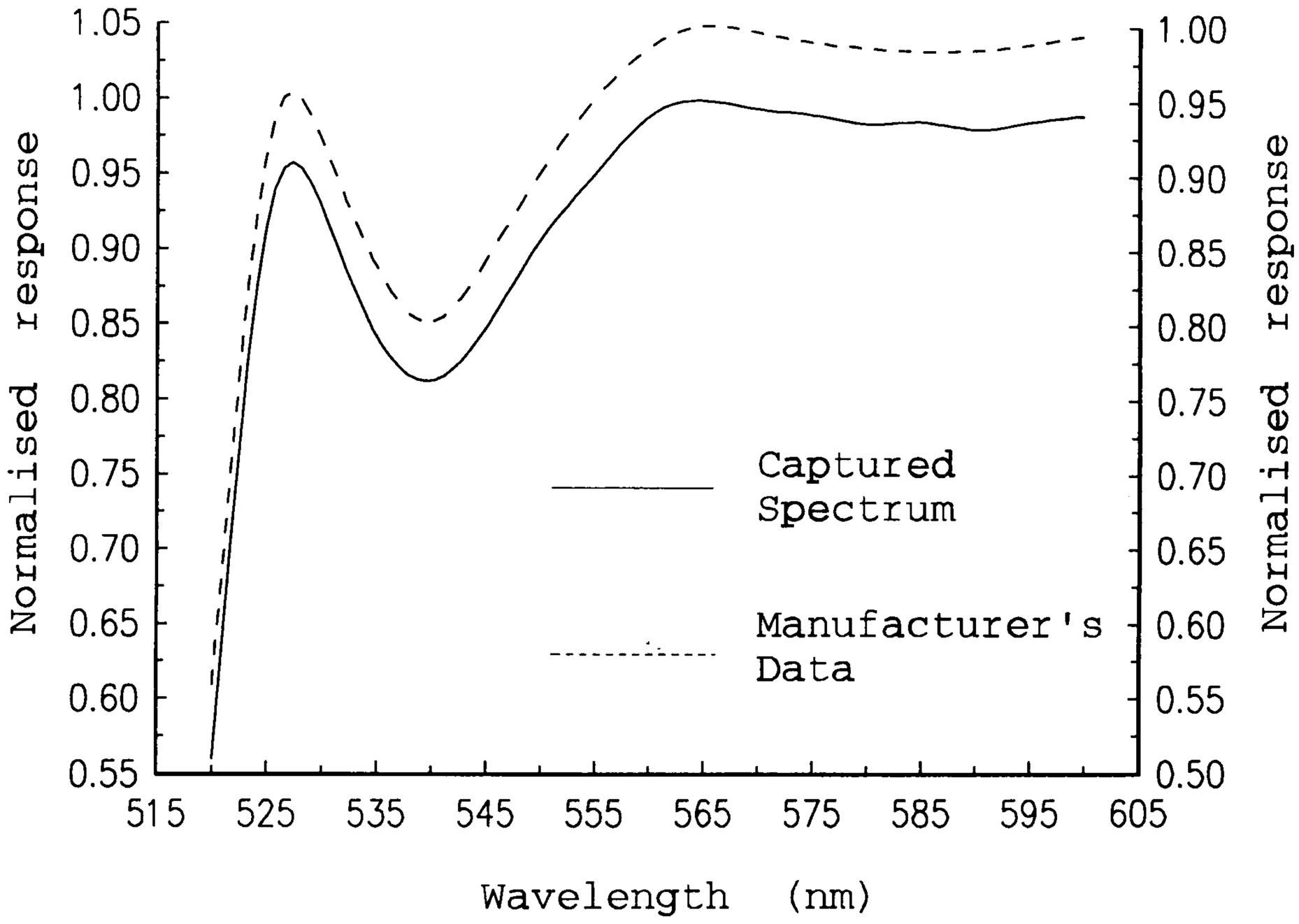

Figure 3.6: Comparison of captured transmission spectrum of long pass optical filter with data provided by the manufacturer, used for testing the developed system. Note offset of right y-axis to facilitate comparison of spectra.

Also the cycle detection function for extracting the AC PPG signal amplitude was tested. Figure 3.7 shows the performance of the cycle detection function on a clean AC PPG signal. The position of the pointers at only the minimum and maximum of each AC PPG cycle, excluding the local minima and maxima of the dicrotic notch, demonstrate the ability of this function for calculating the AC PPG amplitude. Moreover, Figure 3.8 shows that this function can also cope with AC PPG signals that are affected by noise and motion artifacts.

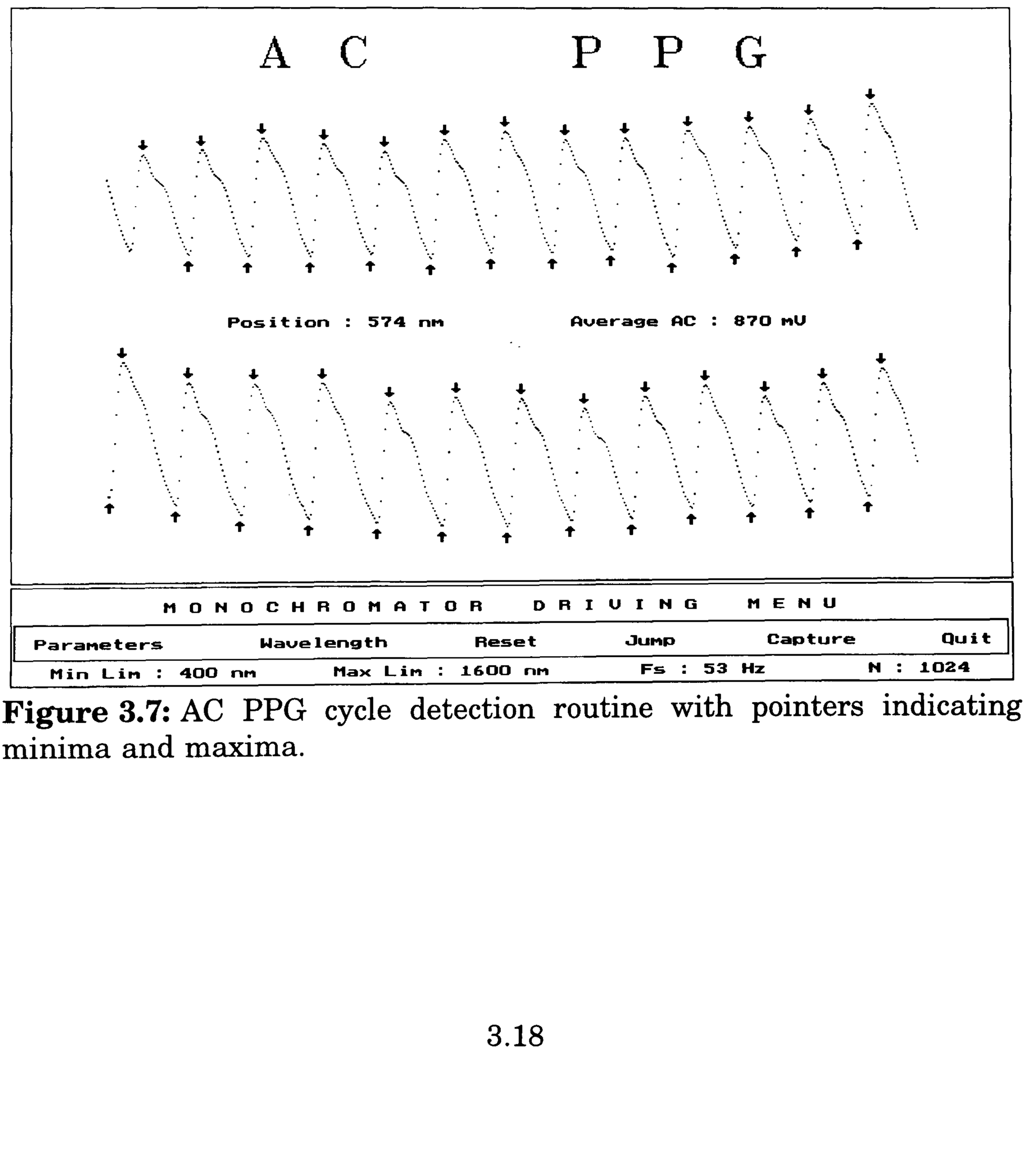

Figure 3.7: AC PPG cycle detection routine with pointers indicating minima and maxima.

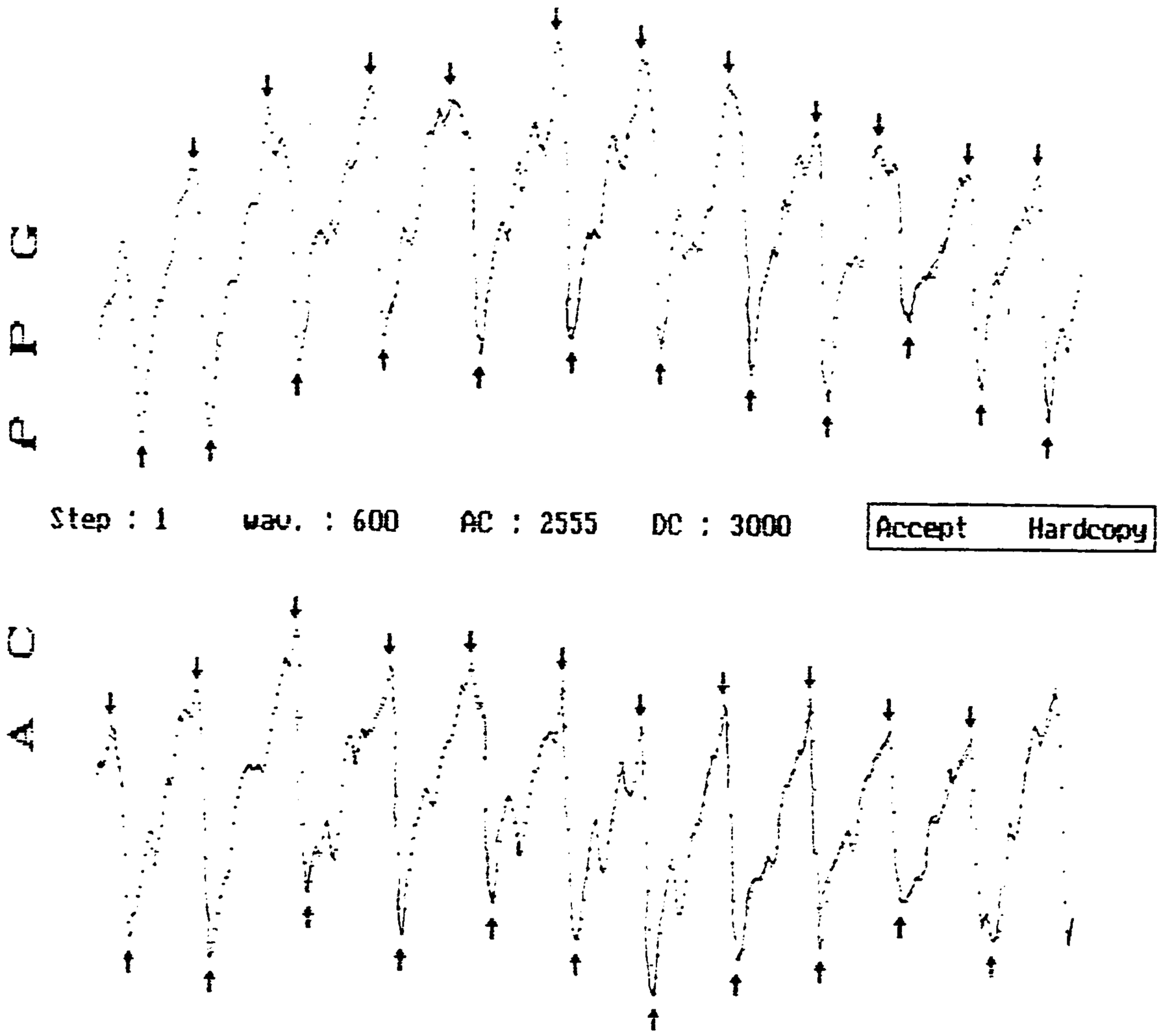

Figure 3.8: The PPG cycle detection function is able to cope with signals affected by noise and motion artifacts.

CHAPTER 4

WAVELENGTH STUDIES

RESULTS AND DISCUSSION

4.1 INTRODUCTION

Before presenting and discussing the results of the wavelength dependence studies of the AC and DC PPG signals and the AC/DC ratio, the current pulse oximetry theory as described in section 2.1 is summarised. The theory of pulse oximetry has evolved from the theory of oximetry and thus is based on the Lambert-Beer law. Pulse oximetry is explained by comparing transmission through tissue with transmission through an imagined cuvette, which contains a non blood compartment (tissue, bone), blood and arterial blood. The DC PPG signal is assumed to be due to the absorption of the non blood compartment and the blood that is present at the end of the outflow phase. The AC PPG signal is assumed to be created by a pulsatile change in the thickness of the cuvette caused

by the flow of arterial blood. The oxygen saturation predicted by this theory given by the ratio of the AC/DC (the **R** ratio) at two wavelengths, is equal to the ratio of the absorption coefficients of arterial blood for these wavelengths. This model, however, does not take into account scattering of light by tissue and blood, even though it is widely acknowledged and accepted that scattering plays an important role. Thus pulse oximeters are calibrated empirically due to the deviations of the **R** ratio versus SpO_2 from the theoretically derived relationship.

From the simple model of a finger described above and shown in Fig. 2.1 and applying the Lambert-Beer law (see eq. 1.4) that pulse oximetry is currently based on, the following expressions for the AC and DC signals are obtained:

$$I = I_{DC} = I_o\ 10^{-A} = I_o\ 10^{-(\varepsilon_t C_t + \varepsilon_b C_b)L} \tag{4.1}$$

$$I' = I_{DC+AC} = I_o\ 10^{-A'} = I_o\ 10^{-(\varepsilon_t C_t + \varepsilon_b C_b)L}\ 10^{-\varepsilon_{ab} C_{ab} \Delta L} \tag{4.2}$$

$$I_{AC} = I_{DC} - I_{DC+AC} = I_o\ 10^{-(\varepsilon_t C_t + \varepsilon_b C_b)L}\ (1 - 10^{-\varepsilon_{ab} C_{ab} \Delta L}) \tag{4.3}$$

where: ε_t absorption coefficient of non blood compartment

C_t concentration of non blood compartment

ε_b absorption coefficient of blood

C_b concentration of blood

ε_{ab} absorption coefficient of extra arterial blood

C_{ab} concentration of arterial blood.

The AC/DC ratio is given by:

$$\frac{I_{AC}}{I_{DC}} = 1 - 10^{-\epsilon_{ab} C_{ab} \Delta L} = 1 - e^{-2.3 \epsilon_{ab} C_{ab} \Delta L} \qquad (4.4)$$

For small ΔL the AC/DC ratio is approximated by:

$$\frac{I_{AC}}{I_{DC}} \approx 2.3 \epsilon_{ab} C_{ab} \Delta L \qquad (4.5)$$

Therefore from the existing theory of pulse oximetry for a healthy subject with normal oxygen saturation levels (assuming $\varepsilon_{ab} = \varepsilon[HbO_2]$), from equation 4.5 the AC/DC ratio should be approximately proportional to the absorption spectrum of oxyhaemoglobin.

In this chapter the results from the studies on the wavelength dependence of both the AC and DC photoplethysmograms, as defined in section 1.3, are presented. Since pulse oximetry uses the AC/DC ratio of the PPG signal at two wavelengths to calculate oxygen saturation, investigation of the behaviour of the AC/DC ratio over the wavelength range that pulse oximeters operate is important in order to observe any deviations either from the wavelength dependence predicted by existing pulse oximetry theory or between reflection and transmission mode.

Therefore, in line with the current pulse oximetry theory the AC/DC ratio is compared and discussed in relation to the absorption spectrum of oxyhaemoglobin. Moreover, the calibrated AC and DC PPG signals are compared with the absorption spectrum of oxyhaemoglobin to

examine the effect of oxyhaemoglobin in their behaviour.

It must be emphasised that all results obtained are based simply on the direct comparison of the experimental behaviour of the AC/DC ratio and the ratio expected from the existing theory, for each mode and range. Due to the shape of the absorption spectra of oxy- and deoxyhaemoglobin (see section 1.2.1 and Fig. 1.4), which present a steep increase below 600nm, the results were split at 600nm. This was necessary due to the technical limitations of the optical system as explained in detail in sections 3.5 and 3.7. The results above 600nm in each mode are presented first, followed by the results below 600nm.

The majority of the experiments were performed on the left index finger of the same subject in the sitting position. The finger rested loosely in a custom made holder, shown in Appendix B, designed to minimise movement artifacts. The subject was a healthy male Caucasian nonsmoker, aged 27. Similar measurements were performed on the same finger of different subjects for comparison and reasons of verification. Since a non modulated optical set up was used, all measurements were performed in a dark room to minimise any interference from background light.

The common problem of reproducibility of *in vivo* optical measurements was experienced as expected. This meant that although the nature of the individual graphs of AC and DC signals versus wavelength for a specific range were similar, the absolute values of the measurements differed. Consequently, averaging the results without

normalisation cannot be achieved without giving a negatively false impression of the accuracy of the measurements. Therefore, for the purposes of discussing the wavelength dependence of the PPG signals, typical AC and DC PPG signals are presented for each range and mode. A condensed version of the results presented here is situated in a fold-out page at the end of this chapter for ease of reference. More results for each range and mode and for different subjects are shown in Appendix E.

4.2 WAVELENGTHS ABOVE 600nm

All commercially available pulse oximeters are reliant on measurements at wavelengths in the red and near infrared (usually 660nm and 940nm) to calculate the oxygen saturation. Therefore, this wavelength range is considered first.

4.2.1 The DC PPG signals

Figure 4.1 shows the wavelength dependence of the DC PPG signals from 600nm to 1000nm in transmission and reflection modes in comparison to the absorption spectrum of oxyhaemoglobin.

In transmission the DC signal presents a maximum in the region of 660-720nm, this being the region of low oxyhaemoglobin absorption. The overall behaviour of the signal is that of an inverse relationship with the absorption spectrum of oxyhaemoglobin.

In reflection the DC signal also presents a maximum in the region of 660-720nm due to the influence of oxyhaemoglobin. However, this influence is not as clear as in the transmission mode especially in the lower part of this range.

The effect of the water absorption peaks at 975nm and at 760nm (not so clearly) can also be seen.

4.2.2 The AC PPG signals

Figure 4.2 shows the wavelength dependence of the AC PPG signals from 600nm to 1000nm in transmission and reflection modes in comparison to the absorption spectrum of oxyhaemoglobin.

In transmission the AC signal in this range follows the inverse of the absorption spectrum of oxyhaemoglobin.

In reflection the AC signal follows the absorption spectrum of oxyhaemoglobin up to about 800nm. In the range 800 - 1000nm the AC signal shows a response similar to the one observed for the transmission studies, that is, it follows the inverse of the absorption spectrum of oxyhaemoglobin. The AC signal also presents a minimum at 660nm and the importance of this is discussed later.

4.2.3 The AC/DC ratio

Figure 4.3 shows the wavelength dependence of the AC/DC ratio from 600nm to 1000nm in transmission and reflection modes in

comparison to the absorption spectrum of oxyhaemoglobin.

In transmission mode the behaviour of the DC and AC PPG signals is very similar, with the general trend being inverse to the absorption of oxyhaemoglobin. However, there are slight differences in the individual trends over the whole range. These differences seem to be giving the AC/DC ratio structure which follows the absorption spectrum of HbO_2 (from 600-840nm).

In reflection the AC/DC ratio follows the absorption spectrum of HbO_2 up to 720nm, but above this range it increases at a steeper rate.

4.3 WAVELENGTHS BELOW 600nm

The interest in the wavelength dependence of the PPG below 600nm lies with whether or not these wavelengths can be of any practical use in future pulse oximeters, by exploiting the more pronounced absorption spectra of haemoglobin derivatives, in order, for example, to increase the accuracy of pulse oximetry and its ability to distinguish between other forms of haemoglobin but oxy- and deoxyhaemoglobin.

The wavelength range studied is from 450 to 590nm. However, for the transmission studies, weak signals due to the higher absorption involved, resulted in unreliable readings below 490nm. Consequently, results for this mode are presented from 490 to 590nm only.

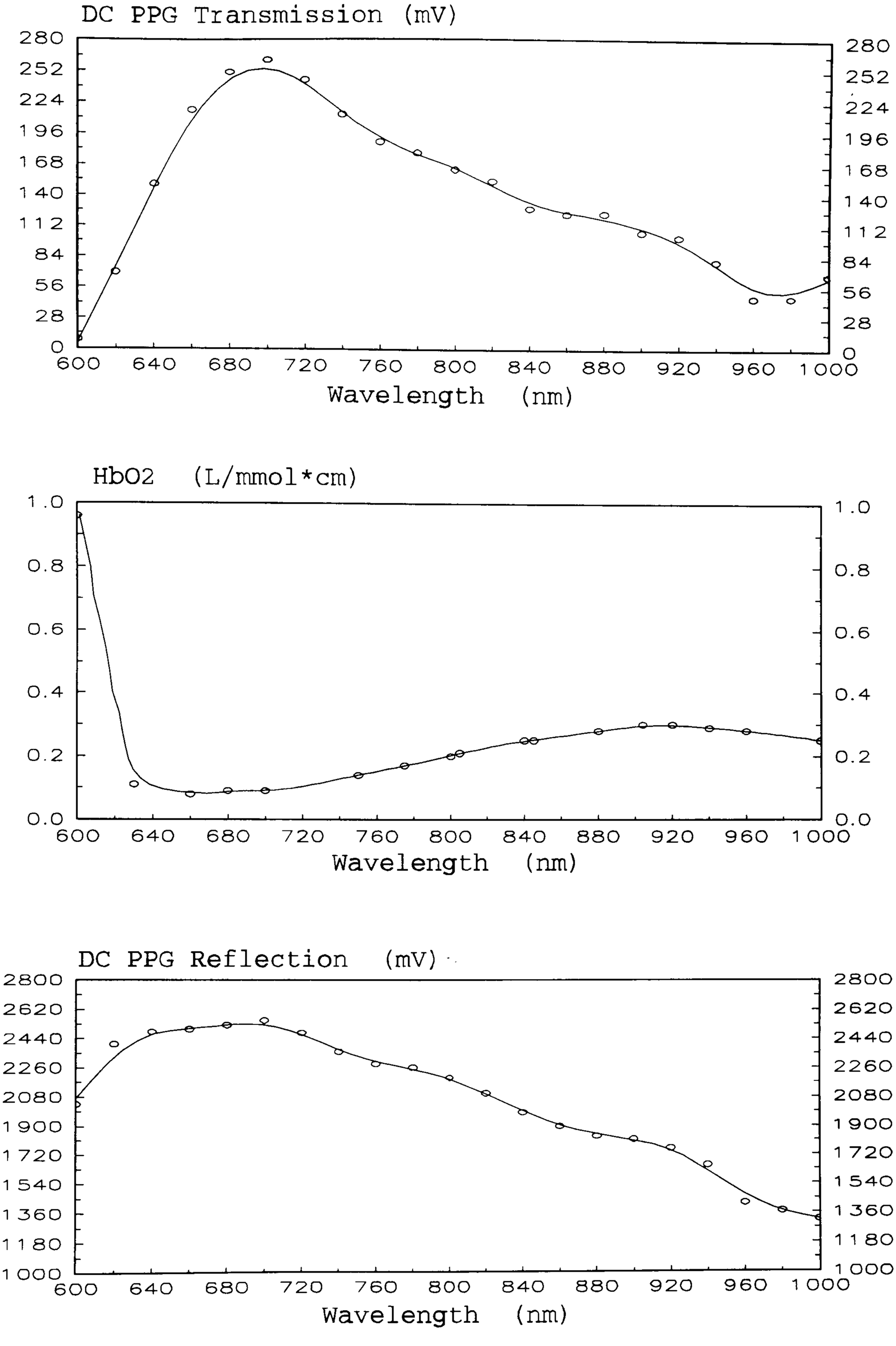

Figure 4.1: The DC PPG signals in transmission mode (top) and reflection mode (bottom) compared in relation to the absorption of oxyhaemoglobin.

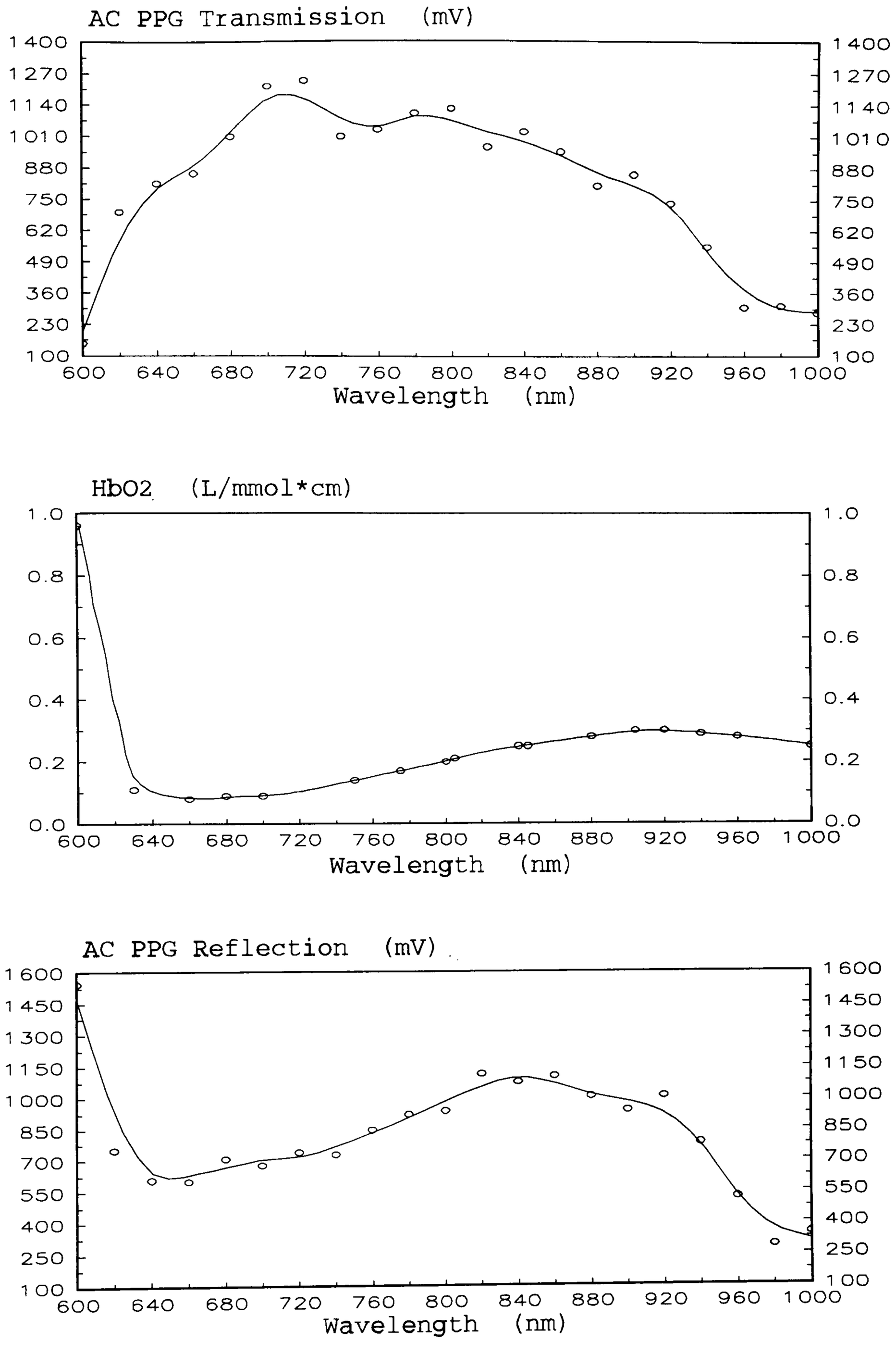

Figure 4.2: The AC PPG signals in transmission mode (top) and reflection mode (bottom) compared in relation to the absorption of oxyhaemoglobin.

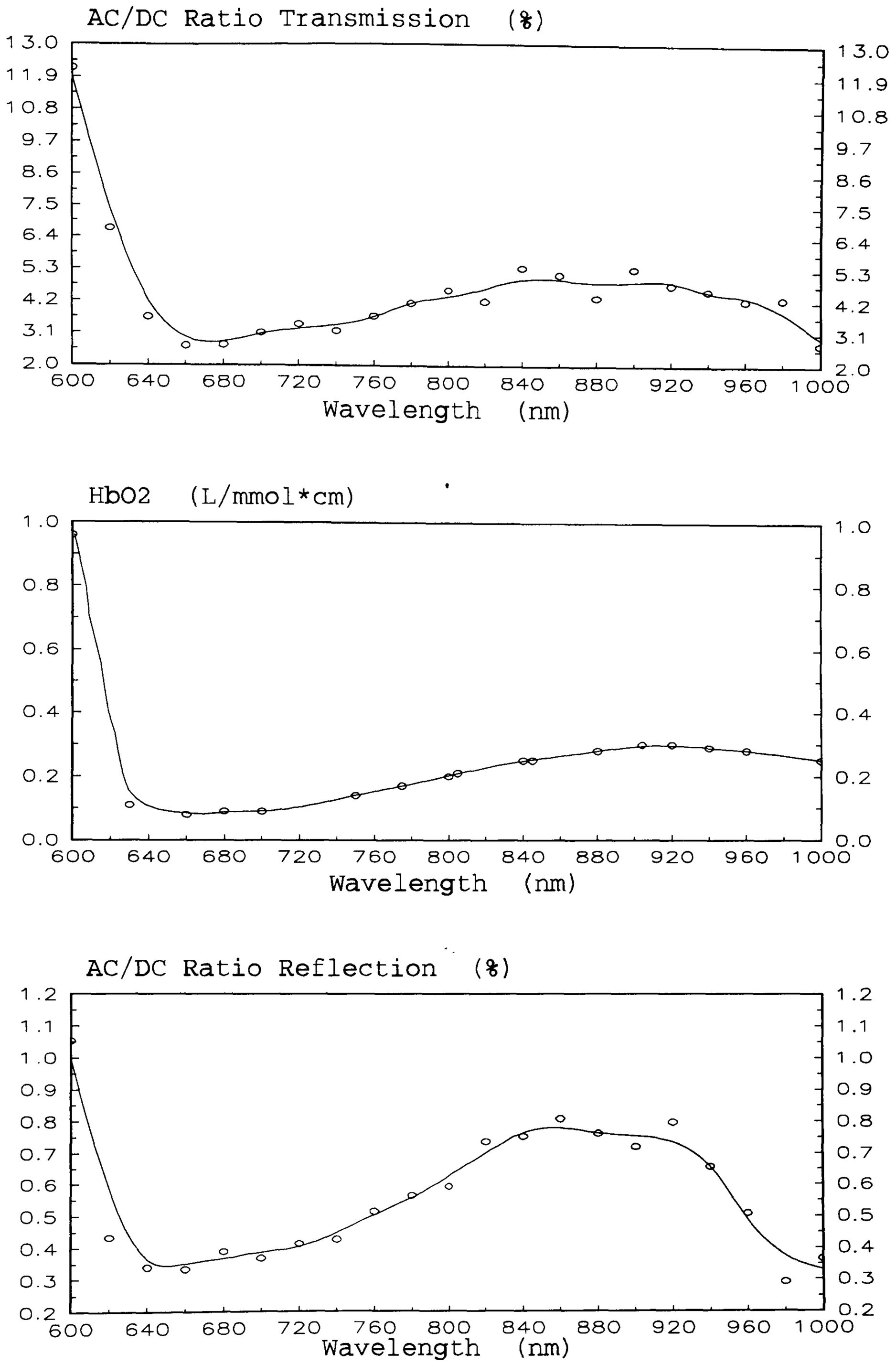

Figure 4.3: The AC/DC ratio in transmission mode (top) and reflection mode (bottom) compared in relation to the absorption of oxyhaemoglobin.

4.3.1 The DC PPG signals

Figure 4.4 shows the wavelength dependence of the DC PPG signals from 450nm to 590nm in transmission and reflection modes in comparison to the absorption spectrum of oxyhaemoglobin.

In transmission as in the above 600nm range, the DC signal below 600nm follows the inverse of the absorption spectrum of oxyhaemoglobin.

In reflection again the DC signal presents an inverse relationship with oxyhaemoglobin

4.3.2 The AC PPG signals

Figure 4.5 shows the wavelength dependence of the AC PPG signals from 450nm to 590nm in transmission and reflection modes in comparison to the absorption spectrum of oxyhaemoglobin.

In transmission the AC signal follows the inverse of the absorption spectrum of oxyhaemoglobin, in the same way as the DC signal.

In reflection the AC signal follows the absorption spectrum of oxyhaemoglobin with the two peaks at 542 and 578nm clearly defined.

4.3.3 The AC/DC ratio

Figure 4.6 shows the wavelength dependence of the AC/DC ratio from 450nm to 590nm in transmission and reflection modes in comparison to the absorption spectrum of oxyhaemoglobin.

In transmission although the data here seems to be more scattered, the AC/DC ratio clearly exhibits an inverse relationship with HbO_2 which is in contrast to the AC/DC ratio at wavelengths above 600nm. The transition from the inverse relationship to the proportional relationship appears at around 590nm. This was examined in more detail by performing a further set of experiments shown in Fig. 4.7 that zoomed into the wavelength range of interest, with data taken at much shorter sampling intervals.

In reflection the percentage modulation of the PPG signal, that is the AC/DC ratio, is higher than for wavelengths above 600nm and follows the absorption spectrum of oxyhaemoglobin. A higher AC/DC ratio below 600nm was also observed by Crowe (Crowe, 1986) and Cui (Cui, 1990). Moreover, for wavelengths shorter than 600nm the shape of the AC PPG signal was smoother and the amplitude was higher (see Fig. 4.10).

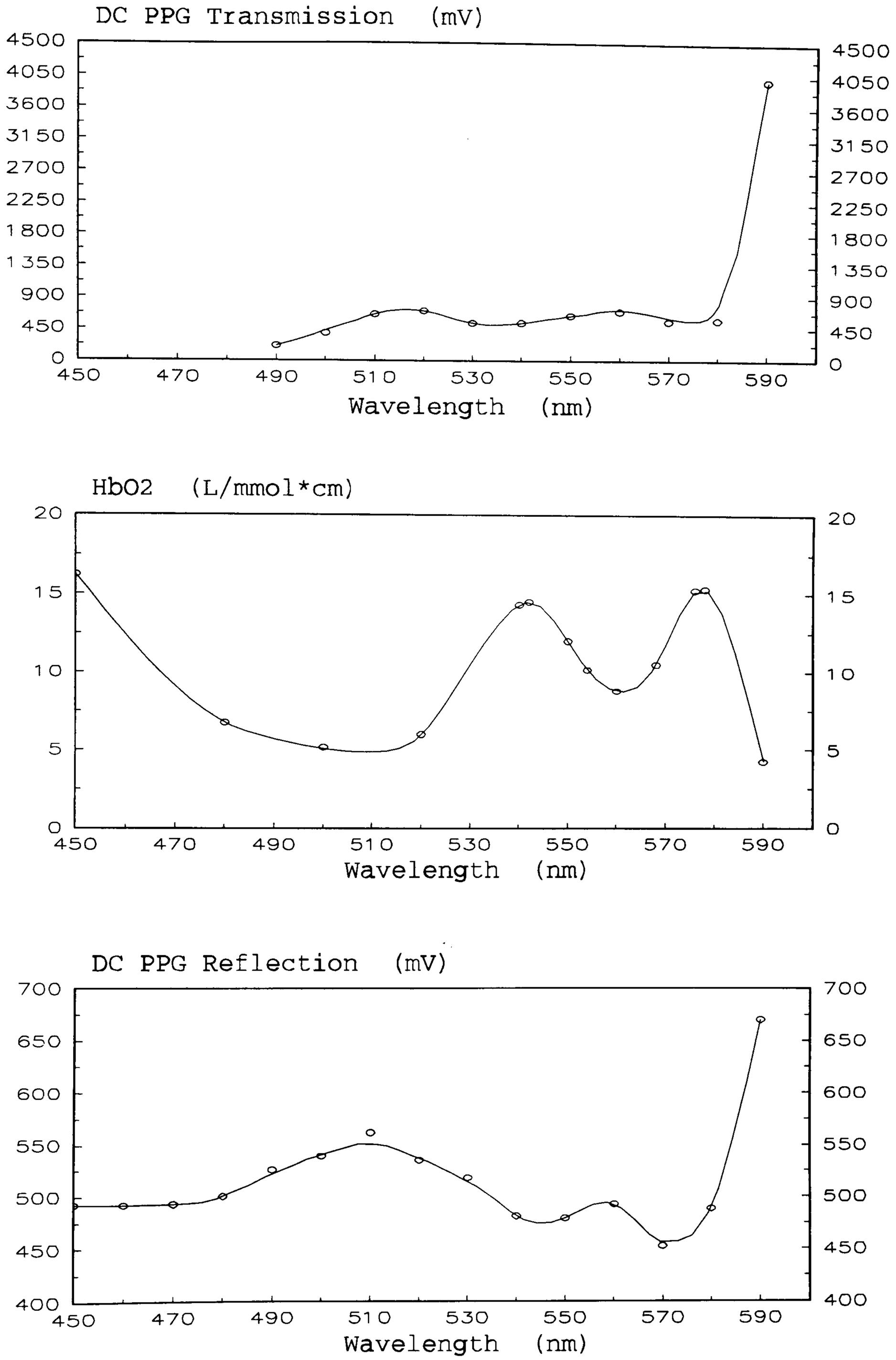

Figure 4.4: The DC PPG signals in transmission mode (top) and reflection mode (bottom) compared in relation to the absorption of oxyhaemoglobin.

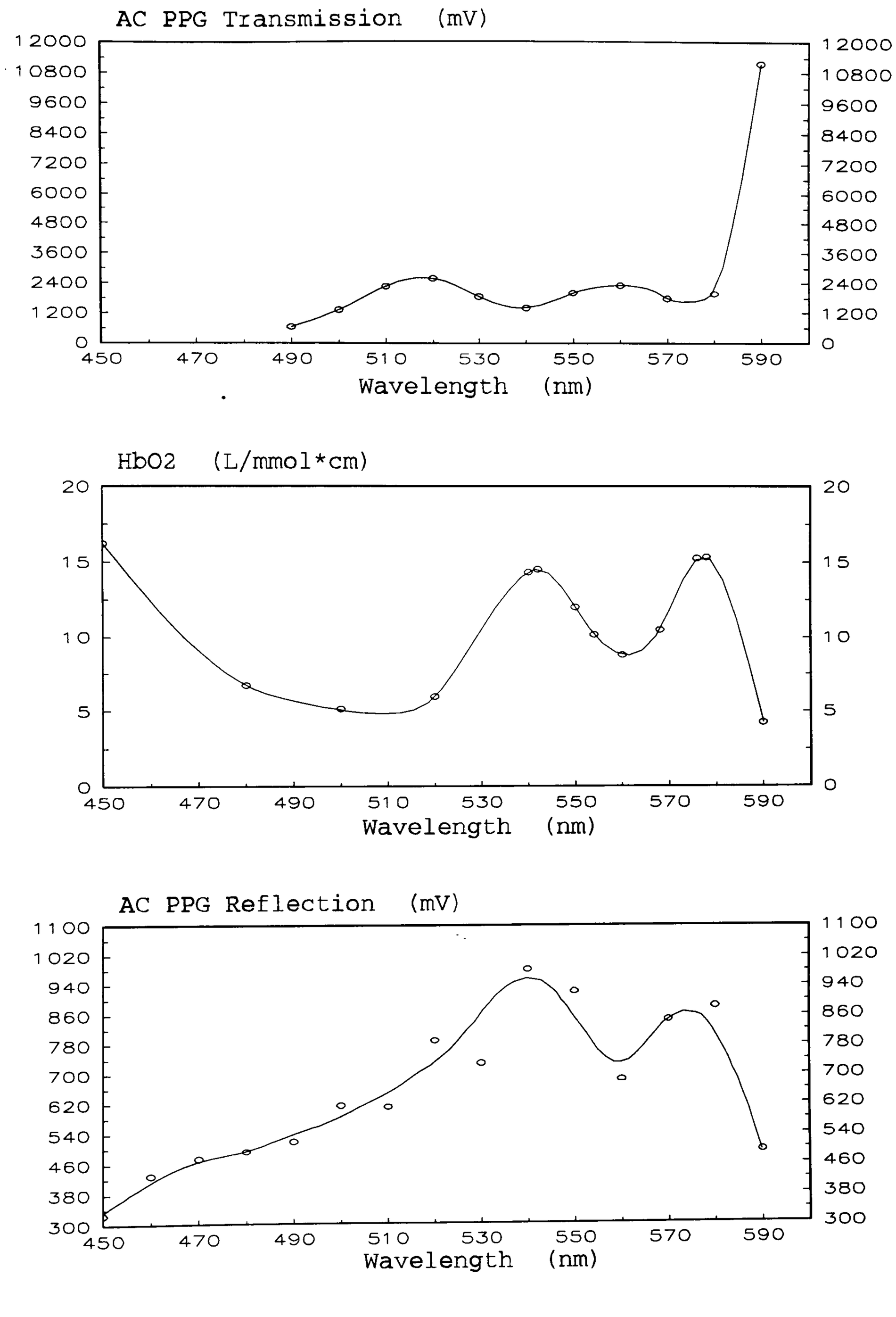

Figure 4.5: The AC PPG signals in transmission mode (top) and reflection mode (bottom) compared in relation to the absorption of oxyhaemoglobin.

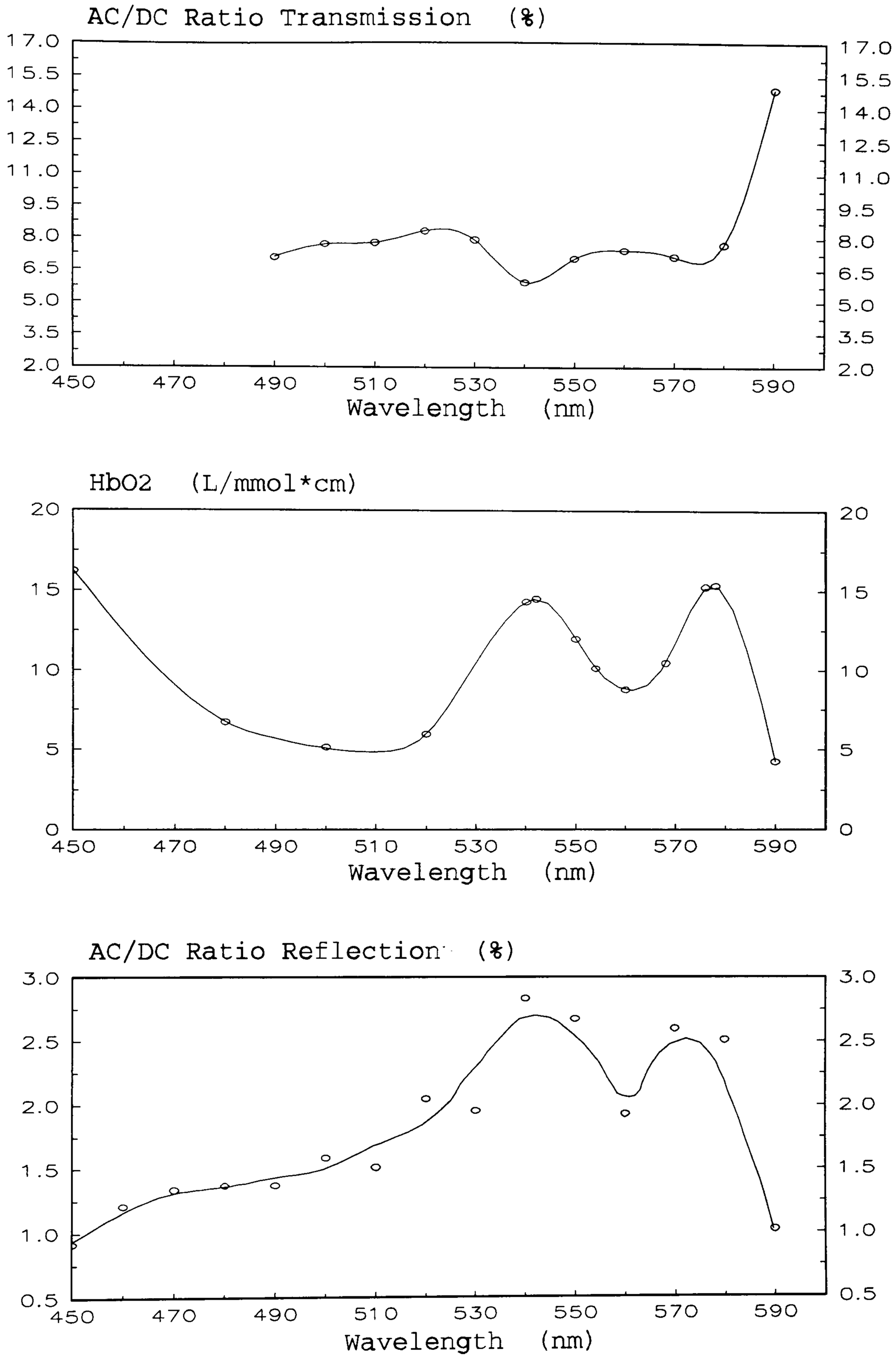

Figure 4.6: The AC/DC ratio in transmission mode (top) and reflection mode (bottom) compared in relation to the absorption of oxyhaemoglobin.

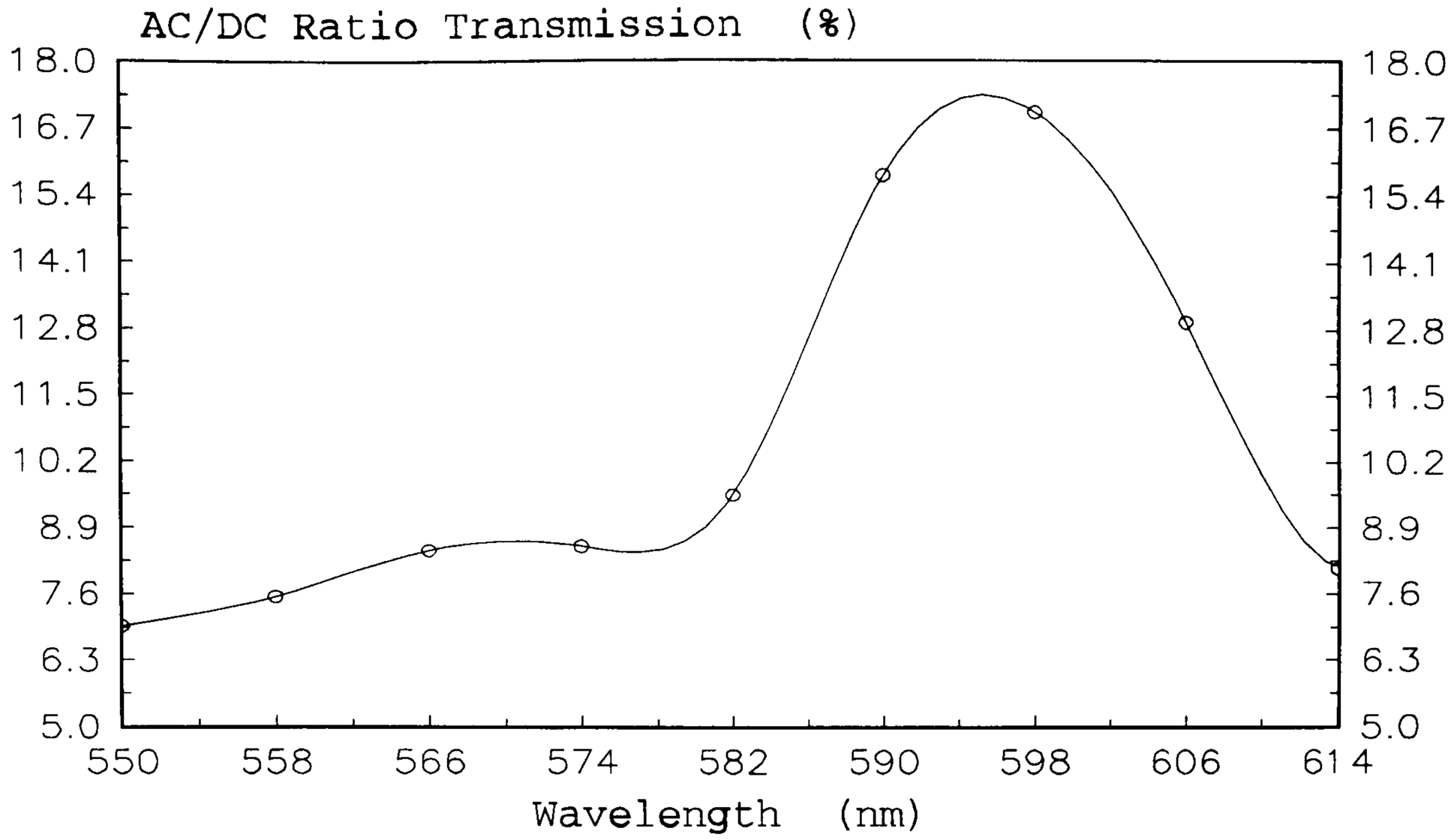

Figure 4.7: The AC/DC ratio in transmission indicating the transition in its behaviour.

4.4 REFLECTION OR TRANSMISSION ?

Further experiments were carried out in reflection mode with two 1.5mm fibres placed side by side. The distance between the two fibres was increased from the original of 3mm to 7mm, in order to study the effect of this change on the wavelength dependence of the AC/DC ratio. These results (Fig. 4.8) show a transition from reflection to transmission behaviour with increasing separation between the two fibres.

4.5 DISCUSSION

The results obtained in sections 4.2 - 4.4 above are discussed and compared here with the behaviour expected from a Lambert-Beer based

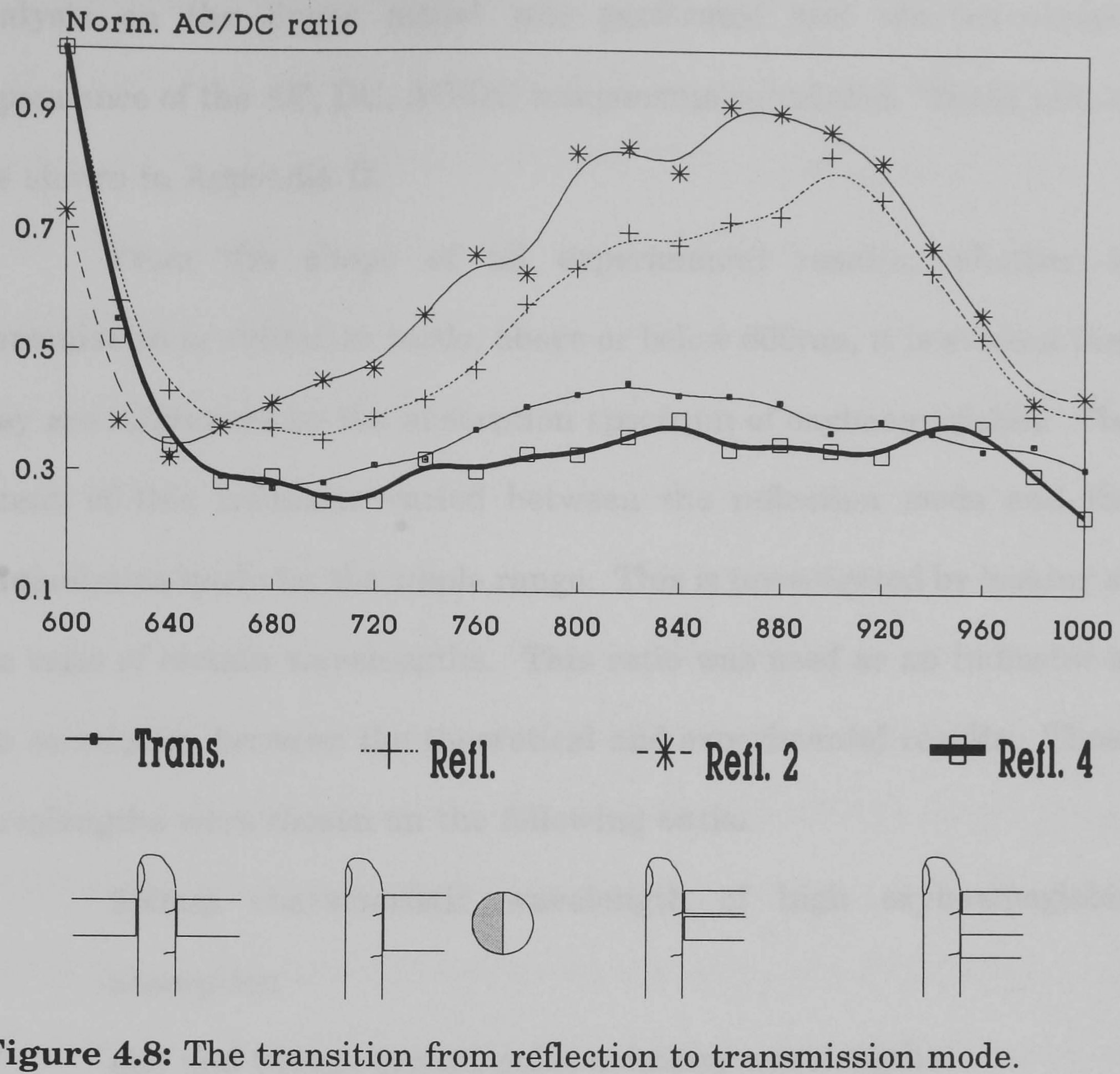

Figure 4.8: The transition from reflection to transmission mode.

model used to describe pulse oximetry in chapter 2 and in the introductory section of this chapter.

4.5.1 Comparison of experimental results with Lambert-Beer model

In this model the finger was approximated as a system of three concentric cylinders representing three different layers; dermis-blood, fat-blood and bone. The blood was assumed to be homogeneously distributed with a base volume of 10% which increased by a further 10%, simulating the influx of arterial blood. This model and the absorption characteristics

of the constituents are described in detail in section 5.4. A Lambert-Beer analysis on the finger model was performed and the wavelength dependence of the AC, DC, AC/DC components calculated. These results are shown in Appendix D.

From the shape of all experimental results, whether in transmission or reflection mode, above or below 600nm, it is evident that they are influenced by the absorption spectrum of oxyhaemoglobin. The extent of this influence varied between the reflection mode and the transmission mode for the whole range. This is investigated by looking at the ratio of certain wavelengths. This ratio was used as an indicator of the correlation between the theoretical and experimental results. These wavelengths were chosen on the following basis:

560nm characteristic wavelength of high oxyhaemoglobin absorption

660 and 940nm typical pulse oximetry wavelengths

In the case of the transmission mode the DC PPG signal follows a pattern similar to the inverse of the absorption spectrum of oxyhaemoglobin, with the characteristic absorption peaks at the known wavelengths. However, it does not follow the magnitude predicted by the model. The DC ratio at 660 to 560 is of 22 orders of magnitude (as shown in Appendix D, table D.2) whereas the experimental results show a ratio of approximately only 2 orders of magnitude (see Fig. E.13).

In reflection mode the DC PPG signal also follows a pattern similar to the inverse of the absorption spectrum of oxyhaemoglobin, with

the characteristic absorption peaks at the known wavelengths. As with the transmission mode it does not follow the magnitude predicted by the model and in this case the experimental 660/560 ratio is only 2 (see Fig. 4.9). This is probably due to lower average pathlengths and also may be due to lower concentration of blood in the outer layers of the fingertip; the end result being a reduced influence due to oxyhaemoglobin absorption. A similar wavelength dependence for the DC signal was observed by Takatani (Takatani, 1989).

The value of the AC/DC ratio for both reflection and transmission modes is higher for wavelengths below 600nm than for wavelengths above 600nm. Again for both modes the experimental AC/DC values for the 560/660 ratio are much smaller in magnitude compared to the values obtained from the model. However, the experimental values (which are in agreement with published data, Fig. 2.4) for the 660/940 ratio are approximately twice the values obtained from the model. The results from the model also fail to explain the transitional behaviour (Fig. 4.7) of the transmission AC/DC ratio in the below 600nm range. In reflection mode the experimental value of 5 for the AC/DC ratio at 560/660nm is of the same order observed by Cui (Cui, 1990).

These experimental results clearly show that the existing simple model for pulse oximetry, which is still based on the Lambert-Beer law, is inadequate. Furthermore, it does not explain the wavelength dependence of the photoplethysmogram for the wavelength range 450 - 1000nm studied here for the two modes.

In the model used it has been assumed that the layers of dermis-blood and fat-blood are homogeneous. Even the introduction of scattering would not solve the problem, it would actually produce greater fluctuations due to the extra attenuation from scattering losses. However, in practice the tissues are structurally inhomogeneous usually consisting of multiple layers with the red blood cells contained within the capillaries and within larger and smaller blood vessels. Thus the discrepancies from the experimental results and the behaviour expected from the model could be due to the inhomogeneties where the received light does not interact with blood in such a way as the homogeneous model suggests. These discrepancies are higher in the below 600nm region. A plausible explanation for this behaviour of the existing model could be due to the fact that the absorption coefficient of blood in this range is much higher (by 2 orders of magnitude) and any errors due to blood concentration and distribution are exaggerated. For wavelengths above 600nm the absorption coefficient of blood is lower and of similar value to the surrounding tissue. Therefore any errors due to the distribution or total amount of blood in the model are small.

4.5.2 The AC signal in reflection mode

The AC signal in reflection (for the whole 450 - 800nm range) follows the absorption of oxyhaemoglobin, and this is in direct contrast to the transmission results. In the range 800 - 1000nm it follows the inverse of the absorption spectrum of oxyhaemoglobin, a response similar to the

one observed for the transmission studies. This change in proportionality in the AC signal in reflection could be due to the fact that the received light interacted with deeper layers of tissue (therefore longer pathlength), since light at longer wavelengths penetrates deeper because of a decrease in scattering and absorption.

Moreover, the amplitude of the AC signal was higher below 600nm than above, and this is in direct contrast to the transmission results. The income of arterial blood changes the original blood concentration by introducing extra blood absorption. The greater the absorption coefficient of blood at a certain wavelength with respect to the surrounding tissue absorption the bigger the drop in reflected intensity and the bigger the amplitude of the AC signal. This explains the observed response of the AC signal. This is in direct agreement with results obtained by Cui (Cui, 1990) and Lindberg (Lindberg, 1991). The behaviour of the AC and DC PPG signals from 540 - 680nm indicating the above point is shown in Fig. 4.9. The behaviour of the reflection AC signal could be explained by assuming that most of the signal is modulated by the arterial pulse. On the contrary, in the case of the transmission AC the behaviour is different because there is less light (due to higher overall absorption) to be modulated.

The fact that the AC signal below 600nm in reflection mode is higher than above 600nm, could be utilised by incorporating extra wavelengths below 600nm, where haemoglobin has characteristic spectra, in the reflection oximeter's probe. This could be of great clinical

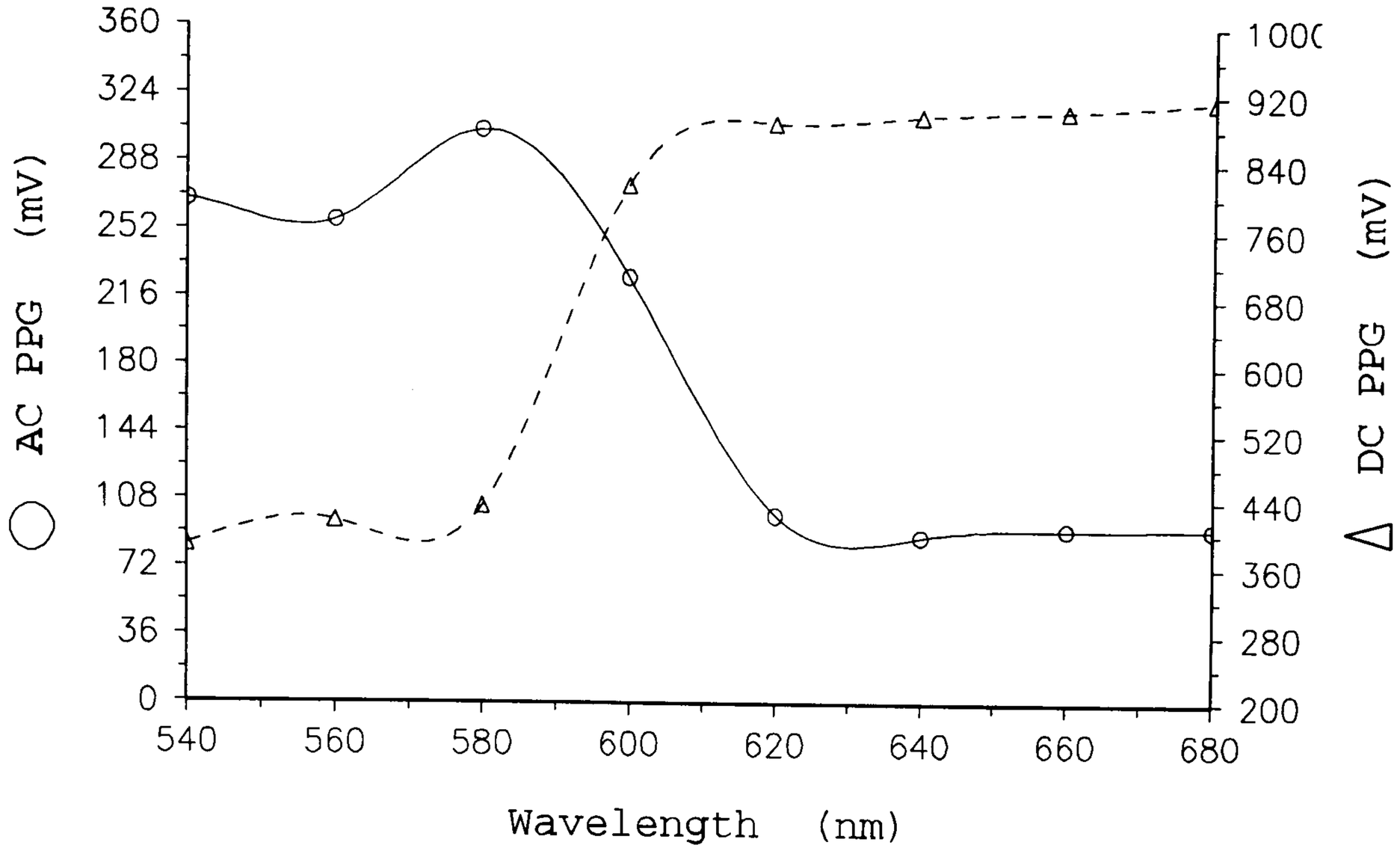

Figure 4.9: AC and DC PPG components in reflection for the 540 - 680nm range.

importance, as the introduction of the extra wavelengths means that the oximeter could account for all forms of haemoglobin other than oxyhaemoglobin and deoxyhaemoglobin, in its calculation of oxygen saturation. Thus a limitation of present pulse oximeters would be overcome, with the scope of being used in new areas. For example, it could be used in relation to fire victims that have higher levels of carboxyhaemoglobin without the uncertainty of false or ambiguous oxygen saturation readings.

In reflection mode again, of great concern is the fact that the AC signal amplitude at 660nm presented a minimum and also had the worst signal to noise ratio. Two typical traces of AC PPG signals, one at 660nm the other at 570nm, are shown in Fig. 4.10.

The importance of this is that the 660nm wavelength is used by the pulse oximeter algorithm in order to calculate oxygen saturation. Most

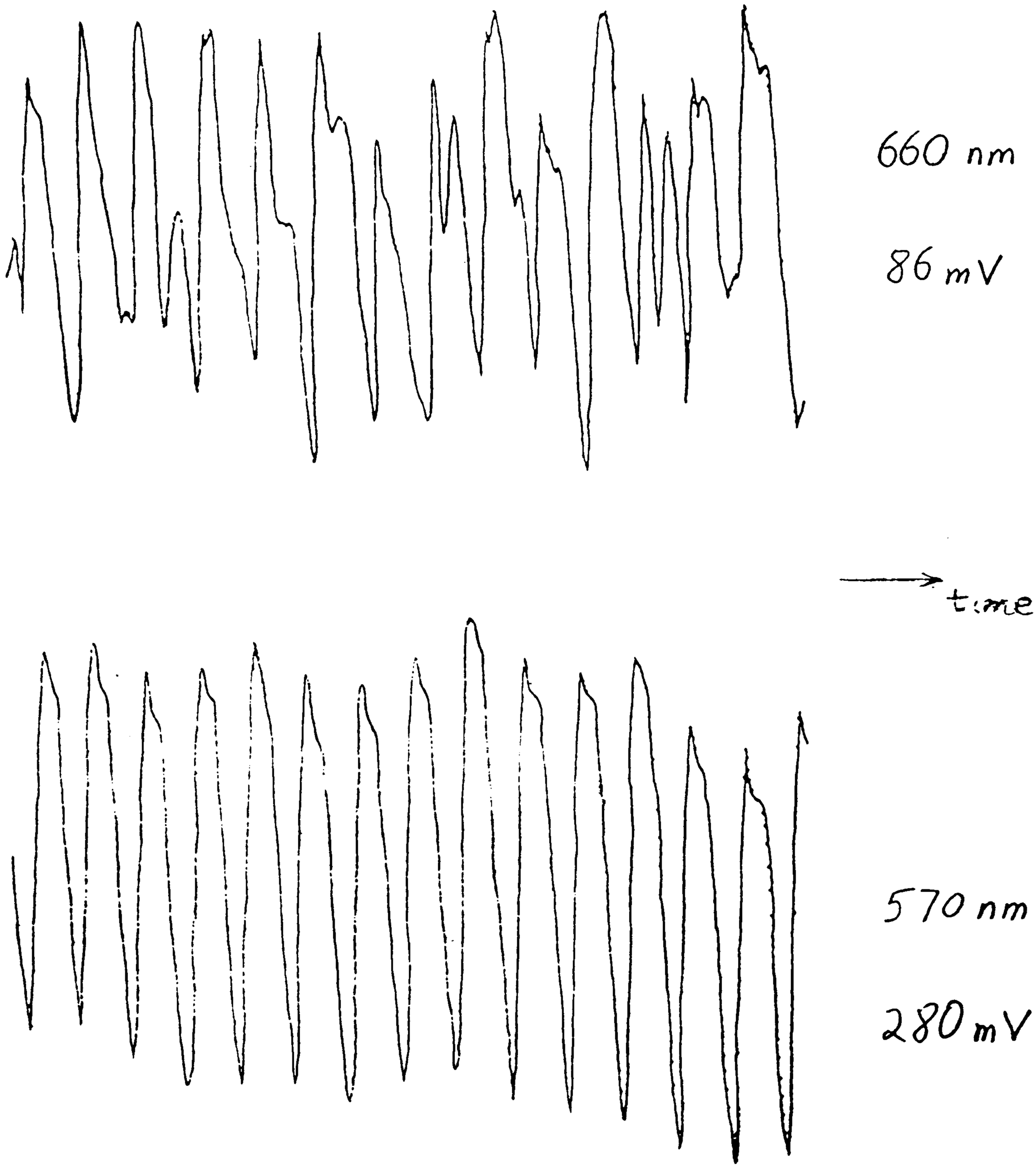

Figure 4.10: Typical AC PPG signals at 660nm (top) and 570nm.

modern pulse oximeters offer a plethysmographic display along with oxygen saturation values and heart rate. The displaying of the pulsatile signal is used to validate (in a way) the oxygen saturation reading, since the physician can check whether the oximeter is locked on a good signal.

However, most pulse oximeters tend to display only the infrared (940nm) channel, and in reflection mode this can be misleading taking into consideration the problems reported here with the 660nm wavelength (see section 4.2.2 and figures 4.2, 4.10). The possibility of using other suitable wavelengths for reflection mode pulse oximetry should be investigated.

4.5.3 Comparison of Transmission and Reflection

Luckily, for pulse oximetry for the two wavelengths employed in the calculation of SpO_2 the shortcomings of this simple model are not so evident. This is apparent from the very similar values recorded for the ratio **R** (the AC/DC ratio of 660 over 940nm as used by commercial pulse oximeters) for transmission and reflection modes. It is for this reason that pulse oximeters used with either a transmission probe or a reflection probe seem to be giving the same results. If however, another wavelength but 940nm was employed then the values of the ratio for transmission and reflection would have been very different (see Fig. 4.3). This coincidence prevented research like the work performed here from being carried out earlier, the result being an over simplified Lambert-Beer law based model being used to explain pulse oximetry.

The results presented in section 4.4 where the separation distance between two reflection fibre bundles was increased, demonstrate that the underlying processes of reflection and transmission photoplethysmography are different. With increasing distance between the fibre bundles the wavelength behaviour of the photoplethysmogram

changed from a reflection one to a transmission one. These results are of significance to reflection probe designers and are supported by results by Mendelson (Mendelson, 1988a) and Graaff (Graaff, 1991) where they found that oxygen saturation readings also varied with distance of detector from emitter.

4.6 FURTHER WORK

Some new areas of further work can be identified following these results. As mentioned earlier these studies were performed on healthy volunteers with the assumption of normal oxygen saturation levels. The same studies could be performed on healthy volunteers undergoing a controlled study of reducing SaO_2 levels. This will give further valuable information on the relationship between the AC, DC and AC/DC components with respect to the reduced value of SpO_2 at each wavelength and mode. Information of this type is critical for the accurate development of a model on pulse oximetry.

Secondly the same study as above could be performed on the model finger developed by De Kock and Reynolds. Comparisons of these results with the ones performed on volunteers will provide a further test on the behaviour and accuracy of the model finger, and assist in its further development. A successful development of a model finger would facilitate beneficial research to be carried out in assessing new pulse oximeter models, comparison of the performance of different models and testing of

existing monitors.

Following observations made here regarding the size of the AC PPG signals in reflection mode for wavelengths below 600nm, the possibility of utilising these wavelengths in future designs of pulse oximeters should be seriously considered. This possibility is examined and described in more detail in chapter 7 where a new type of reflection pulse oximeter is proposed.

4.7 CONCLUSION

The experimental results on the wavelength dependence of the AC, DC and AC/DC PPG components for the 450 - 1000nm range are without doubt different to the ones predicted by the current pulse oximeter model. Moreover, the results obtained thus far show distinct differences between the reflection and transmission modes.

In conclusion these results suggest that perhaps the wavelengths used for pulse oximetry should be reconsidered, together with the assumption that oxygen saturation readings taken in this manner will always be independent of the mode of operation.

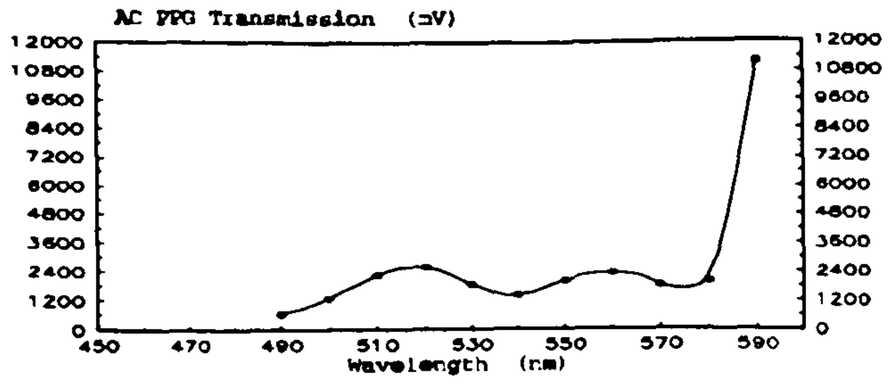
AC PPG Transmission (mV)
Wavelength (nm)

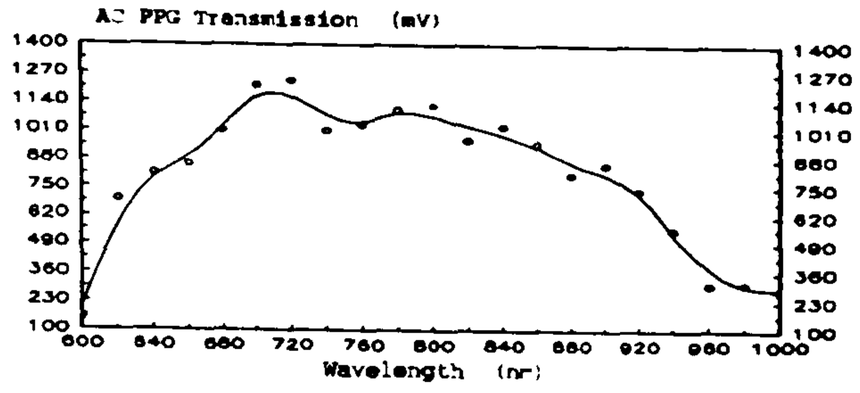
AC PPG Transmission (mV)
Wavelength (nm)

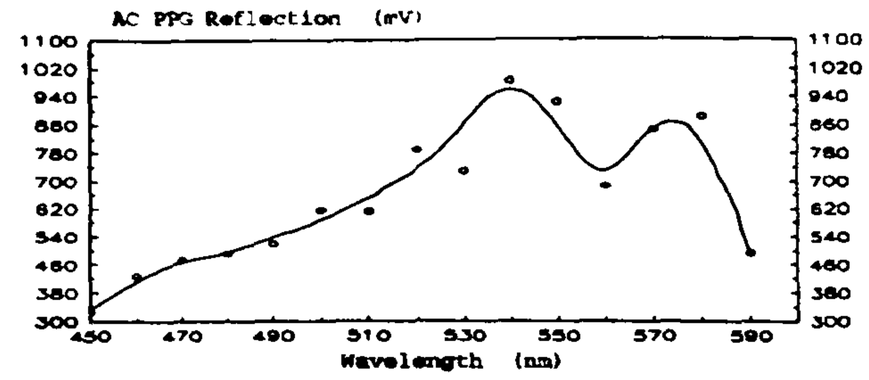
AC PPG Reflection (mV)
Wavelength (nm)

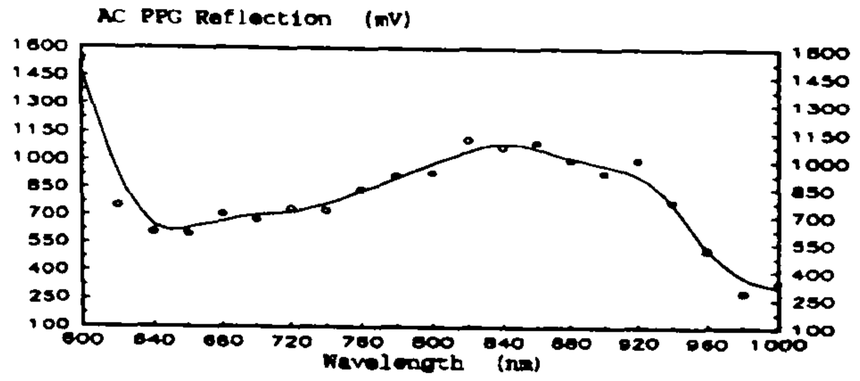
AC PPG Reflection (mV)
Wavelength (nm)

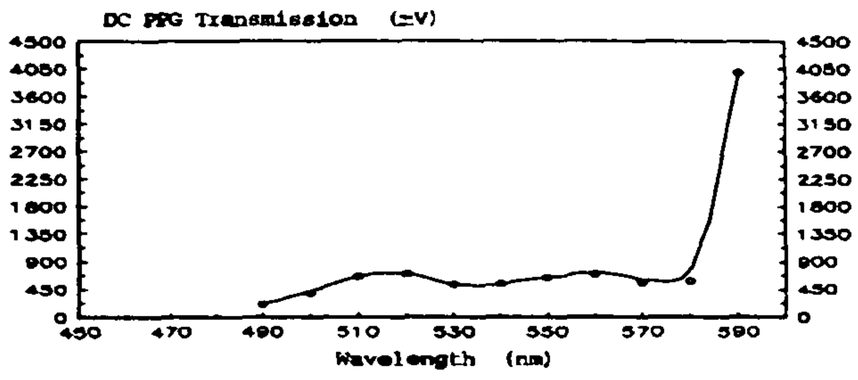
DC PPG Transmission (mV)
Wavelength (nm)

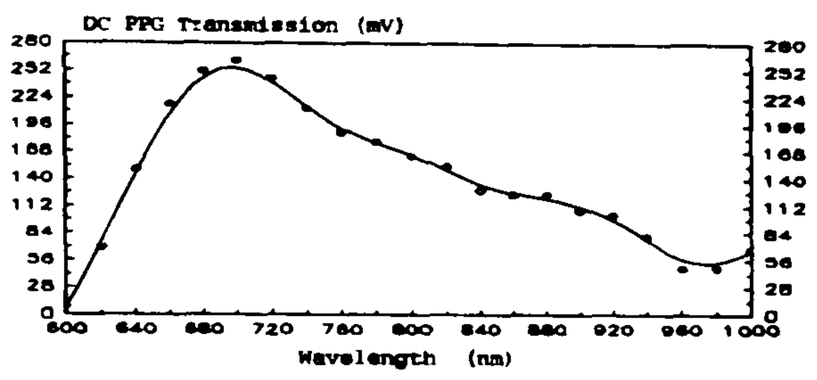
DC PPG Transmission (mV)
Wavelength (nm)

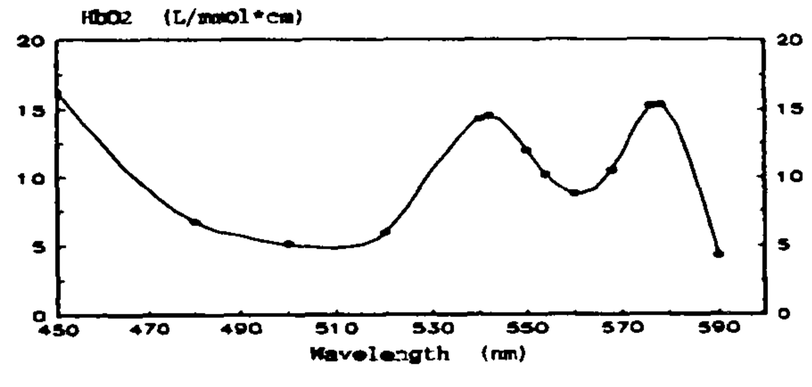
HbO2 (L/mmol*cm)
Wavelength (nm)

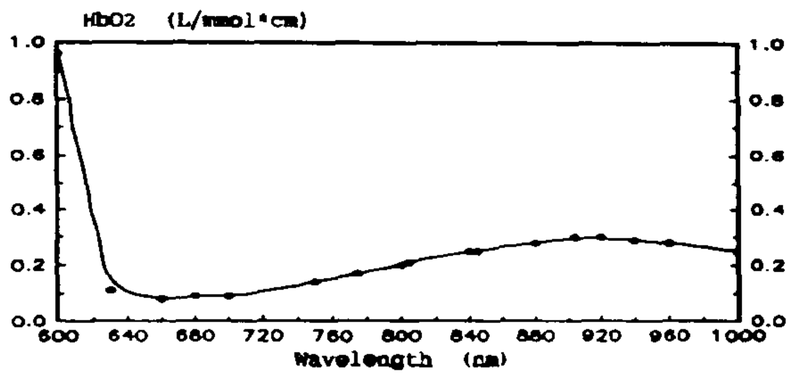
HbO2 (L/mmol*cm)
Wavelength (nm)

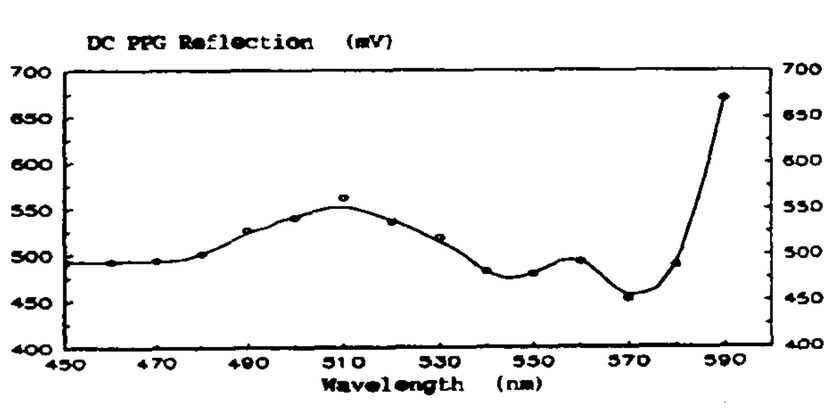
DC PPG Reflection (mV)
Wavelength (nm)

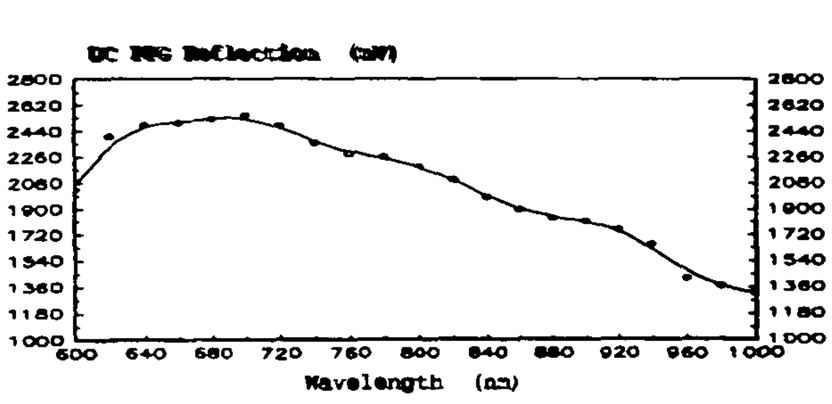
DC PPG Reflection (mV)
Wavelength (nm)

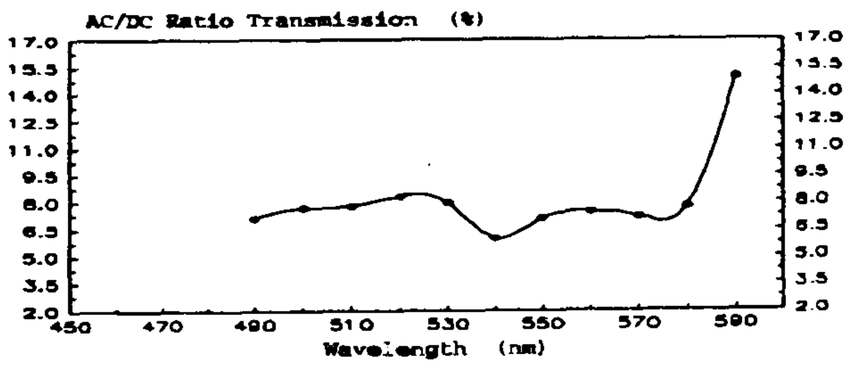
AC/DC Ratio Transmission (%)
Wavelength (nm)

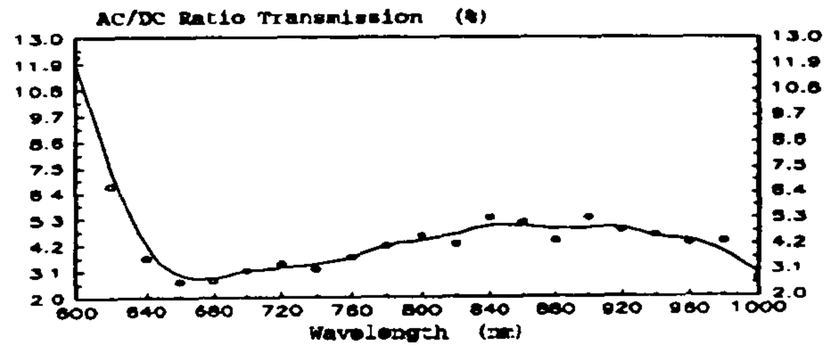
AC/DC Ratio Transmission (%)
Wavelength (nm)

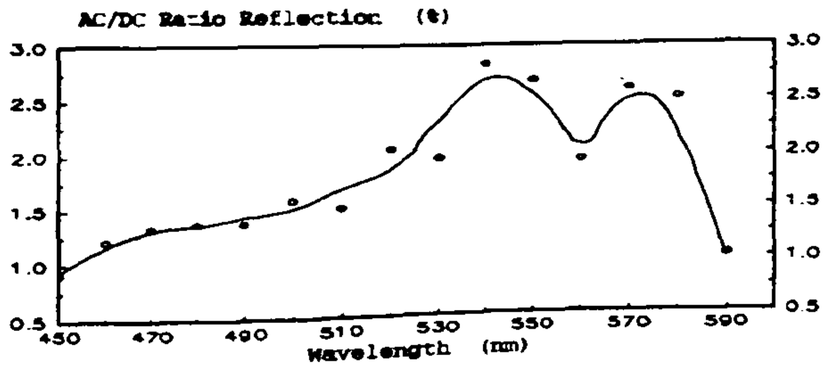
AC/DC Ratio Reflection (%)
Wavelength (nm)

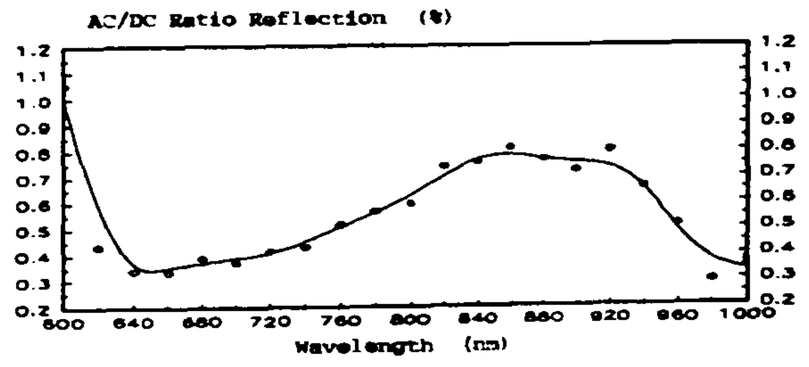
AC/DC Ratio Reflection (%)
Wavelength (nm)

CHAPTER 5

MONTE CARLO MODELLING

5.1 INTRODUCTION

Several theoretical methods exist to calculate the transmittance and reflectance characteristics of tissue when the absorption and scattering coefficients of the tissue are available. Examples are the Kubelka Munk Theory and the Photon Diffusion Theory. However, in the last few years the technique which has become widely accepted to be suitable for simulating light transport in tissue is the Monte Carlo method. This provides a model for simulating light propagation in tissue, where the effects of scattering and absorption are equally important and geometrically complex volumes are to be studied. It is a statistical technique which uses experimentally derived probabilities for photon absorption and scattering, in order to predict the likely path of a photon entering and propagating through a sample. By recording the path, scattering and absorption history of a large number of photons, an

approximation of the overall optical characteristics of the sample can be computed.

Light propagation in tissue is characterised by the scattering coefficient, absorption coefficient and the scattering phase function which is the distribution of scattering angles per scattering event. This method however, demands explicit values of the optical parameters of the media in the model. It also requires a lot of computing resources and it is only on very fast computers that simulation times become practical. A major limitation at present is the lack of widely available data giving the values of the above parameters for different types of samples and at different light wavelengths.

Moreover, it is important to understand and be aware of the limitations of Monte Carlo modelling, realising that it may not provide the answers to all problems simulated. Tests and comparisons should be performed either with other simulation methods or experimentally derived data.

5.2 STRUCTURE AND *IN VIVO* OPTICS OF SKIN

The entire surface of the human body is covered by a layer of skin which presents a tough but flexible barrier to the exterior. Its most obvious role is that of protection against physical trauma. However, it has a number of other important functions by being the interface between our organism and the outside environment. These are temperature regulation and also formation of an extensive sensory surface. These last two are

highly developed at the fingertips. This is shown by the number of nerve endings at the pulps which is more than elsewhere a fact that is also mirrored by the size of the sensory area devoted to them in the brain (Helal, 1989). The function of thermoregulation is discussed in section 5.3.

The structure of the skin is usually described as consisting of three main parts. These are the epidermis, the dermis and the subcutaneous tissue. The optical properties of all these parts are different and are described below. Understanding the optical properties of tissue is vitally important in phototherapy, photochemotherapy and in non invasive *in vivo* optical measurements for monitoring purposes (pulse oximetry being one of them).

5.2.1 Epidermis

The top layer, the epidermis, is avascular (blood free). It is about 50 to 150 μm thick and consists of an uppermost layer of tough dead cells called the stratum corneum. The stratum corneum can be 10 to 20 μm thick, depending on the region. The epidermis contains melanin which is the pigment responsible for the dark coloration of negroid and tanned skin. Melanin strongly absorbs ultra violet and shorter wavelength visible light. Although some scattering occurs in this layer it is not considered to be important.

5.2.2 Dermis

The dermis is 1 to 4mm thick and consists of a complicated

matrix structure of elastic collagen fibres, blood vessels, sweat glands, sebaceous glands and hair follicles all embedded in a viscous gel of water and mucopolysaccharides. Although collagen absorbs very little in the visible and near infra red spectrum, a great deal of scattering occurs due to the geometry of the collagen fibres. The scattering is of the Rayleigh type, with transmission increasing with wavelength.

Scattering also occurs in whole blood. Since the size of erythrocytes is large compared to visible light, it has been shown that red blood cells are highly forward scatterers and wavelength independent. *In vivo* the blood borne pigments haemoglobin, betacarotene and bilirubin are the major absorbers of visible radiation in the dermis (with haemoglobin being the major absorber). Scattering increases the average path length the photons must take to reach a given depth in tissue and increases their chances of being absorbed before reaching deeper within the tissue. Therefore, the strong scattering in conjunction with the high absorption in this layer leads to very high light attenuation, and largely determines the penetration of optical radiation in tissue.

5.2.3 Subcutaneous tissue

The subcutaneous layer contains varying amounts of fat according to the sex and the region of the body. It also contains the larger blood vessels and nerves from which arise superficial cutaneous branches to supply the skin.

5.2.4 Summary

To summarise, the epidermis is primarily an absorptive layer and its absorbance is dependent upon the concentration of melanin. The dermis scatters light because of the collagen matrix and blood and also absorbs depending upon the volume and oxygen saturation of haemoglobin. A representation of the different optical processes in skin is shown in Fig. 5.1.

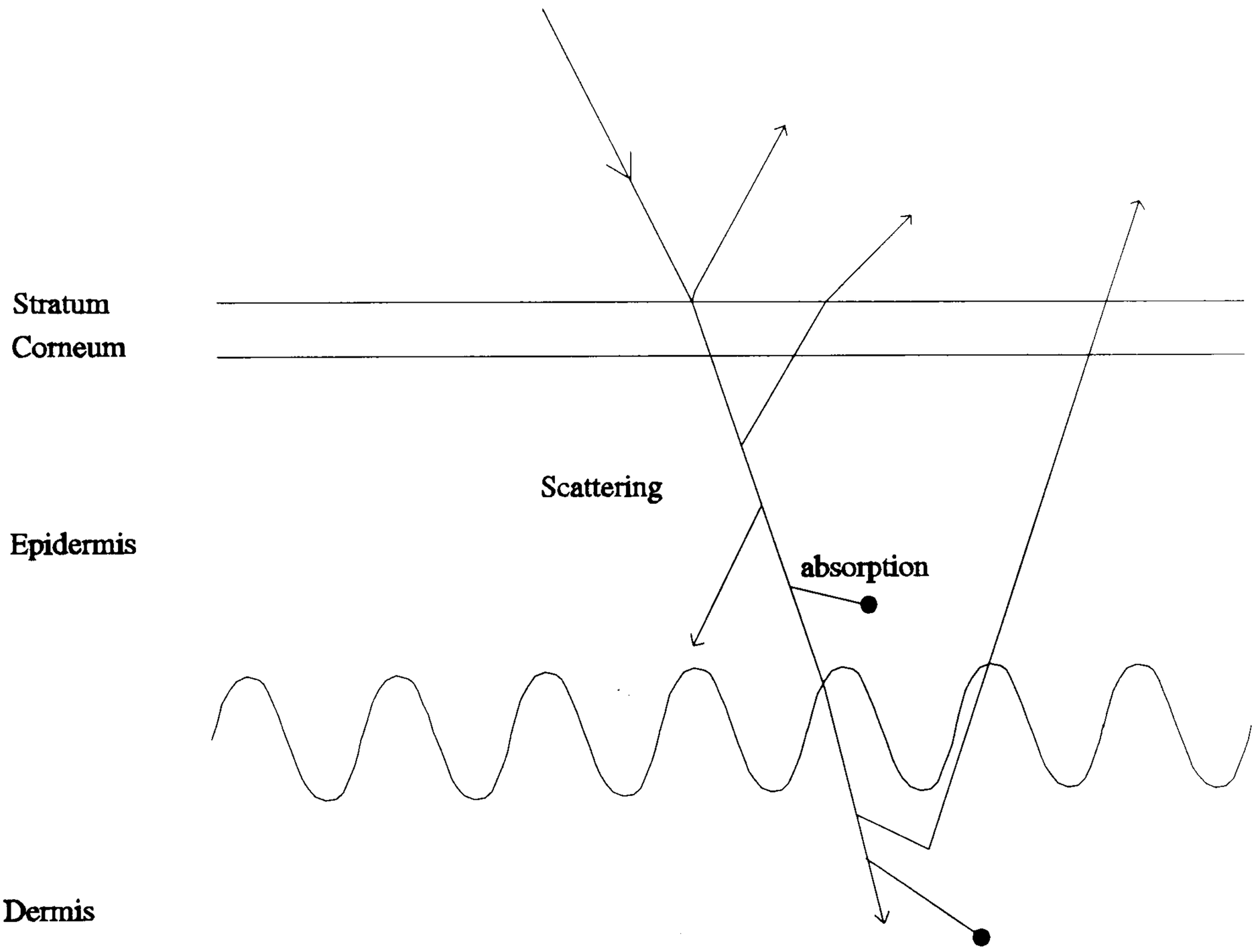

Figure 5.1: A representation of the optical processes in skin.

5.3 BLOOD SUPPLY TO THE SKIN

The topic of blood supply to the body in general, has been dealt

with in section 1.1.1. The blood supply to the skin, and specifically the finger, is now considered. The vascular supply of human skin is schematically represented in Fig. 5.2. It originates in medium size arteries that enter the subcutaneous fat and begin to branch at the level of the junction of the dermis into a horizontally disposed plexus of vessels. These then give rise to several vertical arcades whose caliber becomes progressively diminished as they extend upwards in the dermis. In the upper part of the dermis these arcade vessels give rise to a plexus of horizontally oriented arterioles. From this plexus afferent branches arise, extend into the dermal papillae, loop and return to the upper dermis, forming a venous plexus that extends above and beneath the arteriolar plexus. Thereafter the venous circulation parallels that of the arterial.

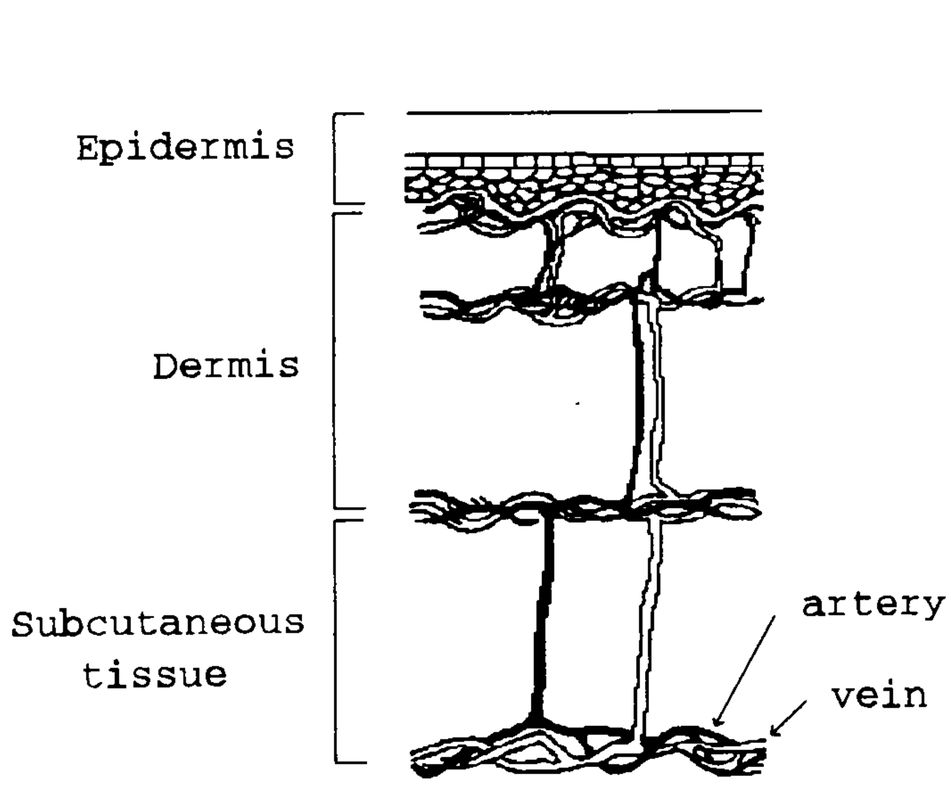

Figure 5.2: The blood supply of the skin.

The anatomy of the blood supply of the skin is further complicated by the presence of arteriovenous anastomoses. These are artery-vein shunts and are well developed in areas of the skin which are

concerned with thermoregulation. In the case of the fingertip the numbers range up to 500 per cm^2 (Thomine, 1981). The total blood flow, which determines the rate of heat loss, can thus be increased irrespective of the nutritional needs of the tissue. It has been found, by using photoplethysmography, that blood volume especially in the pulp is highly variable and can vary between 0.5 and 100 cc per 100 cc of tissue.

The blood volume fraction in normal dermis is quite small, probably around 5 - 10 % (Cui, 1990). The oxygen requirement for normal skin is quite low and since skin blood flow is primarily a thermal regulation mechanism for the body, the oxygen saturation of blood in normal dermis will generally remain close to the arterial level of 98%.

5.4 MONTE CARLO MODELLING

A Monte Carlo model of a human finger has been devised and the Monte Carlo technique is used to simulate light propagation. The results can then be compared with the ones found experimentally concerning the wavelength dependence of the photoplethysmogram. The specifications of the model adopted in these studies are described below.

5.4.1 Geometry of Finger Model

The finger was approximated as a system of three concentric cylinders with a length of 28mm, representing three different layers. The

third and inner layer was bone with a radius of 3.5mm, the middle layer was a mixture of fat and blood with a radius of 6mm and the outer layer was a mixture of dermis and blood with a radius of 7mm. In both layers 1 and 2 the blood volume was set to 10%, and was assumed to be homogeneously distributed, with the rest of the volume being dermis and fat respectively. The influx of arterial blood was simulated by a 10% increase in the blood volume for layers 1 and 2. This increase in blood content changed the total volume and therefore the physical dimensions of the model as well. A section of the model in the plane defined by the y-z axis is shown in Fig. 5.3. The coordinate system was set at the middle of the model. The x-axis is coming out of the paper and is the one that runs along the middle of the finger bone (distal phalanx).

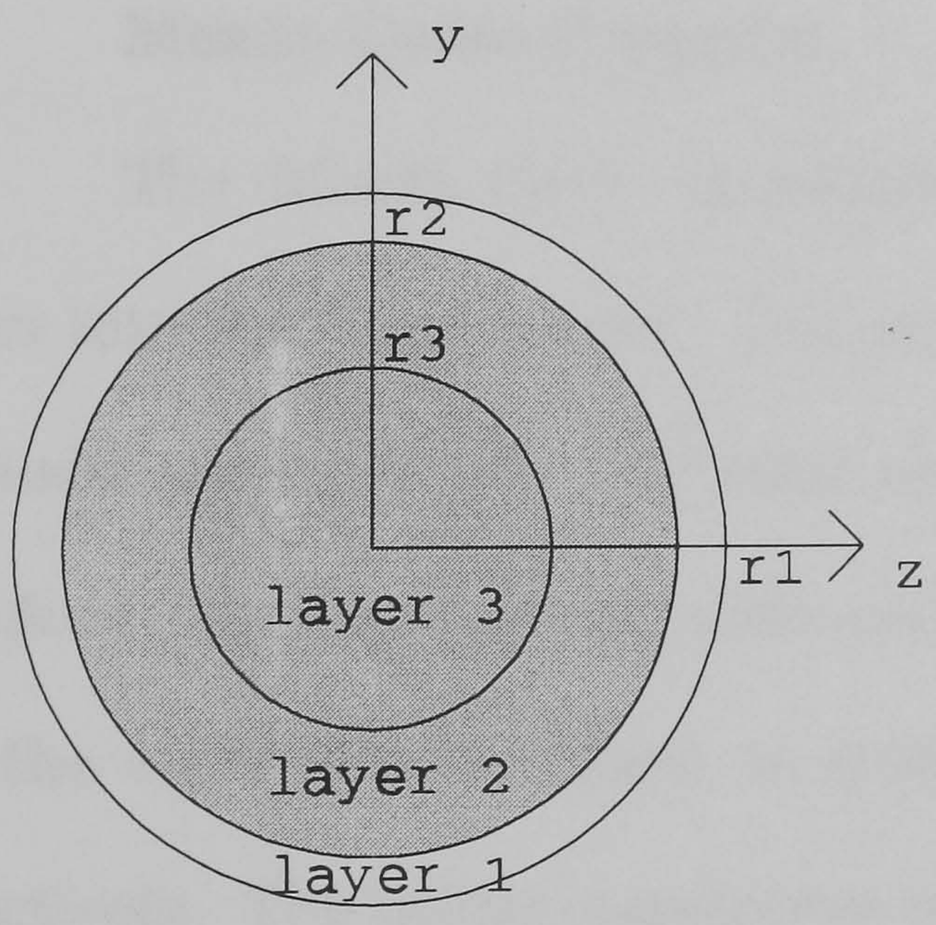

	Standard Blood	Extra Blood
r1	7.0	7.024
r2	6.0	6.018
r3	3.5	3.5

Figure 5.3: Section of the Monte Carlo model of a human finger, showing the model's layers and dimensions at standard and extra blood volumes.

The anatomy of a finger is shown in Fig. 5.4 for comparison and as a reminder of the limitations of the model discussed above.

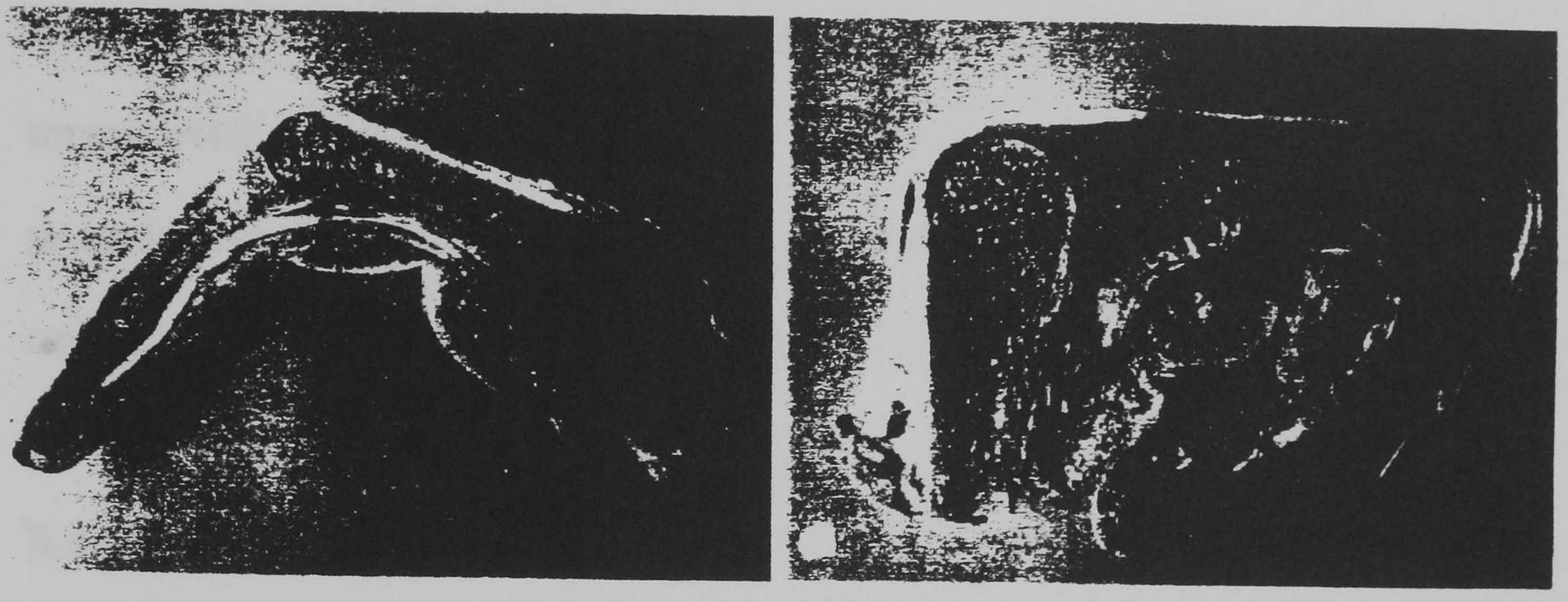

Figure 5.4: The anatomy of a human finger.

5.4.2 Monte Carlo Program

The Monte Carlo simulation process begins by launching a photon into the finger model. For each simulation the input photons to the model were 900000. For each wavelength two modes of simulation were done, the first one was with standard blood content, the second one with the extra arterial blood, to model the DC and DC+AC intensities respectively. The initial coordinates of the launched photon are the same for all photons and are (0,0,-7) for standard simulation and (0,0,-7.024) for simulations with the extra 10% blood. The initial direction is again the same for all photons and is one where the photon travels along the z-axis. Once the photon is launched it interacts with the tissue. The program monitors the scattering distance, direction of travel and coordinates

between each scattering event, the length a photon has travelled in each layer, the total path length and finally the time taken for each simulation. The photon movement continued until the photon exited the model. A photon was considered lost if its x-coordinate was bigger than ±14mm and simulation for that particular photon was stopped. The simulation terminated when all input photons were launched. The Monte Carlo program was developed using the Borland Turbo C programming language and its function is described in Appendix C.

5.4.3 Photon Detection

Three detection modes were employed, one transmission and two reflection. In the first reflection mode the distance between emitter and detector was 2mm and in the second 4mm. These modes were chosen to cover the same area as the optical fibres used in the practical experiments. A detection routine was applied on the photons that exit the model to check whether they fall into the specified detection mode. If a photon was detected, the photon counter for that specific detection mode was increased and the distances travelled in each medium of the model were saved in a file. The disadvantage of this detection technique is that if the detection modes are altered in any way the simulation would have to be re run, which is time consuming. However, the advantage is that the results data files are of reasonable size.

5.4.4 Scattering Distance

The distance Δs represents the distance that a photon travels between scattering events. It is given by:

$$\Delta s = \frac{-\ln \xi}{\mu_s}$$

where ξ is a random variable between zero and one. The variable μ_s is the scattering coefficient and describes the scattering properties of the medium the photon is propagating through.

5.4.5 Scattering Angles - Photon Direction

The direction of travel of a photon after a scattering event is represented by two directional angles, the azimuthal angle θ and the longitudinal angle ϕ. The longitudinal angle ϕ is uniformly distributed between 0 and 360° and is derived by multiplying 2π by a random number. Therefore,

$$\phi = 2\ \pi\ \xi$$

The azimuthal angle θ for non isotropic scattering taking into account that scattering in tissue is characterised by the Henyey-Greenstein phase function (Prahl, 1989) is given by:

$$\cos\theta = \frac{1}{2g}\ \{\ 1 + g^2 - [\frac{1 - g^2}{1+g-2g\xi}]^2\ \}$$

where ξ is a random variable between zero and

one and g is the anisotropy coefficient, where g=0 denotes isotropic scattering and g=1 is totally forward scattering.

5.4.6 Photon Position

The position of a photon in tissue is described by the three spatial coordinates x, y, z and its direction of travel by the two angles ϕ and θ. Another way of representing the direction of travel is by the direction cosines μ_x, μ_y, μ_z, that is the cosine of the angle the photon's direction makes with each of the x, y and z axis respectively. The new direction cosines after a scattering event taking into account its previous direction of travel are given by the following equations:

$$new\mu_x = \frac{\sin\theta}{\sqrt{1-\mu_z^2}} (\mu_x\mu_z\cos\phi - \mu_y\sin\phi) + \mu_x\cos\theta$$

$$new\mu_y = \frac{\sin\theta}{\sqrt{1-\mu_z^2}} (\mu_y\mu_z\cos\phi + \mu_x\sin\phi) + \mu_y\cos\theta$$

$$new\mu_z = -\sin\theta\cos\phi\sqrt{1-\mu_z^2} + \mu_z\cos\theta$$

In case of the angle being too close to the normal (abs[cosz] >

0.99999), the following equations are used to obtain the new direction cosines:

$$new\,\mu_x = \sin\theta\,\cos\phi$$

$$new\,\mu_y = \sin\theta\,\sin\phi$$

$$new\,\mu_z = \frac{\mu_z\,\cos\theta}{abs(\mu_z)}$$

The new position of the photon after a scattering event is given by:

$$newx = x + \mu_x\,\Delta s$$

$$newy = y + \mu_y\,\Delta s$$

$$newz = z + \mu_z\,\Delta s$$

5.4.7 Absorption

Photon absorption is considered at the end of the simulation. Since the program keeps track of the total path length in each layer, the detected light "intensity" is calculated by applying the Lambert-Beer law. This is the same technique as applied by Van der Zee and Delpy (Van der Zee, 1987) and is different from the way Prahl (Prahl, 1989) introduces absorption in the model, where he assumes that absorption takes place at the discrete scattering sites.

5.4.8 Model's Optical Parameters

Optical parameters are obtained by observing measurable quantities, as for example reflected light intensity, and converting them into specific parameters that characterise light propagation in tissue. This model's optical parameters, that is absorption coefficient, scattering coefficient and anisotropy factor for each constituent and at each wavelength, have been obtained from several sources as shown in table 5.1. In the case of mixed layers 1 and 2 the scattering and absorption coefficients were the average of the two constituents for each layer, taking into account their relative concentrations. Table 5.2 lists the absorption and scattering coefficients used for each layer, at each wavelength and type of simulation.

λ	DERMIS (a)			FAT (b)		
	u_a	u_s	g	u_a	u_s	g
545	0.23	23	0.78	0.02	30	0.95
560	0.22	22	0.785	0.02	29.5	0.95
577	0.22	21	0.787	0.02	29.5	0.95
660	0.21 *	19 *	0.813 #	0.02	28.5	0.95
800	0.19 *	18 *	0.852 #	0.02	28	0.95
940	0.175 *	17.5 *	0.896 #	0.02	27	0.95

λ	BLOOD (a)			BONE (c)		
	u_a	u_s	g	u_a	u_s	g
545	33	47.2	0.995	1.983 ■	39.5 ♦	0.91 ♦
560	20	47	0.995	1.20 ■	38.5 ♦	0.915 ♦
577	35.4	46.8	0.995	2.13 ■	37.5 ♦	0.918 ♦
660	0.182 †	45.5	0.995	0.032	34	0.925
800	0.456 †	44	0.955	0.024	28	0.935
940	0.661 †	43	0.955	0.045	24.5	0.945

(a) Data from Verkruysse, 1993.
(b) Data from Key, 1991.
(c) Data from Firbank, 1993.
* Extrapolated and compared with results from Van Gemert, 1989.
\# Calculated from Van Gemert, 1989.
† Extrapolated having in mind extinction coefficients of HbO_2.
♦ Extrapolated.
■ Calculated from Firbank, 1993.

Table 5.1: Monte Carlo parameters for each constituent.

PARAMETERS FOR DC SIMULATIONS						
λ	LAYER 1		LAYER 2		LAYER 3	
	u_a	u_s	u_a	u_s	u_a	u_s
545	3.507	25.42	3.318	31.72	1.983	39.5
560	2.198	24.5	2.018	31.25	1.2	38.5
577	3.738	23.58	3.558	31.23	2.13	37.5
660	0.2072	21.65	0.0362	30.2	0.032	34
800	0.2166	20.6	0.0636	29.6	0.024	28
940	0.2236	20.05	0.0841	28.6	0.045	24.5

PARAMETERS FOR DC+AC SIMULATIONS						
λ	LAYER 1		LAYER 2		LAYER 3	
	u_a	u_s	u_a	u_s	u_a	u_s
545	3.8347	25.662	3.6478	31.892	1.983	39.5
560	2.3958	24.75	2.2178	31.425	1.2	38.5
577	4.0898	23.838	3.9118	31.403	2.13	37.5
660	0.20692	21.915	0.03782	30.37	0.032	34
800	0.21926	20.86	0.06796	29.76	0.024	28
940	0.22846	20.305	0.09051	28.76	0.045	24.5

Table 5.2: Calculated u_a and u_s Monte Carlo parameters for each layer for each model taking into account constituent concentrations.

However, in the case of the anisotropy factor a different regime was used. Taking as an example layer 1, at every scattering event a random number was used to decide whether the photon was scattered by blood or dermis, having of course in mind the concentrations of dermis and blood in the layer. Once this was decided the appropriate anisotropy

factor was used.

5.4.9 Modelling Assumptions

For the setup of this finger model several assumptions were made, and these are clearly defined below :

i) The finger was of cylindrical shape with an outside diameter of 14mm, with well defined concentric cylindrical layers representing dermis and blood, fat and blood and bone, as described in section 5.4.1. Although, this is not strictly true in real life, it simplified program flow in the tracking of photon position, with the aim of achieving greater speed in simulation execution.

ii) The length of the model was 28mm. Any photons propagating outside this length were considered lost. This again was introduced to speed up simulation. Although some photons that exceeded this limit might have been scattered back and eventually exit the model and be detected, it was assumed that the scattering distance they might have travelled would be that great that by applying the appropriate absorption coefficients would have made their contribution to the overall detected signal negligible. This particular length was chosen having in mind the fibre bundles dimensions used in reflection mode in the practical experiments.

iii) The possibility of internal reflections occurs when a photon is propagated from one layer to another with a different refraction index. In this program possible internal reflections were ignored. However, when

a photon was propagated from one layer to another, its position was brought back to the layer interface and a new scattering was allowed to happen.

iv) Any effect of the epidermis and finger nail was ignored. Since the epidermis is assumed to be mainly an absorptive medium, it was not introduced in the simulation process. Also the inclusion or exclusion of the finger nail in the model in reflection mode is of no importance, since photons were injected at the pulp side. It was only in transmission mode that any effects of the finger nail would manifest themselves.

5.5 MONTE CARLO RESULTS

Monte Carlo simulations have been performed on the finger model at the following wavelengths: 545, 560, 577, 660, 800 and 940nm. These are characteristic oxyhaemoglobin and pulse oximetry wavelengths. Table 5.3 gives the number of photons that were detected at each of the modes. The trend of these results was as expected, with fewer photons generally being detected for the DC+AC simulations. Moreover, the number of detected photons increased progressively from the transmission to reflection2 and reflection1 modes.

Wavelength	Photons IN	Photons OUT		
		Transmission	Reflection1	Reflection2
DC545	900000	858	8763	2855
DC+AC	900000	870	8730	2902
DC560	1800000	1818	18931	5962
DC+AC	1800000	1766	18632	5901
DC577	1800000	1848	19684	6471
DC+AC	1800000	1746	19539	6017
DC660	2700000	3102	38443	11161
DC+AC	2700000	3306	37864	11040
DC800	2700000	4236	51839	13340
DC+AC	2700000	4377	51354	13697
DC940	2700000	5553	73349	17422
DC+AC	2700000	5355	72671	17917

Table 5.3: Number of photons detected at each wavelength and each mode following Monte Carlo simulations.

From each simulation the AC and DC intensities, as defined for the photoplethysmogram, were recorded. The DC intensity was given by the results of the standard simulation runs. The results of the simulations with the extra 10% arterial blood produced the AC+DC intensity, and therefore the AC intensity was calculated by subtracting the DC intensity

from the above. Finally the AC/DC ratio was calculated. These results are shown in table 5.4.

Wavelength	**Itr**	**Ir1**	**Ir2**
DC545	1.12384e-93	4.96319e-10	2.76313e-27
DC+AC	2.74553e-107	4.41568e-11	3.5666e-31
AC545	1.123839e-93	4.521622e-10	2.76277e-27
AC/DC	0.9999	0.911	0.999
DC560	1.510823e-62	12.29936e-6	5.26128e-16
DC+AC	3.66234e-56	9.96448e-6	4.42994e-18
AC560	-3.66234e-56	2.33488e-6	5.21698e-16
AC/DC	2.42406e6	0.1898	0.9916
DC577	1.02053e-87	4.20974e-9	18.94066e-27
DC+AC	11.175e-116	2.72178e-10	7.85382e-27
AC577	1.02053e-87	3.82522e-9	11.08684e-27
AC/DC	1	0.9086	0.58535
DC660	0.784672	1046.474	86.4625
DC+AC	1.00964	988.009	79.1755
AC660	-0.224967	58.465	7.287
AC/DC	0.2867	0.05586	0.08427
DC800	1.776388	1692.918	98.7362
DC+AC	1.30256	1608.071	83.119
AC800	0.473828	84.847	15.6172
AC/DC	0.26674	0.05012	0.15817
DC940	1.086996	3172.34	133.0276
DC+AC	0.764413	2965.313	117.3634
AC940	0.322583	207.027	15.6642
AC/DC	0.29676	0.06526	0.11775

Table 5.4: Monte Carlo results on model finger.

The model's behaviour for wavelengths below and above 600nm was again examined by looking at the 660/560 ratio. For the transmission results the DC ratio for the 660/560nm is by 62 orders of magnitude bigger than the experimental results obtained in chapter 4, and by 46 orders of magnitude bigger than the results obtained by the Lambert-Beer analysis of the same model in Appendix D.

The difference between the Monte Carlo results and the Lambert-Beer results are explained by the fact that the effects of scattering have been taken into account in the case of the Monte Carlo analysis. This resulted in increased pathlengths which in combination with higher absorption coefficients below 600nm resulted in a much bigger 660/560 ratio. A histogram of the pathlengths in the transmission and the two reflection modes is shown in Fig. 5.5.

The results obtained in reflection mode are still not in close agreement with the experimental results, but are not in any way as far out as the transmission results. This would suggest that until a better understanding of the underlying processes in transmission mode is reached, Monte Carlo modelling would be of better use in reflection mode.

The results obtained in the second reflection mode where the distance between the emitter and receiver was bigger, are in between the results obtained in transmission and first reflection mode. This is of the same trend observed for the experimental results in section 4.4.

It has to be emphasised that a Monte Carlo simulation is as accurate as the model used. Therefore, these results suggest that the

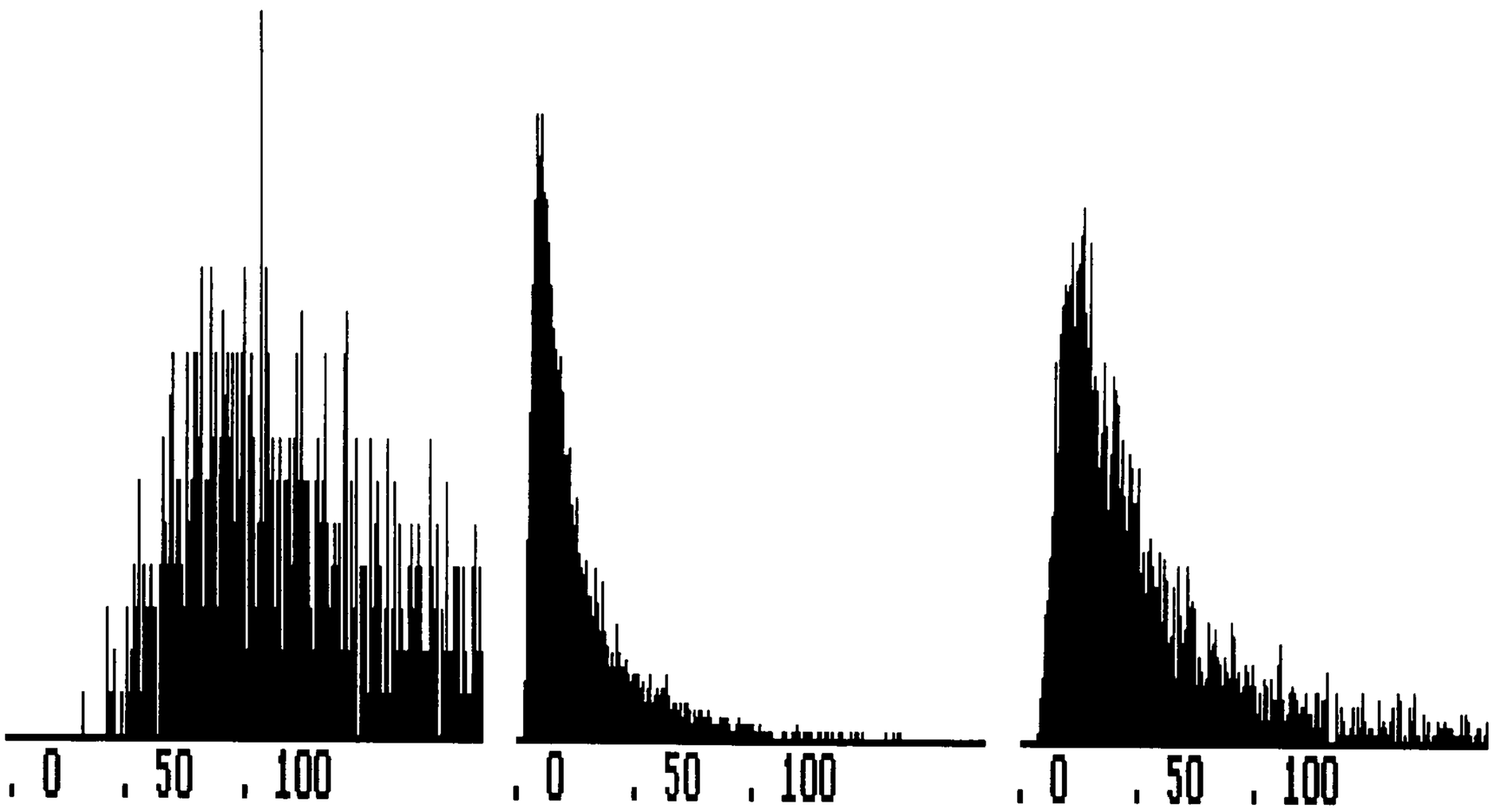

Figure 5.5: A histogram of the pathlengths for each mode.

model used here is in need of modification. This model was based on the one currently used to explain pulse oximetry, as presented in the literature. Clearly the introduction of scattering effects has pushed these results further apart from the ones obtained in our experiments in chapter 4, pointing to the fact that this model is inappropriate and fundamentally wrong.

Moreover, the accuracy of Monte Carlo simulations is affected by the scattering and absorption parameters used. In this case the parameters used were ones published in the literature. Most of them however, are parameters for thin slabs in studies performed *in vitro*. Recent research casts doubts on whether these parameters are appropriate

for use in *in vivo* models. A study by Graaff et al (Graaff, 1993) resulted in *in vivo* values for the absorption coefficients and the reduced scattering coefficients to be much smaller from the *in vitro* ones.

Further research for determining the optical parameters of several types of human skin *in vivo* and at different wavelengths is necessary before models like the above would of any use in Monte Carlo simulations. The setup of a database for Monte Carlo parameters would facilitate and encourage more research in this field.

In conclusion a new model for pulse oximetry needs to be developed, that would take into account the heterogeneous structure and concentration of blood in the skin.

CHAPTER 6

THE CONSEQUENCES OF PROBE MALPOSITION IN REFLECTION PULSE OXIMETRY

6.1 INTRODUCTION

As mentioned in previous chapters pulse oximetry has revolutionised monitoring in anaesthesia, intensive care and neonatology. In the last few years apart from the standard stick on, clip on transmission probes, reflectance probes for pulse oximetry have become available. One area in which the use of reflection pulse oximetry is currently under investigation is that of fetal monitoring during labour (Gardosi, 1991; Johnson 1991; Mendelson, 1992). The aim of fetal monitoring is to detect and of course prevent hypoxia. Adapting pulse oximetry to be used in fetal monitoring is not easy and its successful application has so far been hampered by many problems. This is mainly

due to the limited access to the fetus, appropriate probe design and its application. The following work was performed in collaboration with physicians at the Queens Medical Centre, Nottingham and is related to artifacts observed in reflection pulse oximetry readings due to variations in probe to skin surface separation, caused by poor probe application.

Probe application in adult or neonatal pulse oximetry does not usually present a problem. This is because first one can see whether the probe is applied properly and also most modern oximeters offer an ambient light warning; that is if the level of the ambient light is above some preset threshold this would suggest that the probe has come off. However, in the birth canal the scenario is very much different. The probe has fluids, edema, hair, maternal movements and contractions to contend with. Moreover, the absence of any background light makes the ambient light warning of the pulse oximeter unable to function.

There are several ways of applying the probe to the fetal scalp, ranging from simply positioning the probe and hoping that it will stay there by pressure from the maternal tissue, to gluing the probe in position or using modified spiral scalp electrodes. A different approach was used by Johnson (Johnson, 1991) by incorporating suction to the probe's design to ensure good application at all times. However, in practice it was found that suction did not always work and therefore good probe application could not be guaranteed. Although, many times the probe was just sitting there, oxygen saturation readings were still obtained.

Physicians at the Perinatal Research and Monitoring Unit,

Queen's Medical Centre, Nottingham used a probe with a pair of Copeland-type arcuate needles (Gardosi, 1991), in order to solve the problem of good probe application. Results obtained from both Johnson and Gardosi showed that on occasions the SpO_2 level varied unaccountably. It was later noticed that some of the variations coincided with contractions. At this stage it was not clear whether these variations in SpO_2 readings were genuine or just an artifact of poor probe application.

6.2 PRELIMINARY INVESTIGATIONS

A simple experiment was devised to investigate how important adequate probe application is to reflection pulse oximetry. A commercially available pulse oximeter (Criticare 504) was used with a multi-site probe on an adult finger in darkness. The probe was first attached to the finger firmly, that is with both emitter and detector in complete contact with the skin and a normal 98 - 99 % SpO_2 reading was obtained. Then the probe to skin contact was broken and this resulted in an artificially low SpO_2 level reading. As the distance between the probe and the skin increased the SpO_2 level decreased. The results from this experiment (Gardosi, 1991) are shown in Fig. 6.1.

It was interesting to note that in all cases what appeared to be normal PPG signals were obtained. This did not give any indication about incomplete probe application.

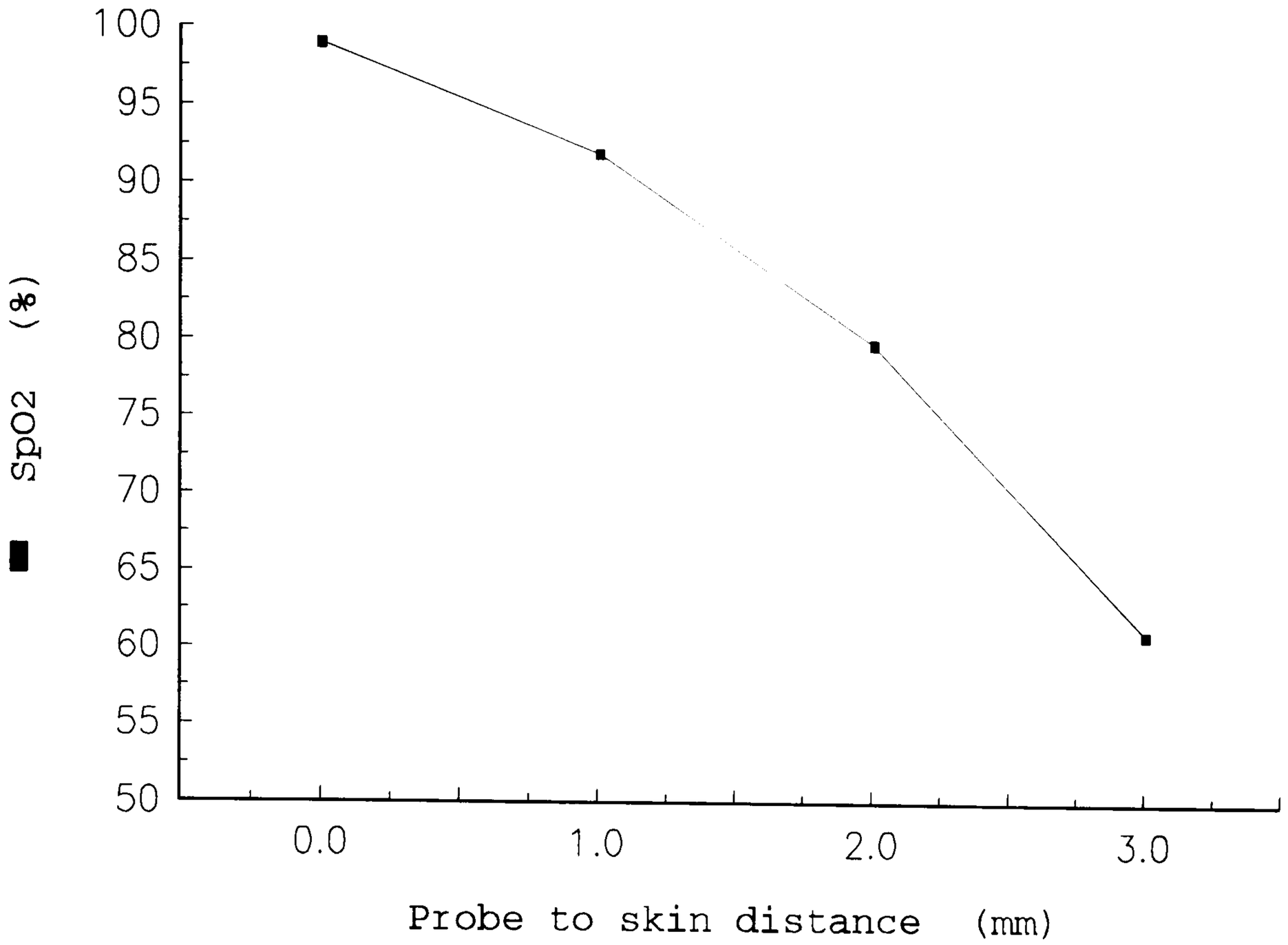

Figure 6.1: Increasing the gap between the probe and the skin surface results in an artificial low oxygen saturation reading from the pulse oximeter.

6.3 EXPERIMENTAL PROCEDURE

Once this artifact was established an experiment was set up aiming to verify and quantify this effect under laboratory conditions. This was performed by examining the effect of varying the distance of the reflectance probe from the subject's finger upon the ratio **R** (and consequently SpO_2). The subject was a healthy male caucasian, nonsmoker, aged 27. The ratio **R** was defined in section 2.1.1 and is:

$$R = \frac{\frac{AC_{red}}{DC_{red}}}{\frac{AC_{ir}}{DC_{ir}}} \qquad (6.1)$$

Commercial pulse oximeters use the ratio **R** to calculate SpO_2 from empirically derived data as explained in section 2.1.1. From Fig. 2.2 it is clear that as the ratio **R** increases, SpO_2 decreases. All the variables from which **R** was calculated were monitored in order to establish their effect upon the ratio **R**.

The main system set up was the one designed for the wavelength dependence studies and is described in detail in chapter 3. The probe used consisted of two 1.5 mm diameter bundles. The acceptance angle of the fibres was ±34.5°. As the LEDs used by commercial pulse oximeters are of the surface mount type offering a wide viewing angle, the two fibre bundles were placed at an angle of 17°, thus offering a better approximation to the commercial type probe. The probe arrangement is shown in Fig. 6.2 with the dotted line representing the skin surface. The acceptance angles are shown in the figure. Light from the emitter illuminates the skin within the limits of the acceptance angles. However, not all light emerging from the skin area S will be detected. For light to be detected it must fall within the solid angle Φ, thus for example light emerging from the point P in the direction shown will not be detected. Therefore, probe geometry is important and has to be kept in mind when analysing the results.

A special finger holder was designed in order to prevent finger movements during the experiments. The finger rested loosely in the holder and the holder was attached firmly on the experimental jig. The probe's position from the finger was varied from contact up to a maximum

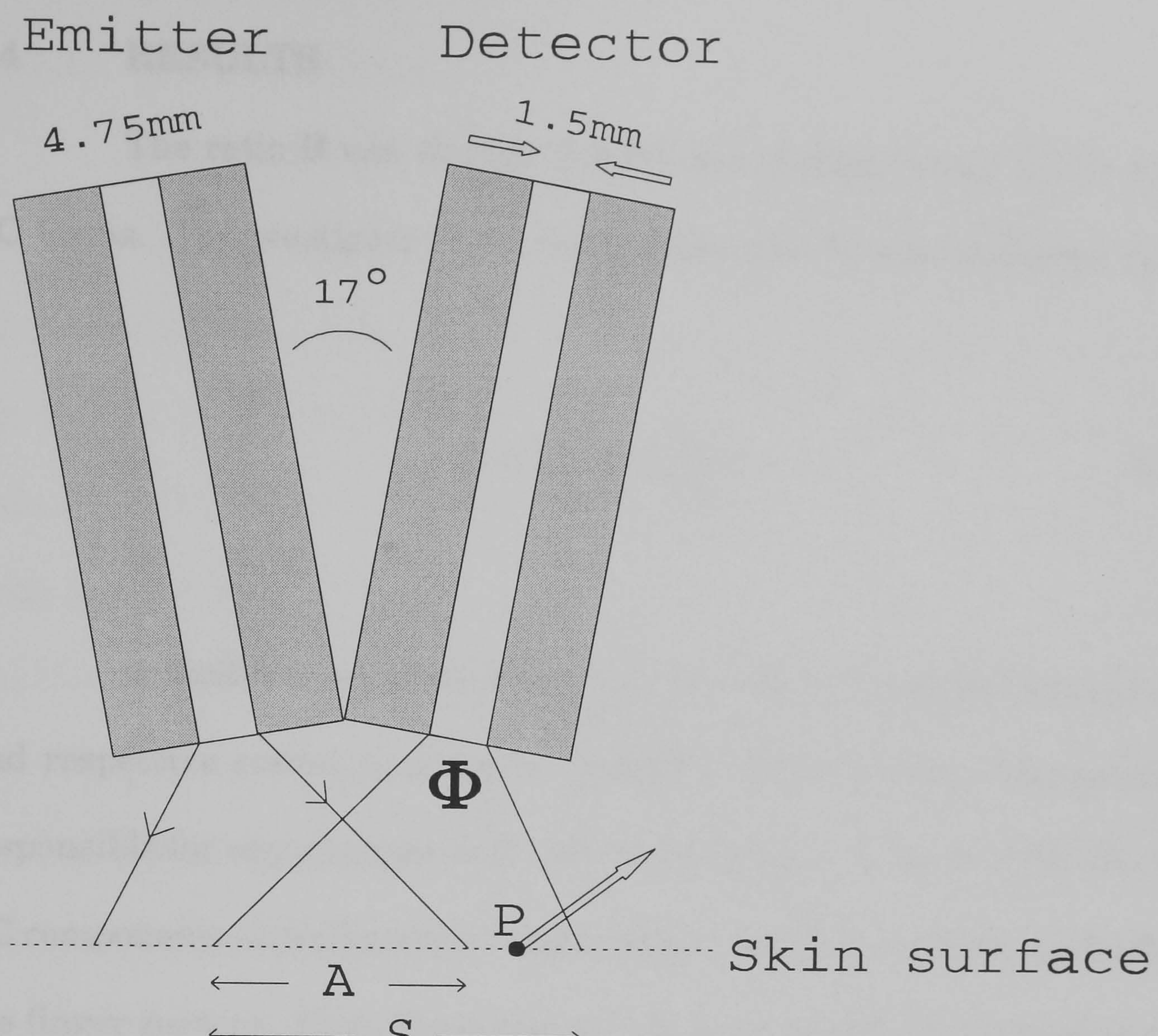

Figure 6.2: Reflection probe configuration.

of 4mm, in steps of 1mm, using a lead-screw arrangement. The finger holder and the experimental jig are shown in Appendix B.

AC and DC PPG measurements were taken at the two wavelengths most commonly used by pulse oximeters, namely 660 and 940nm. These measurements were taken with the probe initially in good contact with the finger (zero separation distance), and repeated with the probe moved at distances of 1, 2, 3 and 4mm away from the finger. The same procedure was repeated at least 5 times.

6.4 RESULTS

The ratio **R** can change if there is a change in any of the AC or DC terms. To investigate these results the ratio **R** was rewritten as:

$$R = \left(\frac{AC_{red}}{AC_{ir}}\right)\left(\frac{DC_{ir}}{DC_{red}}\right) \tag{6.2}$$

to facilitate separate investigation of the AC and DC components and respective ratios, in order to identify which of these components is responsible for any changes in **R**. The results take the form of the DC and AC components and respective ratios versus the distance of the probe from the finger surface. From these the ratio **R** is calculated and plotted versus the probe distance. They are all presented as the mean plus and minus one standard deviation.

Results are presented here from three different sets of experiments. In section 6.4.1 the results are from experiments using the reflectance probe as described in section 6.3 above. Section 6.4.2 covers preliminary results obtained with a new reflectance probe which incorporates a redesigned geometry with the aim of reducing the importance of this artifact. Finally in section 6.4.3 results are presented from malposition experiments with a transmission probe.

6.4.1 Original Reflectance Probe

6.4.1.1 The DC components

Looking at the DC components first it appears that both DC_{red} and DC_{ir} follow the same trend, their amplitude increasing with increasing separation distance between the probe and the finger surface, as shown in Fig. 6.3. If the two DC signals followed exactly the same trend, then their ratio would have been constant for all probe positions. However, there are some small variations in the relative performance of the two DC signals and this is apparent in the shape of the DC_{ir}/DC_{red} ratio, as shown in Fig. 6.4. Although the variations of the DC_{ir}/DC_{red} ratio will produce a change in the ratio **R**, these variations alone (assuming a constant AC ratio) are slight and their effect on the ratio **R** and consequently on the SpO_2 readings is minimal. Therefore, any major changes in the ratio **R** should be reflected by the behaviour of the AC_{red}/AC_{ir} ratio.

From Fig. 6.3 it can be seen that as the probe to skin distance is increased, the DC component increases. Once contact with the skin is broken the DC signal becomes a composite one, of back scattered light from within the finger and scattering from the skin surface. The influence of the light scattered from the skin surface is dependent on the probe geometry and specifically on the overlap area **A**, as defined in Fig. 6.2. This can be seen in Fig. 6.5 where the increase of the DC signal follows the same trend as the increase of the overlap area **A** as the probe is moved away from the skin surface.

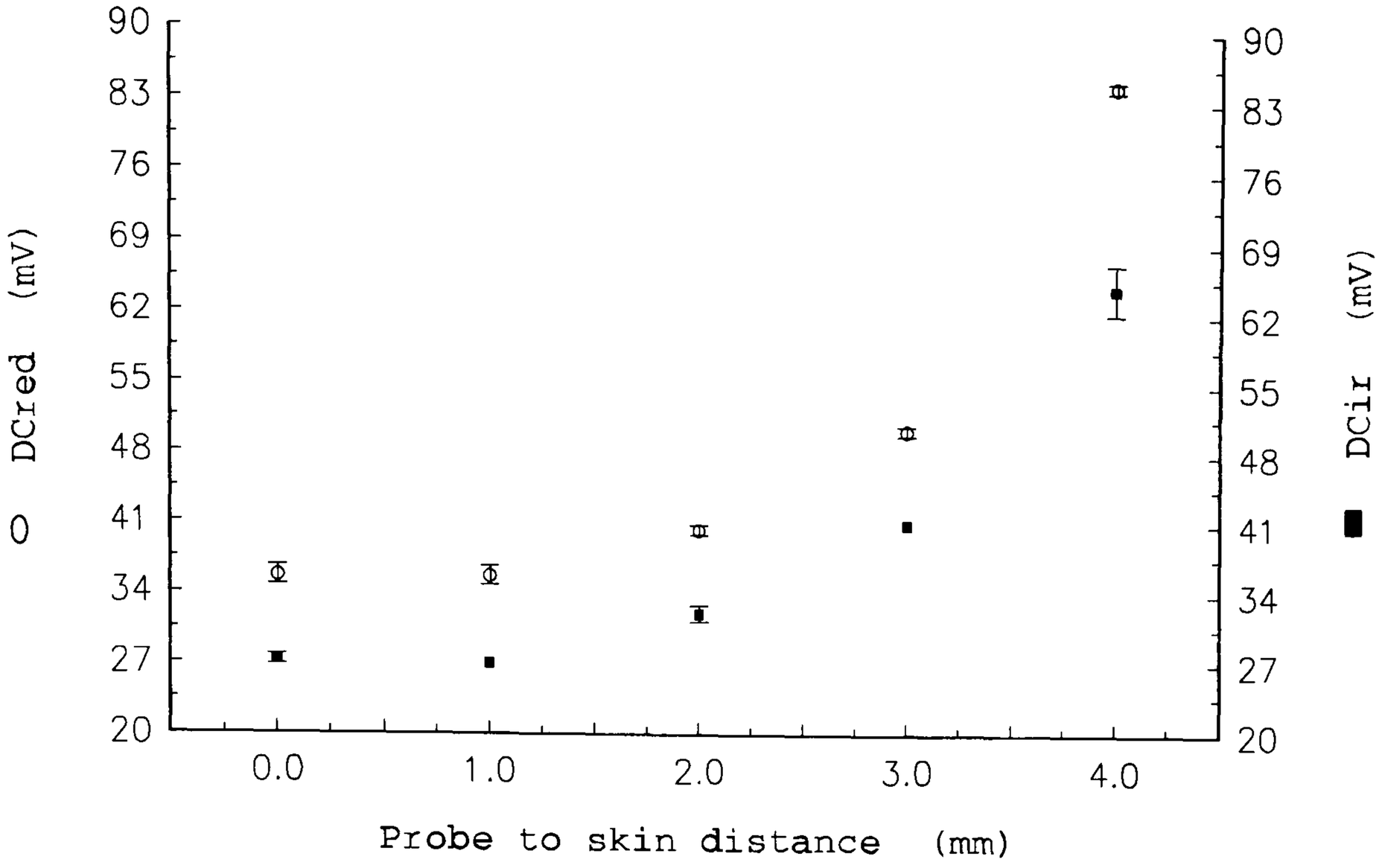

Figure 6.3: The effect of increasing the probe to skin distance on the DC_{red} and DC_{ir} components.

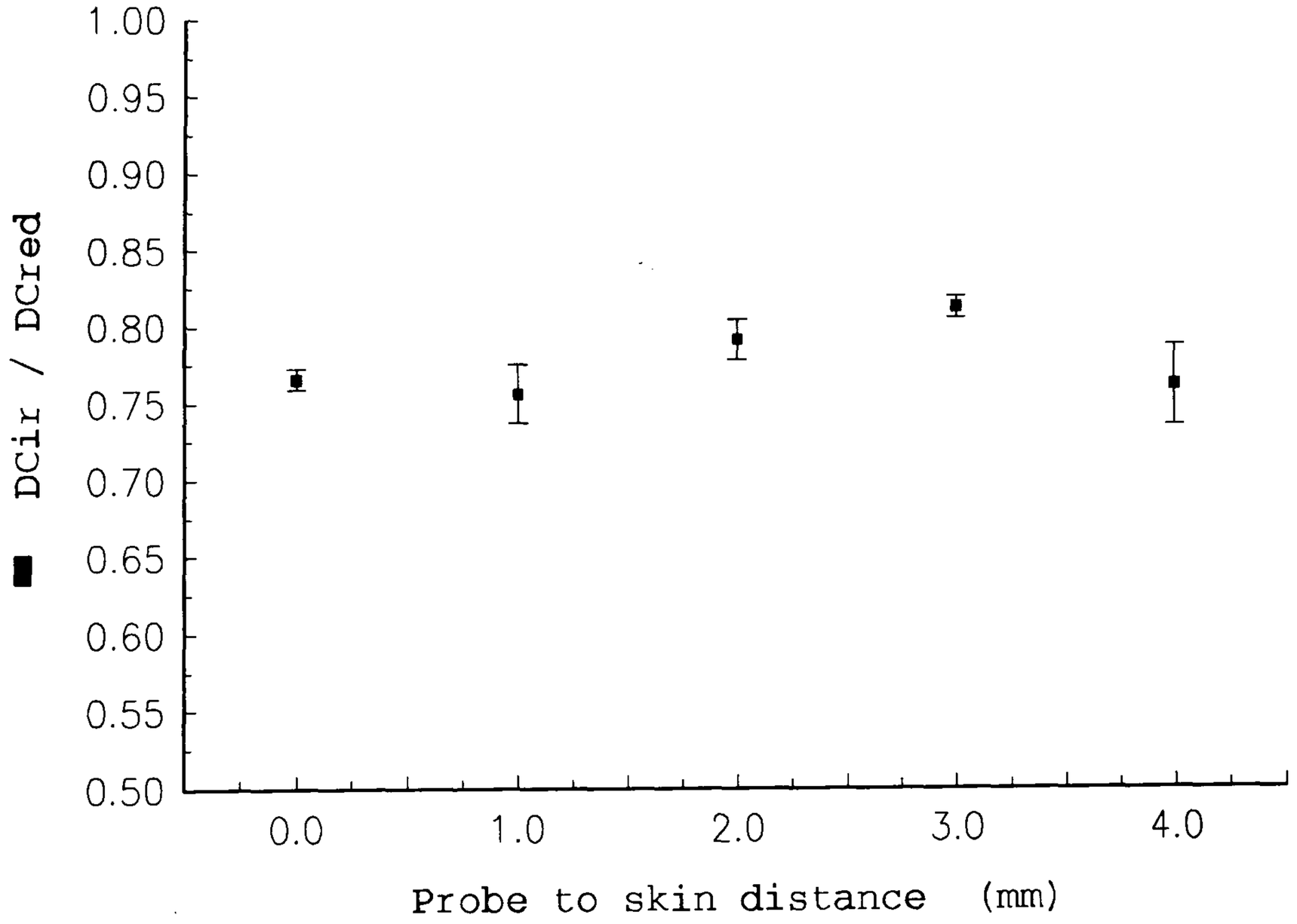

Figure 6.4: The effect of increasing the probe to skin distance on the DC_{ir}/DC_{red} ratio.

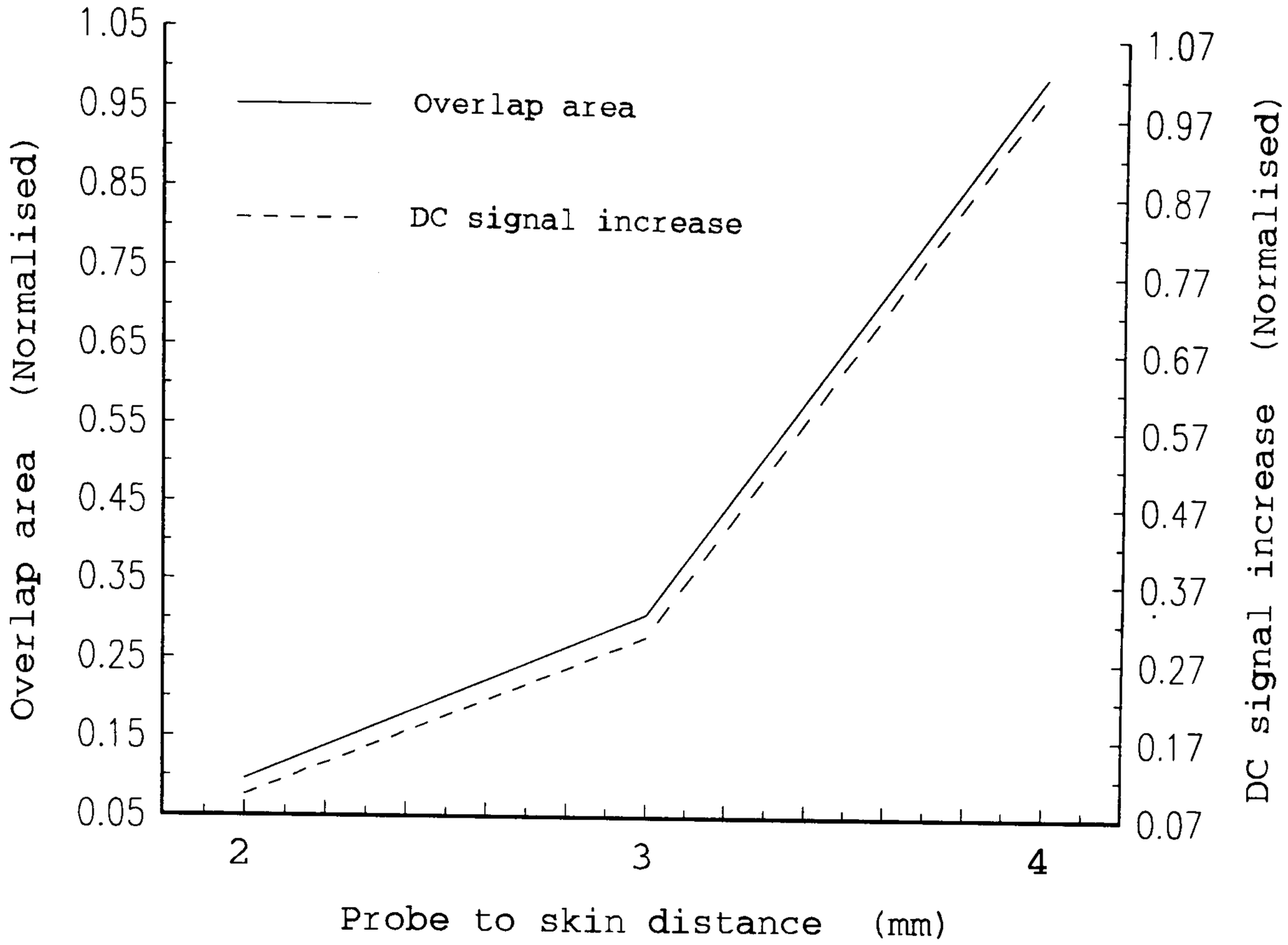

Figure 6.5: Comparison of overlap area and increase in the DC signal as the probe is moved away from the skin surface. Please note offset of right y-axis to facilitate comparison of data.

6.4.1.2 The AC components

As shown in Fig. 6.6 the AC components follow a similar pattern, both decreasing for a distance of 4mm. However, the rate of increase and decrease for the two signals is different. At contact the amplitude of the AC_{ir} is almost twice that of the AC_{red}, whereas at 4mm the amplitude of the AC_{red} is bigger.

The different behaviour of the AC_{red} and AC_{ir} signals produces the AC_{red}/AC_{ir} ratio in Fig. 6.7.

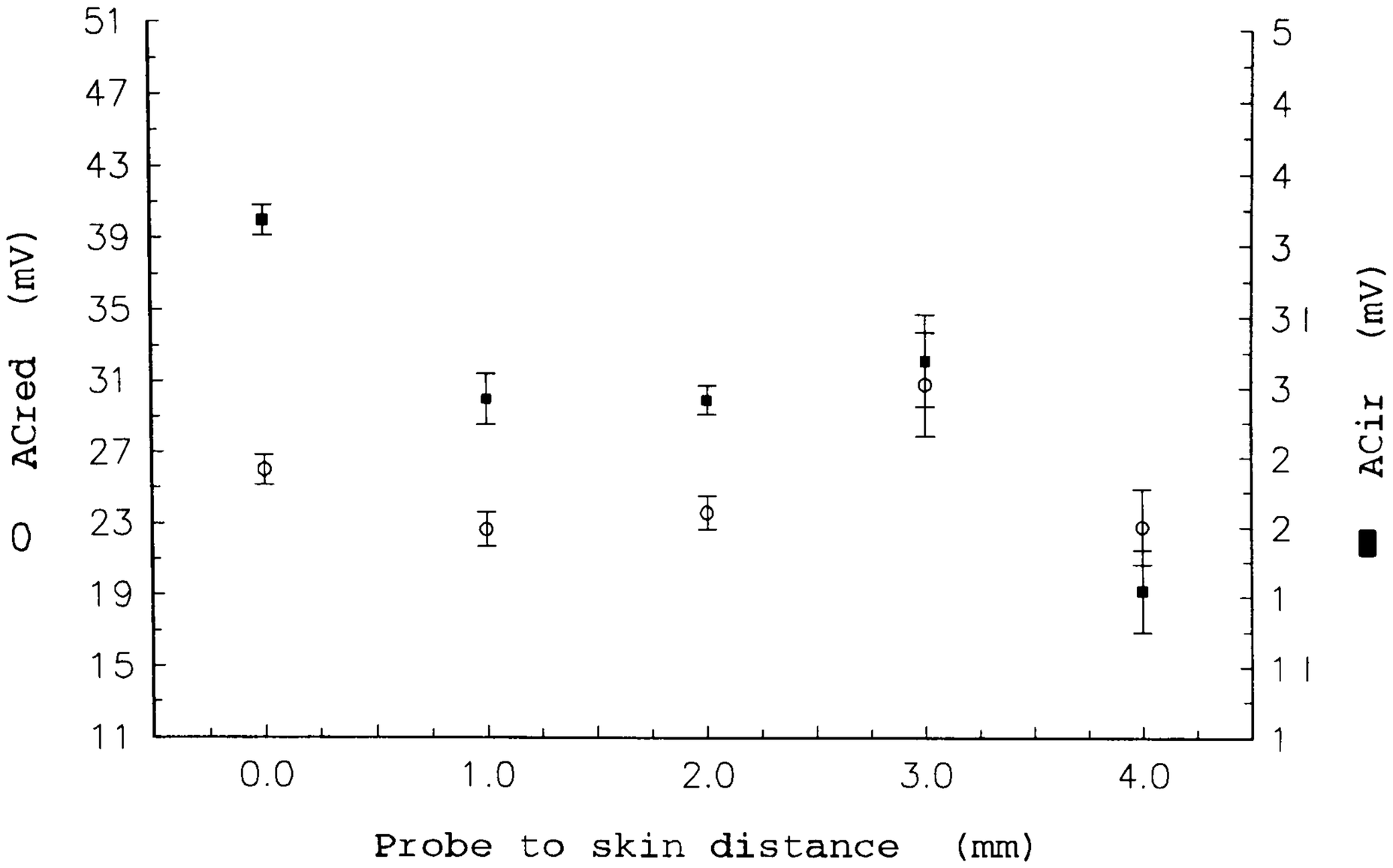

Figure 6.6: The effect of increasing the probe to skin distance on the AC_{red} and AC_{ir} components.

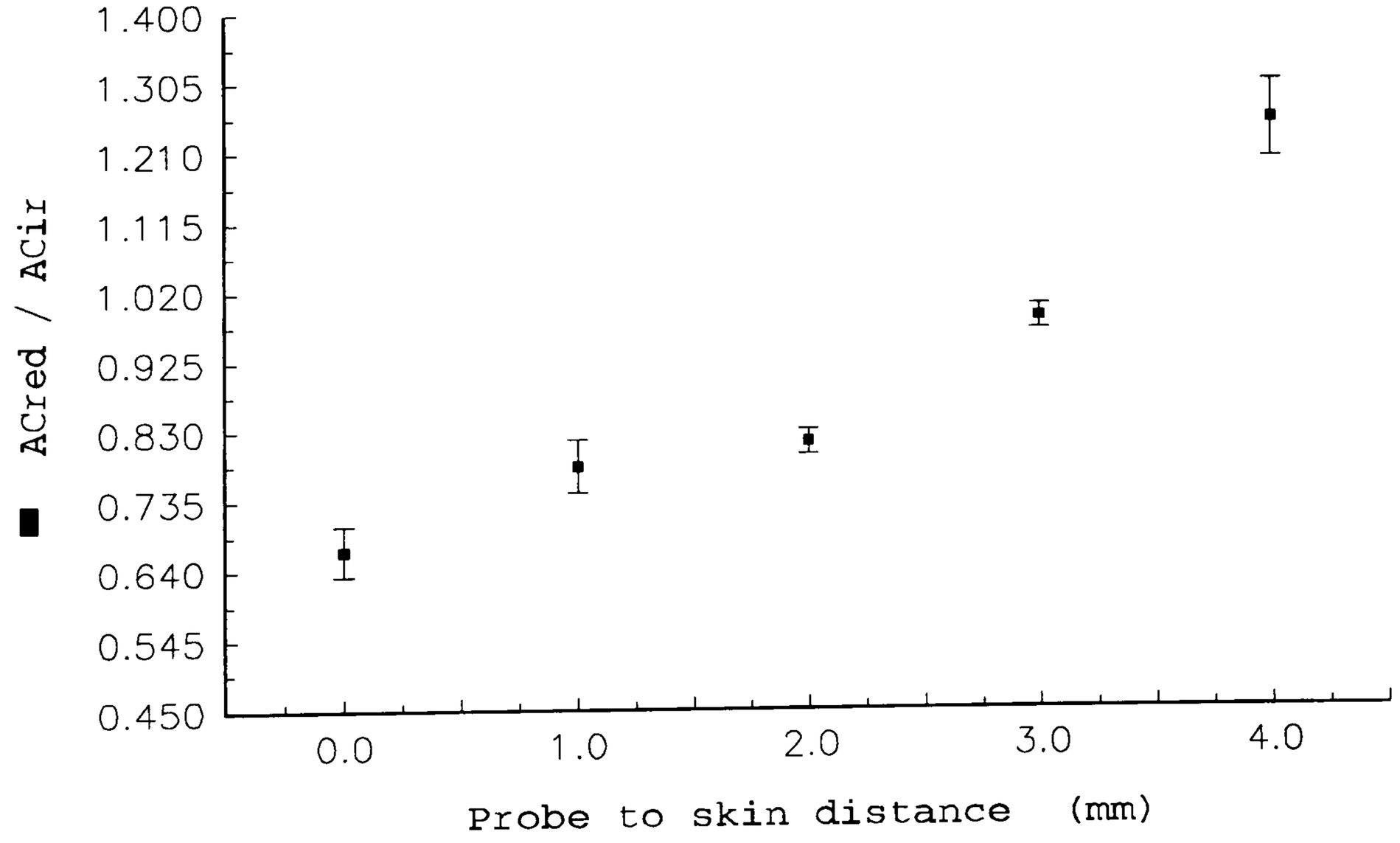

Figure 6.7: The effect of increasing the probe to skin distance on the AC_{red}/AC_{ir} ratio.

A plausible explanation of these results is that the red and infrared AC differences are caused by different pathlengths due to scattering. Once contact with skin is broken the geometry between probe and skin changes and the difference in scattering between the red and infrared signals results in the ACred/ACir variations observed. This of course means that a Lambert-Beer model for pulse oximetry is rejected, which was discussed in chapter 2. In support of these findings is a different observation made by Mendelson (Mendelson, 1988a) and Graaff (Graaff, 1991) regarding the ratio **R** and the distance between emitter and detector in a reflectance probe. In their experiments the probe remained in good contact with the skin at all times but the distance between the emitter and detector was varied. This resulted in differences in the ratio **R** caused again by a varying AC_{red}/AC_{ir} ratio.

Again, as in all cases what appeared to be normal AC PPG signals (in terms of shape) were obtained. This did not give any indication about incomplete probe application. A typical AC PPG at a distance of 3mm is shown alongside one at contact in Fig. 6.8.

6.4.1.3 The R ratio

The increase of the AC_{red}/AC_{ir} ratio with increasing probe to skin distance, and the relatively unchanged DC_{ir}/DC_{red} ratio, results in an increase of the ratio **R**, Fig. 6.9. This increase of the ratio **R**, results in a decrease in the calculated oxygen saturation (SpO_2) in a similar way as described in the preliminary investigation section 6.2. This is shown in

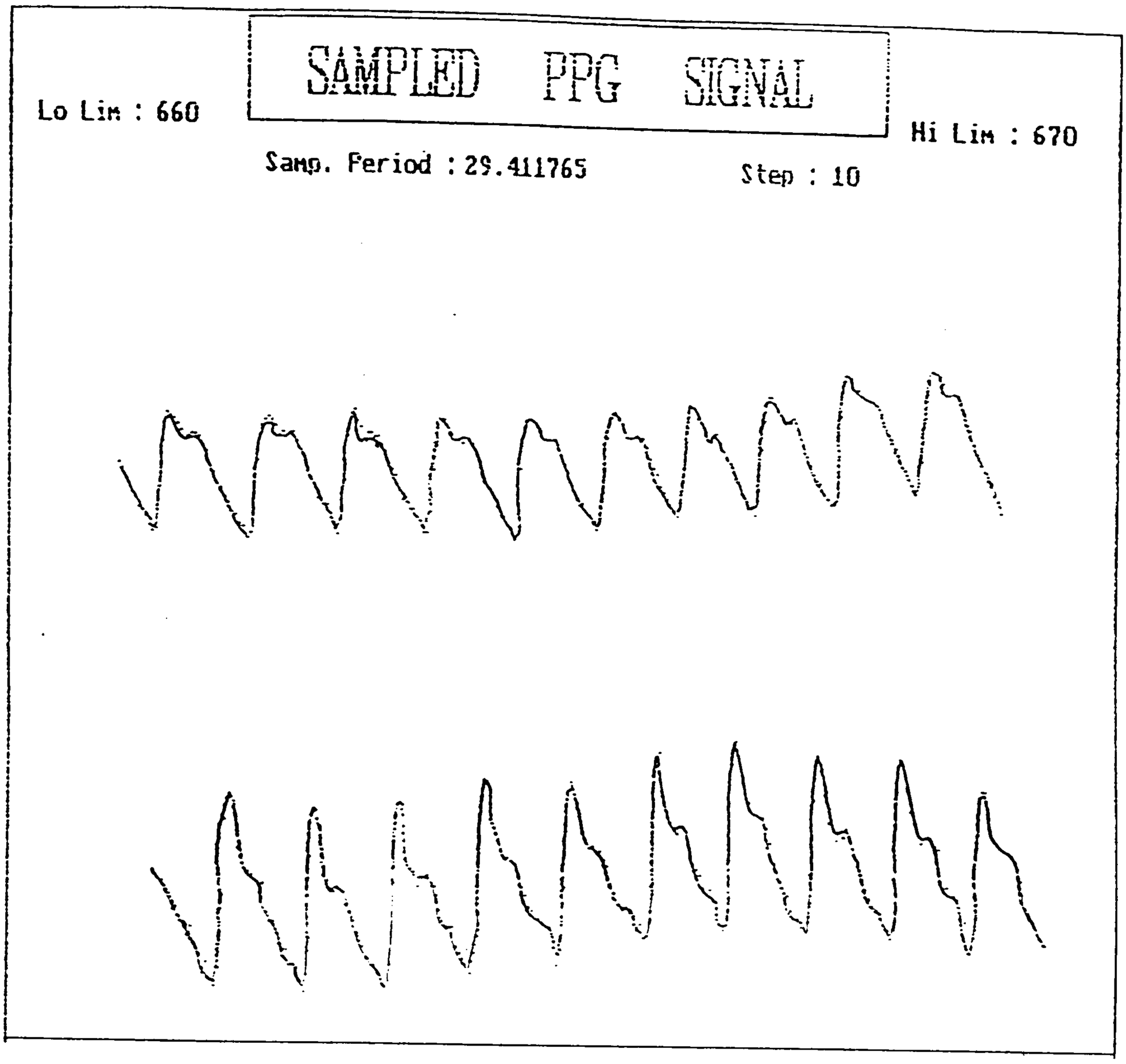

Figure 6.8: AC photoplethysmograms. The top signal is at contact and the bottom one at 3mm away from the skin.

Fig. 6.10 where the decrease of oxygen saturation is plotted against the increasing probe to skin distance. Please note that oxygen saturation readings shown above are only approximate, since a general calibration curve (Fig. 2.4) shown in section 2.1.1 was used and not one specifically derived for this instrument. This however, does not affect or invalidate in any way the above observations with regards to the increase in **R** with increasing distance.

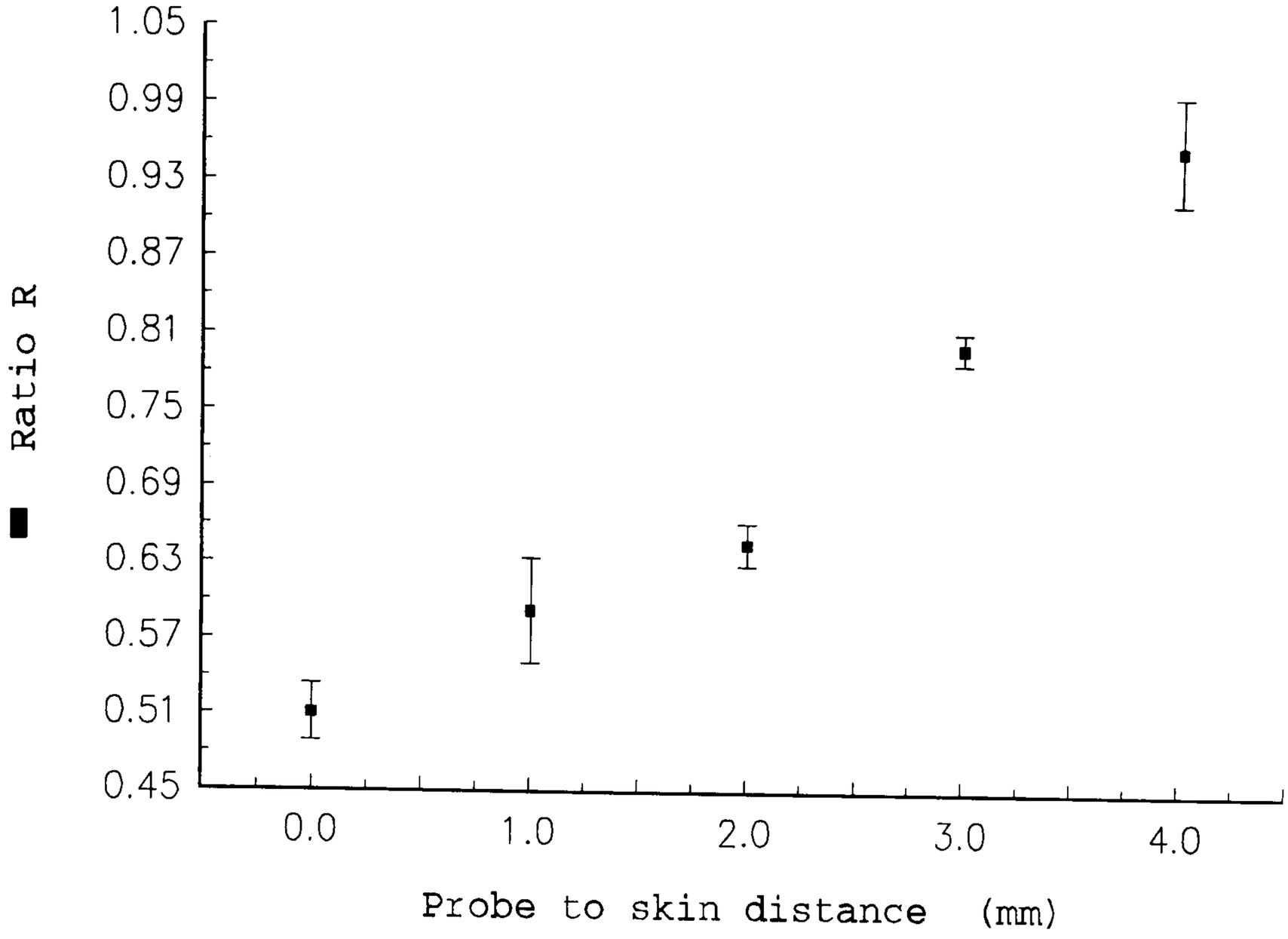

Figure 6.9: The affect of increasing the probe-skin distance on the ratio **R**, in reflection mode.

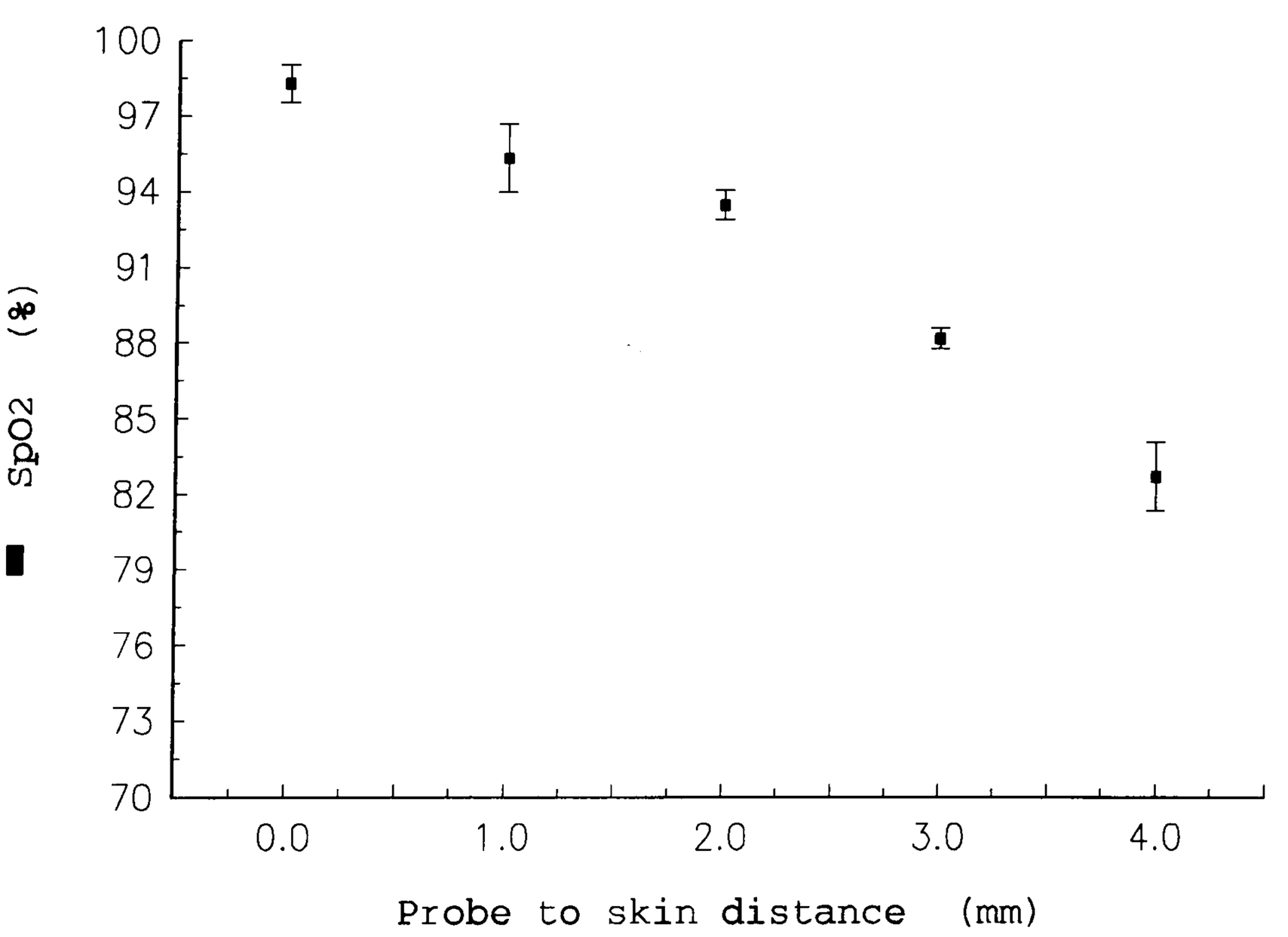

Figure 6.10: The effect of increasing the probe to skin distance on the SpO_2 readings. Please note that SpO_2 values are only approximate. See text for details.

6.4.2 New Reflectance Probe

The probe design in Fig. 6.2 was modified to the one shown in Fig. 6.11.

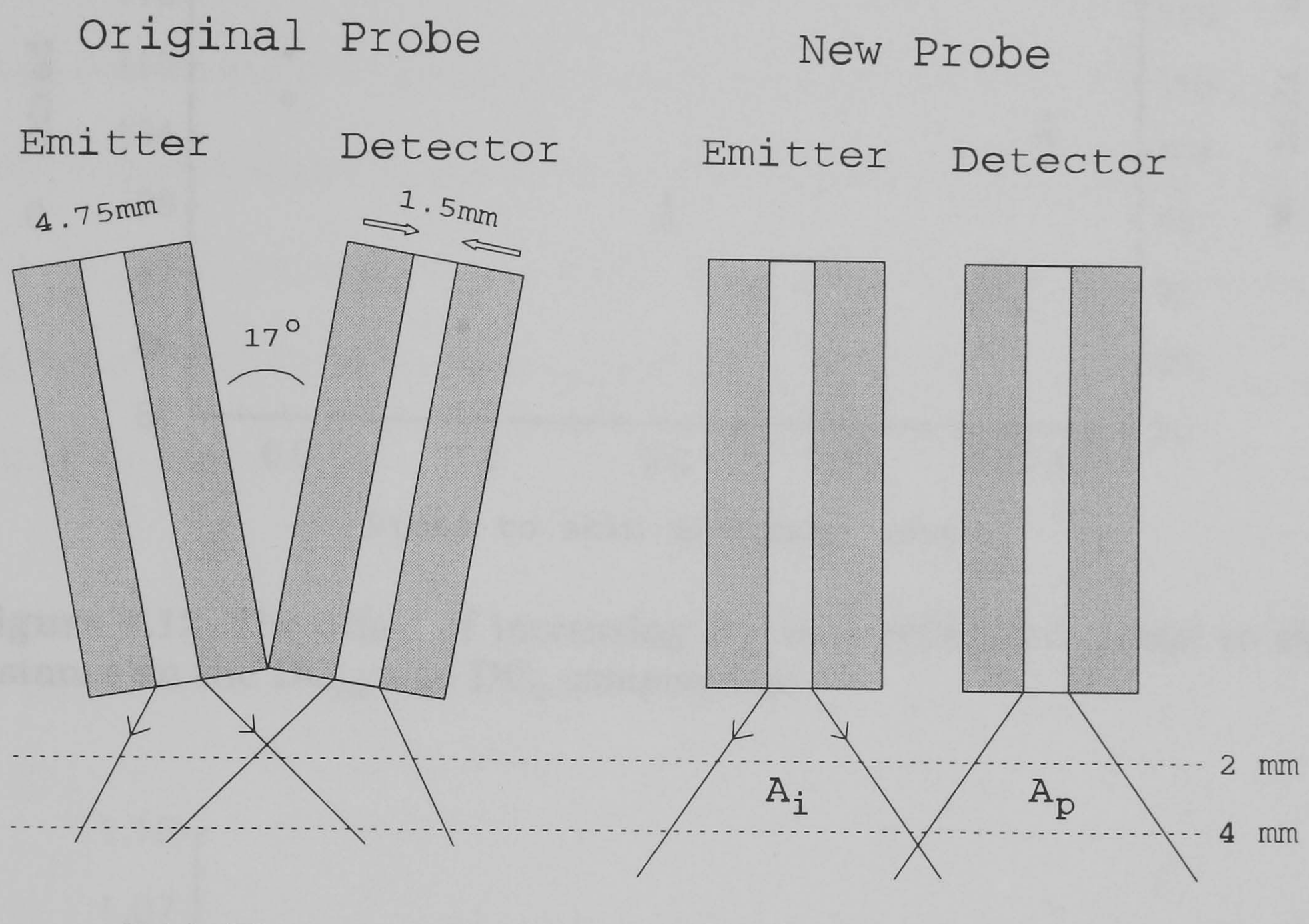

Figure 6.11: The new reflectance probe design as shown on the right, compared to the original design.

The fibre bundles were placed next and parallel to each other. Measurements in this case were only taken at contact, 2mm and 4mm away from the skin.

6.4.2.1 The DC components

This arrangement prevented any direct reflections from the skin to be picked up by the receiving bundle for up to a distance of just over 4mm. This was reflected by the resulting DC signals shown in Fig. 6.12 and the DC_{ir}/DC_{red} ratio which remained constant as shown in Fig. 6.13.

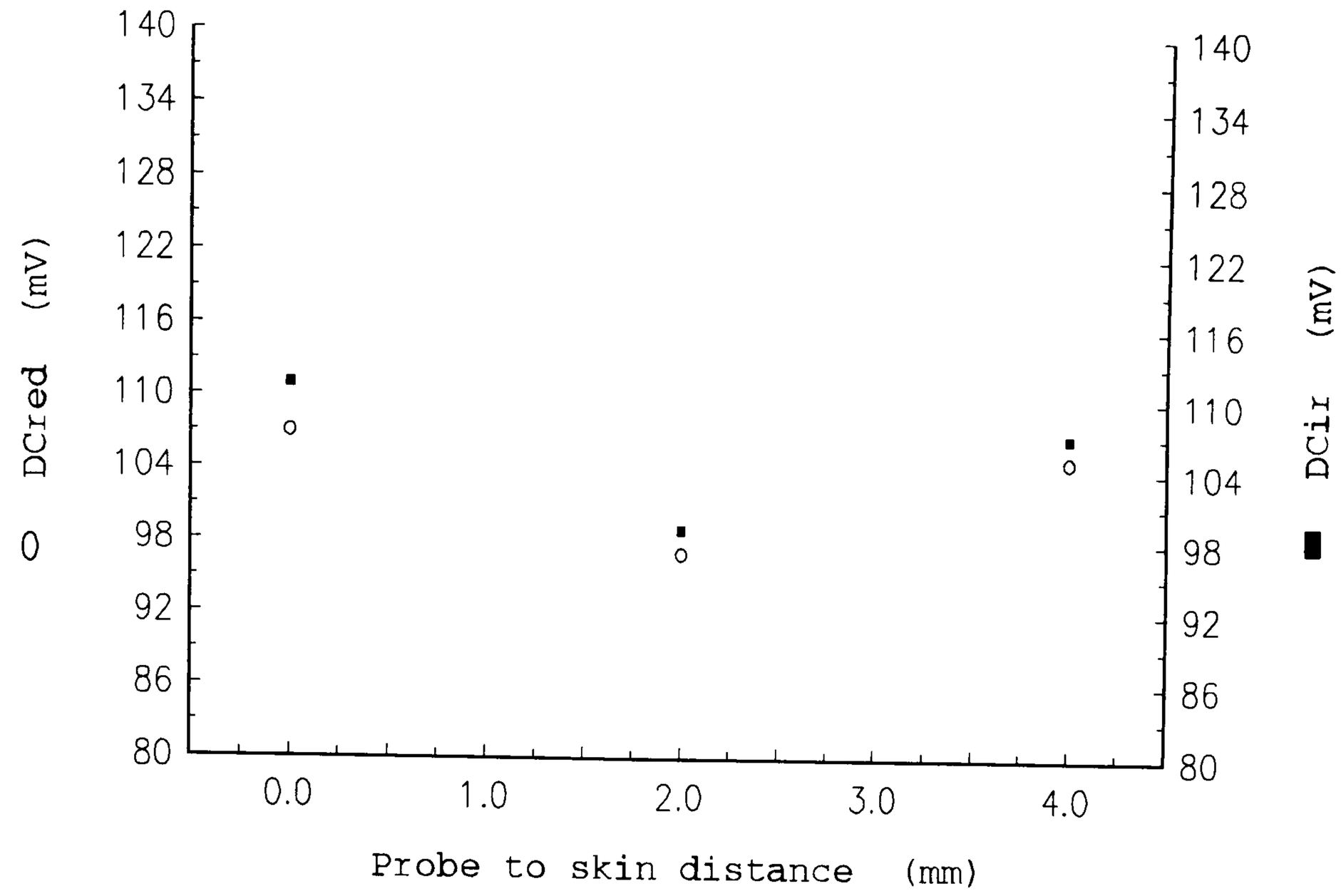

Figure 6.12: The effect of increasing the new reflectance probe to skin distance on the DC_{red} and DC_{ir} components.

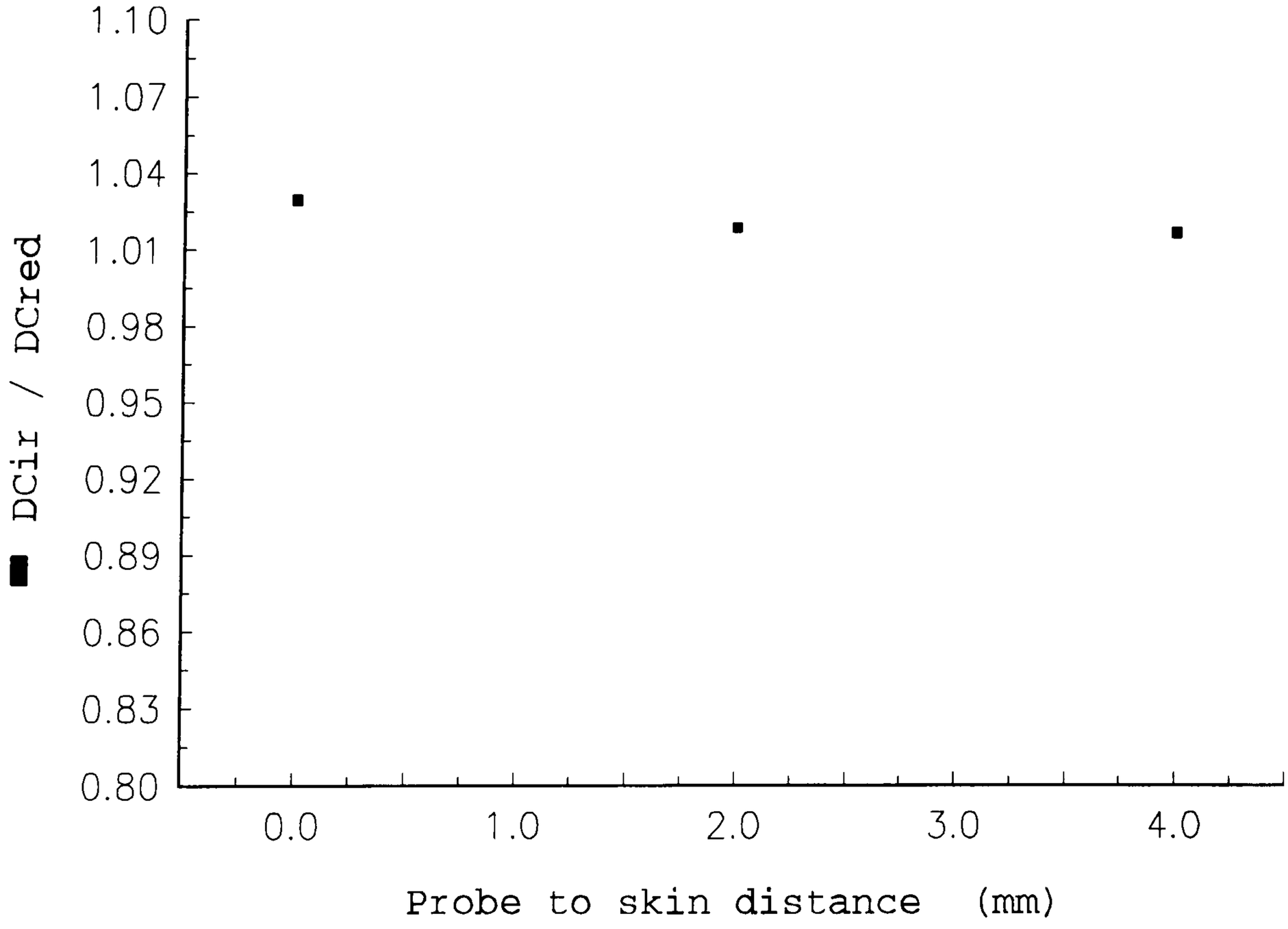

Figure 6.13: The effect of increasing the new reflectance probe to skin distance on the DC_{ir}/DC_{red} ratio.

6.4.2.2 The AC components

Similar to the AC components for the original reflection probe the AC components for the new reflectance probe follow a similar pattern, both decreasing for a distance of 4mm, as shown in Fig. 6.14. Again, the rate of increase and decrease for the two signals is different, resulting in the AC_{red}/AC_{ir} ratio as shown in Fig. 6.15. The AC_{red}/AC_{ir} ratio increased again as it did for the original probe design, but in this case with a lower rate of increase.

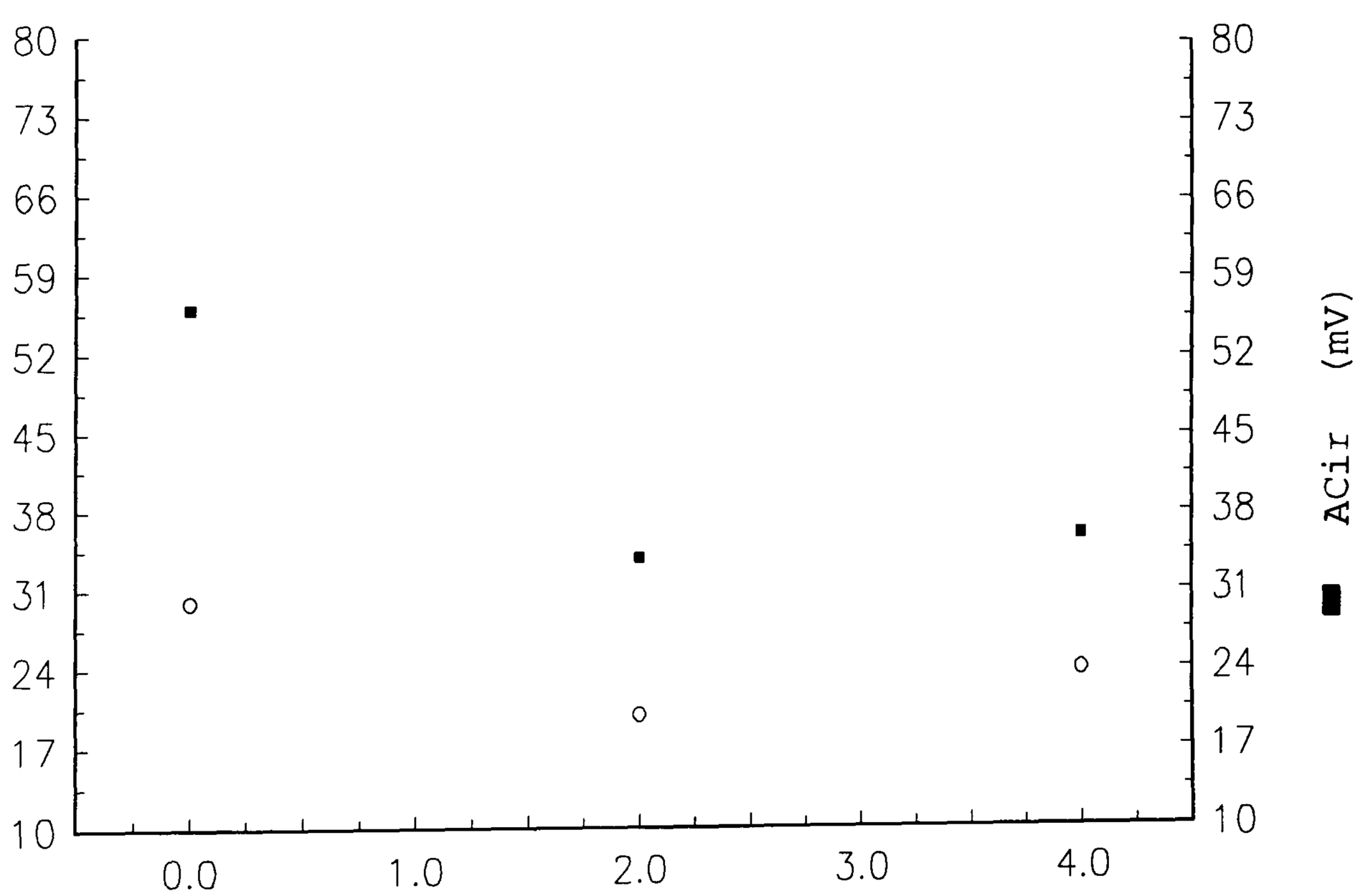

Figure 6.14: The effect of increasing the new reflectance probe to skin distance on the AC_{red} and AC_{ir} components.

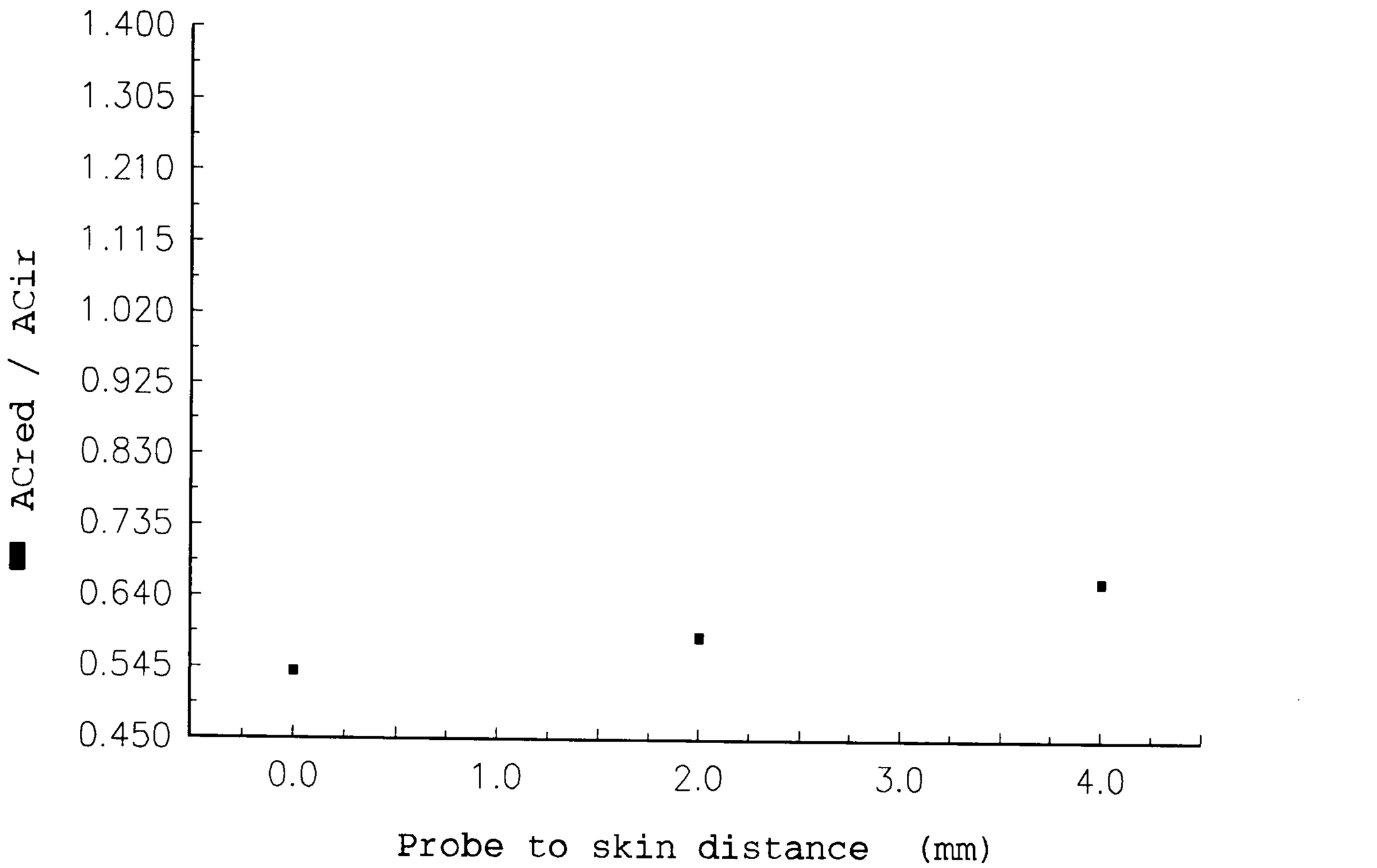

Figure 6.15: The effect of increasing the new reflectance probe to skin distance on the AC_{red}/AC_{ir} ratio.

6.4.2.3 The R Ratio

The resulting **R** ratio again increased with distance from the skin as shown in Fig. 6.16. Comparison, however, of Fig. 6.16 and Fig. 6.9 shows that the increase of the ratio **R** as the probe is moved away from the skin was less for the new probe design. Consequently, the resulting decrease in oxygen saturation calculation as shown in Fig. 6.17 is less for this new probe and the gravity of this artifact reported here less severe.

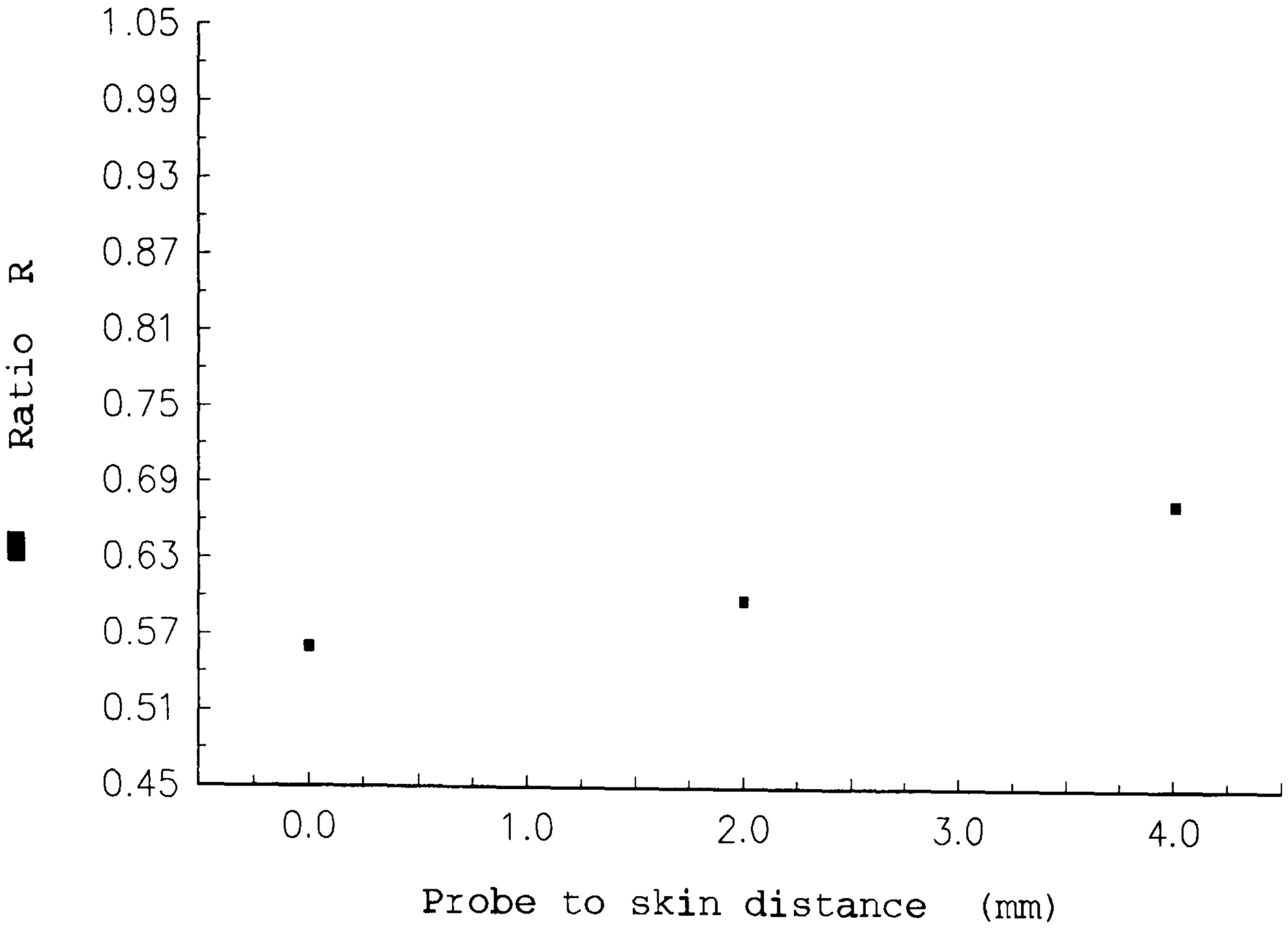

Figure 6.16: The effect of increasing the new reflectance probe to skin distance on the ratio **R**.

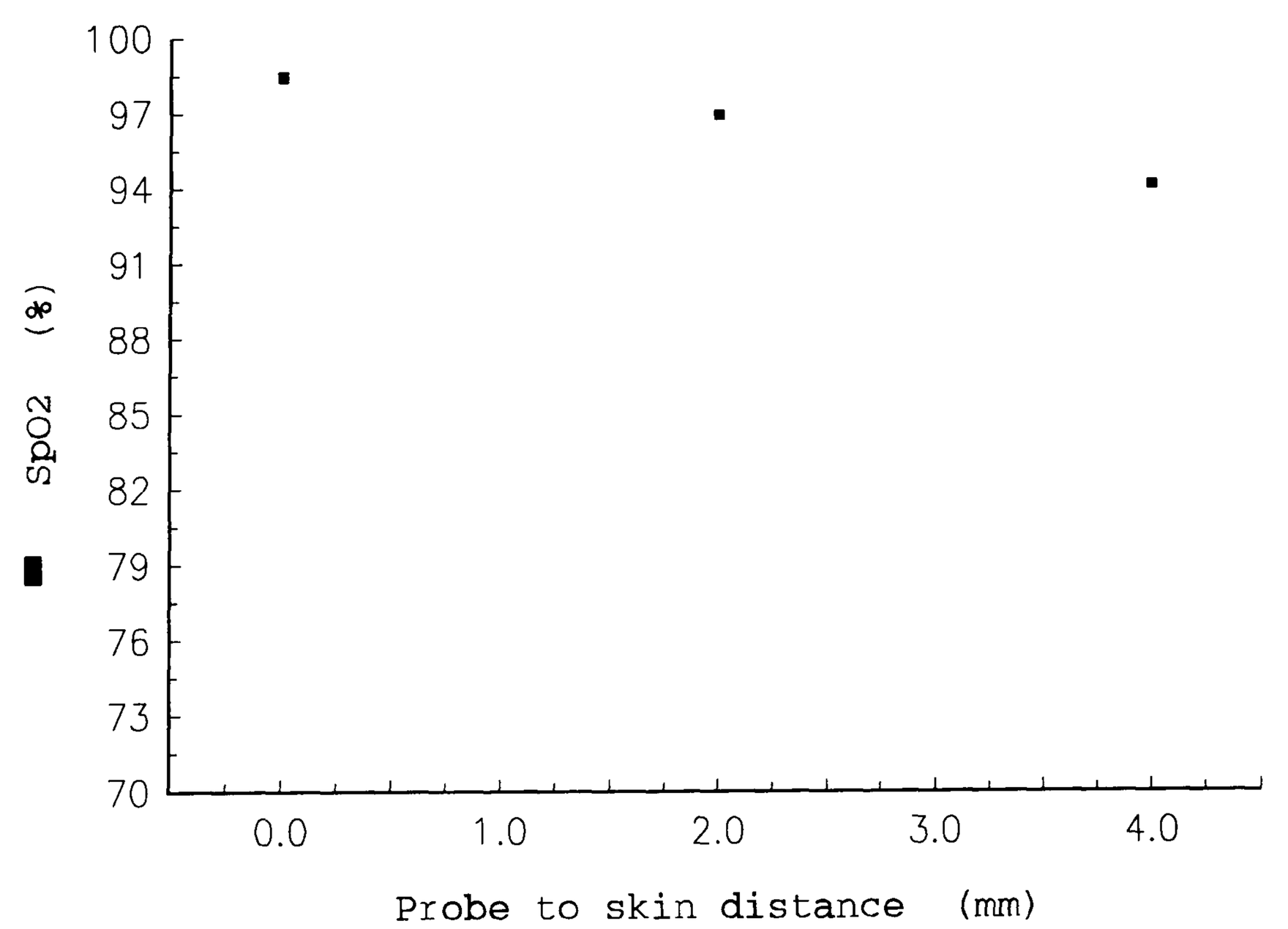

Figure 6.17: The effect of increasing the new reflectance probe to skin distance on the SpO_2 readings.

6.4.3 Transmission Probe

The transmission probe employed the same two fibre bundles as the reflection probe above, with each on either side of the fingertip. The receiving fibre bundle was kept in good contact with the skin at all times, whereas the position of the transmitting fibre bundle with respect to skin surface was varied from contact to 4mm away in steps of 1mm. Again, AC and DC PPG measurements were taken at the 660 and 940nm wavelengths for each probe position. Direct shunting was avoided in this case since the finger rested loosely in the custom made holder which was constructed from an opaque material.

In this case even though the individual AC and DC components varied with the changes in the probe to skin surface distance, the AC and DC ratios remained unaffected. Consequently, the ratio **R** remained constant for all probe to skin separation distances as shown in Fig. 6.18, ensuring oxygen saturation readings remained unaffected.

6.5 DISCUSSION

These laboratory results verified the original observation with a commercially available reflectance pulse oximeter, that with increasing probe to skin distance the ratio **R** is increased, resulting in a false low SpO_2 reading. Therefore, incomplete probe application in reflection pulse oximetry would result in a false low SpO_2 reading. The clinical importance of this artifact is well illustrated with an effect that sometimes can be observed during labour, where on occasions, the oxygen saturation value

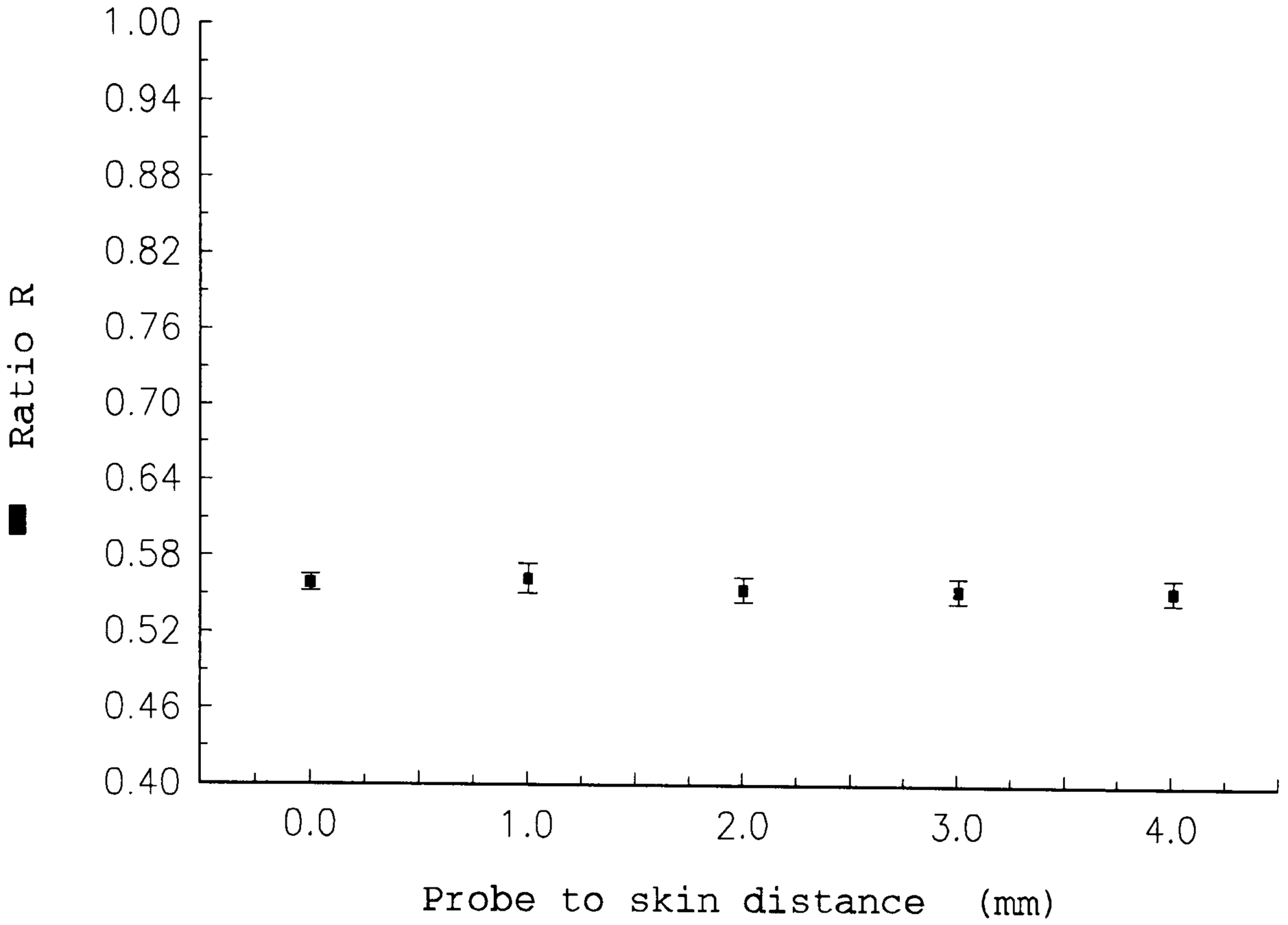

Figure 6.18: The effect of increasing the probe to skin distance on the ratio **R**, in transmission mode.

was found to be increasing. In fact, this artifact was recorded unnoticed in another fetal oximetry study (Johnson, 1991) where a graph displays a regular increase in saturation with each contraction. Many different theories have been put forward as to reasons for such an increase, but a simpler explanation based on these findings is that with every contraction a poorly applied probe is temporarily pressed into better contact giving an increased SpO_2 reading which is probably closer to the true baseline for that fetus. Clearly, fetal pulse oximetry can only establish itself as a reliable adjunct or alternative to current techniques, if this artifact is excluded.

There are several ways of rectifying this problem. One way is to design a new probe that will ensure good skin contact at all times. This

seems to be the route preferred by the teams of physicians and engineers working on this problem. Another way is to incorporate software in the pulse oximeter that would correct any false low readings. Of course, such correction could only be possible if means for establishing any probe malposition and more importantly measuring the probe to skin separation distance are built into the probe design.

A different approach would be to modify probe geometry in such a way that will make the system immune to changes of probe to skin distance variations. This approach was examined in section 6.4.2 and the preliminary results presented in that section, from experiments with a new redesigned fibre bundle reflectance probe, suggest that this is possible. The new design was a result of observations regarding the size and relative positioning of the illuminating area A_i and the probing area A_p, as shown in Fig. 6.11. In the new probe the areas A_i and A_p increased at a slower rate with increasing distance, compared to the original probe design. Moreover, with the new probe design the two areas remained distinct up until a distance of 4mm from the skin. In contrast, with the original probe design the two areas started to merge at a distance of 2mm from the skin.

A probe that is always illuminating and "looking" at the same area irrespective of its position from the skin, would decrease this type of artifact. This could be achieved either by introducing fibres with smaller acceptance angles or introducing extra optical components.

6.6 CONCLUSION

Poor probe to skin contact in reflectance pulse oximetry may cause false oxygen saturation readings despite the presence of good photoplethysmograms and hence go unrecognized. This artifact should be excluded before pulse oximetry can become useful for intrapartum fetal monitoring. A new reflectance probe design, as discussed above, with improved geometry that allows a smaller increase or even better no increase in the probing area as it is moved away from the skin surface, would decrease this type of artifact.

CHAPTER 7

PROPOSAL OF A NOVEL, VISIBLE WAVELENGTH, REFLECTANCE PULSE OXIMETER

7.1 INTRODUCTION

In the first two chapters of this thesis the operation and uses of pulse oximetry have been extensively explained. Although the current situation regarding pulse oximetry is that of an extremely commercially successful instrument, its operation is nevertheless widely acknowledged to be incompletely understood. Original pulse oximeter theory purported to show that use of a pulsatile waveform meant that arterial oxygen saturation was being calculated, hence its advantage over earlier oximeters which gave tissue oxygen saturation. However, as explained in detail in chapter 2 and by the results obtained and discussed in chapters 4, 5 and 6 these early theories are now universally agreed to be too simplistic to apply to instrument calibration and this procedure is now

performed empirically. A more probable reason for the success of pulse oximetry is its ease of use, with a very easy to apply sensor and no calibration procedures to be followed before monitoring. A technical reason for its success is due to the fact that the cardiac derived photoplethysmographic (AC PPG) signal is used in the derivation of oxygen saturation. The use of this modulated signal facilitates a much more reliable form of monitoring.

Although several problems have been reported relating to the use of pulse oximeters, it has to be emphasized again that pulse oximeters are very reliable clinical instruments in most cases, and this has been clearly proved over the last few years. However, the reservations reported here regarding the underlined theory of pulse oximetry in some specific uses of this type of monitoring, is that in certain circumstances its use should be reconsidered pending further investigations or a redesign.

7.2 THE PROPOSAL

The study of the wavelength dependence of the AC and DC components of the photoplethysmogram in chapter 4, was not only concerned with the wavelength range from 650 - 1000nm where pulse oximeters operate, but also the visible region below these wavelengths where the absorption of light by haemoglobin compounds is much stronger, by approximately two orders of magnitude. Indeed it is for this reason that the whole visible region is not used in transmission pulse oximetry

because of the resultant low level of light emerging from the tissue surface.

To briefly summarise, our results show unexpected phenomena regarding the levels of detected light and confirm that the mechanisms underlying transmission and reflection pulse oximetry are undoubtedly different. However, of particular relevance to this proposal was the finding that it was possible to obtain reliable pulsatile signals in reflectance mode using the visible region of the spectrum where the spectra of haemoglobin compounds possess characteristic features.

The proposal is to construct an instrument that will obtain both the non-pulsatile and pulsatile components of backscattered light from tissue (ie in reflectance mode) over the 500-600nm wavelength region. These signals will then be processed to produce oxygen saturation measurements. Firstly the equipment needed to construct this novel pulse oximeter is described and then its advantages and potential use are described.

7.2.1 Equipment

The form that the instrument would take would be of a continuous (white light) source, with band pass filters restricting the output to approximately 500 to 600nm. Light would be piped to and from the tissue by using fibre bundles. A fibre bundle delivers the filtered light to the finger and a second one collects the backscattered light after its interaction with the finger tissue and blood. In practice two individual

fibre bundles placed next to each other could be used or a bifurcated one. The backscattered light needs to be split into its constituent colours in order to be able to identify the level of interaction of different wavelengths within the 500 to 600nm range and the finger. This function can be performed by a dispersive element, such as a prism or a grating, coupled to a photodetector array. The resolution of such an arrangement is mainly dependent on the size (pixel number) of the photodetector array. The output of this would be passed to a digital signal processor (DSP) board hosted by a PC for subsequent processing and display of results. A schematic diagram of this is shown in Fig. 7.1.

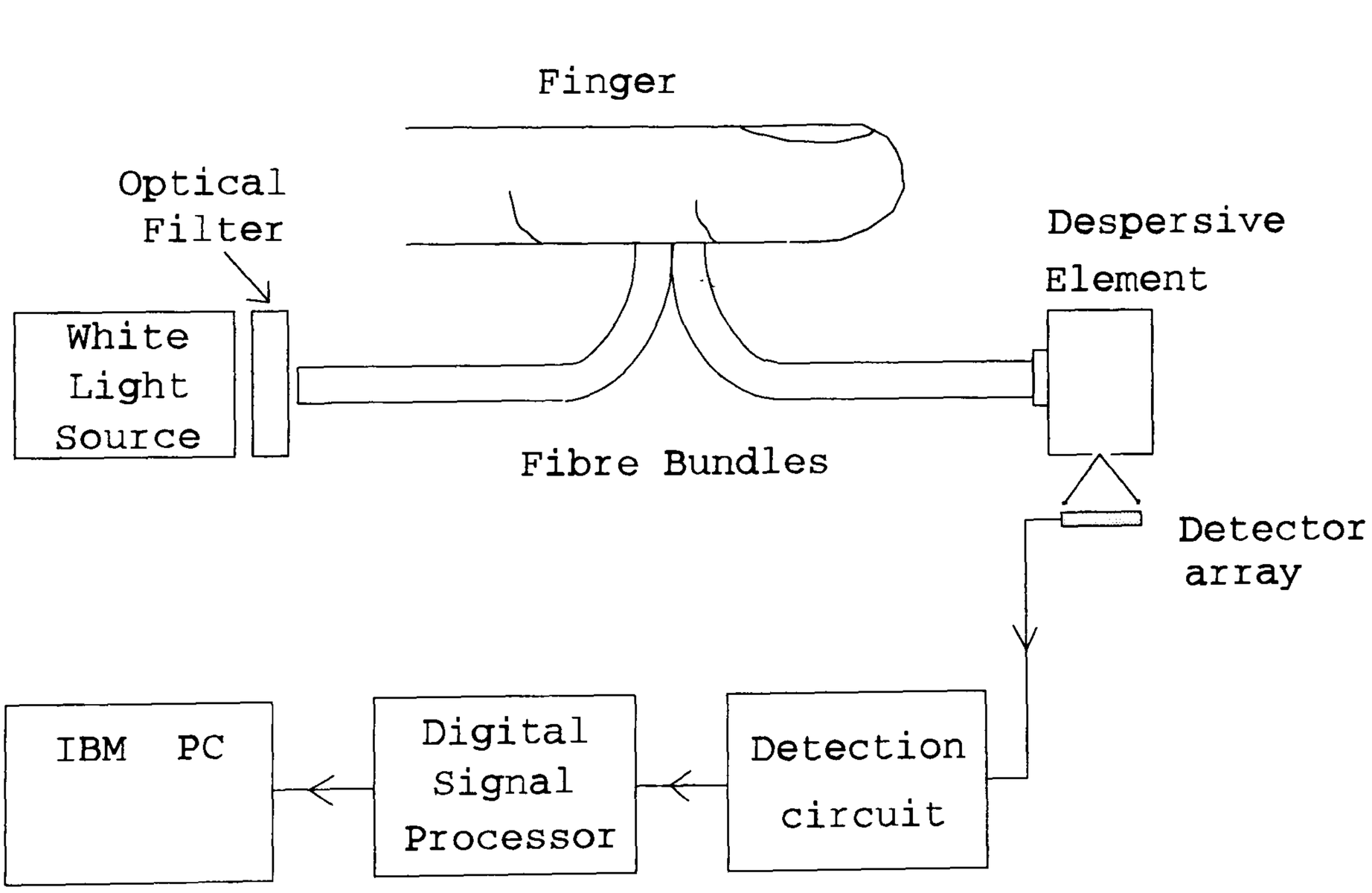

Figure 7.1: Schematic diagram of the proposed visible wavelength, reflectance pulse oximeter.

7.2.2 Advantages of the new monitor

Use of non-pulsatile signals (DC PPG) alone for *in vivo* spectroscopic analysis (including tissular oxygen saturation) has already been practised whereas pulse oximetry requires both sets of data, since it depends upon the pulsatile/non-pulsatile ratio (AC/DC), and in principle gives arterial $Sp0_2$. The aim here would be to use both techniques together which could lead to both tissue and arterial monitoring of oxygen saturation being possible with a single instrument.

Use of a continuous source rather than the LEDs would appear to be a disadvantage of the proposed instrument over usual pulse oximeters (in terms of size and expense since a dispersive element and photodiode array are required), but the potential advantages are considered to outweigh this in the following three ways.

Firstly, because with non-pulsatile measurements there is no signal to 'lock' onto it is difficult to discern what is noise and what is artefact (eg movement) when using single wavelength measurements. When the whole spectra is recorded this problem is largely overcome simply because the volume of data is larger and it is possible to look for spectral signatures, hence the type of analysis of the non-pulsatile signals proposed becomes possible.

Secondly, in the proposed region to be monitored the various forms of haemoglobin that can be produced, all possess distinctive spectra and can therefore be distinguished. This is of extreme significance since one of the problems with current pulse oximeters is that they assume only

two forms of haemoglobin are present (Hb and HbO_2) which in the case of both heavy smokers and victims of smoke inhalation is certainly not so, where higher concentrations of carboxyhaemoglobin are present. The inability of current pulse oximeters to distinguish all the forms of haemoglobin stems from the fact that only two measuring wavelengths are used and thus only two forms of haemoglobin (Hb and HbO_2) can be discriminated. Moreover, in the near infrared the absorption spectra of different haemoglobins are less distinct, thus usage of extra wavelengths in this region in order to facilitate differentiation of all haemoglobin derivatives would be harder to achieve. Consequently, for two classes of patient who are likely to be in need of such technology its use is compromised. Both of these problems would be solved by this new instrument. In addition a reflectance probe design as described in chapter 6 would be a distinct advantage in the case of burns victims, where reliable oxygen saturation readings could be obtained remotely, in case it is practically difficult to attach the probe on the patient.

The third advantage of using a continuous source is related to the empirical calibration of pulse oximeters and in some instances almost arbitrary choice of transmission or reflectance modes for monitoring, which means that their use for accurate quantitative measurement is questionable. For **qualitative monitoring** where changes in oxygen saturation are being looked for, this is much less of a problem. However, pulse oximetry, because of its ease of use, is now being used in applications where it is most inappropriate.

An example of this is in the measurement of oxygen tension in premature infants undergoing oxygen therapy. Due to incomplete lung development in such neonates oxygen is given to maintain adequate oxygen tension, however it is known that too much oxygen may lead to blindness via retrolental fibroplasia. Therefore accurate knowledge of oxygen tension is vital. This can be obtained directly via electrochemical oxygen electrodes, but their use has recently given way to pulse oximetry whose "sensors" are far easier to apply for clinical staff. The unsuitability for this task in particular is because it only measures oxygen **tension** (PO_2) indirectly via its relationship with oxygen **saturation** given by the oxygen dissociation curve, as explained in section 1.1.2.1. The problem is that in the region of SaO_2 of interest, the right upper portion of the oxygen dissociation curve as shown in Fig. 1.2, the gradient of $d(SaO_2)/d(PO_2)$ is extremely small and therefore using SpO_2 as an indicator of PO_2 is ill-advised. This is because it is the oxygen tension that is the important parameter as far as tissue damage is concerned. Clearly oximetry alone cannot guard against hyperoxia on the upper reaches of the dissociation curve and in the case of preterm babies receiving oxygen, partial pressure should be monitored when SpO_2 readings are higher than 90% (Dear, 1987). To date no firm guidelines in the usage of pulse oximetry regarding minimum and maximum SpO_2 limits, for the monitoring of premature and newborn babies are enforced.

As explained earlier the use of pulse oximeters as a quantitative monitor is questionable and sometimes too much reliance is given in pulse

oximeters readings, maybe due to incomplete understanding of pulse oximetry theory and limitations and also maybe due to over familiarisation with this method of monitoring due to its ease of use. In a recent communication (Lakanpaul, 1994) nursing staff were increasing levels of oxygen therapy to newborn babies because the pulse oximeter reading was lower than what thought to be the "normal" 98%, even though other methods of blood gas analysis did not indicate the need for such a procedure.

Consequently, pulse oximetry in reflectance (arguably the least reliable) mode is now being used for an important operation where the technique is known to be problematic. If it is to remain to be applied to this task, it is suggested that an instrument such as the one proposed would, via multiple wavelength pulse oximetry, be more likely to provide accurate results.

As a final point it should be noted that to the best of the author's knowledge neither a visible nor multiple wavelength oximeter, has been constructed previously. Although very early (non-pulse) oximeters used visible wavelengths in reflection mode, recent oximeters work in transmission mode with near-IR wavelengths coinciding with the so called "transmission window" in the attenuation of light by tissue. Naturally the development of transmission pulse-oximeters utilised similar wavelengths.

This proposal is to turn away from this convention, and attempt to use the visible region where haemoglobin compounds have characteristic spectra, employ scanning spectrophotometry and process both non-

pulsatile and pulsatile data simultaneously to discern as much as possible about the haemodynamic status of the tissue and arterial and venous systems.

It is appreciated that the proposed instrument would be more bulky and complex than current pulse oximeters. However, the aim is not to replace all such devices rather only those where their use may lead to incorrect results. Furthermore it is realised that what is given above are suggestions as to where use of such an instrument would be of benefit without specific reference to the signal processing requirements. It is assumed that the necessary data will be present and is therefore simply a matter of extracting it. This is in fact quite similar to the way in which the algorithms used within pulse oximeters have been latterly developed, ie in a semi empirical manner.

CHAPTER 8

CONCLUSIONS

Although the principles of oximetry (the determination of oxygen saturation using optical measurements) have been known since the turn of the century it was not until the early 1980s that the technique found widespread clinical use in the form of pulse oximetry. Since then, the increase in use of pulse oximeters in all critical care situations has been quite remarkable, turning it into one of the most important methods of monitoring in use today. All forms of oximetry rely upon the differences in the absorption spectra of haemoglobin (Hb) and oxyhaemoglobin ($Hb0_2$) which mean that by measuring light attenuation at two wavelengths the oxygen saturation (SaO_2) can be determined. Pulse oximeters use the ratio of the pulsatile and non pulsatile components of light scattered from tissue at two wavelengths (typically 660 and 940nm) to calculate oxygen saturation. The factors that have made pulse oximetry a success where

other earlier oximeters failed is its processing of the cardiac synchronous component of light backscattered from tissue, related to the arrival of the "pulse", and also the exploitation of recent technological advances in light emitting diodes and microprocessors.

Original pulse oximeter theory purported to show that use of a pulsatile waveform meant that arterial oxygen saturation was being calculated, hence its advantage over earlier oximeters which gave tissue oxygen saturation. However, these early theories are now universally agreed to be too simplistic to apply to instrument calibration and this procedure is now performed empirically.

The current situation regarding this technique is therefore that of a commercially successful instrument whose operation is nevertheless widely acknowledged to be incompletely understood. This is not to say that pulse oximeters are not valuable clinical instruments, which is clearly proven, but that perhaps their use in **certain** circumstances should be reconsidered along with a possible redesign.

Therefore the study of the wavelength dependence of the magnitude of the pulsatile and non-pulsatile components of light scattered from tissue, is of extreme importance in trying to assess and understand the way that pulse oximeters really operate, whether in reflection or transmission mode. This ties in with a new trend of using transmission pulse oximeters with multi-site sensors which can be used in either transmission or reflection mode. Consequently any observed deviations either from the wavelength dependence predicted by existing pulse

oximetry theory or between reflection and transmission mode would suggest that the output from pulse oximeters should perhaps be viewed with caution.

The wavelength dependence of the photoplethysmographic signals in both refection and transmission modes in studies on the fingertip was therefore investigated. This work has not only used the wavelength range from 650 - 1000nm where pulse oximeters operate, but also the visible region below these wavelengths where the absorption of light by haemoglobin compounds is stronger by approximately two orders of magnitude, thus covering the 450-1000nm range. The possibilities of using other wavelengths, instead of 660 and 940nm, especially in the visible region was examined with the aim of improving the accuracy and overcoming certain limitations of existing instruments.

The experimental results obtained on the wavelength dependence of the AC, DC and AC/DC PPG components for the 450 - 1000nm range are undoubtedly different to the ones predicted by the current simple pulse oximeter model based on the Lambert-Beer law. Moreover, they show unexpected phenomena regarding the magnitude of the above components over the whole range, with distinct differences between the reflection and transmission modes. However, for the two most common wavelengths used today (660 and 940nm) the behaviour of the normalised AC components is similar; this probably being a reason why oximeters operating in transmission and reflection give similar results. In contrast, in reflection it was noted that the signal to noise ratio of the 660nm AC

PPG was low, thus potentially having an adverse effect on the monitoring reliability of reflection pulse oximeters. Furthermore, of particular importance was the finding that it is possible to obtain reliable pulsatile signals in reflectance mode using the visible region of the spectrum where the spectra of haemoglobin compounds possess characteristic features.

These results suggest that perhaps the wavelengths used for pulse oximetry should be reconsidered, together with the assumption that reliable oxygen saturation readings taken in this manner will always be independent of the mode of operation.

The possibility of defining a model finger for Monte Carlo simulations of light transport in tissue was also investigated. The aim was to compare the simulation results on the wavelength dependence of the photoplethysmograph with the experimental results. A successful definition of such a model would allow future simulation prediction of the behaviour of pulse oximeters due to the variation of relevant parameters.

The preliminary results obtained from the Monte Carlo simulations in reflection and transmission modes were not in agreement with the experimental results. This was attributed to two reasons. Firstly, further research for determining the optical parameters of several types of human skin *in vivo* and at different wavelengths is necessary before models like the above would be of any use in Monte Carlo simulations. The setup of a database for Monte Carlo parameters would facilitate and encourage more research in this field. Secondly, a new model for pulse oximetry needs to be developed, that would take into

account the heterogeneous structure and concentration of blood in the skin.

A new area in which the use of reflection pulse oximetry is currently under investigation is that of fetal monitoring during labour. Recent advances have raised the question of possible artifacts which may arise due to inadequate probe application in the birth canal. In adult or neonatal pulse oximetry, application does not create a problem, but in the birth canal, the probe has fluids, edema, hair, maternal movements and contractions to contend with. In addition because of the absence of light, the 'ambient light' warning signal that the probe is incorrectly applied is unable to function. Preliminary observations with a commercial pulse oximeter on an adult finger in darkness, reported false low SpO_2 readings associated with malpositioned reflectance probes, even though an apparently normal photoplethysmogram was obtained. This means that any separation of the sensor from the fetal head is likely to lead to similarly low oxygen saturation readings. This new artifact was examined here in detail, using a reflectance probe on an adult finger. This was performed by examining the effect of varying the distance between the reflectance probe and the subject's finger upon the ratio **R**.

With the original reflectance probe, whose geometry resembled the geometry of commercially available ones, an increase in the ratio **R** and consequently a drop in oxygen saturation reading was recorded for every subsequent movement of the probe from the skin, with a final reading of 83% at a distance of 4mm. The generation of this artifact was

traced at the differing behaviour of the AC_{red} and AC_{ir} PPG signals when incomplete probe to skin application was allowed to take place.

This artifact should be excluded before pulse oximetry can become useful for intrapartum fetal monitoring. A new probe design with modified geometry was examined which offered an improved performance in reducing this artifact, with a final SpO_2 reading of 94% (compared to 83% for the original probe). Further suggestions were made for new designs that would further decrease this type of artifact.

Finally, a proposal for a novel, visible multi-wavelength reflection pulse oximeter was given. This was based upon the observations in chapter 4 relating to the size of the AC PPG and the possibility of obtaining reliable pulsatile signals in reflectance mode using the visible region of the spectrum. The proposal turns away from the current convention and attempts to use the visible region where haemoglobin compounds have characteristic spectra, will employ scanning spectrophotometry and will process both non-pulsatile and pulsatile data simultaneously to discern as much as possible about the haemodynamic status of the tissue and arterial and venous systems. It is appreciated that the proposed instrument would be more bulky and complex than current pulse oximeters but the aim is not to replace all such devices rather only those where their use may lead to incorrect results.

In conclusion pulse oximeters are extremely valuable and popular instruments. However, the outcome of this study suggests that more work is necessary in order to further understand their operation. This would

improve their accuracy and use in situations where their use is currently limited and thus increase their spectrum of operation.

APPENDIX A

OXIMETRY ON HAEMOLYSED BLOOD

Haemolysed blood gives a clear solution of purely absorbing media with no scattering material. Therefore, light transmission through haemolysed blood is described theoretically by the Lambert-Beer law. The implementation of oximetry on haemolysed blood in a cuvette is a simple technique, with a fully understood and solid theory behind it.

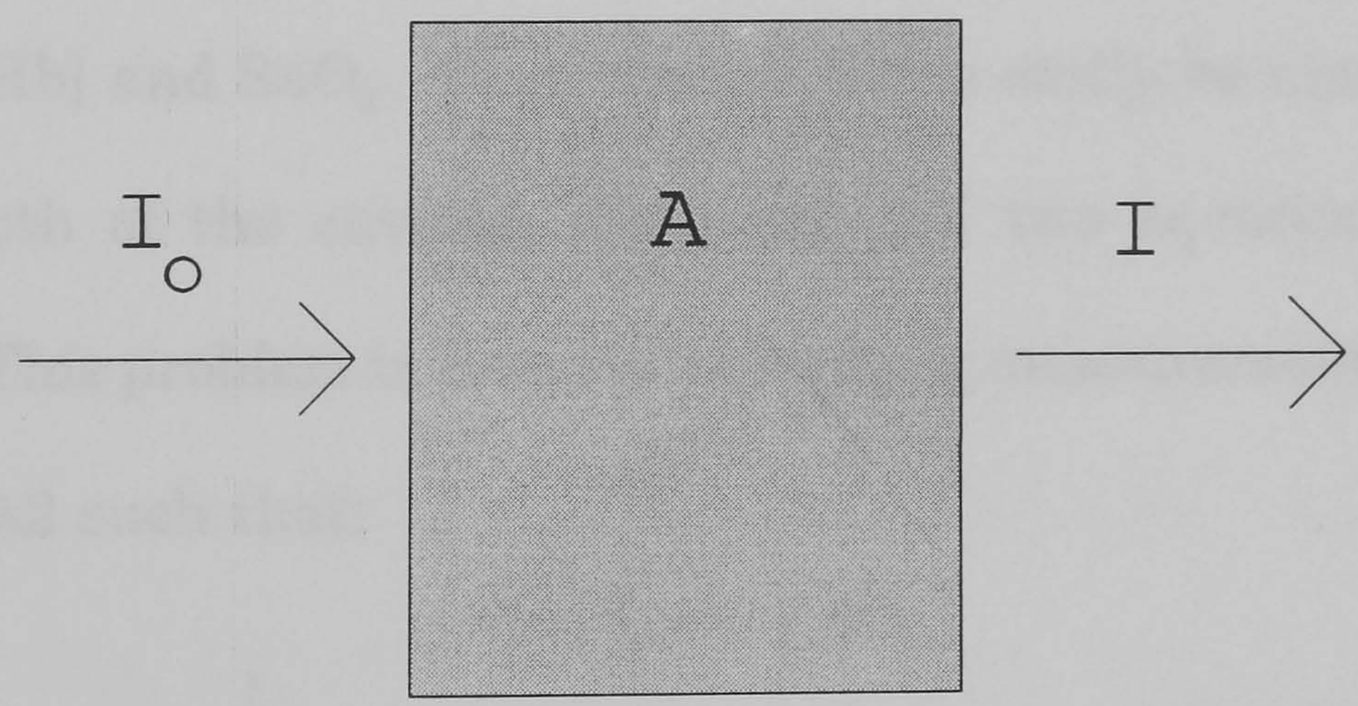

Figure A.1: Application of Lambert-Beer law to a cuvette containing haemolysed blood.

Assuming that haemolysed blood will consist of only haemoglobin, Hb, and oxyhaemoglobin HbO_2 (that is neglecting carboxyhaemoglobin and methaemoglobin) and these have absorption coefficients of $\varepsilon_{\lambda 1}[Hb]$ and $\varepsilon_{\lambda 1}[HbO_2]$ at wavelength λ_1 respectively, then the absorbance $A_{\lambda 1}$ of the solution will be given by:

$$A_{\lambda 1} = \log\frac{I_o}{I_{\lambda 1}} = L\ (\epsilon_{\lambda 1}[HbO_2]C[HbO_2] + \epsilon_{\lambda 1}[Hb]C[Hb]) \qquad \textbf{(A.1)}$$

where L is the path length through the sample, $C[HbO_2]$ and C[Hb] are the HbO_2 and Hb concentrations respectively.

The functional oxygen saturation as defined in chapter 1 is given by:

$$SaO_2 = \frac{C[HbO_2]}{C[HbO_2] + C[Hb]} \qquad \textbf{(A.2)}$$

In the above two equations there are four unknowns, namely L, $C[HbO_2]$, C[Hb] and SaO_2. Even though L can easily be measured, since it is the depth of the cuvette, there are still two equations and three unknowns. This problem is overcome by taking measurements at a second wavelength $\lambda 2$ such that:

$$A_{\lambda 2} = \log\frac{I_o}{I_{\lambda 2}} = L\ (\epsilon_{\lambda 2}[HbO_2]C[HbO_2] + \epsilon_{\lambda 2}[Hb]C[Hb]) \qquad \textbf{(A.3)}$$

where $\varepsilon_{\lambda 2}$ are the respective absorbtion coefficients at the second

wavelength $\lambda 2$.

Solving for C[HbO2] and C[Hb] from equations (A.1) and (A.3) and substituting to equation (A.2) and rearranging, the following expression for the oxygen saturation is obtained:

$$SaO_2 = \frac{\epsilon_{\lambda 1}[Hb] - \frac{A_{\lambda 1}}{A_{\lambda 2}}\epsilon_{\lambda 2}[Hb]}{(\epsilon_{\lambda 2}[HbO_2] - \epsilon_{\lambda 2}[Hb])\frac{A_{\lambda 1}}{A_{\lambda 2}} - (\epsilon_{\lambda 1}[HbO_2] - \epsilon_{\lambda 1}[Hb])} \qquad \textbf{(A.4)}$$

Equation A.4 is independent of L because SaO_2 is a ratio of $C[HbO_2]$ and C[Hb] and therefore the dependence upon L cancels out. This means, though, that only SaO_2 can be found and not the absolute concentrations of haemoglobin and oxyhaemoglobin, without measuring the path length L. Even if a third wavelength is used it will not help since L and haemoglobin concentrations cannot be separated. In other words this optical technique cannot distinguish between and increase in absorbance due to a greater path length or an overall increase in total haemoglobin concentration. However, this analysis shows that absorption measurements at two wavelengths are sufficient to calculate SaO_2 on a haemolysed blood sample.

In this form all four absorption coefficients must be known previously. The two wavelengths are chosen having in mind the absorption spectra of haemoglobin and oxyhaemoglobin. They are usually in the range of red to near infrared.

In practice an isobestic wavelength is usually employed (805nm

at near infrared), which means that at this wavelength the absorption coefficients for Hb and HbO_2 are the same. In this case, assuming that $\varepsilon_{\lambda 2}[HbO_2] = \varepsilon_{\lambda 2}[Hb]$, then equation (A.4) above becomes:

$$SaO_2 = \frac{\epsilon_{\lambda 1}[Hb] - \frac{A_1}{A_2}\epsilon_{\lambda 2}[Hb]}{\epsilon_{\lambda 1}[Hb] - \epsilon_{\lambda 1}[HbO_2]} \qquad \textbf{(A.5)}$$

APPENDIX B

SYSTEM

This appendix presents information on the technical specifications of the photodetectors and the light source used in the instrumentation for the experimental studies in chapters 4 and 6.

A typical spectral response curve for the Hamamatsu 1P28 photomultiplier tube is shown in Fig. B.1 and for the Centronics OSD60-5T silicon photodiode in Fig. B.2. The relative spectral distribution of the light source used by the monochromator is shown in Fig. B.3.

The diagram in Fig. B.4 shows the finger holder(1), the fibre probe holder(2) and the lead-screw arrangement(3) used for the experiments in chapters 4 and 6.

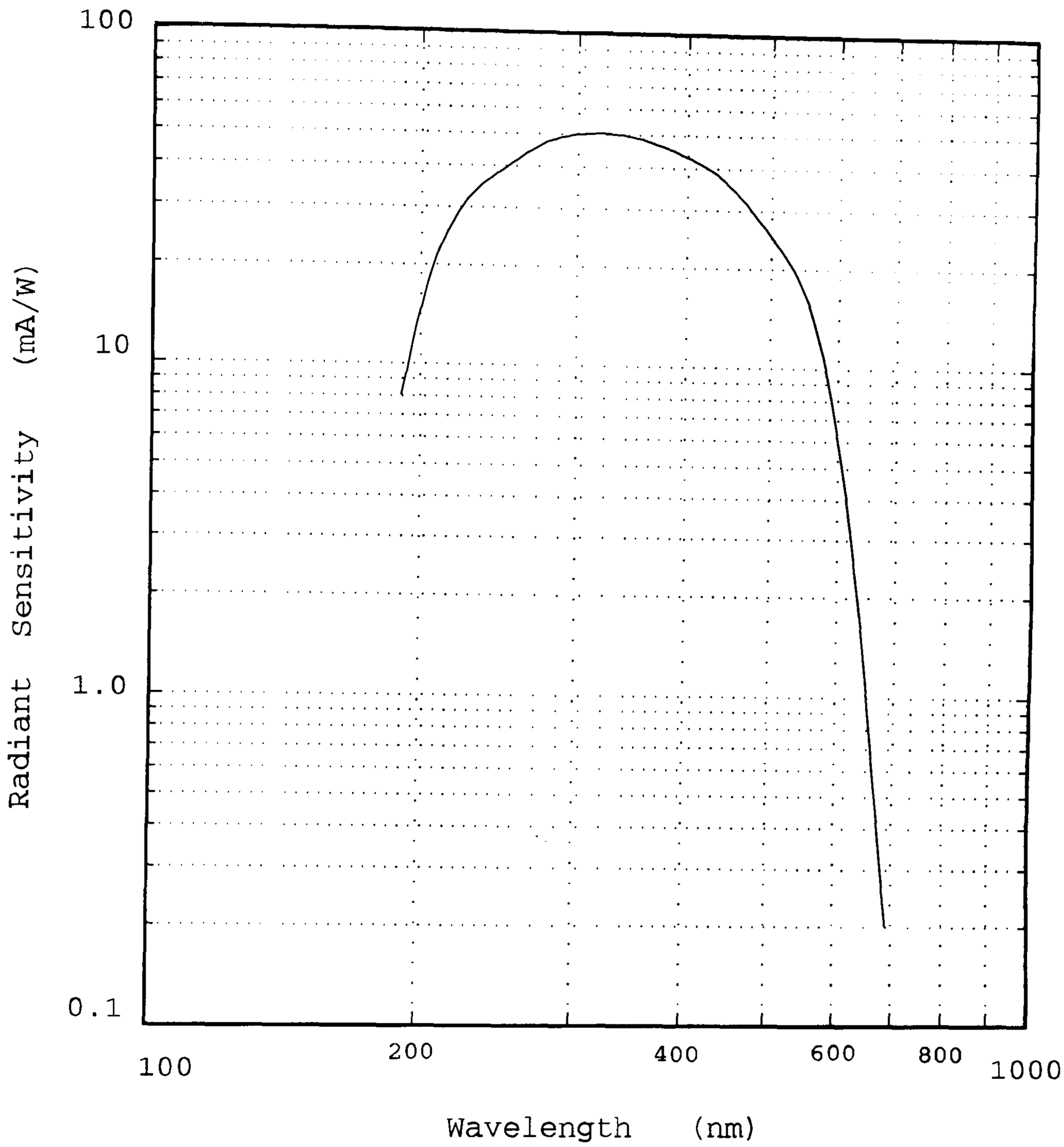

Figure B.1: Radiant sensitivity vs wavelength for the Hamamatsu 1P28 photomultiplier tube.

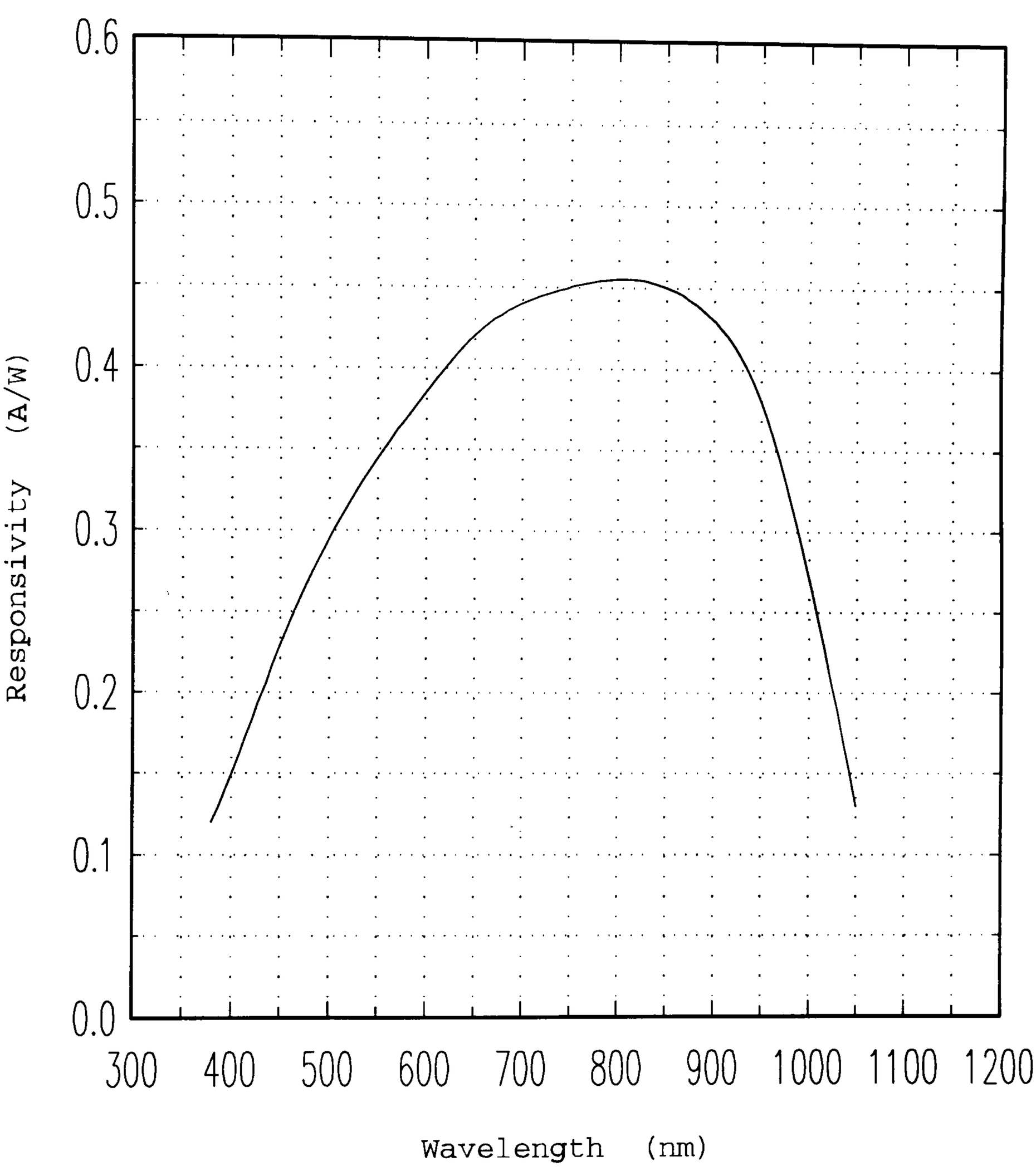

Figure B.2: Responsivity of the Centronics OSD60-5T silicon photodiode.

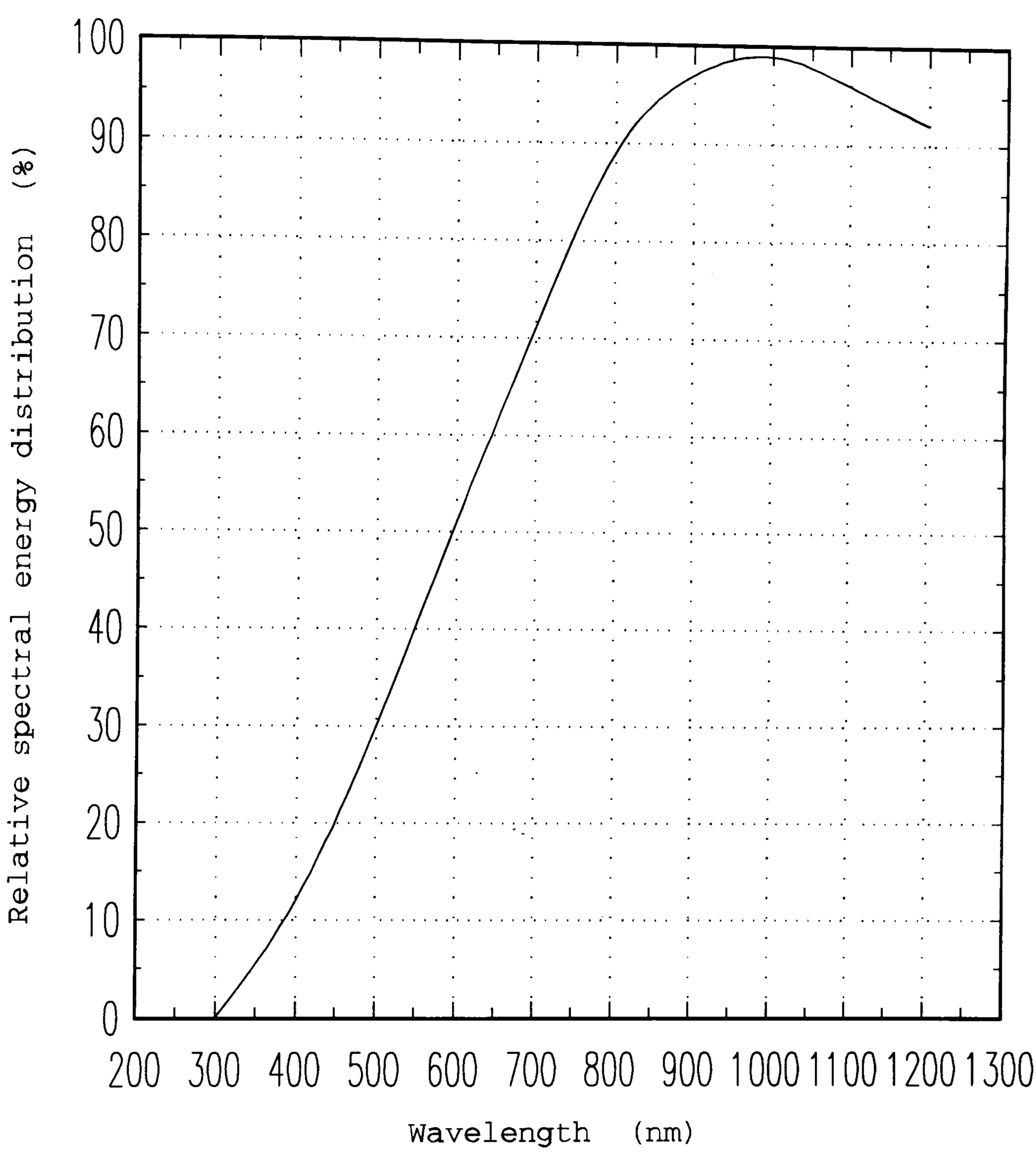

Figure B.3: Relative spectral energy distribution of the tungsten-Halogen light source.

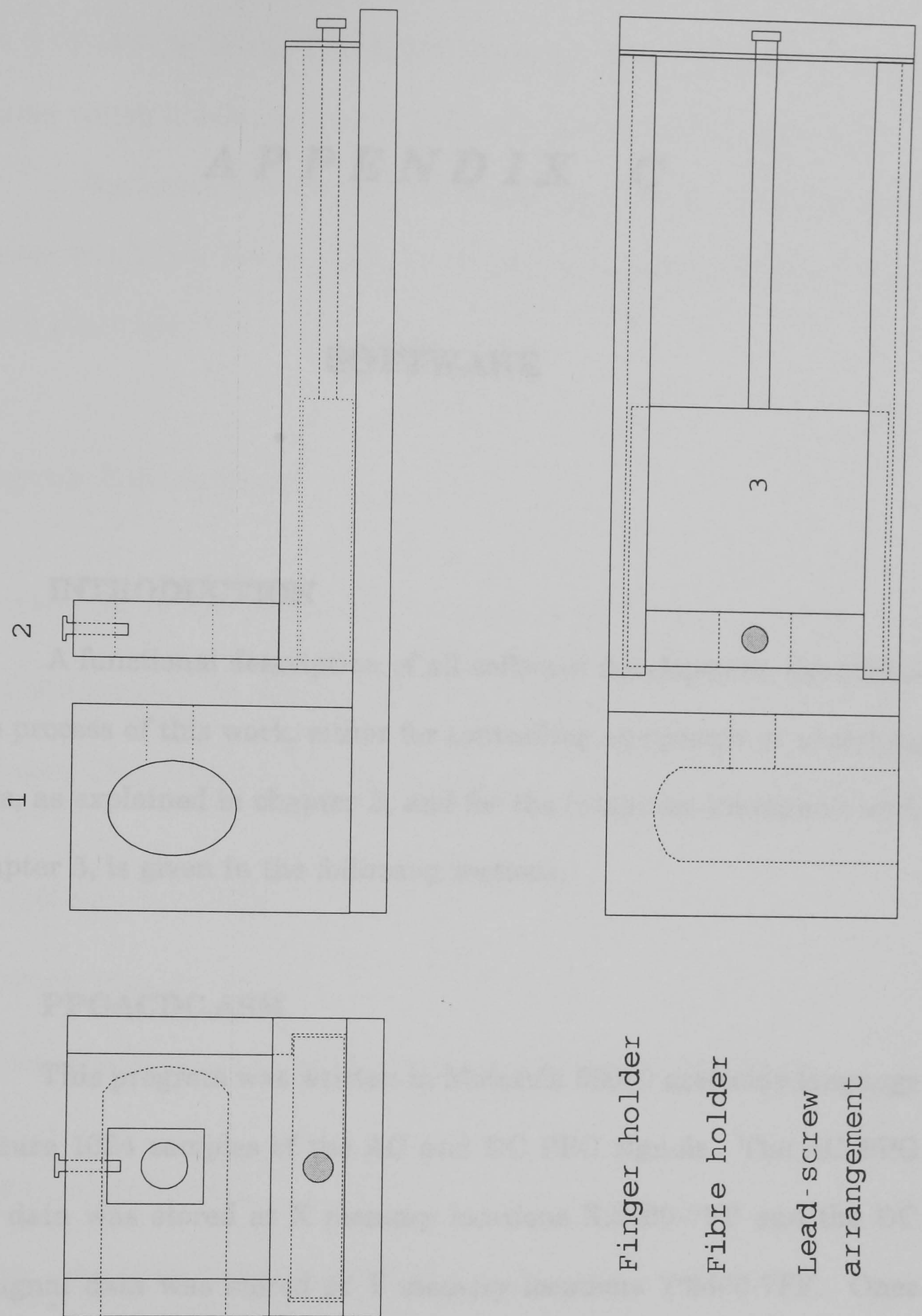

Figure B.4: The experimental setup for the investigation of the positioning of the reflectance probe with respect to the skin surface.

APPENDIX C

SOFTWARE

C.1 INTRODUCTION

A functional description of all software developed by the author in the process of this work, either for controlling equipment or analysing results, as explained in chapter 3, and for the computer simulation work in chapter 5, is given in the following sections.

C.2 PPGACDC.ASM

This program was written in Motorola 56000 assembly language to capture 1024 samples of the AC and DC PPG signals. The AC PPG signal data was stored at X memory locations X:$400-7FF and the DC PPG signal data was stored at Y memory locations Y:$400-7FF. Once sampling was finished the DSP signalled to the PC that it was ready to transfer the captured data. Handshaking with the PC was implemented by using the HF3 flag.

The A/D converters were clocked by using the on board interval

timer. This timer is a 16 bit counter, which can be loaded and read as port 3 (Y:$FFC3) of the DSP56001 I/O map. Writing to port 3 loads a register which is reloaded into the counter at the end of each count.

The value N expressed in hexadecimal value, that the counter register should be loaded with, for a certain sampling frequency Fs (in Hz), is given by: $N = - 10^6 / Fs$.

Program Description

Set interrupt vector for IRQB in program memory position 0A Hex

Set main program in progarm memory position 90 Hex

Initialise data pointers for sample (samp_no) and interrupts counters (cnt_int)

Samples no set to 1024

Interrupts counter set to 2

Set sampling frequency at 159Hz and enable IRQB interrupts.

for (samp_no; 0; 1024)
  Wait for Interrupt();

disable interrupts and flag (HF3) PC.

end of progarm

```
Wait for Interrupt()
  if (cnt_int = 2)
            clear cnt_int
            select input channel 0
            get sample and save at X data memory
            select input channel 1
            get sample and save at Y data memory
            increment sample counter by 1
  else
            increment cnt_int by 1
```

C.3 PPGACDC.C

A block diagram showing the function of this program is shown in Fig. C.1 and hardcopies of consecutive screen displays following the **Analyse** function are shown in Figures C.2 - C.5.

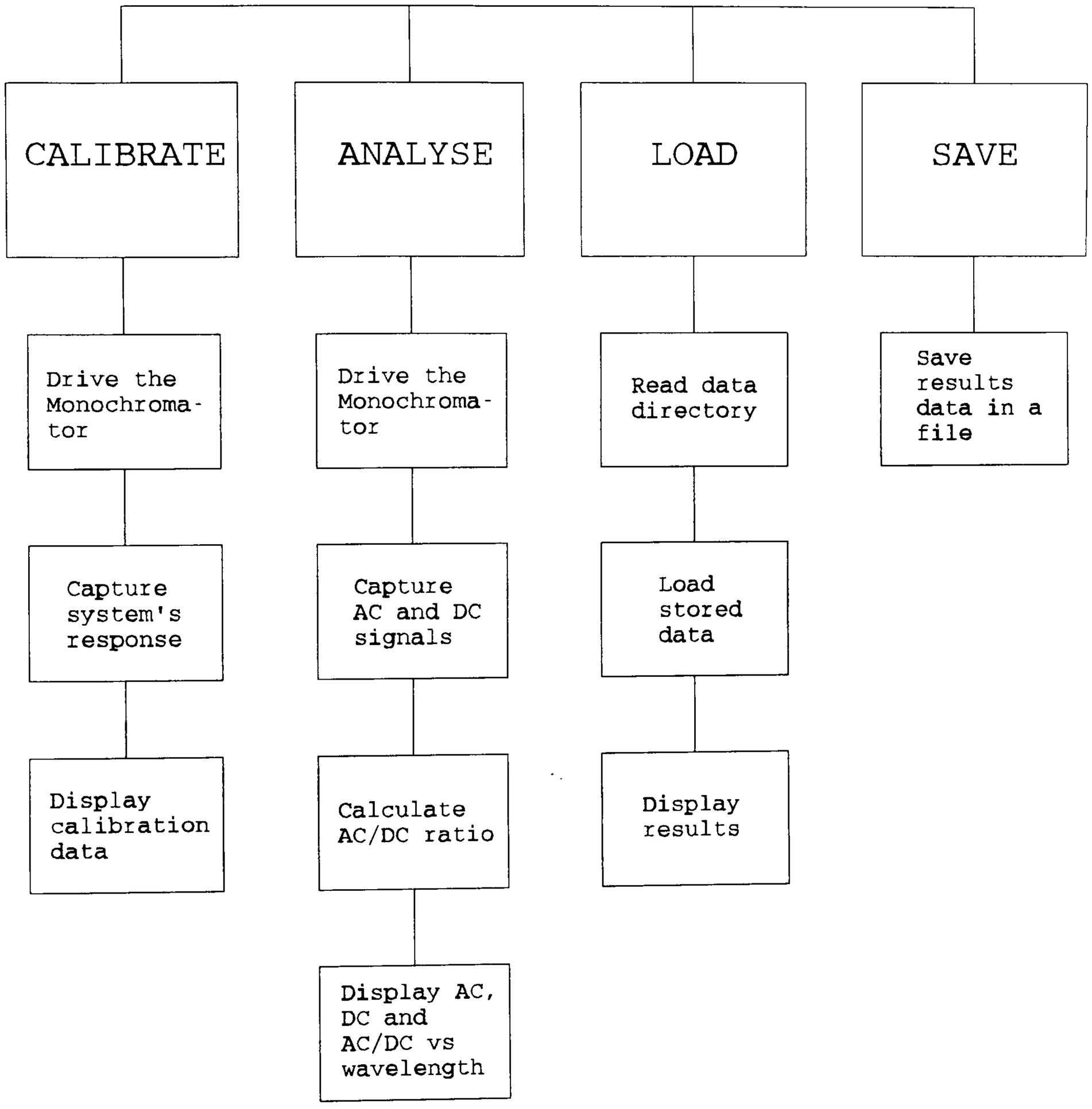

Figure C.1: Block diagram of PPGACDC.C.

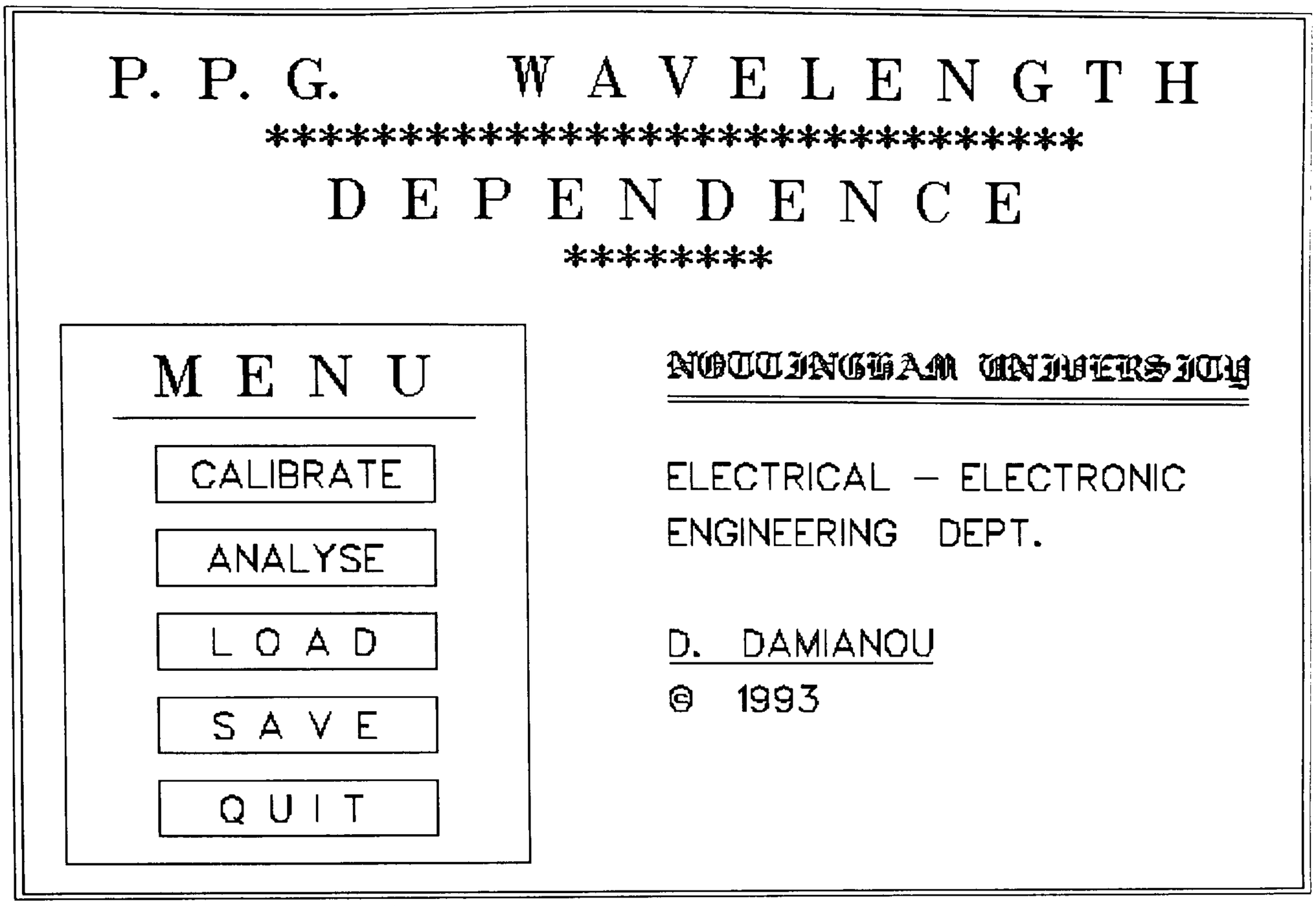

Figure C.2: The main menu.

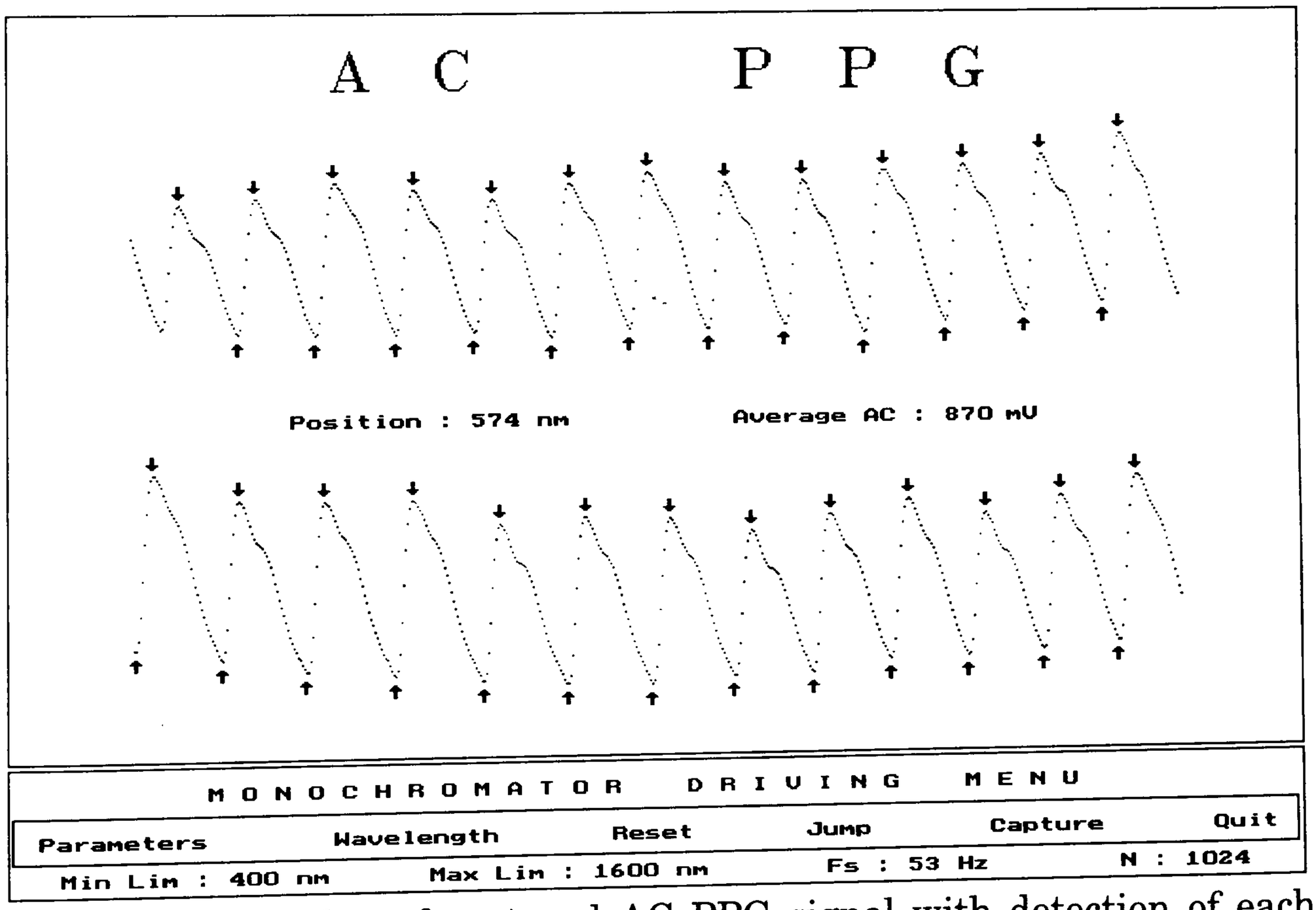

Figure C.3: Display of captured AC PPG signal with detection of each cycle and calculation of its amplitude.

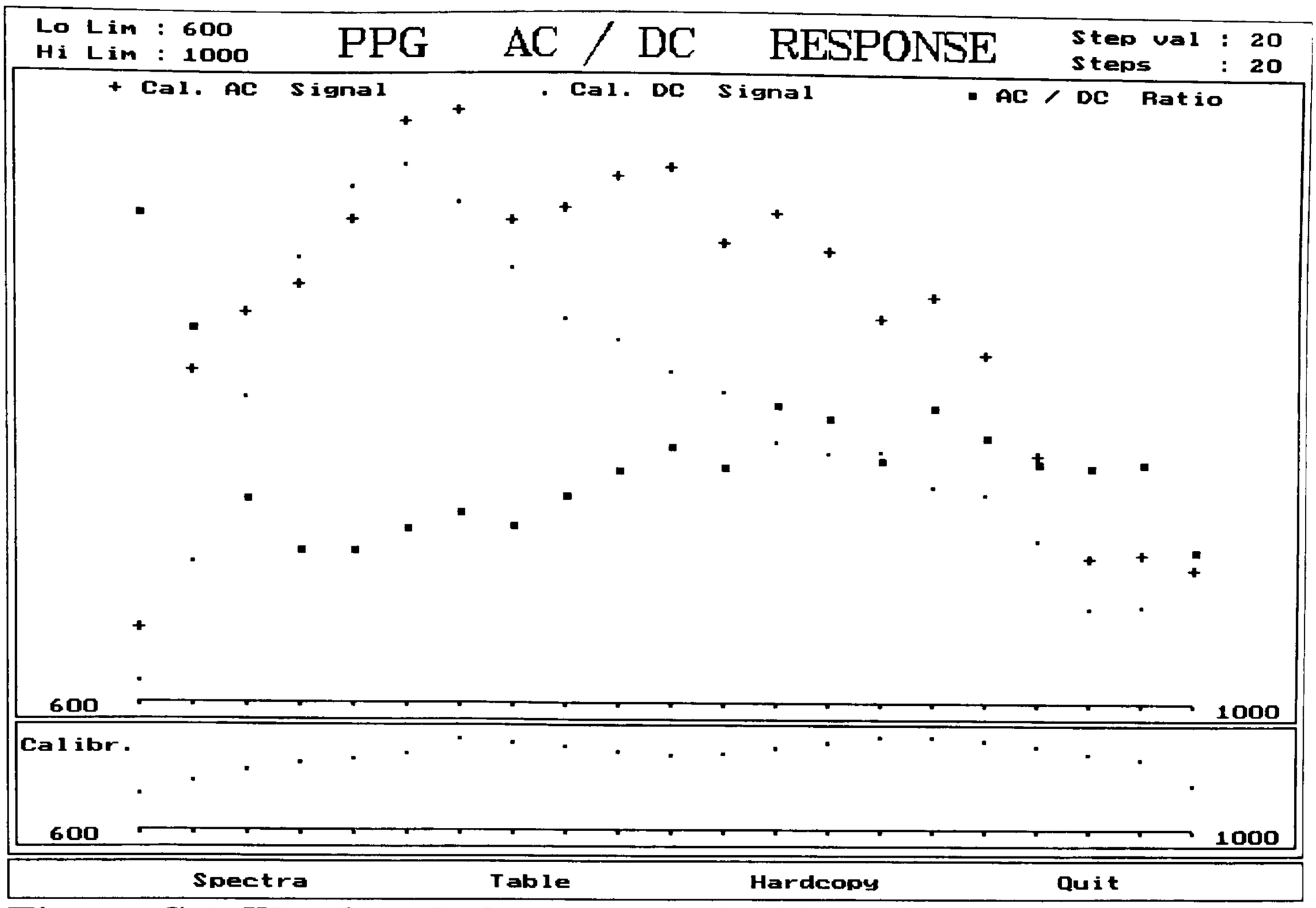

Figure C.4: Wavelength dependence of calibrated AC, DC PPG signals and AC/DC ratio.

PPG AC / DC RESPONSE

Wavelength	A C	D C	(AC / DC) %	Calibration
600	172164	-13105	8.7582	-344
620	1063360	-106088	6.6823	-461
640	1494318	-274471	3.6296	-552
660	1784022	-443054	2.6844	-614
680	2174128	-540818	2.68	-648
700	2792357	-601133	3.0968	-690
720	3401400	-668601	3.3916	-825
740	2650184	-559035	3.1604	-790
760	2624867	-475026	3.6838	-760
780	2621661	-422155	4.1401	-713
800	2562064	-371805	4.5939	-685
820	2230310	-352589	4.217	-693
840	2523878	-314355	5.3525	-737
860	2518116	-327148	5.1315	-797
880	2262582	-347229	4.3441	-840
900	2396672	-299669	5.3318	-841
920	1984974	-276531	4.7854	-808
940	1317913	-204077	4.3053	-758
960	705220	-110518	4.254	-698
980	665748	-103015	4.3084	-647
1000	387928	-94731	2.73	-418

AC PPG amplification factor : 150

Spectra Table Hardcopy Quit

Figure C.5: Tabular presentation of wavelength dependence results.

Program Description

```
main()
{

Initialise graphics
Open_Menu();

do {
Main_Menu();
options are:
 Calibrate: Monochr_Driver_Menu();
            Monochrom_Management();

 Analyse :  Monochr_Driver_Menu();
            Monochrom_Management();
            Calculate AC/DC;
            Results_Menu();
            Screen_Management();

 Load: Read_Directory();
        if (calibration file)
            Load calibration data
        else
            Load PPG data
            Results_Menu();
            Screen_Management();

Save: Read_Directory();
        if (in calibration mode)
            Save calibration data in a file
        else
            Save PPG data in a file

    Quit

  } while (not Quit)

}       /* End of main  */
```

```
/*********************************/
/*  Screen management of results  */
/*********************************/
void Screen_Management(void)

{

if (calibration array empty)
{
  Read directory
  Load calibration file
}

Calibrate_Ampl();
Plot_Results();
do {
options are:
      Spectra : Plot_Results();
      Table   : Results_Table();
      Hardcopy
      Quit
                  }
  }  while ( not Quit);
}
```

```
/*************************************/
/*  Select monochromator command and  */
/*  monochromator management          */
/*************************************/
void Monochrom_Management(void)

{
  Load "calib.lod";

  do {
    options are:
          Offset:     Capture Offset DC voltage;

          Parameters :Specify wavelength range

          Wavelength :set starting wavelength

          Reset :     reset to starting wavelength

          Jump :      go to wavelength

          Step :      Jump_Step();

          Quit

                }
  }  while (not Quit);
}
```

```
/*********************************/
/*   Get data in steps           */
/*********************************/
void Jump_Step()

{
if (in calibration mode)
    Calibration();
else
    {
        Load "ppgacdc.lod"
        Plot_AC_DC();
    }
}

/*****************************************************/
/*  Get the DC offset value of A/D channel 1  */
/*****************************************************/
void Capture_C1_Offset()

{
keep Channel 1 at Ground Potential
Start DSP;
Wait For Dsp to finish
Read channel 1 data
Scale();
Plot channel 1 data
dc_offset = Average();
}
```

```
/*****************************/
/*  Estimate System's response  */
/*****************************/
void Calibration()

{
  for (start wavelength; end wavelength; step value)
  {
            Move monochromator
            Start_DSP(0x90);
            Wait For Dsp to finish
            Read channel 1 data
            Scale();
            Display channel 1 data
            calib factor = Average() - dc_offset;
  }

  Plot system's calibration spectrum
}

/*****************************/
/*  Plot 2 channels signal data */
/*****************************/
void Plot_AC_DC()

{
  for (start wavelength; end wavelength; step value)
  {
            Move monochromator
            Start_DSP(0x90);
            Wait for Dsp to finish
            Read channel 0 and channel 1 data
            Scale();
            Display channel 0 and channel 1 data
            Detect_AC_Amplitude();
            DC amplitude = Average() - dc_offset;
            Options are to print screen or recapture data
  }
}
```

```
/*****************************/
/*  Display AC, DC and AC/DC  */
/*  at each wavelength        */
/*****************************/
void Results_Table()

{
Display raw AC and DC PPG data, AC/DC in percent and calibration
factors at each wavelength
}

/*****************************/
/*  Plot AC, DC and AC/DC at  */
/*  each wavelength           */
/*****************************/
void Plot_Results()

{
Scale calibrated AC, DC, AC/DC results and calibration factors.
Plot Calibrated AC PPG
Plot Calibrated DC PPG
Plot AC/DC Ratio
Plot calibration data
}

/*****************************/
/*  Calibrate  AC  DC amplitudes  */
/*****************************/
void Calibrate_Ampl()

{
Divide AC and DC PPG data by calibration factors stored in calibration
array
}
```

```
/*************************************/
/*  Calculate AC PPG average amplitude  */
/*************************************/
long Detect_AC_Amplitude(long inp[], long sc)

{
Search for global minima and maxima (ignoring any local ones) by looking
at min and max and checking change of sign avoiding localised changes
Put pointers at detected minima and maxima for visual checking
AC amplitude is average of amplitudes of all captured cycles
}

/*************************************/
/*          Function to scale data */
/*************************************/
long Scale(data array, size of array, available display space)

{
Detect max element;
scale = max / space;
return(scale);
}

/*****************************/
/*  Set up COM1 and Drive    */
/*****************************/
void Set_Up_Drive()

{
Initialise  COM1  to  N,8,1
Set up Drive with type of grating used (600 lines/mm), min wavelength
(400nm), max wavelength (1600nm) and scanning speed (200 nm/min)
}
```

```
/******************/
/* Opening menu  */
/******************/
void Open_Menu(void)

{
Set up openning menu
  if (option == 'Y')
  {
     DSP56000 board initialised
     Set_Up_Drive();
  }
}

/******************/
/* Main  menu    */
/******************/
void Main_Menu(void)

{
Set up of main menu displaying aim of software
Options are calibrate, analyse, load, save and quit.
}

/*************************************/
/* The menu for the monochromator driver */
/*************************************/
void Monochr_Driver_Menu(void)

{
Set up of menu for driving the monochromator
Displays wavelength limits, sampling frequency and number of samples
taken, photodetector used.
Options are Parameters setting, Starting wavelength, Reset to starting
wavelength, Jump to specific wavelength, Step acquisition, Capture of DC
offset voltage and Quit.
}
```

```
/*****************************/
/*  Plot  Results  Menu  */
/*****************************/
void Results_Menu(void)

{
Set up of menu for displaying results
Options are display of captured spectra, data in tabulated form, plotting
display and quit.
}
```

C.4 MCARLO.C

Program Description

```
main()
{
  Select number of input photons.

  Read model's optical parameters from file.
  Create results files for transmission and 2 reflection modes.

  for (i=1; i<=max_photons_in; i++)
  {
        Initialise_Photon();
        Model_Photon();
  }
```

Display simulattion time, number of photons out, lost and detected in each mode and save these at the end of transmitted results data file.

```
} /* End of main */


/*************************************************/
/*  Initialise the photon. Photon 'enters'       */
/*  normal to model but scatters at (0,0,-radius_1)  */
/*************************************************/
void Initialise_Photon()

{
Input photon at position (0,0,-z)
Set direction cosines cosx = cosy = 0, cosz = 1.
Zero distances in each layer.
Optical parameters for layer1 to begin with.
}
```

```
/*********************************/
/*  Calculate new position of photon   */
/*  after change of layer              */
/*********************************/
void Change_Layer(float r)

{
  Calculate distance travelled out of previous layer.
  Subtract this from last scattering distance.
  Move photon position at layer interface.
}

/*****************************/
/*  Select optical parameters   */
/*****************************/
void Select_Parameters()

{
  Set optical parameters to the ones for particular layer
  if (photon in layer 1 or 2)
          Select whether scattered by blood or not

}
```

```
/*********************************/
/*  Calculate new direction cosines   */
/*  and new position of photon        */
/*********************************/
int Model_Photon()

{
  do
  {
```

Generate scattering distance and angles ϕ and θ from optical parameters.

Calculate new photon position.

Add new scattering distance to total distance for appropriate layer

```
Check to see where photon is
If (Photon changed layer)
    Change_Layer();
    Select_Parameters();
else
{ if (photon still in layer 1 or 2)
    Select whether scattered by blood or not
        }

  }
  while ((|x| < 14) or distance from origin < radius 1);
  if (|x| > 14)
    increment photons lost counter.
  else
    { increment photons out counter.
      Detection_Mode();
    }
}
```

```
/*****************************************/
/*  Check to see whether exiting  */
/*  photon will be detected       */
/*****************************************/
void Detection_Mode()

{
  if (|x| < 2) AND (|y| < 2) AND (z > 0))
  {
        increase transmitted photons counter.
        save scattering distances for each layer in transmission file.
}
if (2 < x < 4) AND (|y| < 2) AND (z < 0))
{
        increase reflected mode 1 photons counter.
        save scattering distances for each layer in reflection 1 file.
}
if (4 < x < 6) AND (|y| < 2) AND (z < 0))
{
        increase reflected mode 2 photons counter.
        save scattering distances for each layer in reflection 2 file.
  }
}
```

APPENDIX D

LAMBERT-BEER ANALYSIS OF MODEL FINGER

In this appendix the values for the DC, AC and AC/DC components following a Lambert-Beer analysis on a finger model are calculated. The finger was approximated as a system of three concentric cylinders representing three different layers; dermis-blood, fat-blood and bone. The blood was assumed to be homogeneously distributed with a base volume of 10% which increased by a further 10%, simulating the influx of arterial blood. This finger model is explained in detail in chapter 5.

The absorption characteristics and physical dimensions of each layer used for the DC and DC+AC calculations are shown in Table D.1, where u_a is the absorption coefficient, L the pathlength for base blood volume and L' the pathlength for the increased blood volume.

PARAMETERS FOR DC CALCULATIONS						
λ	LAYER 1		LAYER 2		LAYER 3	
	u_a	L	u_a	L	u_a	L
545	3.507	2	3.318	5	1.983	7
560	2.198	2	2.018	5	1.2	7
577	3.738	2	3.558	5	2.13	7
660	0.2072	2	0.0362	5	0.032	7
800	0.2166	2	0.0636	5	0.024	7
940	0.2236	2	0.0841	5	0.045	7

PARAMETERS FOR DC+AC CALCULATIONS						
λ	LAYER 1		LAYER 2		LAYER 3	
	u'_a	L'	u'_a	L'	u'_a	L'
545	3.8347	2.0129	3.6478	5.0395	1.983	7
560	2.3958	2.0129	2.2178	5.0395	1.2	7
577	4.0898	2.0129	3.9118	5.0395	2.13	7
660	0.20692	2.0129	0.03782	5.0395	0.032	7
800	0.21926	2.0129	0.06796	5.0395	0.024	7
940	0.22846	2.0129	0.09051	5.0395	0.045	7

Table D.1: The absorption characteristics and physical dimensions of each layer of the finger model.

In the following calculations it was assumed that in transmission mode the detected light interacted with all three layers of the model. Contrary in reflection it was assumed that the detected light interacted only with the first (dermis-blood) layer of the model.

Using Lambert-Beer analysis the corresponding DC and DC+AC components for each mode are:

In transmission

$$DC = 10^{-(u_{a1}L_1 + u_{a2}L_2 + u_{a3}L_3)}$$

$$DC+AC = 10^{-(u'_{a1}L'_1 + u'_{a2}L'_2 + u'_{a3}L'_3)}$$

In reflection

$$DC = 10^{-(u_{a1}L_1)}$$

$$DC+AC = 10^{-(u'_{a1}L'_1)}$$

The AC component was calculated by subtracting the DC+AC component from the DC one. The calculated results for transmission mode are shown in Table D.2 and for reflection mode in Table D.3.

Wavel.	DC	DC+AC	AC	AC/DC
545	3.2734e-38	1.04e-40	3.2629e-38	0.9968
560	1.3002e-23	3.989e-25	1.2603e-23	0.96932
577	6.668e-41	1.3936e-43	6.6541e-41	0.99791
660	0.151565	0.1475356	0.004029	0.02658
800	0.120448	0.1117293	0.008718	0.07238
940	0.065659	0.058749	0.0069	0.105225

Table D.2: Transmission results.

Wavel.	DC	DC+AC	AC	AC/DC
545	9.683e-8	1.91e-8	7.772e-8	0.8027
560	4.0179e-5	1.5048e-5	2.5131e-5	0.6254
577	3.3419e-8	5.8565e-9	2.75629e-8	0.8247
660	0.385123	0.383257	0.001866	0.00485
800	0.368807	0.361952	0.006855	0.01858
940	0.357108	0.346842	0.010265	0.02874

Table D.3: Reflection results.

APPENDIX E

FURTHER WAVELENGTH DEPENDENCE RESULTS

In chapter 4 typical AC and DC PPG signals were presented for each range and mode. In this appendix further results are presented for the two modes. In addition results are presented for expanded wavelength ranges and with smaller step sizes for improved resolution. In some of these results, the problems associated with slight finger movements (caused by the long capturing times) are apparent.

These results are for the same subject (healthy male caucasian, nonsmoker, aged 27), unless otherwise stated.

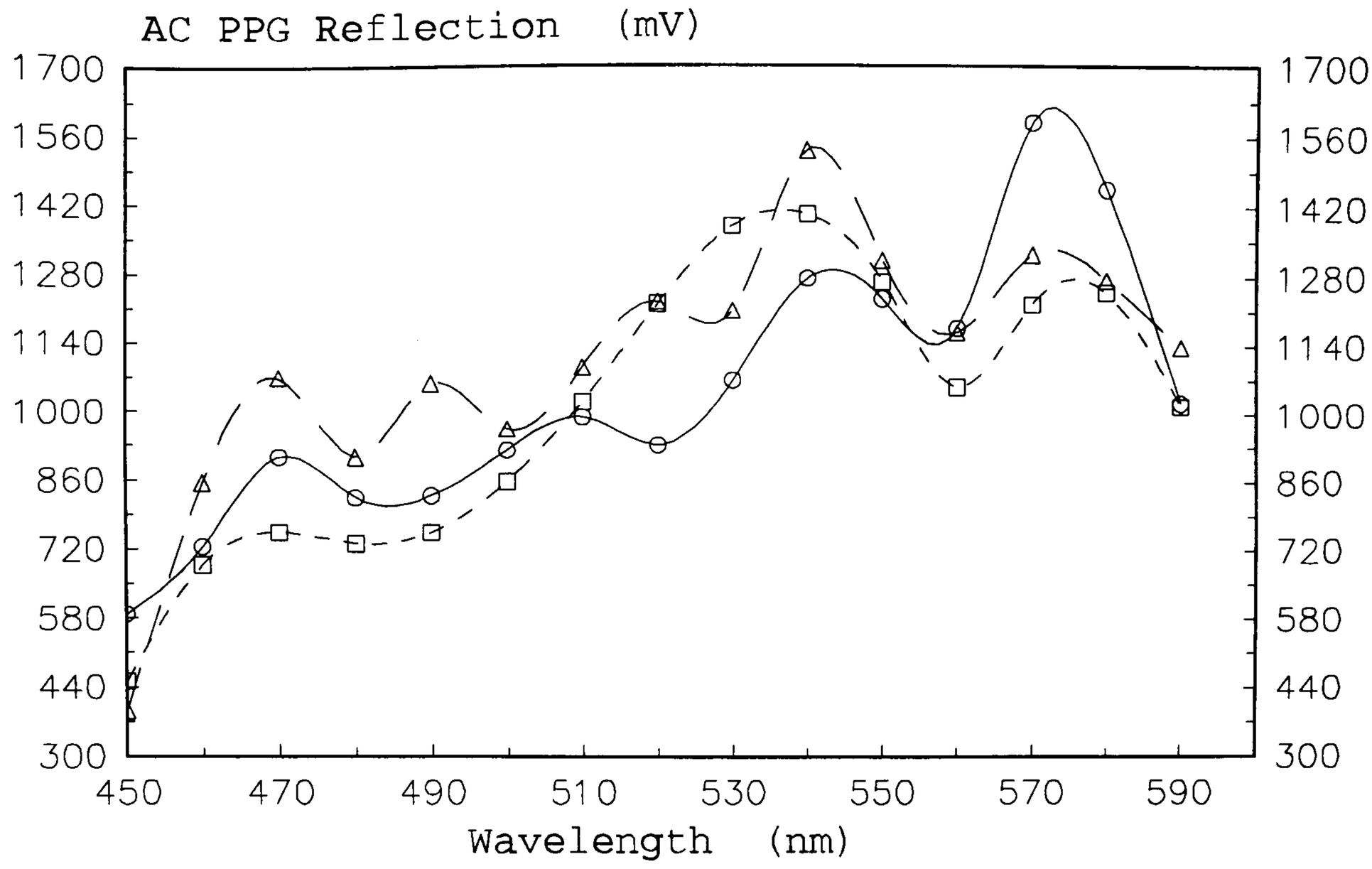

Figure E.1: AC PPG signals in reflection from 450 - 490nm.

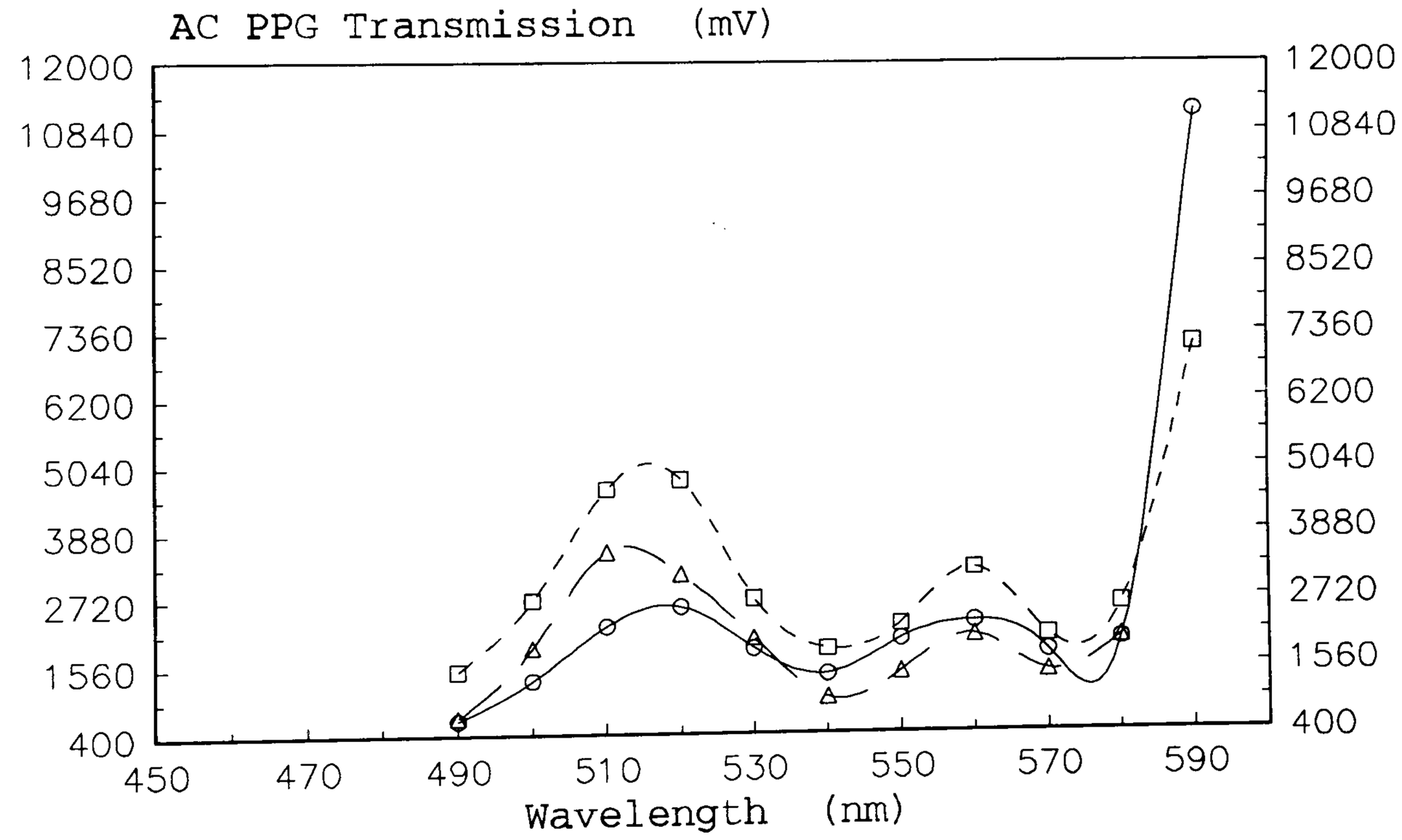

Figure E.2: AC PPG signals in transmission from 490 - 590nm.

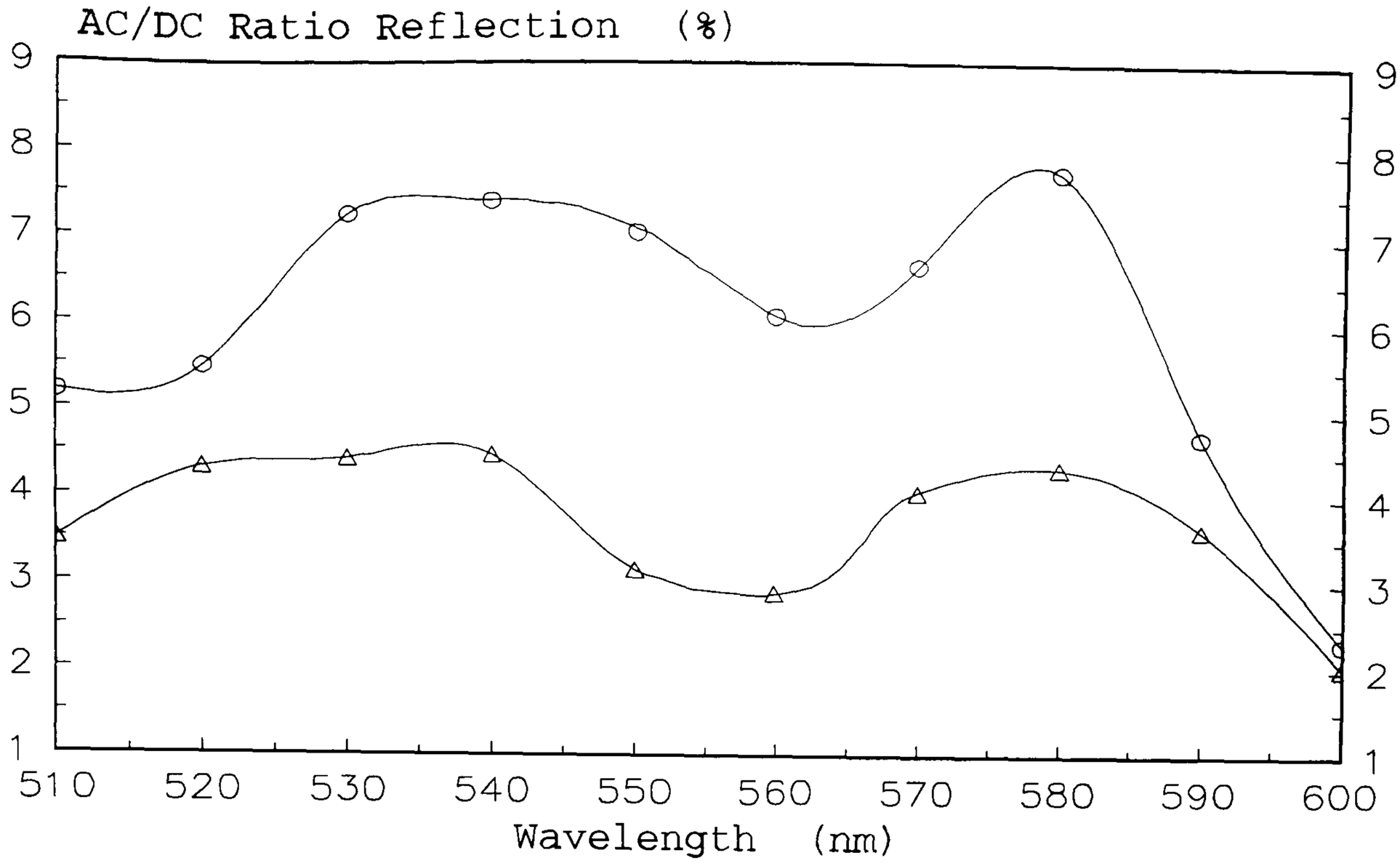

Figure E.3: AC/DC ratio in reflection mode from 510 - 600nm. Top trace is for a male chinese subject, 28 the bottom for a male caucasian, 22.

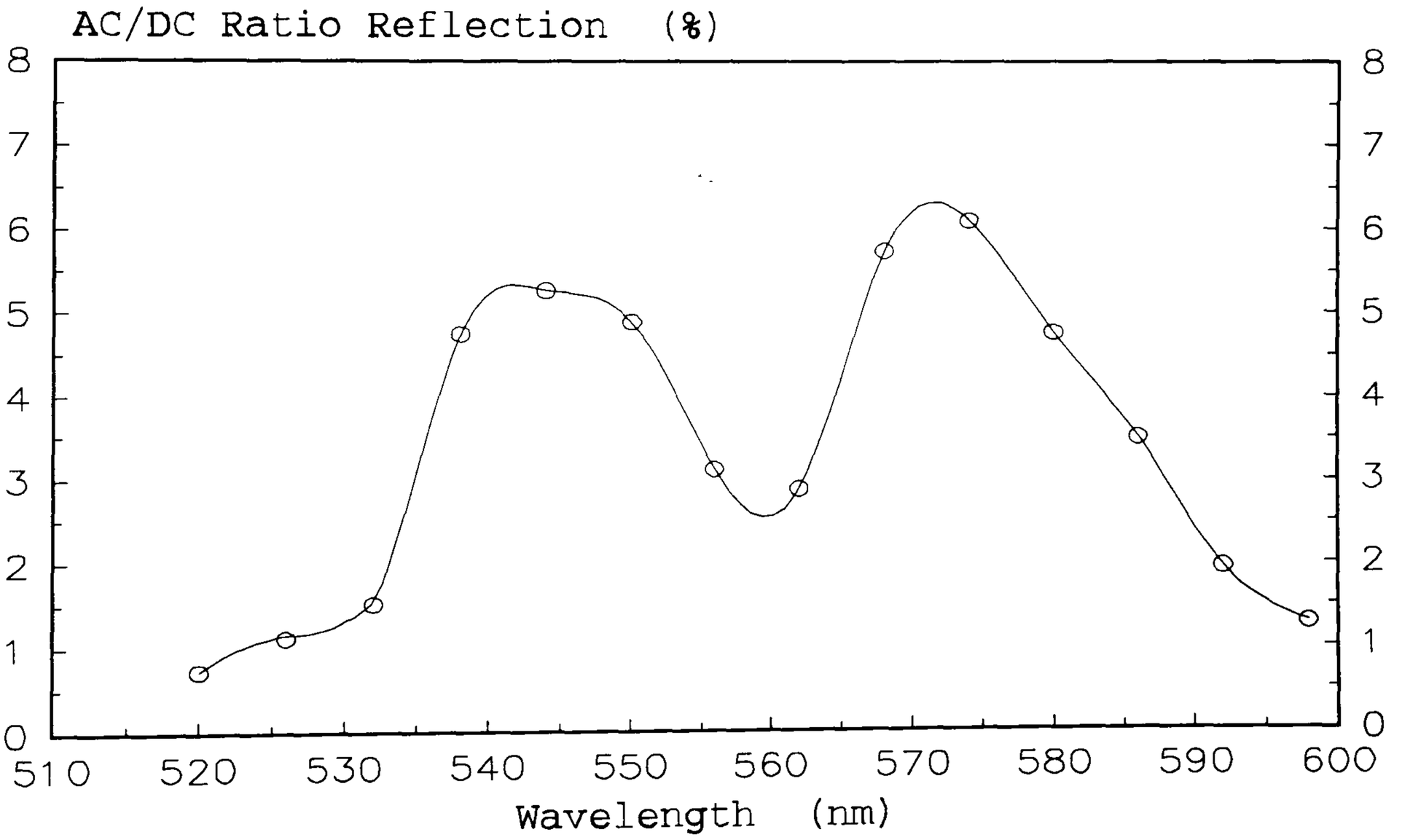

Figure E.4: AC/DC ratio in reflection mode from 520 - 598nm with increased resolution.

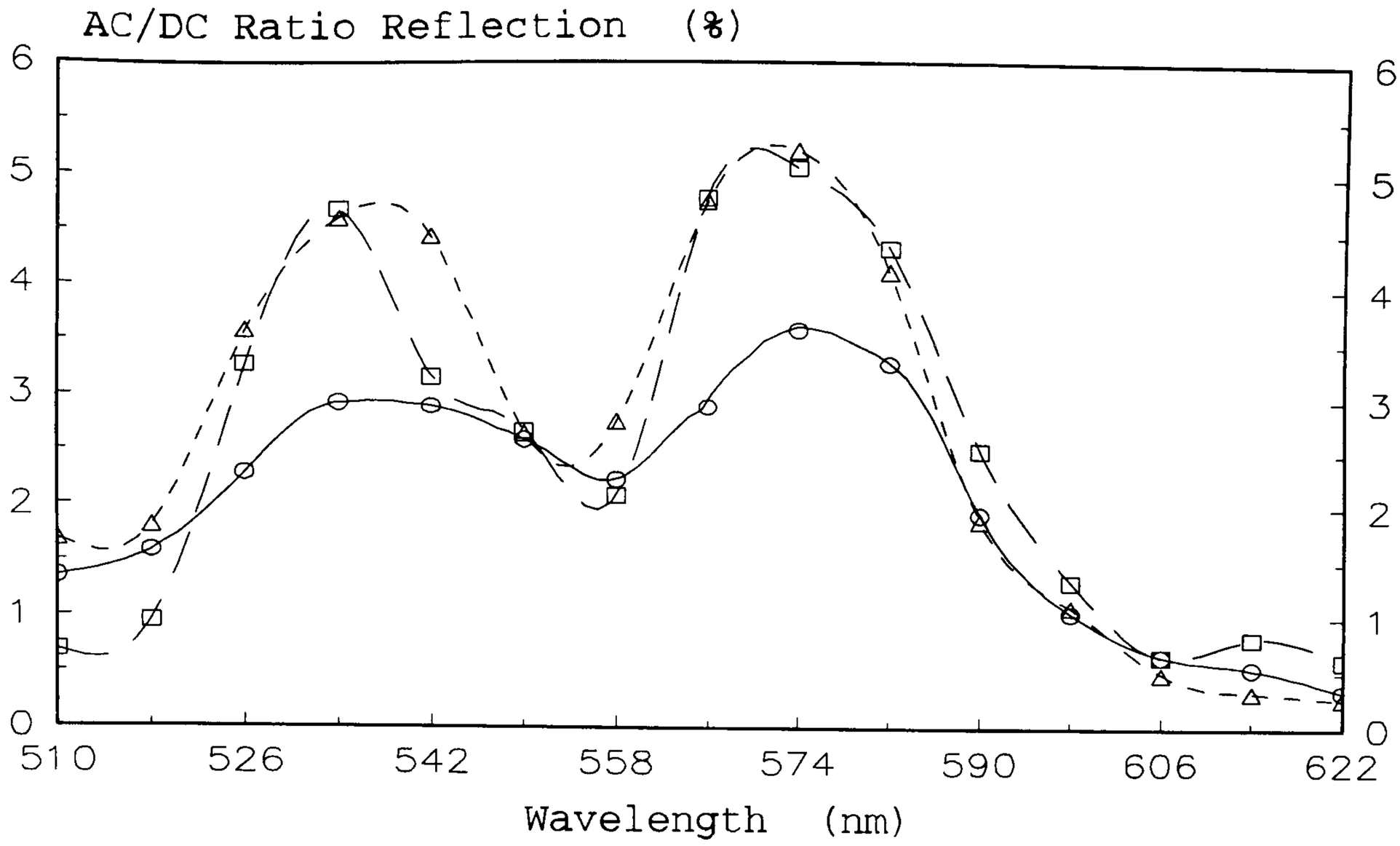

Figure E.5: AC/DC ratio in reflection mode from 510 - 622nm with increased resolution.

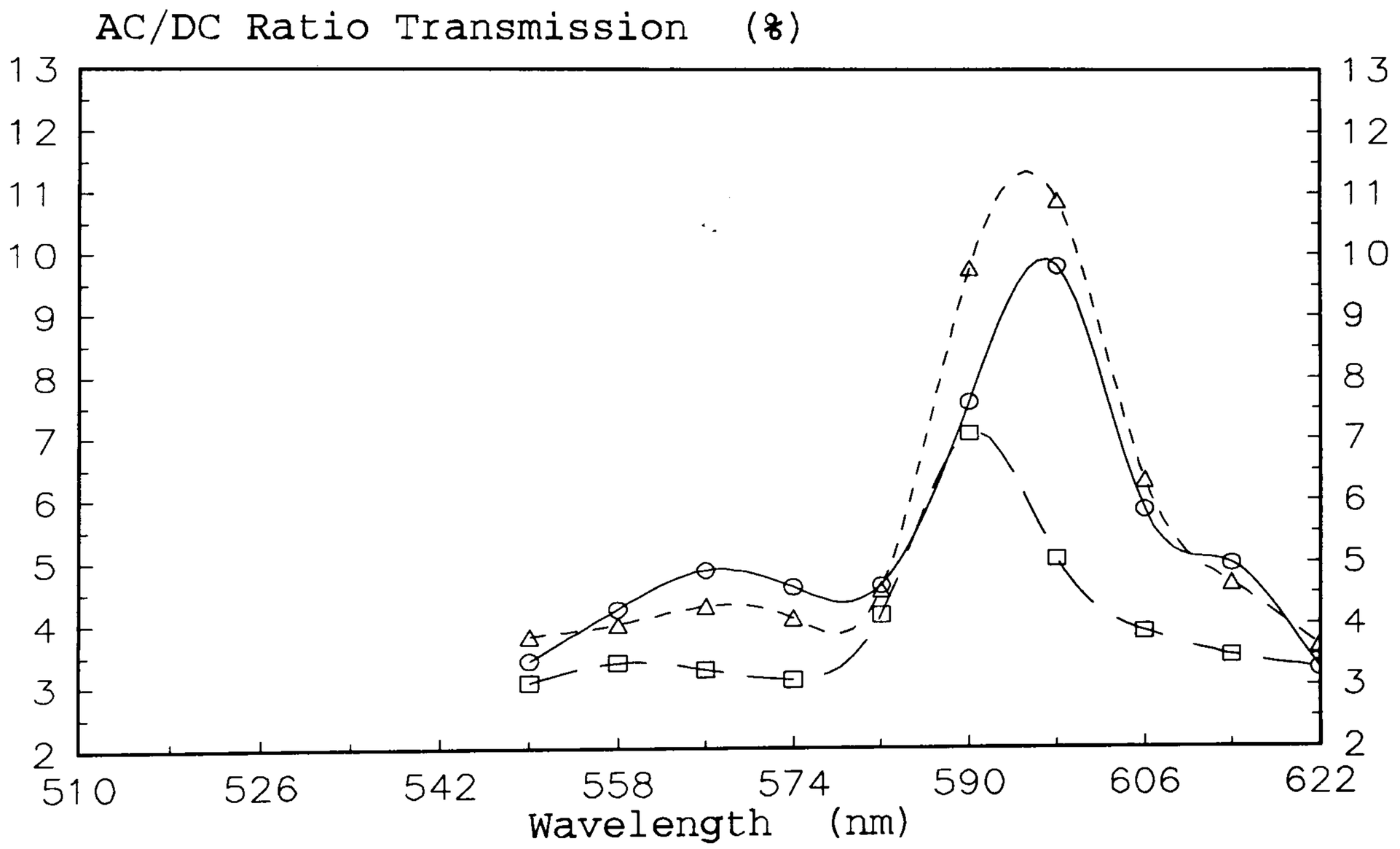

Figure E.6: AC/DC ratio in transmission mode from 550 - 622nm with increased resolution. Long dashed trace for a female caucasian, 23.

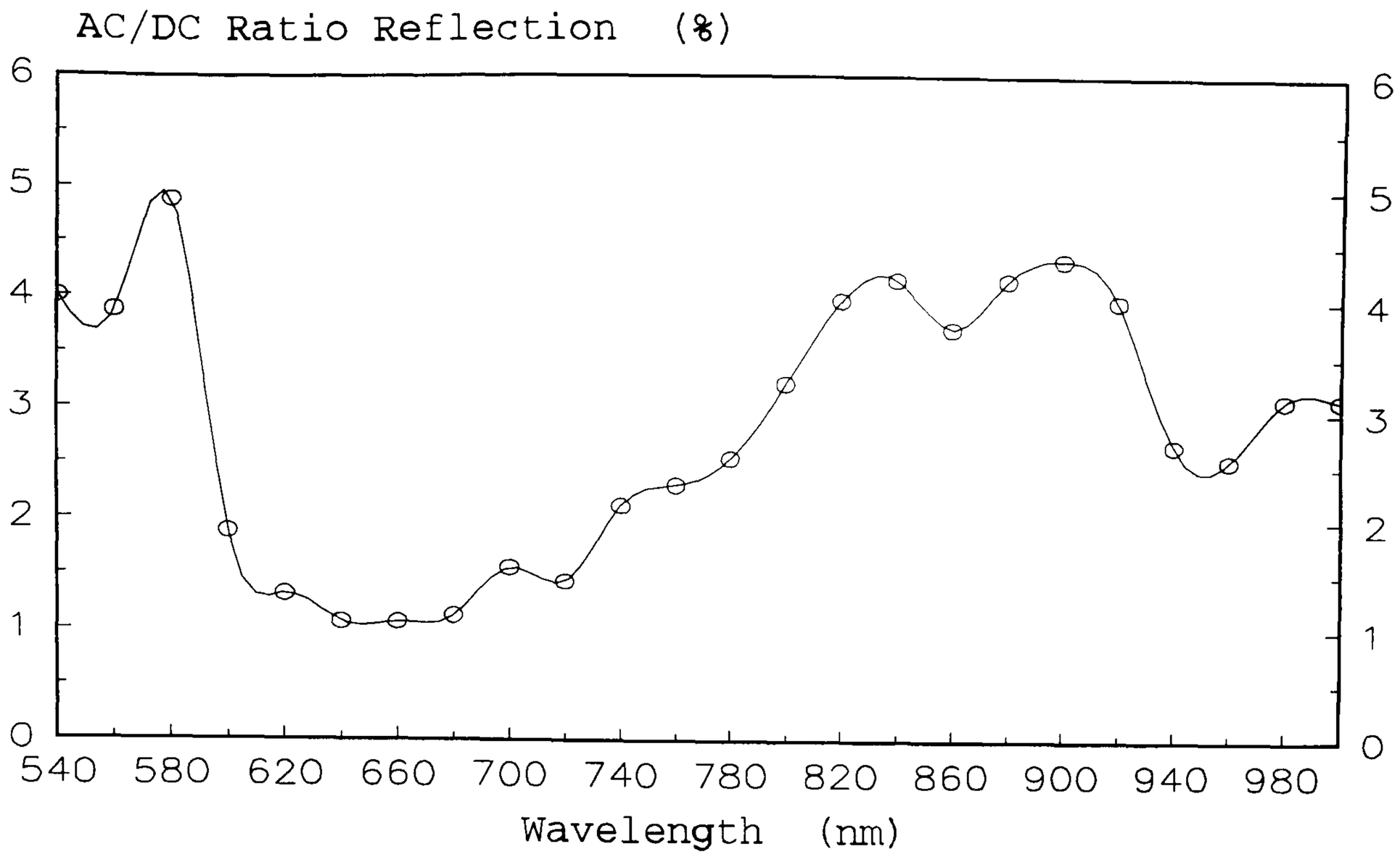

Figure E.7: AC/DC ratio in reflection mode for expanded range 540 - 1000nm.

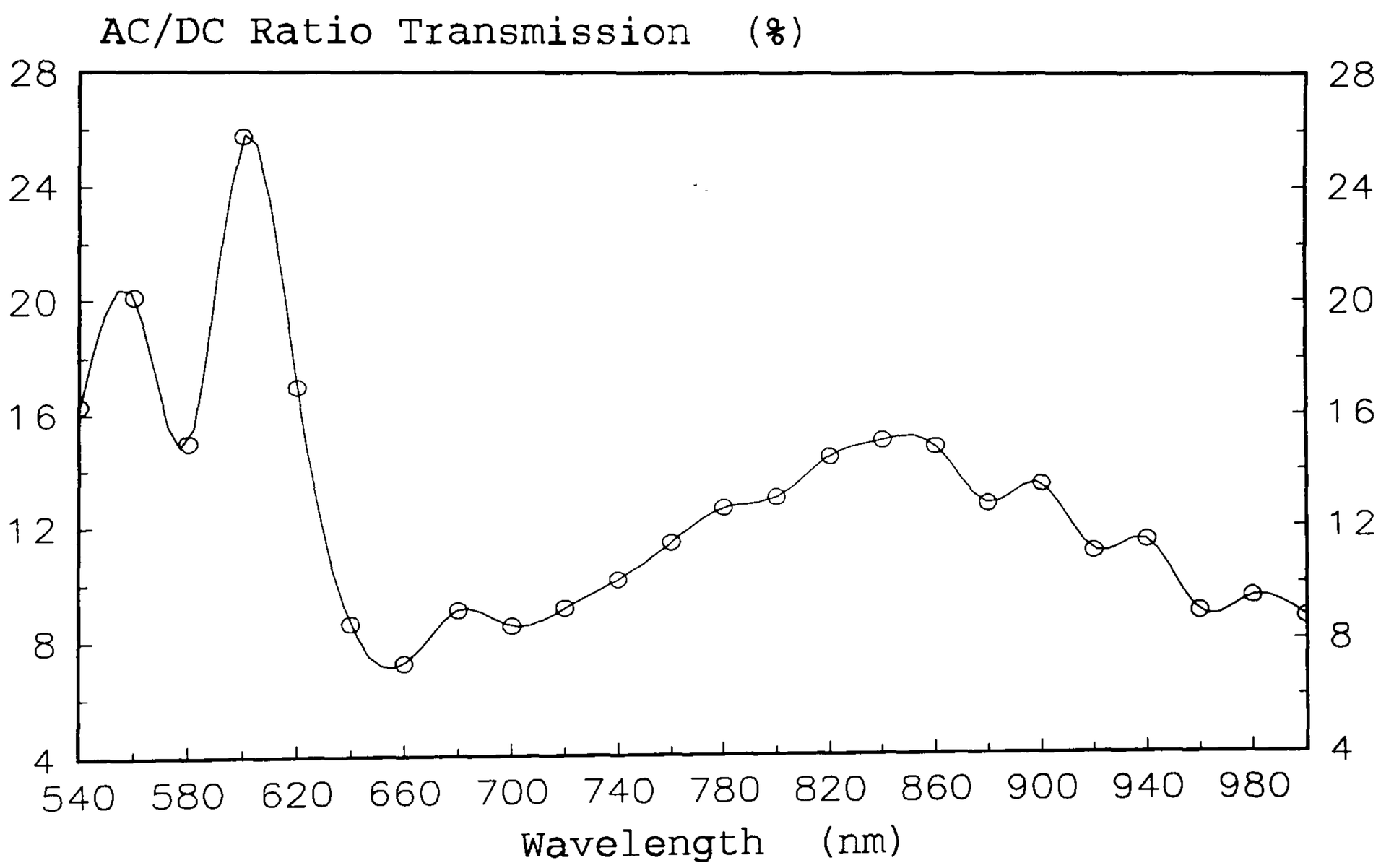

Figure E.8: AC/DC ratio in transmission mode for expanded range 540 - 1000nm.

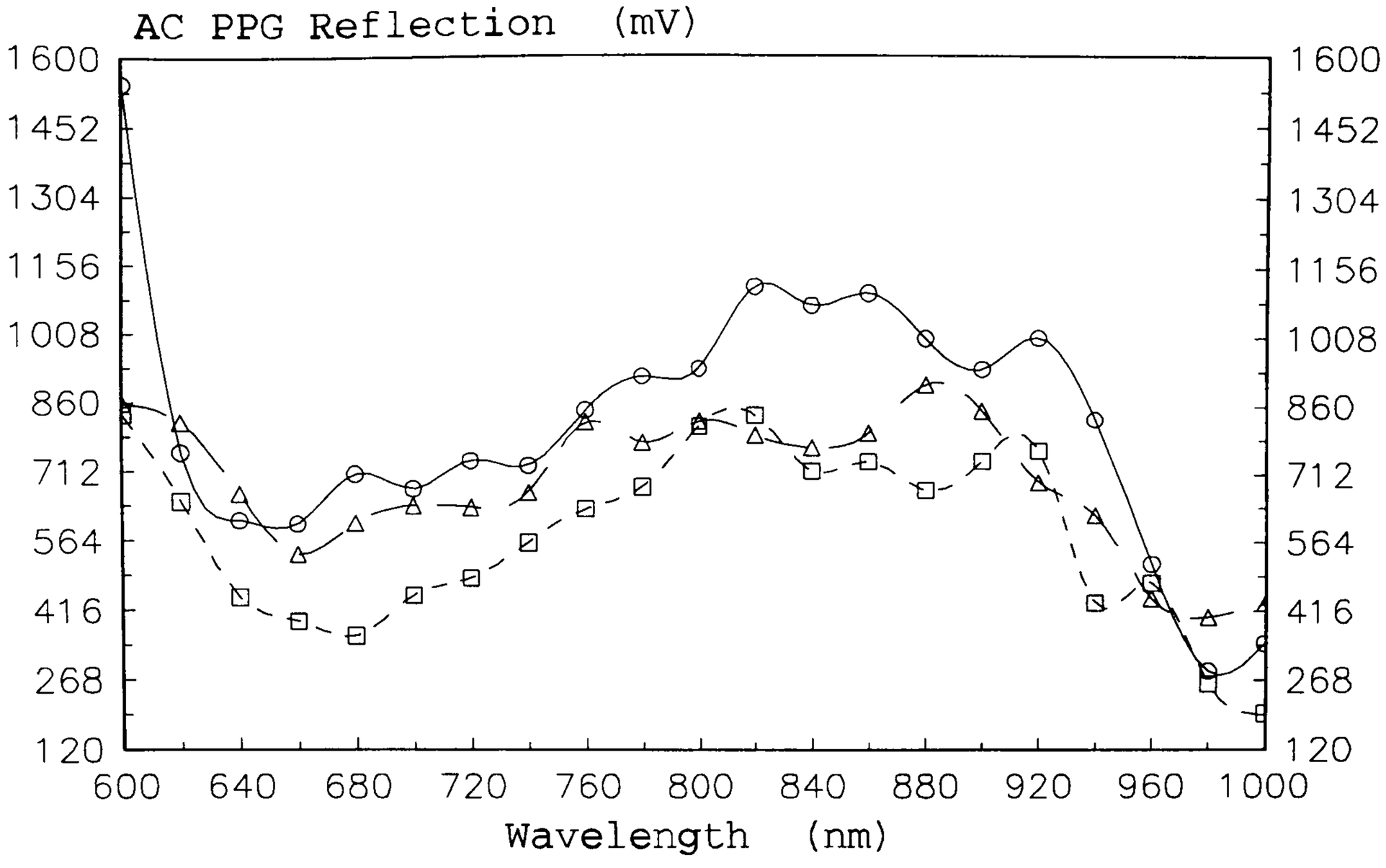

Figure E.9: AC PPG signals in reflection mode from 600 - 1000nm. Long dashed trace for a male chinese, 28 subject.

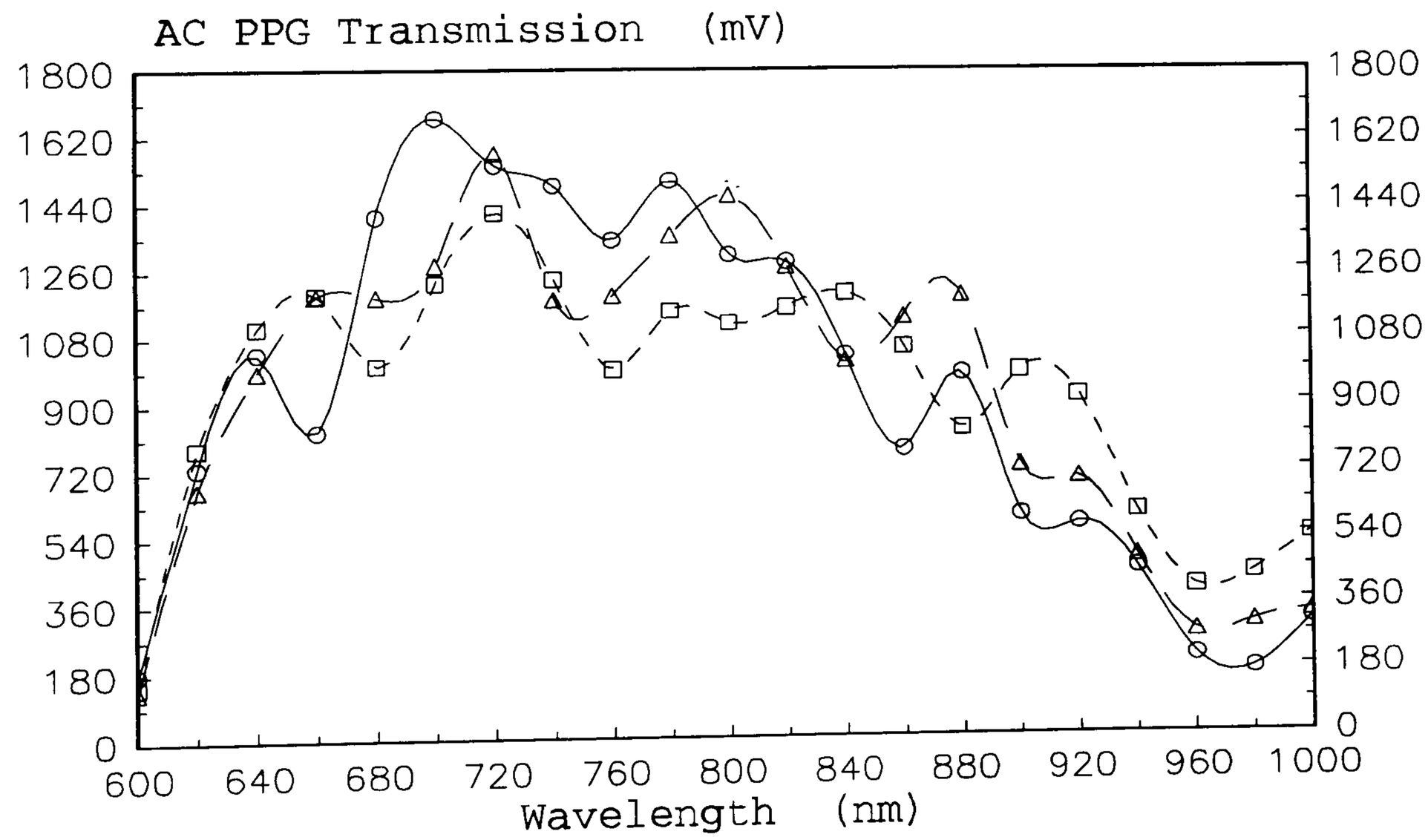

Figure E.10: AC PPG signals in transmission mode from 600 - 1000nm.

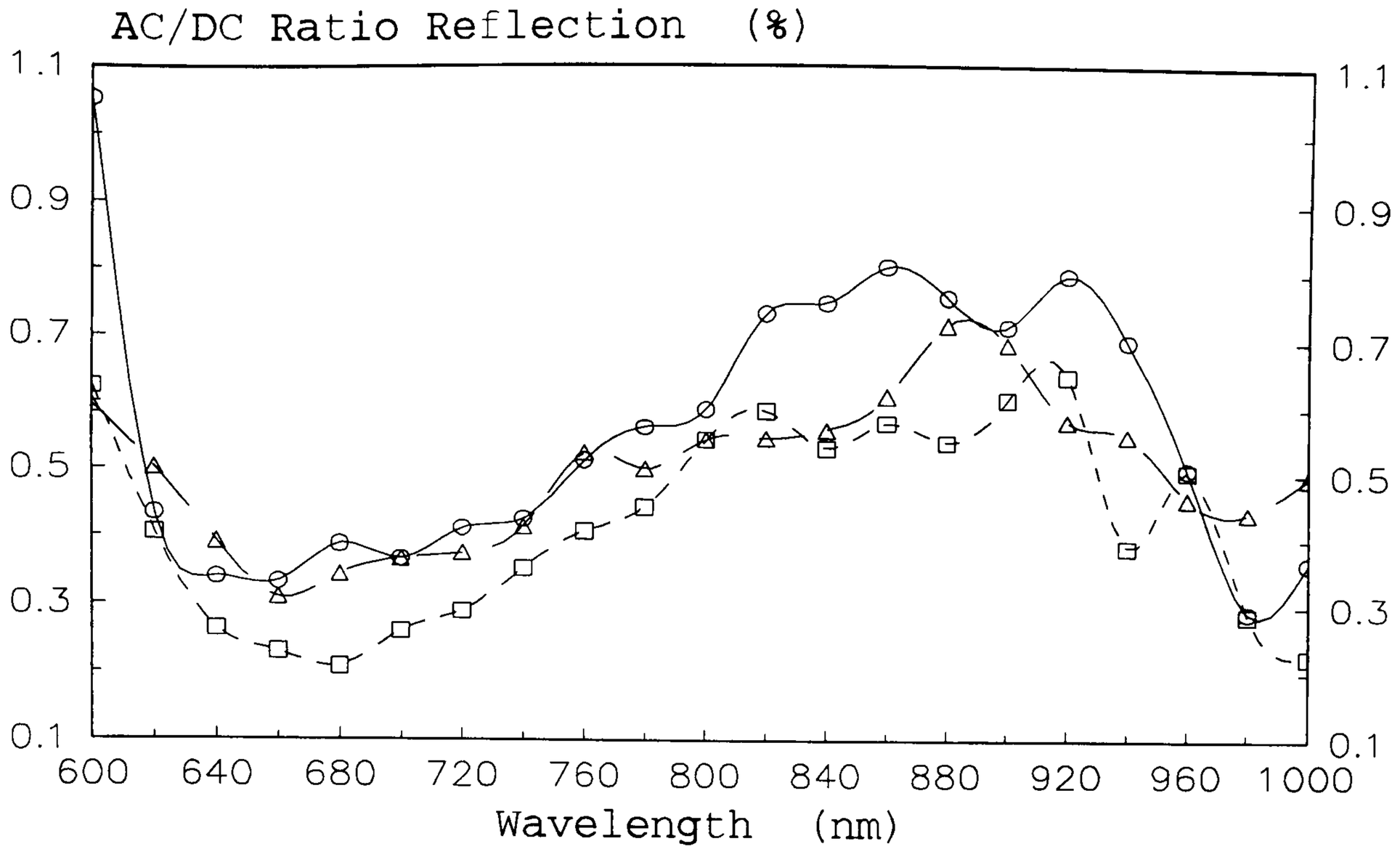

Figure E.11: AC/DC ratio in reflection mode from 600 - 1000nm. Long dashed trace for a male chinese, 28 subject.

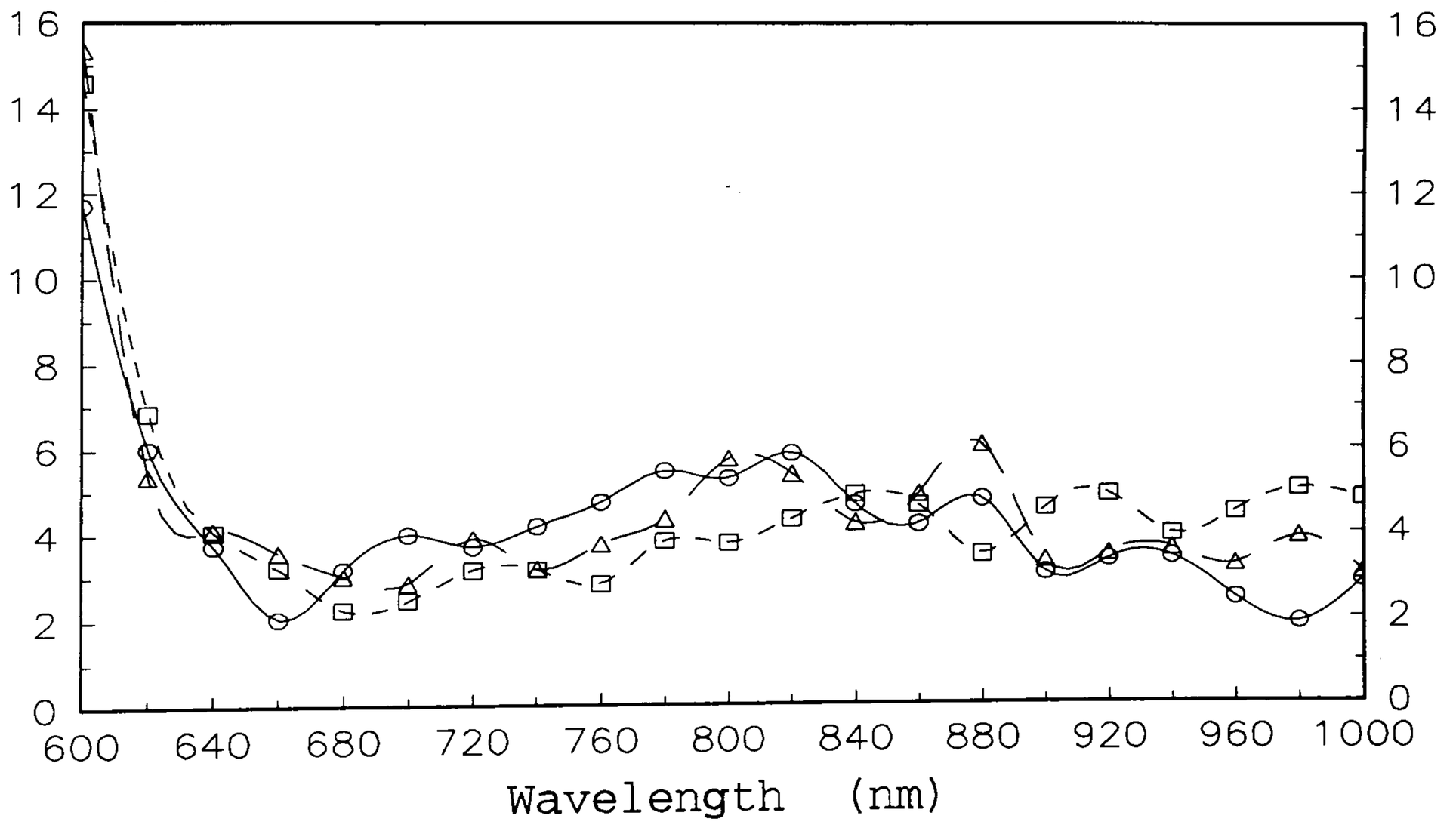

Figure E.12: AC/DC ratio in transmission mode from 600 - 1000nm.

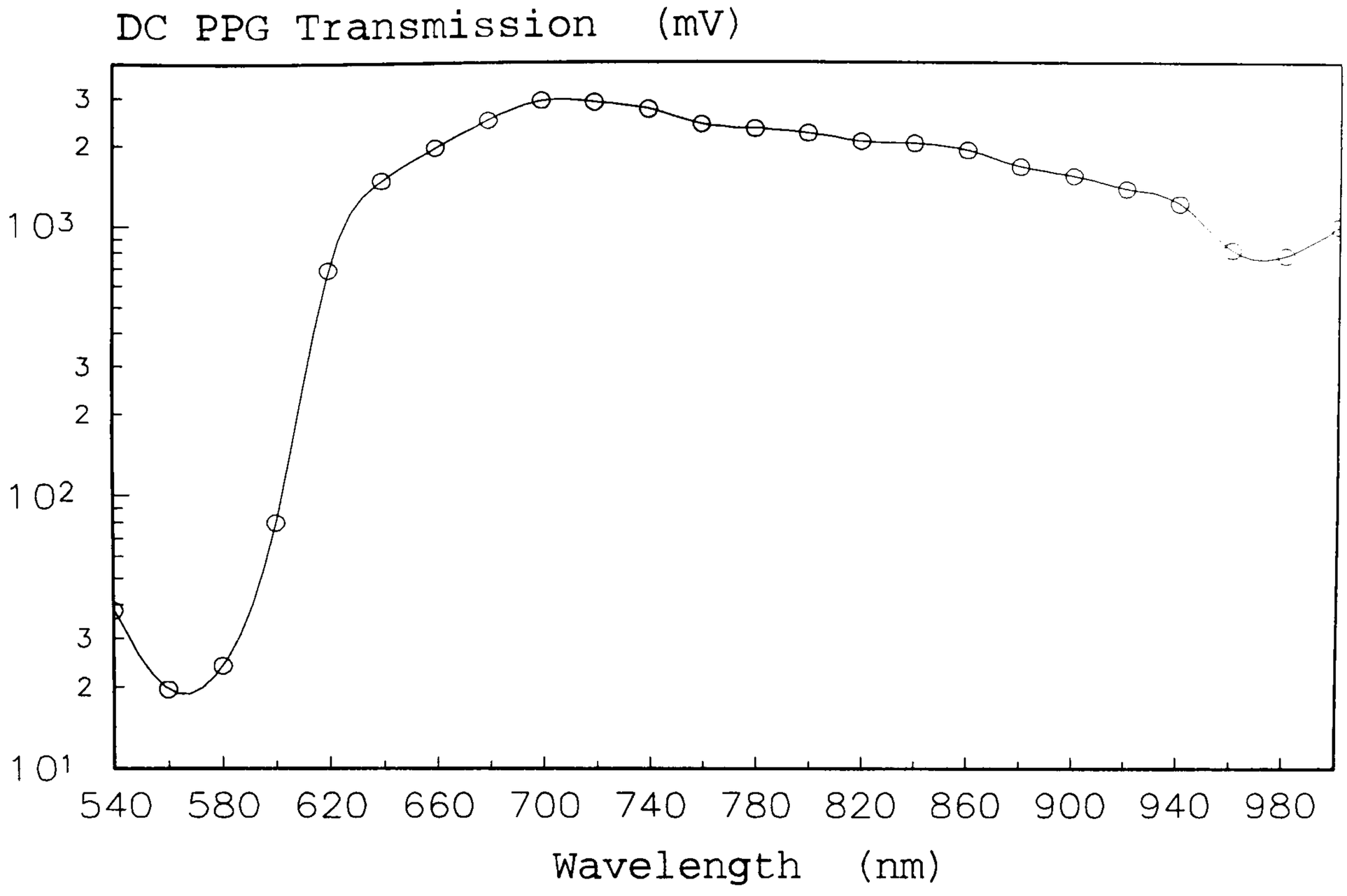

Figure E.13: DC PPG signal in transmission mode from 540 - 1000nm.

BIBLIOGRAPHY

Adriano, K.P. et al : Intraoperative transcutaneous PO_2 ($TcPO_2$) monitoring quantitates PaO_2. Fact or fiction ?
Anesth. Analg., 1984, **63**, p. 178.

Alexander, C.M., Teller, L.E. and Gross, J.B. : Principles of pulse oximetry: theoretical and practical considerations.
Anesth. Analg., 1989, **68**, (3), pp. 368 - 376.

Amar, D. et al : Fluorescent light interferes with pulse oximetry.
J. Clin. Monit., 1989, **5**, pp. 135 - 136.

Amoore, J.N., Stay, D.G. : Pulse Oximeters: An equipment management perspective.
IPSM & BES 1st joint annual scientific conference, 1994, p. 107.

Anderson, N.M. and Sekelj, P. : Light absorbing and scattering properties of non-haemolysed blood.
Phys. Med. Biol., 1967, **12**, pp. 173 - 184.

Astrup, P. and Severinghaus, J.W. : The history of blood gases, acids and bases.
1st edition, Munksgaard International Publishers, Copenhagen 1986.

Barker, S.J. and Tremper, K.K. : The effect of carbon monoxide inhalation on pulse oximetry and transcutaneous Po_2.
Anesthesiology, 1987, **66**, pp. 677 - 679.

Barker, S.J. et al : Comparison of three oxygen monitors in detecting endobronchial intubation.
J. Clin. Monit., 1989a, **4**, pp. 240 - 243.

Barker, S.J., Tremper, K.K. and Hyatt, J. : Effects of methemoglobinemia on pulse oximetry and mixed venous oximetry.
Anesthesiology, 1989b, **70**, pp. 324 - 326.

Barker, S.J., et al : The effect of sensor malpositioning on pulse oximeter accuracy during hypoxemia.
Anesthesiology, 1993, **79**, (2), pp. 248 - 254.

Blackwell, G.R. : The technology of pulse oximetry.
Biomed. Instrum. Technol., 1989, **23**, (3), pp. 188 - 193.

Blitt, C.D. : Monitoring in anesthesia and critical care medicine.
Second edition, Churchill Livingstone, 1990.

BIDS, 1995 : Computer search.

Bowes, W.A. and Corke, B.C. : Pulse oximetry: a review of the theory, accuracy and clinical applications.
Obstet. Gynecol., 1989, **74**, (3). pp. 541 - 546.

Brooks, T.D., Paulus, D.A. and Winkle, W.E. : Infrared heat lamps interfere with pulse oximeters.
Anesthesiology, 1984, **61**, p. 630.

Challoner, A.V.J. : Photoelectric plethysmograph for estimating cutaneous blood flow.
Non invasive physiological measurement, Rolfe P. (Ed.), Academic Press, London, 1979, pp. 125-151.

Challoner, A.V.J. and Ramsay, C.A. : A photoelectric plethysmograph for the measurement of cutaneous blood flow.
Phys. Med. Biol., 1974, **19**, (3), pp. 317 - 328.

Cornelissen, P.J.H. et al : Correction factors for hemoglobin derivatives in fetal blood, as measured with the IL CO-Oximeter.
Clin. Chem., 1983, **29**, p. 1555.

Costarino, A.T., Davis, D.A. and Keon, T.P. : Falsely normal saturation readings with the pulse oximeter.
Anesthesiology, 1987, **67**, pp. 830 - 831.

Cote, C.J et al : A single-blind study of pulse oximetry in children.
Anaesthesiology, 1988, **68**, pp. 184 - 188.

Crowe, J.A. : Optical methods for monitoring physiological and biochemical variables.
D.Phil. thesis, Green College, Oxford, Trinity term, 1986.

Cui, W., Ostrander, L.E. and Lee, B.Y. : In vivo reflectance of blood and tissue as a function of light wavelength.
IEEE Trans. Biomed. Eng., 1990, **37**, pp. 632 - 639.

Damianou, D. : Frequency analysis of PPG signals.
M.Sc. thesis, Nottingham University, 1989.

Damianou, D., Crowe, J.A. et al : Artefacts in reflection pulse oximetry readings due to variations in probe to skin surface separation.
IEE Colloquium on pulse oximetry, April 1991, Digest No: 1991/089.

Dear, P.R.F. : Monitoring oxygen in the newborn: saturation or partial pressure.
Arch. Dis. Child, 1987, **62**, p. 879.

Desiderio, D.P. et al : Pulse oximetry during thoracic surgery: not the 'gold standard' for oxygenation.
Anesth. Analg., 1988, **67**

de Kock, J.P. : Pulse Oximetry: Theoretical and experimental models.
Ph.D. thesis, St Hugh's college Oxford, 1991.

Enson, Y. et al : In vivo studies with an intravascular and intracardiac reflection oximeter.
J. Appl. Physiol., 1962, **17**, pp. 552 - 558.

Eisenkraft, J.B. : Pulse oximeter desaturation due to methemoglobinemia.
Anesthesiology, 1988, **68**, pp. 279 - 282.

Firbank, M. et al : Measurement of the optical properties of the skull in the wavelength range 650-950nm.
Phys. Med. Biol., 1993, **38**, (4), pp. 503 - 510.

Ganong, W.F. : Review of medical physiology, 6th edition.
Lange medical publications, Los Altos, 1973.

Gardosi, J.O., Schram, C.M. and Symonds, E.M. : Adaptation of pulse oximetry for fetal monitoring during labour.
The Lancet, May 1991, **337**, pp. 1265 - 1267.

Gardosi, J.O., Damianou, D. and Schram, C.M. : Artifacts in fetal pulse oximetry: Incomplete sensor-to-skin contact.
Am. J. Obstet. Gynecol., 1994, pp. 1169 - 1173.

Graaff, R. et al : Biophysical aspects of reflection pulse oximetry.
Fourth International conference on fetal and neonatal physiological measurements, Lafeber, H. N. (Ed.), 1991, Elsevier Science Publishers, Amsterdam, pp. 129-134.

Graaff, R. et al : Optical properties of human dermis *in vitro* and *in vivo*.
Applied Optics, 1993, **32**, (4), pp. 435 - 447.

Gravenstein, J.S. : Gas monitoring and pulse oximetry.
Butterworth-Heinemann, USA, 1990.

Griffiths, D. M. et al : Pulse meters and Pulse Oximeters.
Anaesth. Intens. Care, 1988, **16**, (1), pp. 49 - 53.

Helal, B. : Injuries to the fingertip.
The practice of hand surgery, second edition, edited by Lamb, D.W., Blackwell Scientific Publications, Oxford 1989.

Hertzman, A.B. : Observations on the finger volume pulse recorded photoelectrically.
Amer. J. Physiol., 1937, **119**, pp. 334 - 335.

Hertzman, A.B. : The blood supply of various skin areas as estimated byawhe photoelectric plethysmograph.
Amer. J. Physiol., 1938, **124**, pp. 328 - 340.

Hertzman, A.B., Randall, W.C. and Jochim, K.E. : The estimation of the cutaneous blood flow with the photoelectric plethysmograph.
Amer. J. Physiol., 1946, **145**, pp. 716 - 726.

Johnson, C.C. et al : A solid state fiberoptics oximeter.
J. Assoc. Adv. Med. Inst., 1971, **5**, pp. 77 - 83.

Johnson, N. et al : Fetal monitoring with pulse oximetry.
Brit. J. Obst. Gynaec., January 1991, **98**, pp. 36 - 41.

Kagle, D.M. et al : Evaluation of the Ohmeda 3700 pulse oximeter: steady state and transient response characteristics.
Anesthesiology, 1987, **66**, pp. 376 - 380.

Kamal, A.A.R. et al : Skin photoplethysmography- a review.
Comp. Meth. Progr. Biomed., 1989, **28**, pp. 257 - 269.

Kapany, N.S. et al : Fiber optics oximeter-densitometer for cardiovascular studies.
Appl. Opt., 1967, **6**, pp. 565 - 570.

Kelleher, J.F. : Pulse oximetry.
J. Clin. Monit., 1989a, **5**, (1), pp. 37 - 62.

Kelleher, J.F. and Ruff, R.H. : The Penumbra effect: vasomotion dependent pulse oximeter artefact due to probe malposition.
Anaesthesiology, 1989b, **71**, pp. 787 - 791.

Kessler, M.R. et al : Spurious pulse oximeter desaturation with methylene blue injection.
Anesthesiology, 1986, **65**, pp. 435 - 436.

Key, H. et al : Optical attenuation characteristics of breast tissues at visible and near infrared wavelengths.
Phys. Med. Biol., 1991, **36**, (5), pp. 579 - 590.

Konishi, M. et al : Photoelectric Oximeter.
United States Patent 3,998,550, 1976.

Kramer, K. et al : Influence of oxygen saturation, erythrocyte concentration and optical depth upon the red and near-infrared light transmittance of blood.
Amer. J. Physiol., 1951, **165**, pp. 229 - 246.

Lakanpaul, M. : Personal communication.

Lindberg, L. G., Oberg, P. A. : Photoplethysmography: influence of light source wavelength.
Med. & Biol. Engin. & Comput., 1991, **29**, pp. 48 - 54.

Loewinger, E. et al : Analysis of a micromethod for transmission oximetry in whole blood.
J. Appl. Physiol., 1964, **19**, pp. 1179 - 1184.

Mearns, A.J. et al : Forcing frequency testing, a new approach to physiological measurement.
Psychophysiology of cardiovascular control - Models, methods and data, eds. Orlebeke, J.F., Mulder, G. and Van Doorman, L.J.P., Plenum, New York, 1985, pp. 425 - 436.

Mendelson, Y. et al : Non invasive Pulse Oximetry utilizing Skin Reflectance Photoplethysmography.
IEEE Trans. on Biomed. Eng., 1988a, **35**, (10), pp. 798 - 805.

Mendelson, Y. et al : Design and evaluation of a new reflectance pulse oximeter sensor.
Medical Instrumentation, 1988b, **22**, (4), pp. 167 - 173.

Mendelson, Y. and Kent, J.C. : Variations in optical absorption spectra of adult and fetal hemoglobins and its effect on pulse oximetry.
IEEE Trans. on Biomed. Eng., 1989, **36**, p. 844

Mendelson, Y. and Yocum, L. : Noninvasive measurement of arterial oxyhemoglobin saturation with a heated and a non-heated skin reflectance pulse oximeter sensor.
Biomed. Instrum. & Technol., 1991, **25**, pp. 472 - 480.

Mendelson, Y. and Solomita, M.V. : The feasibility of spectrophotometric measurements of arterial oxygen saturation from the fetal scalp utilizing noninvasive skin-reflectance pulse oximetry.
Biomed. Instrum. & Technol., 1992, **26**, pp. 215 - 224.

Meuwissen, I. and Over, R. : Multidimensionality of the content of female sexual fantasy.
Behav. Res. Ther., 1991, **29**, pp. 179 - 189.

Millikan, G.A. : The Oximeter, an instrument for measuring continuously oxygen saturation of arterial blood in man.
Rev. Sc. Instr., 1942, **13**, pp. 434 - 444.

Nakajima, S. et al : New pulsed-typed earpiece oximeter.
Kokyu to Junkan, 1975, **23**, pp. 709 - 713.

Nellcor Incorporated : Improved method and apparatus for detecting optical pulses.
European Patent Application EP 0 335 357 A2, 1989.

O'Reilly, G. et al : A survey on pulse oximeter performance.
IPSM & BES 1st joint annual scientific conference, 1994, p. 108.

Physio-Control Corporation : Method and apparatus for the automatic calibration of signals employed in oximetry.
European Patent Specification EP 0 262 779 B1, 1993.

Pologe, J.A. : Pulse oximetry: technical aspects of machine design.
Int. Anesthesiol. Clin., 1987a, **25**, (3), pp. 137 - 153.

Pologe, J.A. : The theory and principles of pulse oximetry.
J. Perinatol., 1987b, **7**, (4), pp. 320 - 322.

Polyani, M.L. and Hehir, R.M. : New reflection oximeter.
Rev. Sci. Instr., 1960, **31**, pp. 401 - 403.

Polyani, M.L. and Hehir, R.M. : In vivo oximeter with fast dynamic response.
Rev. Sci. Instr., 1962, **33**, pp. 1050 - 1054.

Prahl, S.A. et al : A Monte Carlo model of light propagation in tissue.
SPIE Institute Series, 1989, **IS 5**, pp. 102 - 111.

Rasanen, J. et al : Titration of continuous positive airway pressure by real-time dual oximetry.
Chest, 1988, **92**, pp. 853 - 856.

Reynolds, K.J. et al : In vitro performance test system for pulse oximeters.
Med. Biol. Eng. Comput., 1992a, **30**, pp. 629 - 635.

Reynolds, K.J. et al : Response of 10 pulse oximeters to an in vitro test system.
Br. J. Anaesth., 1992b, **68**, pp. 365 - 369.

Runciman, W.B. et al : The pulse oximeter: Applications and limitations - an analysis of 2000 incident reports.
Anaesth. Intens. Care, 1993, **21**, (5), pp. 543 - 550.

Sarnquist, F.H., Todd, C. and Whitcher, C. : Accuracy of a new non-invasive oxygen saturation monitor.
Anesthesiology, 1980, **53**, S163.

Saunders, N.A., Powles, A.C.P. and Rebuck, A.S. : Ear oximetry: Accuracy and practicability in the assessment of arterial oxygenation.
Am. Rev. Resp. Dis., 1976, **113**, pp. 745 - 749.

Southall, D.P. and Samuels, M. : Inappropriate sensor application in pulse oximetry.
Lancet, 1992, **340**, (8817), pp. 481 - 482.

Scheller, M., Unger, R. and Kelner, M. : Effects of intravenously administered dyes on pulse oximeter readings.
Anesthesiology, 1986, **65**, pp. 550 - 552.

Severinghaus, J.W. and Naifeh, K.H. : Accuracy response of six pulse oximeters to profound hypoxia.
Anesthesiology, 1987, **67**, pp. 551 - 558.

Shapiro, B.A., Harrison, R.A. and Walton, J.R. : Clinical application of blood gases, 3rd edition, 1982, Year Book Medical Publishers INC.

Sherebrin, M.H. and Sherebrin, R.Z. : Frequency analysis of the peripheral pulse wave detected in the finger with a photoplethysmograph.
IEEE Trans. on Biomed. Eng., **37**, (3), pp. 313 - 317.

Shimada, Y. et al : Effects of multiple scattering and peripheral circulation on arterial oxygen saturation measured with a pulse-type oximeter.
Med. Biol. Eng. Comput., 1984, **22**, pp. 475 - 478.

Sidi, A. et al : Methylene blue and indocyanine green artificially lower pulse oximetry readings of oxygen saturation: studies in dogs.
J. Clin. Monit., 1987, **3**, pp. 249 - 256.

Takatani, S. : Toward absolute reflectance oximetry: I. Theoretical consideration for noninvasive tissue reflectance oximetry.
Adv. Exp. Med. Biol., 1989, **248**, pp. 91 - 102.

Takatani, S. et al : Experimental and clinical evaluation of a noninvasive reflectance pulse oximeter sensor.
J. Clin. Monit., 1992, **8**, (4), pp. 257 - 266.

Taylor, M.B. et al : The current status of Pulse Oximetry. Clinical value of continuous noninvasive oxygen saturation monitoring.
Anaesthesia, 1986, **41**, (9), pp. 943 - 949.

Thilo, E.H. et al : Saturation by pulse oximetry: Comparison of the results obtained by instruments of different brands.
Journal of Pediatrics, 1993, **122**, (4), pp. 620 - 626.

Thomine, J.M. : The skin of the hand in The Hand, volume 1, edited by Raoul Tubiana, 1981, W.B. Saunders company, Philadelphia.

Tremper, K.K. and Barker, S.J. : Pulse oximetry.
Anesthesiology, 1989, **70**, (1), pp. 98 - 108.

Van der Zee, P. and Delpy, D.T. : Simulation of the point spread function for light in tissue by a Monte Carlo method.
Adv. Exp. Med. Biol., 1987, **215**, pp. 179 - 191.

Van Gemert, M.J.C. et al : Skin optics.
IEEE Trans. Biomed. Eng., 1989, **36**, (12), pp. 1146 - 1154.

Verkruysse, W. et al : Modelling of the effect of wavelength on the pulsed dye laser treatment of port wine stains.
Applied Optics, 1993, **32**, (4), pp. 393 - 398.

Webb, R.K. et al : Which monitor? An analysis of 2000 incident reports.
Anaesth. Intens. Care, 1993, **21**, (5), pp. 529 - 542.

Wood, E.H. and Geraci, J.E. : Photoelectric determination of arterial oxygen saturation in man.
J. Lab. Clin. Med., 1948, **34**, pp. 387 - 401.

Wukitsch, M.W. : Pulse oximetry: Historical review and Ohmeda functional analysis.
Int. J. Clin. Monit. Comput., 1987, **4**, (3), pp. 161 - 166.

Wukitsch, M.W. et al : Pulse oximetry: analysis of theory, technology and practice.
J. Clin. Monit., 1988, **4**, (4), pp. 290 - 305.

Yelderman, M. and New, W. : Evaluation of pulse oximetry.
Anesthesiology, 1983, **59**, pp. 349 - 352.

Yoshiya, I., Shimada, Y. and Tanaka, K. : Spectrophotometric monitoring of arterial oxygen saturation in the fingertip.
Med. Biol. Eng. Comput., 1980, **18**, pp. 27 - 32.

Zijlstra, W.G. : Fundamentals and applications of clinical oximetry.
1953, 2nd Ed., Van Gorcum, Assen.

Zijlstra, W.G. et al : Correction factors for hemoglobin derivatives in fetal blood, as measured with the IL CO-Oximeter (Reply to letter to the editor).
Clin. Chem., 1983, **29**, p. 1556.

Zijlstra, W.G., Buursma, A.A. and Meeuwsen van der Roest W.P. : Absorption spectra of human fetal and adult oxyhemoglobin, de-oxyhemoglobin, carboxyhemoglobin and methemoglobin.
Clin. Chem., 1991, **37**, pp. 1633 - 1638.